

You Choose, We Do it

St. JOSEPH'S COLLEGE OF ENGINEERING

Old Mamallapuram Road, Semmencherry

Chennai - 600 119



National Conference on Emerging Techniques in Electrical Engineering

15th April 2015



Organized by

**Department of Electrical and Electronics Engineering
Institute of Electrical and Electronics Engineers (IEEE)**

&

ISTE Chapter

PREFACE

We, the staff of Department of Electrical and Electronics Engineering are happy to present this preface of proceedings of national level conference on Emerging Techniques in Electrical Engineering, EtEE – 15, being conducted in our college on April 15, 2015.

We are very proud that we have received an overwhelming response to our call of papers. The selected papers have been scheduled for presentation in three different sessions on April 15, 2015.

Dr. David B.Durocher, President, IEEE IAS Society and **Dr. Peter Magyar**, Chair & Managing Director, IEEE IAS, has kindly accepted to deliver the keynote address of the conference. The detailed program is presented in the subsequent pages.

We also thank the Managing Director, Director, Principal and Dean for their kind co-operation, guidance in conducting the conference

Dr. T D Sudhakar

Organizing Secretary

ORGANIZING COMMITTEE

Chief Patron	Dr. B. Babu Manoharan, M.A.,M.B.A.,Ph.D., Managing Director
Patron	Mr. B. Jaikumar Christhu Rajan, M.E., M.B.A., Director
Chair-Person	Dr. Vaddi Seshagiri Rao M.E., M.B.A., Ph.D., Principal
Convener	Mrs. Jayarama Pradeep M.E., (Ph.D.), Associate Professor/Head, Dept. of EEE
Organizing Secretary	Dr. T D Sudhakar, M.E., Ph.D., Associate Professor, Dept. of EEE
Organizing Members	Dr. Ramani Kalpathi, M.S., Ph.D., Dr. C. Baskaran, M.E., Ph.D., Dr. T.V.Narmadha M.E., Ph.D., Mr. K.Mohanadasse M.E., (Ph.D.) Dr. M.Ramesh Babu M.E., Ph.D., Dr. S.Arunachalam, M.E., Ph.D.,
Coordinators	Mr. N.Chidambararaj, M.E.,(Ph.D.), Mr. S Nishant, M.E.,

CONTENTS

Sl No	Title	Page No.
1	Thermal Analysis of A 3 Phase, 550 W Switched Reluctance Machine	001
2	Analysis Of Global Maximum Power Point For Partially Shaded PV Module Using Fuzzy Logic Controller	006
3	Comparative Study On Various Bipolar PWM Strategies For Seven Level Symmetrical Inverter	013
4	Congestion Management Based on Active Power Rescheduling of Generator Units Using Bacterial Swarming Algorithm	021
5	Design And Implementation of ANFIS Controller for Solid Oxide Fuel Cell System	027
6	Design and Implementation of Water Pumping System Using SEPIC Converter	032
7	Energy Management System For Hybrid Renewable Energy Sources Using Adaptive Neural Network	036
8	A Grid Connected Solar Energy System Using LQR Based P&O MPPT Algorithm	041
9	Fuel Cost Function For Economic Load Dispatch Using Particle Swarm Optimization Algorithm	046
10	High Efficient Current Controlled Converter For SRM	052
11	Implementation Of Single Phase Matrix Converter	058
12	Load Based Pricing In Demand Side Management Through Ant Colony Optimization	063
13	Maximum Power Tracking In Solar System In Uncertain Environment Using Robust Optimization	067
14	Minimization Of Load Forecast Uncertainty For Reliable Supply	071
15	Enhance The Performance Of Hierarchical Control In Microgrid Application	077
16	Optimal Placement Of Distribution Generator To Maximize The Net Savings Of The Distribution Network	082
17	Performance Analysis On Multi Carrier Trapezoidal PWM Strategies For Symmetrical Multilevel Inverter	087

18	PV Based Cascaded Sepic Converter For Battery Charging	092
19	Reconfiguration For Loss Reduction And Sensitivity Analysis For Simultaneous Optimal Placement Of Fc Banks And Dg In Radial Distribution Network	097
20	Resonant Boost Converter For PV Based Pumping Application	105
21	Security Constrained Unit Commitment Problem Based On Memetic Algorithm In Thermal-Wind Generation	111
22	Self Hiring Using Secured Embedded System	117
23	Simulation And Implementation Of Mixed Conduction Mode Control For Boost Power Factor Conduction Conversion	121
24	Voltage Sag Compensation In Stand Alone Power System Using SRF Theory	130
25	Wireless Control Of Prototype Of PMDC Motor Using PI And Fuzzy Logic	133
26	Congestion Management In Electricity Market By Demand Response Program	143
27	A Structure Of 360° Solar Tracking System Using PLC And SCADA	149
28	Performance Analysis Of PMSM Using Direct Torque Control	156
29	A Stability Analysis For Grid Connected Wind Farm With Battery	159
30	A Power Oscillation Damper For Variable Speed Wind Generator	163
31	Dynamic Mathematical Modelling Of PMSM And Parametric Sensitivity Analysis Using Vector Control	167
32	A Probability Based Approach for Unit Commitment and Economic Dispatch in Powered Microgrids	171
33	Quasi Z Source Inverter For Consumer Application	177
34	Analysis With PWM Control of Cuk and Boost Dual Input Dual Output Dc-Dc Converter	185
35	Soft Start Methods Of Dc Motor Fed By A PV Source	189
36	Design Of H6 Transformer Less Full Bridge Grid Tied Inverters	192

Thermal Analysis of a 3 phase, 550 W Switched Reluctance Machine

A. Pavan

School of Mechanical and Building Sciences
VIT University
Chennai, India
pavan.a2013@vit.ac.in

Sathyaranarayanan N

School of Electrical Engineering
VIT University
Chennai, India
sathyaranarayanan.n2014@vit.ac.in

Rajesh Kumar R

Research Department
CD-Adapco
Bengaluru, India
rajesh.kumar@cd-adapco.com

N.C. Lenin

School of Electrical Engineering
VIT University
Chennai, India
lenin.nc@vit.ac.in

Sivakumar R

School of Mechanical and Building Sciences
VIT University
Chennai, India
sivakumar.r@vit.ac.in

Abstract—The purpose of this paper is to observe the heat distribution inside the Switched Reluctance Machine (SRM) through Computational Fluid Dynamics (CFD). Electromagnetic losses such as copper and core losses are considered as the heat sources in the machine. Initially, a three dimensional (3-D) steady state thermal analysis is carried out to determine the film coefficient of machine parts. Further, a transient thermal analysis is performed to predict the temperature rise. From the transient analysis, heat distribution for the given speed and time taken to reach the steady state are observed.

Keywords— computational fluid dynamics; switched reluctance motor; thermal analysis; flow analysis; core loss; copper loss

I. INTRODUCTION

Nowadays the attention towards the energy saving electrical machines has increased. Switched reluctance machines are most popular and have been generating attention of electrical researchers due to its robustness, simplicity and low cost manufacturing for the past 3 decades [1]. The losses in SRM originates mainly due to two things; electrical and mechanical. The friction in machine parts and electric currents are the beginnings of heat propagation. Hence the temperature rise in different components of the machine could cause deterioration of insulation in the windings, thermal stress, efficiency reduction and this may contribute to motor failure [2]. Also under high loads, temperature rise influences the motor's electrical and magnetic parameters. It is thus necessary to keep the temperature of the machine components within permissible bounds for safety performance. Due to this, thermal analysis plays prominent role in the analyses of electrical machines [3]. There are two basic types of thermal analysis of electric machines: Analytical lumped-circuit and numerical methods. To design energy saving electrical machine, numerical methods are the most prominent technique. There are several packages of numerical methods to perform thermal analysis such as Finite element analysis (FEA), Motor-CAD, CFD etc.

Among these CFD is a virtual modeling technique with powerful visualization capabilities which can be used to evaluate the performance of a wide range of applications [4]. This paper presents the CFD based thermal analysis of SRM with steady and transient conditions.

II. DESIGN SPECIFICATION

In SRM, the stator and rotor have salient poles. The machine has six stator poles and four rotor poles which are uniformly placed. The windings are present only in the stator which is wounded around the stator teeth. A 3 phase, 6/4 3-D SRM model is shown in Fig. 1 and the geometric dimensions of the corresponding model is presented in Table I.

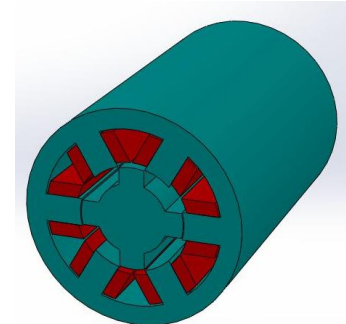


Fig. 1. 3-D Geometric model of SRM

TABLE I. DIMENSIONS OF 6/4 SRM

No of stator Poles	6
No of rotor poles	4
Stator outer diameter (m)	0.055
Rotor outer diameter (m)	0.026
Stack length (m)	0.08522
Air gap length (m)	0.00025

III. NEED FOR FLOW ANALYSIS

The fluid that flows inside the SRM is air. Heat transfer inside the SRM mainly depends on the air velocity. When the rotor begins its rotation, the air inside the SRM is highly turbulent. To investigate the air flow inside the SRM, the air region is split into two areas i.e. the area near to the rotor is taken as rotor air region and the region close to the stator is taken as stator air region. An interface was created in the middle of air gap to interpolate the above two regions. The air gap and the air pockets of SRM is shown in Fig. 2. Air gap means the gap in between the stator and rotor poles. For the given SRM, the rotor is rotating at a speed of 1000 rpm and it is assigned to rotor air regions. To find the air velocity, the flow analysis is carried out for both stator and rotor air regions. The fluid properties shown in Table II are attributed to both stator as well as rotor air regions and a steady state analysis is carried out using STAR-CCM+.

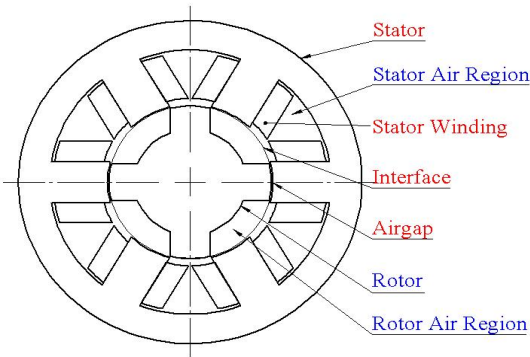


Fig.2 .Front View of SRM

TABLE II. PROPERTIES OF MATERIALS

Material	Thermal conductivity (W/m·K)	Density (kg/m ³)
Air	0.024	1.165
Steel	40	7850
Copper	380	8940

A. Results of Flow Analysis

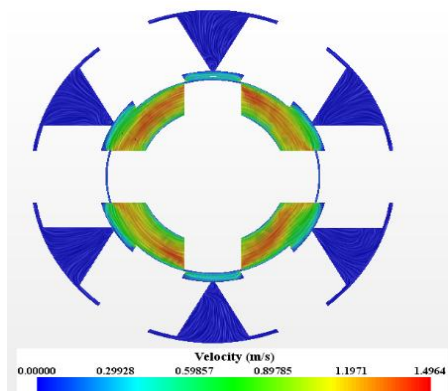


Fig. 3. Velocity distribution in SRM

Figure 3 shows the air velocity distribution inside the SRM for the speed of 1000 rpm. From the simulation results, it is observed that the air velocity at stator and rotor interface is 0.6 m/s. The outcomes of the analysis show higher air speed in the middle of the rotor air region and it is low near to back iron as well as interpolar region. The air flow inside the stator air region is very low due to the flow obstructions by the stator windings. This reduces the convection coefficient on the stator's inner surface area and increases the stator temperature.

IV. HEAT SOURCE

The two primary elements of electromagnetic losses in a motor are copper losses in the windings and core losses in the laminations. These losses are the heat source for the temperature rise. For any motor, the copper loss can be estimated from the formula given in (1). Due to proximity and skin effects, the value of R is greater than the DC resistance. The value of core loss in a separated conductor depends on the proximity of the conductor to the steel core. In addition, the magnetic field created by a single conductor influences other conductors [5]. This is known as proximity effect. Considering the above effects, the expression for the calculation of core losses in the SRM is given as in (2).

$$\text{Core loss} = I^2 R \quad (1)$$

Where

I = Rms Average Current (Ampere)

R = Effective resistance of one phase winding (Ohm)

$$\text{Total loss} = \text{Copper loss} + \text{Core loss}$$

$$\text{Mechanical losses (watts)} \quad (2)$$

$$\text{Core loss} = \text{Total loss} - \text{Copper loss} - \text{Mechanical losses}$$

Where

Mechanical losses = Friction Loss + Windage Loss

$$\text{Total losses} = \text{Input Power} - \text{Output Power} \quad (3)$$

$$\text{Input power} = \frac{\text{Output Power}}{\text{Efficiency}} \text{ (Watts)} \quad (4)$$

The specifications of SRM along with core and copper losses are presented in Table III.

TABLE III. SPECIFICATIONS OF 6/4 SRM

Rotational Speed (RPM)	1000
Average Current (Ampere)	6
Copper loss (watts)	57.15
Core loss (Watts)	18.376

V. STEADY STATE THERMAL ANALYSIS

In steady state analysis, conduction heat transfer with different boundary conditions [5] is obtained from the Fourier law as

$$\frac{1}{r} \frac{\partial}{\partial r} \left(kr \frac{\partial T}{\partial r} \right) + \frac{1}{r^2} \frac{\partial}{\partial \theta} \left(k \frac{\partial T}{\partial \theta} \right) + \frac{\partial}{\partial Z} \left(k \frac{\partial T}{\partial Z} \right) + q = 0 \quad (5)$$

TABLE IV. PHYSICAL DIMENSIONS OF SRM

Area of the coil segment (m^2)	27.68×10^{-6}
Total coil area (m^2)	332.16×10^{-6}
Shaft length (m)	0.08522
Volume of the coil (m^3)	2.83066×10^{-5}
Area of the stator (m^2)	1176.6×10^{-6}
Volume of the stator (m^3)	1.0026×10^{-4}

Agreeing to the physical dimensions given in Table IV and from the core and copper losses of the motor, a quantity of heat generated, Q is computed for different parts like stator core and coils as shown in Table V. The material properties, such as thermal conductivity, density, specific heat, etc, are specified for each part of the machine. The ambient temperature was set as 303K and a steady state CFD based thermal analysis were carried out for the given value of Q (W/m^3).

TABLE V. QUANTITY OF GENERATION

Heat generation in copper(W/m^3)	Heat generation in Core (W/m^3)
2.019×10^7	55322.73

A. Results of Steady State Thermal Analysis

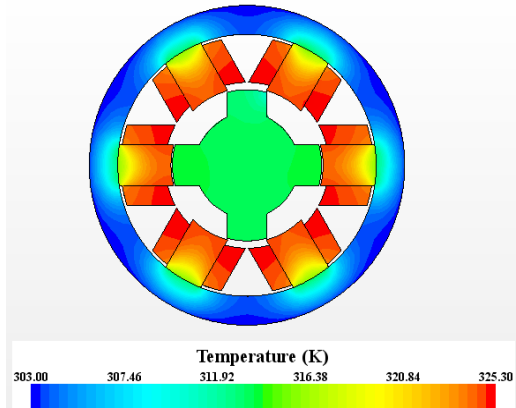


Fig. 3. Steady state temperature distribution.

Figure 4 shows the temperature distribution of SRM in Steady state condition. From the simulations, the maximum temperature generated inside the machine was found to be 325.3 K. The maximum temperature was generated at coils due to higher copper loss. This heat is transferred to the stator poles through conduction. The stator has a larger volume at the back iron to dissipate the heat received by the stator pole from the coils. Hence the temperature is high at stator pole arc and it is low near the back iron of the stator. In steady state, it

is clear that the temperature rise due to copper and core losses depends on the current, flux through the coil and the stator respectively.

VI. TRANSIENT THERMAL ANALYSIS

In transient thermal analysis, the temperature varies with respect to time. In a hollow cylinder containing heat source, conductive heat transfer with various boundary conditions is obtained from the Fourier law in cylindrical coordinate as

$$\frac{1}{r} \frac{\partial}{\partial r} \left(kr \frac{\partial T}{\partial r} \right) + \frac{1}{r^2} \frac{\partial}{\partial \theta} \left(k \frac{\partial T}{\partial \theta} \right) + \frac{\partial}{\partial Z} \left(k \frac{\partial T}{\partial Z} \right) + q = \rho c \frac{dT}{dt} \quad (6)$$

Inside the motor, the developed heat is dissipated mainly through the air flow circulating in between the stator and rotor poles. Due to this, heat in the locality of the excited phase gets transferred to the surfaces of the rotor body through convection. The amount of heat transferred from excited phase to surrounding regions mainly depends upon convection heat transfer coefficient, h. The value of 'h' depends on thermal conductivity, specific heat, fluid dynamic viscosity and other properties of the coolant. With the help of empirical expressions, an approximation of the coefficients is possible. The set of dimensionless numbers used in the calculation of convection heat transfer coefficients are

Reynold's number

$$Re = \frac{\Pi D^2 \omega}{\nu} \quad (7)$$

Where

D - Diameter of the stator up to the stator pole arc (m)

ω - Angular velocity = $2 \Pi N/60$ (rad/s)

N - Speed of the motor (rpm)

ν - Kinematic viscosity (m^2/s)

Grashof number

$$Gr = \frac{\beta g \theta \rho^2 L^3}{\mu^2} \quad (8)$$

Where

β - Coefficient of cubical expansion of fluid (K^{-1})

g - Gravitational force of attraction (m/s^2)

θ - Temperature difference between surface and fluid (K)

ρ - Fluid density (kg/m^3)

L - Characteristic length of the surface (m)

μ - Fluid dynamic viscosity (Kg/m s)

Prandtl number

$$\text{Pr} = \frac{c\mu}{\lambda} \quad (9)$$

Where

c - Specific heat capacity of fluid (J/Kg K)

λ - Thermal conductivity of fluid (W/m K)

Nusselt Number

$$Nu = \frac{hL}{\lambda} \quad (10)$$

Nusselt number is often used for the calculation of the convection heat transfer coefficient (h).

$$h = \frac{Nu(\lambda)}{L}$$

Natural Convection is considered on stator external surface. The natural convection heat transfer mainly depends upon fluid properties and on the temperature difference between the considered solid component and the fluid. The convective heat transfer coefficient for natural convection is calculated using (11)

$$Nu = 0.129(Gr \text{Pr})^{1/3} \quad (11)$$

Internal surfaces are subjected to forced convection due to the rotary motion of the rotor. Forced convection mainly depends upon the fluid properties and velocity and is independent of temperature. The empirical relation to calculate convective heat transfer coefficient inside the machine components [6] is given as

$$Nu = 0.037(Re)^{4/5}(\text{Pr})^{1/3} \quad (12)$$

$$Nu = 65.811$$

$$h = 59 \text{ (W/m - K)}$$

Convection coefficient is calculated for different heat dissipating surfaces depending on the shape of the surface and the velocity of the air in contact with the surface of heat dissipation. The respective convection coefficients are set for the corresponding surfaces. In the steady state simulation, the temperature increases from 303 K and attains the maximum of 325.3 K. This state is considered as the initial boundary conditions for the transient thermal analysis and simulation were carried out.

A. Results of Transient Thermal Analysis

Figure 5 shows the interior temperature distribution of the SRM. From the simulations it is observed that the maximum temperature generated at coil is 324.62 K. This heat is dissipated to stator poles and stator air regions through conduction and convection respectively. The temperature distribution inside the SRM mainly depends upon air flow distribution and convection heat transfer coefficient. The flow

distribution in stator region is low due to which heat distribution in the stator is high, whereas the temperature in the rotor is low because of higher velocities in the rotor air region. Fig. 6 and 7 shows the results obtained in transient analysis. In transient thermal analysis, the time required for the SRM to reach steady state temperature is determined and plotted in fig. 8. It shows that the temperature rise is maximum in coils and it stabilizes after 120 seconds. In rotor, the rise in temperature is initiated after 5 seconds due to higher velocities in rotor air region and rotary motion of rotor. The time taken for conduction and convection process in stator and stator air region delays the temperature rise. The stator is the only part which experiences wide range of temperature variations. The temperature in stator poles is high due to conduction with the coils and it is low in the back iron of stator. The stator poles have direct contact with coils due to which the rise in temperature is logarithmic, similar to coils. When compared to stator the temperature rise in rotor is less. This is because of heat losses due to conduction between stator and coils as well as convection with air. Hence the temperature distribution within the machine parts is analyzed accurately with the help of transient thermal analysis.

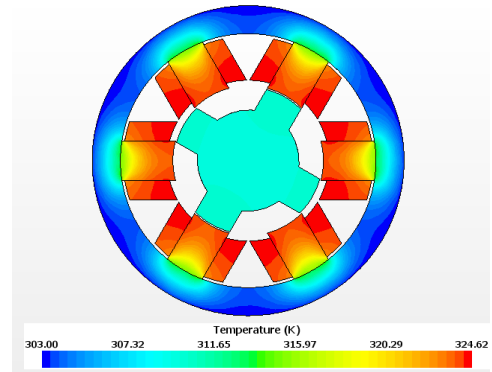


Fig. 2. Temperature distribution in Transient State

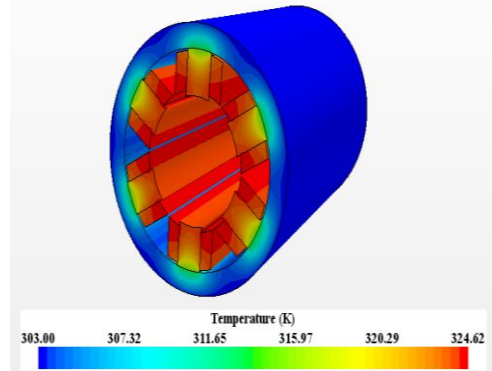


Fig. 3. Temperature distribution in Stator and coils.

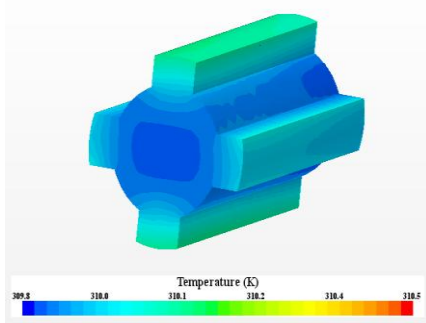


Fig. 4. Temperature distribution in Rotor.

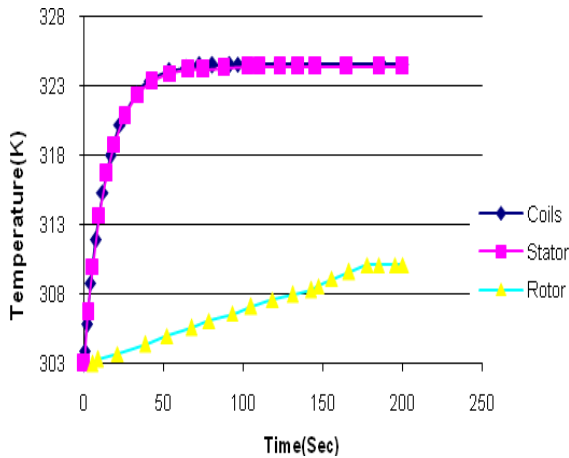


Fig. 6. Variation of Temperature in different parts.

VII. CONCLUSIONS

The flow distribution and temperature rise in the SRM have been analyzed using 3-D analysis. At 1000 rpm, the velocity at the stator and rotor interface is obtained as 0.6 m/s. The coils are the main source of heat which is present in the stator hence the rise in temperature is maximum in coils and stators. The

maximum temperature rise in SRM is 324 K and it is stabilized after 120 s. The result indicates that the flow distribution in stator region is low due to which heat distribution in the stator is high. Whereas, flow of air in rotor region is high thereby heat distribution in this region is very low. Using these results, the weight of materials used and number prototype for testing can be minimized.

ACKNOWLEDGMENT

I would like to thank Dr. Magesh Ramadoss, Program Manager-Academic, who provided me an opportunity to participate in the STAR-CCM+ training and arranged all facilities to make life easier. I perceive as this opportunity as a big milestone in my career development. I will strive to use gained skills and knowledge in the best possible way. I choose this moment to acknowledge his contribution gratefully.

REFERENCES

- [1] R. Satheesh, V. Prakash Kumar, S. Prabhu, V. Chandrasekhar, N.C. Lenin, R. Arumugam, "Flow analysis of switched reluctance hub motor," International Journal of Advanced Scientific and Technical Research, vol. 6, pp. 2249-9954, 2013.
- [2] E. Annie Elisabeth Jebaseeli and S. Paramasivam, "Steady state and transient thermal analysis of switched reluctance machine," International Journal of Computer and Electrical Engineering, vol. 4, pp. 794-798, 2012.
- [3] K.N. Srinivas and R. Arumugam, "Analysis and characterization of switched reluctance motors," IEEE Trans. on Magn., vol. 41, pp. 1321-1332, 2005.
- [4] LukaszSlupik and JacekSmolka, "Experimentally validated numerical model of coupled flow, thermal and electromagnetic problem in small power electric motor," Computer Assisted Methods in Engineering and Science, vol. 20, pp. 133-144, 2013.
- [5] S. Prabhu, V.Chandrasekhar, P. Karthikeyan, N.C. Lenin and R. Arumugam, "Vibration and thermal analysis of switched reluctance hub motor," European Journal of Scientific Research, vol.6, no.1, pp. 12-20, 2012.
- [6] D.A. Staton and A. Cavagnino, "Convection heat transfer and flow calculations suitable for electric machines thermal models," IEEE Trans. on Ind. Electron., vol. 55, pp. 3509-3516, 2008.

Analysis of Global Maximum Power Point for Partially Shaded PV Module using Fuzzy Logic Controller

Praveen Kumar. P

Post Graduate Student

Department of Electrical and Electronics Engineering

K.S. Rangasamy College of Technology

Tiruchengode, Namakkal, 9942051262

praveen.a6623@gmail.com

Jaiganesh.K

Assistant Professor

Department of Electrical and Electronics Engineering

K.S. Rangasamy College of Technology

Tiruchengode-637211, Namakkal, 9841762674

akj_79@yahoo.co.in

Abstract— To convert solar energy more viable, the efficiency of solar array systems should be maximized. An easier approach to maximizing the efficiency of solar array systems is Maximum Power Point Tracking (MPPT). MPPT is used in photovoltaic (PV) systems to maximize the output power of photovoltaic array, irrespective of the irradiation and temperature conditions. Many conventional MPPT fails to attain global maximum power point due to presence of multiple maxima points in shaded solar PV panel. This work proposes a fuzzy based controller which always attains the global maximum point in shaded panels. The proposed MPPT has been implemented by combining fuzzy logic based MPPT with a scanning and storing system. The proposed MPPT is able to reach the global maximum power point (MPP) under any partial shading conditions. Moreover, the controller exhibits a fast speed of convergence, having small oscillation around the MPP during steady state. The proposed method attains global maximum point with fast convergence than the conventional MPPT techniques.

Keywords—MPPT, Shaded solar PV Panel, Fuzzy Logic, Multiple Maxima

I. INTRODUCTION

The generation of energy in our modern industrialized society is still mainly based on a very limited resource: fossil fuels. As the world's energy demands rise and new sources for fossil fuels become scarce, so the search for an alternative energy resources has become an important issue for our time. A large amount of research has been done not only in the area of nuclear power generation but also in the area of unlimited energy sources such as wind power generation and solar energy transformation.

The use of new efficient photovoltaic solar cells (PVSCs) has emerged as an alternative measure of energy conservation, renewable green power, and demand-side management. Because of their high initial cost, PVSCs yet not have been fully an attractive alternative for electricity users who are able to buy cheaper electrical power from the utility grid. However, they can be used extensively for lighting, water pumping and air conditioning in remote and isolated areas, where the utility power is not available or is too expensive to transport.

Modified fuzzy-logic controller for maximum power point (MPP) tracking was proposed to increase photovoltaic (PV) system performance during partially shaded conditions [1]. In place of perturbing and observing the PV system MPP, the

controller will scan and stores the maximum power during the perturbing and observing procedures. The controller provides accurate convergence to the global maximum operating point under different partial shadowing conditions. A technique based on GA was developed to extract the global maximum point for PV panel under shade [2]. The characteristics of PV array are affected by shading, temperature and solar insolation. In reality, under partially shaded conditions, the P-V and I-V characteristics of solar array gets more complex with multiple maxima in the characteristic curves. A new method to track the global MPP based on controlling a dc to dc converter connected to the output of PV array, such that it behaves as a constant input-power load. The power-voltage characteristic of PV arrays operating under partial-shading conditions exhibits multiple local MPP[3]. A novel strategy of maximum power point tracking for photovoltaic power generation systems based on Fibonacci search algorithm to realize simple control system to track the real maximum power point even under non-uniform or for rapidly changing insolation conditions [4].

MATLAB-based modeling and simulation scheme suitable for studying the I-V and P-V characteristics of a PV array was developed under a non uniform insolation due to partial shading [5]. The performance of a PV array is affected by solar insolation, shading, temperature, and array configuration. The PV arrays usually gets shadowed completely or partially, by the neighboring buildings, passing clouds, trees, towers, telephone and utility poles. During partially shaded conditions, the PV characteristics becomes more complex having multiple peaks. still, it is very important to understand and predict them in order to extract the maximum possible power.

New MPPT method for PV array under PSC which is based on IncCond method with step-size variation was proposed [6]. Conventional popular MPPT methods are effective under uniform solar irradiance. However, during partially shaded conditions, these MPPTs may fail to track the originall MPP because of the occurrence of multiple local maxima on the PV characteristic curve.

II. SOLAR PV CHARACTERISTICS

The solar cell is the semiconductor device that directly converts the light energy to the electrical energy. Specifically, the output power of a solar array strongly depends on the irradiance level of sunlight and ambient temperature. The conventional model of a solar cell is the one diode model. During uniform solar insolation, the output power of the solar

PV array is equal the total output power of all solar cells. MPPT is used to track maximum power from a Solar PV panel. But in non uniform insolation condition like shadow on the solar panel, the region of shaded solar module starts working as a load, and it can be expeled by using the bypass and blocking diode[9]. If even one full cell is shaded, the voltage of that module will drop to half of its un-shaded value in order to protect itself. If enough cells are shaded, the module will not convert any energy and will in fact become a tiny drain of energy on the entire system. The effect of shading is occurrence of multiple local maxima points. The conventional algorithms like Perturb and Observe method and Incremental conductance method cannot be applied, as the algorithm stops when they get first local maximum point. These algorithms fail to extract global maximum power point resulting in significant reduction of both the generated power and the PV energy production system reliability.

Photovoltaic modules have a very low conversion efficiency of around 15% for the manufactured ones. The PV plant efficiency is affected mainly by three factors: the efficiency of the PV panel, the efficiency of the inverter and the efficiency of the MPPT algorithm. Improving the efficiency of the PV panel and the inverter is not easy as it depends on the technology available, it may require better components, which may increase extremely the cost of the installation. Instead, improving the tracking of the MPP with new control algorithms is easier, which is not expensive and could be done even in plants which are in use already by updating their control algorithms, which would lead to an effective increase in PV power generation and consequently a reduction in its price. MPPT algorithms are necessary because PV arrays have a non linear voltage-current characteristic with a unique point where the power produced is maximum. This point will depends on the irradiance conditions and temperature of the panels. Both conditions change during the day and are also different depending on the season of the year. In addition, irradiation can change rapidly due to changing atmospheric conditions such as clouds.

Conventional MPPT techniques find the maximum power point voltage (V_{MPP}) and current (I_{MPP}) at which the PV array operates at the MPP. The functioning of a photovoltaic array is impacted by solar irradiance, temperature, array configuration and shading. However, these techniques may malfunction for non uniform insolation of the PV array. Frequently, the PV arrays get shadowed, wholly or partially, by means of moving clouds, adjacent buildings and towers, nearby trees, utility and telephone poles. The situation is of special interest in case of large PV installations such as those used in distributed power generation systems.

Solar PV panel is a power source having non linear internal resistance. A major challenge in using a solar PV source containing a number of cells in series is to deal with its non-linear internal resistance. The problem will be more complex when the array receives non-uniform solar radiation. The shaded cells absorb a large amount of electric power generated by cells receiving high insolation and convert it into heat. This heat under certain conditions may damage the low illuminated cells . To mitigate the stress on shaded cells, bypass diodes are connected across the modules. In such case, power-voltage characteristic curve shows multiple peaks under non uniform illumination. Under partially shaded conditions, the PV characteristics get more tangled with more

than one peak. Yet, it is very crucial to understand and predict them in order to draw out the maximum possible power. A MATLAB-based modeling and simulation scheme is desirable for studying the I-V and P-V characteristics of a photovoltaic array under a non- inhomogeneous insolation due to partial shading[8]. It can also be used for assessing and acquiring new maximum power point tracking methods, particularly for partially shaded conditions. The new method offers a mean to study the effects of shading patterns on PV panels having different forms. It is observed that, for a set number of PV modules, the array configuration (refers to the number of series and parallel connections) importantly bears on the maximum usable power under partially shaded conditions[7]. The PV and IV characteristic of shaded solar PV panel is given in Figure 1 and Figure 2.

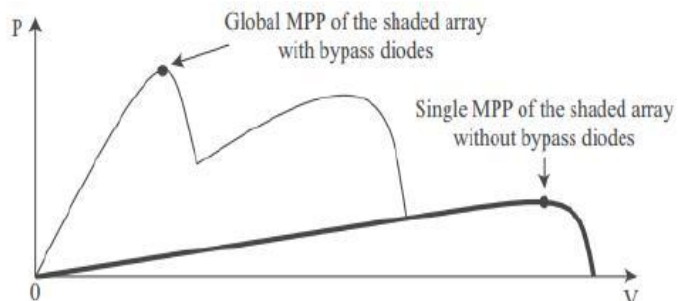


Fig. 1 P-V Characteristics of Shaded PV Solar Cell

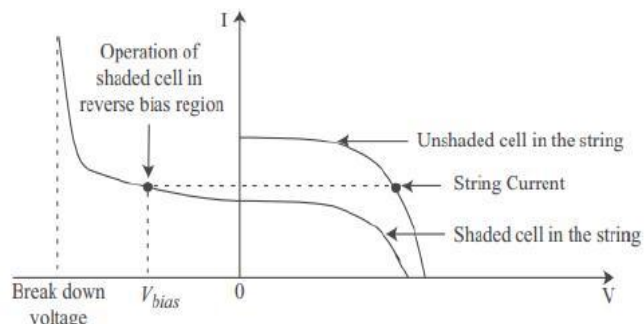


Fig. 2 I-V Characteristics of Shaded PV Solar Cell

The photovoltaic generator model can be found from the electrical equivalent to the source. The equivalent circuit of solar cell is shown in Fig.3. By using single diode model, the equivalent circuit for the solar module in N_s series cells or parallel cells can be studied. The specifications of solar module are illustrated in Table 1.

Table 1. Solar Module Specification

Parameter	Value
Voltage at maximum point(V_m)	26.3 V
Current at maximum point(I_m)	7.61 A
Open circuit voltage(V_{oc})	32.9 V
Short circuit current(I_{sc})	8.21 A
N_s	54
G_{ref}	1000W/m ²
T_{ref}	(25+273.15) K
R_s	0.001Ω
R_{sh}	5Ω

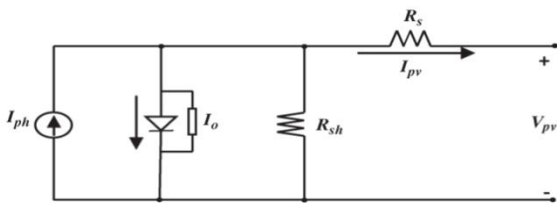


Fig. 3 Equivalent Circuit of PV Cell

III. MAXIMUM POWER POINT TRACKING

Maximum Power Point Tracking, frequently referred to as MPPT, is an electronic system that will operate the PV modules in a manner that allows the modules to produce all the power. It is an electronic DC to DC converter that optimizes the match between the solar array and the battery or utility grid. It converts a higher voltage DC output from solar panel down to lower voltage needed to charge batteries. MPPT is a fully electronic system that varies the electrical operating point of the modules so that the modules are able to deliver maximum available power[10]. Additional power collected from the modules is then made available as increased battery charge current. The following are some of the most commonly used MPPT methods.

A. Perturb and Observe Method

The Maximum Power Point Tracking Algorithm used in this paper is ‘Perturb and Observe (P&O)’ method, in which a slight perturbation is introduced in the system[12]. Owing to this perturbation, the power of the module gets changed. If the power increases due to the perturbation, then the perturbation will be continued in that direction. Once the peak power is reached the power at the next instant decreases and hence after that the perturbation reverses. P&O can be implemented by applying perturbations to the reference voltage of the solar panel. The goal will involve pushing the reference voltage signal towards VMPP thereby causing the instantaneous voltage to track the VMPP. As a result the output power will approach MPP.

B. Incremental Conductance Method

In the incremental conductance method, the controller will measure the incremental changes in array current and voltage to predict the effect of a voltage change. This method requires much more computation in the controller, but it can track the changing conditions more rapidly than perturb and observe method (P&O). Like the P&O algorithm, it can produce oscillations in power output. This method uses the incremental conductance of the photovoltaic array to compute the sign of the change in power with respect to voltage. The incremental conductance method computes the maximum power point by comparison of the incremental conductance to the array conductance. When these two are the same, the output voltage is the MPP voltage. The controller will keep up this voltage until the irradiation changes and the process is repeated.

C. Current Sweep Method

The current sweep method uses a sweep waveform for the PV array current such that the I-V characteristic of the PV array is obtained and updated at fixed time intervals. From the

characteristic curve the maximum power point voltage can then be computed at the same intervals.

IV. FUZZY LOGIC CONTROLLER

Unlike conventional MPPTs where the PV system operating power is perturbed and observed to track the MPP. Scanning, storing, perturbing and observing the operating power of the PV system are used for the proposed MPPT. The proposed method is able to track the MPP under any weather conditions, particularly partial shadowing where local and global maximum points exist. During the initial condition or varying weather conditions, the proposed MPPT makes a wide range search to scan and store the maximum power value on the PV system. A preset value which represents the accepted difference between the identified maximum power and the operated power is stored to decide the controller rules. If the difference between the identified maximum power and the operated power is greater than the pre-set value, the duty cycle is increased, or-else, fuzzy-logic-based MPPT is applied[11]. In this case, the algorithm ensures that the MPPT is not trapped by local maxima and quickly recovers the new global maximum point during varying weather conditions.

The flowchart of the proposed method is shown in Fig.4, where V_{pv} , I_{pv} are the PV output voltage and current respectively, D is the duty cycle, P_{max} is the global MPP, and ΔP_{max} is a constant that identifies the allowable difference between the global maximum point and the operating power point.

Three scanning and storing techniques are proposed to identify the global maximum power during initial conditions or varying weather conditions. The first technique is to initialize the system with maximum duty cycle since the PV output power usually takes some samples before reaching the operating point at maximum duty cycle. The P-V characteristic curve is scanned, and the global MPP is stored. The second technique is to increase the duty cycle from a minimum to a maximum value with a fixed step. In this case, the P-V curve is scanned, and the global MPP is stored. The last technique is to apply a large initial perturbation step to make a wide search range on the PV power locus. The scanning and storing the PV power are accomplished during perturbation and observation.

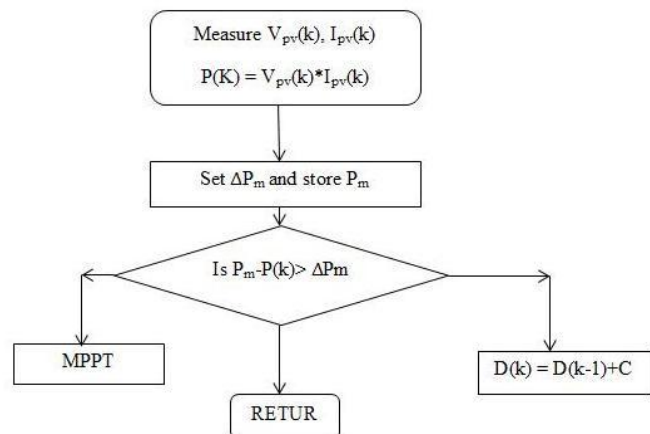


Fig. 4 Proposed method flowchart

Any conventional MPPT method can be used with the proposed method however, fuzzy-logic-based MPPT is preferred specially when using the third technique because the

tracking speed is not constant. Therefore, during initial conditions or varying weather conditions, the initial tracking speed should be fast enough to make a wide range power scan and store the maximum available power. On the other side, when the operating point reaches the global maximum, the tracking speed decreases to minimize any oscillation around the global maximum point. The PV system block diagram along with proposed MPPT controller is shown in Fig.5.

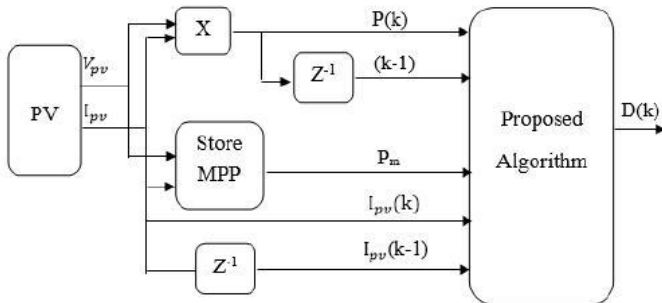


Fig. 5 PV System Block with proposed MPPT Controller

Modification to the fuzzy-logic-based MPPT algorithm using the scanning and storing procedures, is proposed to quickly locate the global MPP. The inputs to the fuzzy logic controller (FLC) are:

$$\begin{aligned}\Delta P &= P(k) - P(k-1) \\ \Delta I &= I(k) - I(k-1) \\ \Delta P_{\max} &= P_{\max}(k) - P(k)\end{aligned}$$

where ΔP , ΔI are the PV array output power change and current change respectively, ΔP_{\max} is the difference between the stored global maximum power (P_{\max}) and the current power, ΔD is the perturbation variation size. To ensure that the PV global maximum power is stored during the scanning procedure, a fast initial tracking speed is used. The change in variable inputs ΔP and ΔI are divided into four fuzzy subsets: positive big (PB), positive small (PS), negative big (NB), and negative small (NS). The variable input ΔP_{\max} is divided into two fuzzy subsets: PB and PS. The output variable ΔD is divided into six fuzzy subsets: PB, positive medium (PM), PS, NB, negative medium (NM), and NS. Therefore, the fuzzy algorithm requires 32 fuzzy control rules. To operate the fuzzy combination, Mamdani's method with max-min combination is used. The fuzzy rules are shown in Table 2.

Table 2 Fuzzy Logic Rules

ΔI ΔP	NB	NS	PS	PB	ΔP_{\max}
NB	PM	PM	NM	NM	PS
NS	PS	PS	NS	NS	
PS	NS	NS	PS	PS	
PB	NM	NM	PM	PM	
NB	PB	PB	PB	PB	PB
NS	PB	PB	PB	PB	
PS	PB	PB	PB	PB	
PB	PB	PB	PB	PB	

V. RESULTS AND DISCUSSION

For the given shaded solar PV panel under study, there are three maximum power points, out of which only one is global maximum power point. Due to the effect of shading, there is an occurrence of more than one maximum point.

In this work, the Simulink model has been developed for 6 cases. The first 3 cases are under constant irradiation and next 3 cases are under varying irradiation conditions. Each case differs in terms of placement of the proposed controller and its actuating signal.

Case I-Individual MPPT Controllers for Shaded & Illuminated PV Arrays,

Case II- MPPT controller based on Illuminated PV Array, Case III - MPPT Controller based on Shaded PV Array.

The conventional MPPT techniques like Perturb & Observe method fails to converge to global maximum power point. In fact it converges to local maximum point and its convergence rate is slower. But the fuzzy logic controller used here converges at global maximum point at a faster manner. The presence of multiple maximum points in shaded solar panel makes the conventional MPPTs to converge at local maxima point instead of global maximum point.

The fuzzy logic controller perturbs and observes the operation at the optimum duty cycle. A wide duty cycle range search is applied to scan for the global maximum point. Once the global maximum power is found, the controller stores the value and compares it with the current operation power. If the difference between the stored global maximum power and the current operating power is greater than a preset value, the duty cycle increases.

During varying weather conditions, the controller resets the stored global maximum value and repeats the same process to find the new global MPP. This technique is slightly faster with less power losses during the initial and varying weather conditions. The duty cycle must return to a minimum value whenever it exceeds the maximum value to track the global MPP.

The proposed fuzzy-logic-based MPPT with a large initial perturbation step scans and stores the power locus during perturbation and observation. The local maxima in the P-V characteristic do not prevent the proposed MPPT from successfully capturing the global MPP in a relatively short time, with small oscillation around the MPP.

Fig.6 gives the designed structure of the MATLAB Simulink model for Case 1. Fig.7 shows the obtained Power from the PV by implementing various MPPT algorithms and comparing them for constant Irradiation condition. Similarly Fig.8 shows the obtained Power from the PV by implementing various MPPT algorithms and comparing them for varying Irradiation condition.

Table 3 gives a quantitative comparison of various performance measures in applying various MPPT algorithms and the proposed Fuzzy Logic Controller based MPPT. In Table 3, P_{ILA} is Power Produced by illuminated array, P_{SH} is the Power Produced by Shaded Array, P_{TOTAL} is the Total Power Produced by both arrays, V_{MIL} is Maximum Power Point Voltage of Illuminated Array, V_{MSH} is Maximum Power Point Voltage of Shaded Array and V_M is Maximum Power Point Voltage

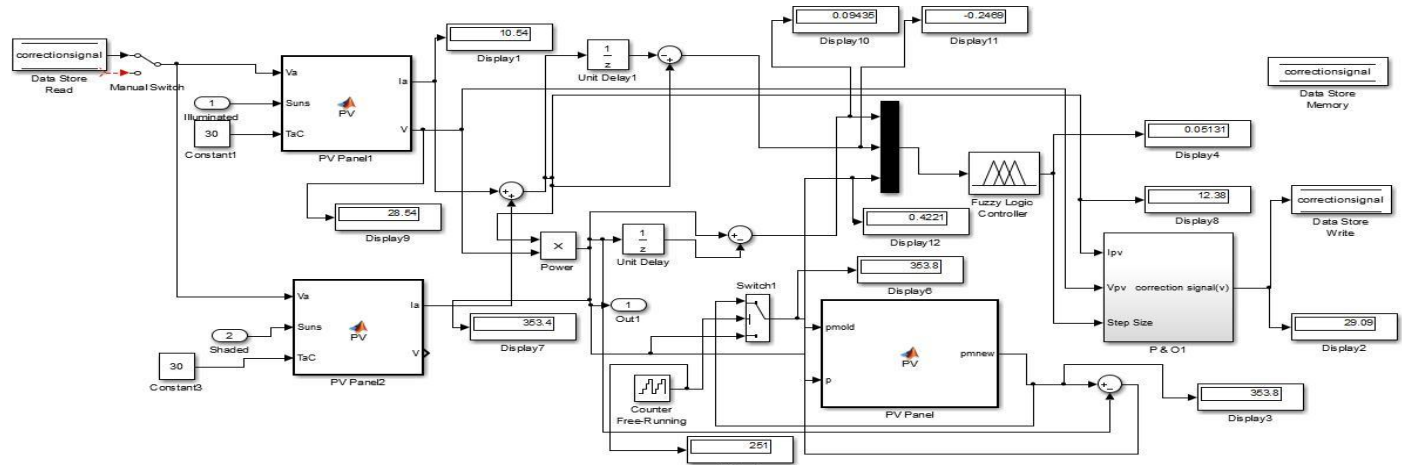


Fig.6 Designed Matlab Shaded PV Array model

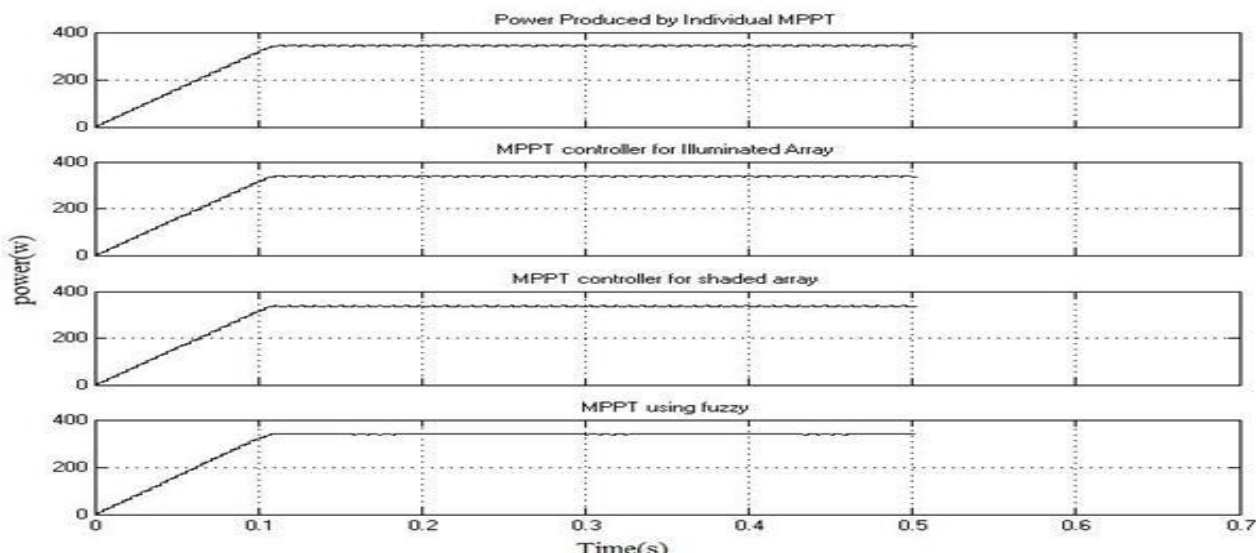


Fig.7 Comparison of Power generated by Various MPPT for constant irradiation

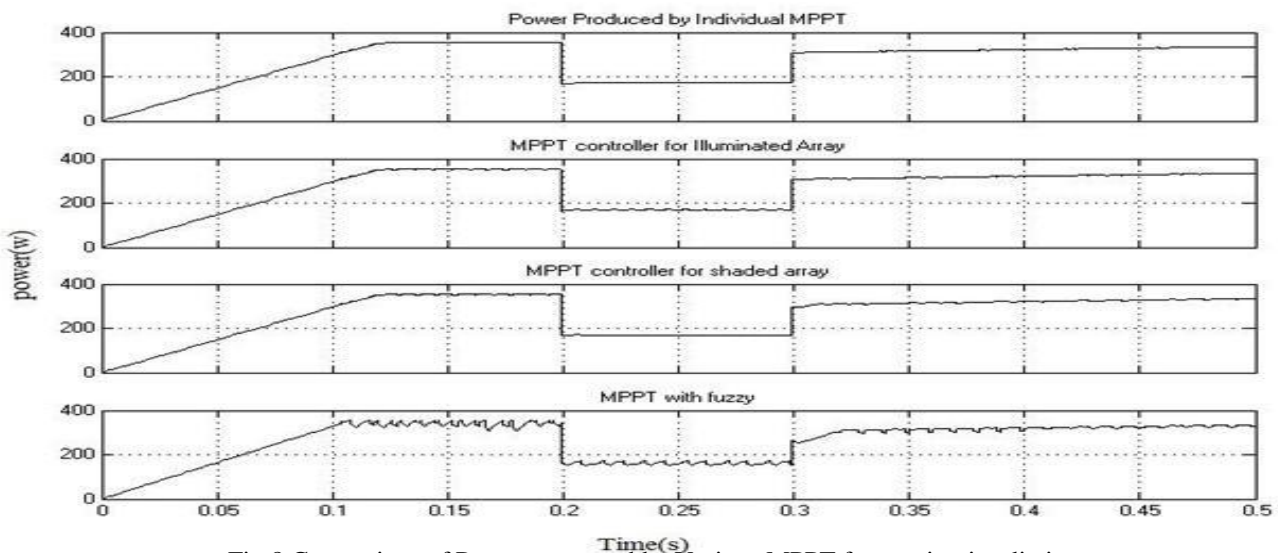


Fig.8 Comparison of Power generated by Various MPPT for varying irradiation

Table 3 Comparison of Performance of Proposed Controller for various Cases

Temperature in °C	Radiation Wb/m ²		MPPT Controllers for Individual Array					MPPT Controller based on Illuminated Array				MPPT Controller based on Shaded Array			
	Illuminated Array	Shaded Array	P _{ILA} (W)	P _{SH} (W)	P _{Total} (W)	V _{MIL} (V)	V _{MSH} (V)	P _{ILA} (W)	P _{SH} (W)	P _{Total} (W)	V _M (V)	P _{ILA} (W)	P _{SH} (W)	P _{Total} (W)	V _m (V)
25	1000	100	291.5	20.15	311.7	28.5	25.5	291.5	14.9	306.4	28	271	20.15	291.1	26
	1000	250	291.5	52.38	343.9	28.5	27.5	291.5	49.57	341.1	28	287.7	52.38	340.1	27
27	1000	100	291.4	20.4	311.5	28.5	25.5	291.4	13.21	304.6	28	273.1	20.14	293.2	26
	1000	250	291.4	52.59	344	28.5	26.5	291.4	48.08	339.5	28	282.1	52.59	334.7	26
30	1000	100	290.3	20.04	310.4	27.5	25.5	290.3	16.6	306.9	28	276.1	20.04	296.2	25
	1000	250	290.3	52.47	342.8	27.5	26.5	290.3	50.89	341.2	28	284.4	52.47	337.1	26

VI. CONCLUSION

The conventional MPPT techniques like Perturb & Observe method fails to converge to global maximum power point. In fact it converges to local maximum point and its convergence rate is mentally dull. But the fuzzy logic controller used here converges at global maximum point at a faster manner. The presence of multiple maximum points in shaded solar panel makes the conventional MPPTs to converge at local maxima point instead of global maximum point.

The fuzzy logic controller perturbs and observes the operation at the optimum duty cycle. A wide duty cycle range search is applied to scan for the global maximum point. Once the global maximum power is founded, the controller stores the value and compares it with the current operation power. If the difference between the stored global maximum power and the current operating power is greater than the preset value and the duty cycle increases. During varying weather conditions, the controller resets the stored global maximum value and repeats the same process to find the new global MPP. The proposed fuzzy-logic based MPPT with a large initial perturbation step scans and stores the power locus during perturbation and observation. The local maxima in the P–V characteristic do not prevent the proposed MPPT from successfully capturing the global MPP in a relatively short time, with small oscillation around the MPP.

VII. REFERENCES

- [1] Alajmi B.N, Ahmed K.H, Finney S.J and Williams B.W, "A Maximum Power Point Tracking Technique for Partially Shaded Photovoltaic Systems in Microgrids", IEEE Transactions on Industrial Electronics, vol.60, no.4, pp.1596-1606, April 2013.
- [2] Ali Reza Reisi, Mohammad Hassan Moradi and Shahriar Jamasb, "Classification and comparison of maximum power point tracking techniques for photovoltaic system", Renewable and Sustainable Energy Reviews, Volume 19, March 2013.
- [3] Bidram A, Davoudi A and Balog R.S, "Control and Circuit Techniques to Mitigate Partial Shading Effects in Photovoltaic Arrays", IEEE Journal of Photovoltaics, vol. 2, no. 4, pp.532-546, Oct 2012.
- [4] Esram T and Chapman P.L, "Comparison of Photovoltaic Array Maximum Power Point Tracking Techniques.", IEEE Transactions on Energy Conversion, vol.22, no.2, pp.439-449, June 2007.
- [5] Femia N, Petrone G, Spagnuolo G and Vitelli M, "Optimization of perturb and observe maximum power point tracking method", IEEE Transactions on Power Electronics, vol.20, no.4, pp.963-973, July 2005.
- [6] Koutroulis E and Blaabjerg F, "A New Technique for Tracking the Global Maximum Power Point of PV Arrays Operating Under Partial-Shading Conditions", IEEE Journal of Photovoltaics , vol.2, no.2, pp.184-190, April 2012.
- [7] Nabil A. Ahmed, Masafumi Miyatake, "A novel maximum power point tracking for photovoltaic applications under partially shaded insolation conditions", Electric Power Systems Research, Volume 78, Issue 5, May 2008.
- [8] Patel, H.; Agarwal, V., "MATLAB-Based Modeling to Study the Effects of Partial Shading on PV Array Characteristics," Energy Conversion, IEEE Transactions on , vol.23, no.1, pp.302-310, March 2008.
- [9] Shiva Maballeghand Jin Jiang, "Modelling, Prediction and Experimental Validations of Power Peaks of PV Arrays under Partial Shading Conditions", IEEE Transactions on Sustainable Energy, Vol. 5, no. 1, pp.293-300, March 2014.
- [10] Subudhi, B.; Pradhan, R., "A Comparative Study on Maximum Power Point Tracking Techniques for Photovoltaic Power Systems," Sustainable Energy, IEEE Transactions on , vol.4, no.1, pp.89-98, Jan. 2013.
- [11] XueFeng, Gooi H.B and Chen S.X, "Hybrid Energy Storage with Multimode Fuzzy Power Allocator for PV Systems", IEEE Transactions on Sustainable Energy, Vol. 5, no. 2, pp.389-397, Oct 2013.
- [12] Yong Yang, Fang Ping Zhao, "Adaptive Perturb and Observe MPPT Technique for Grid- Connected Photovoltaic Inverters", Procedia Engineering, Volume 23, 2011, Pages 468-473, ISSN 1877-7058.
- [13] I. J. Balaguer, L. Qin, Y. Shuitao, U. Supatti, and P. F. Zheng, "Control for grid-connected and intentional islanding operations of distributed power generation," IEEE Trans. Ind. Electron., vol. 58, no. 1, pp. 147–157,

Jan. 2011.

- [14] J. C. Vasquez, R. A. Mastromauro, J. M. Guerrero, and M. Liserre, "Voltage support provided by a droop-controlled multifunctional inverter," *IEEE Trans. Ind. Electron.*, vol. 56, no. 11, pp. 4510–4519, Nov. 2009.
- [15] B. Alajmi, K. Ahmed, S. Finney, and B. Williams, "Fuzzy logic controlled approach of a modified hill climbing method for maximum power point in microgrid stand-alone photovoltaic system," *IEEE Trans. Power Electron.*, vol. 26, no. 4, pp. 1022–1030, Apr. 2011.
- [16] M. Miyatake, M. Veerachary, F. Toriumi, N. Fujii, and H. Ko, "Maximum power point tracking of multiple photovoltaic arrays: A PSO approach," *IEEE Trans. Aerosp. Electron. Syst.*, vol. 47, no. 1, pp. 367–380, Jan. 2011.
- [17] T. L. Nguyen and K.-S. Low, "A global maximum power point tracking scheme employing DIRECT search algorithm for photovoltaic systems," *IEEE Trans. Ind. Electron.*, vol. 57, no. 10, pp. 3456–3467, Oct. 2010.
- [18] H. Patel and V. Agarwal, "Matlab-based modeling to study the effects of partial shading on PV array characteristics," *IEEE Trans. Energy Convers.*, vol. 23, no. 1, pp. 302–310, Mar. 2008.
- [19] A. Safari and S. Mekhilef, "Simulation and hardware implementation of incremental conductance MPPT with direct control method using Cuk converter," *IEEE Trans. Ind. Electron.*, vol. 58, no. 4, pp. 1154–1161, Apr. 2011.
- [20] L. Wuhua and H. Xiangning, "Review of nonisolated high-step-up DC/DC converters in photovoltaic grid-connected applications," *IEEE Trans. Ind. Electron.*, vol. 58, no. 4, pp. 1239–1250, Apr. 2011.
- [21] M. Liserre, T. Sauter, and J. Y. Hung, "Future energy

systems: Integrating renewable energy sources into the Smart power grid through industrial electronics," *IEEE Ind. Electron. Mag.*, vol. 4, no. 1, pp. 18–37, Mar. 2010.

- [22] Y. Mahmoud, W. Xiao, and H. H. Zeineldin, "A simple approach to modeling and simulation of photovoltaic modules," *IEEE Trans. Sustain. Energy*, vol. 3, no. 1, pp. 185–186, Jan. 2012.



P. Praveen Kumar received his B.E degree in Electrical and Electronics Engineering from P.S.G college of technology. Now he is currently pursuing his M.E. degree in Power Systems Engineering from K.S.Rangasamy College of Technology affiliated to Anna University, Chennai. He is a member of ISTE and IEEE



K. Jaiganesh received B.E. degree in Electrical and Electronics Engineering from Periyar University, Salem in 2002 and M.E. degree in Power Electronics and Drives from Anna University, Chennai in 2006. He is currently pursuing his doctoral degree in Anna University, Chennai. He is working as an Assistant Professor in the Department of Electrical and Electronics Engineering at K.S.Rangasamy College of Technology (Autonomous Institution). He is a Life member of ISTE and ISEEE. His research interests are renewable energy sources, inverters, converters.

Comparative Study On Various Bipolar PWM Strategies For Seven Level Symmetrical Inverter

Venkataramanan K¹, Prathapkumar K²

¹ Assistant Professor, Dept of EEE, Arunai Engg College, Tiruvannamalai, Tamilnadu, India

²PG Scholar, Arunai Engg College, Tiruvannamalai, Tamilnadu, India

E-Mail: jkprathap@gmail.com

Abstract— A multilevel inverter is a power electronic device that is used for high voltage and high power applications. This paper represents a new seven level symmetric multilevel inverter with reduced number of switches and gate trigger circuits. Performance analysis has been carried out using triangle as a carrier with sine and trapezoidal as reference. The performance measures like Total Harmonic Distortion (THD), V_{RMS} (fundamental), Distortion factor and lower order harmonics are evaluated. Simulation is performed using MATLAB-SIMULINK.

Key words: *Symmetrical multilevel Inverter, THD, V_{RMS} and DF*

I. INTRODUCTION

Multilevel Inverters are developed to minimizing the switching stress and to obtain the output voltage with multiple steps to achieve the improved fundamental V_{RMS} and lower total harmonic distortion. Teodorescu et al [1] take the survey about multilevel inverter and concluded that the multilevel inverter is working with higher voltage levels. Fang Zheng Peng [2] presented generalized multilevel inverter topology with provides a true multilevel structure that can balance each dc voltage level automatically without need of any other circuits. José Rodríguez et al [3] discussed the survey of multilevel inverter topologies and emerging topologies like soft-switched multilevel inverters and asymmetric hybrid cells. Mariusz Malinowski et al [4] take the Survey on Cascaded Multilevel Inverters. Gierri Waltrich and Ivo Barbi [5] introduced Three-Phase Cascaded Multilevel Inverter and this topology is based Power Cells connected With

Two Inverter Legs in Series. Patricio Cortés et al [6] developed model predictive current control algorithm of three-phase cascaded H-bridge multilevel inverter. Jing Zhao et al [7] proposed a novel pulse width modulation Control Method for One leg of hybrid-

clamped five-level inverter topology. Nho-VanNguyen et al [8] presented an optimized discontinuous pulse width modulation method to minimize switching loss for five-level inverter. Damoun Ahmadi et al [9] developed universal selective harmonic elimination method for high-power multilevel inverters. Bernardo Cougo et al [10] discussed optimal pulse width modulation method for flux reduction in intercell transformers for parallel three-phase multilevel inverters. Soumitra Dasand G. Narayanan [11] investigated alternative switching sequences for a space-vector-modulated three-level inverter. Bernardo Cougo et al [12] analyzed three-phase parallel multilevel inverters using phase disposition modulation scheme. Pradyumn Chaturvedi et al [13] proposed carrier-based neutral point potential regulator for a three-level diode-clamped inverter with reduced switching losses. Ebrahim Babaei et al [14] proposed a new general topology for cascaded H-Bridge multilevel Inverters with reduced number of dc voltage sources and power switches and consists of lower blocking voltage on switches. Ammar Masaoud, et al [15] proposed a new three-phase multilevel inverter topology with reduced number of power electronic components.

II. A NEW SYMMETRICAL MULTILEVEL INVERTER

This new symmetrical multilevel inverter is to reduce the number of switches and to achieve most prominent output with lower output harmonics and low electromagnetic interference. Fig.1 represents a circuit of a new multilevel inverter using four equal numbers of DC input source, and therefore it is called as a Symmetrical multilevel inverter. This new symmetrical multilevel inverter has 5 bidirectional switches S1 to S5. It can synthesize seven output levels are (3Vdc, 2 Vdc, Vdc, 0, - Vdc, -2 Vdc, -3 Vdc) are generated as follows.

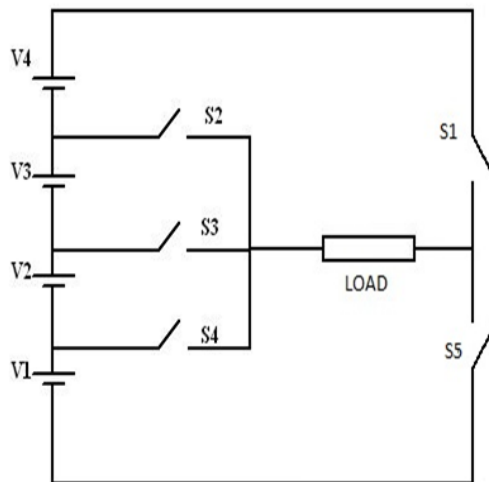


Fig 1: A New Seven Level Multilevel Inverter Topology

The Power Stage Operation of the new multilevel inverter topology is as follows.

1. **Output Voltage $3V_{dc}$:** The switch S_2 , S_5 switches are Kept ON and S_1 , S_3 , S_4 are kept OFF condition.
2. **Output Voltage $2V_{dc}$:** S_3 , S_5 switches are kept ON condition and S_1 , S_2 , S_4 are kept OFF condition.
3. **Output voltage V_{dc} :** S_4 , S_5 switches are kept ON condition and S_1 , S_2 , S_3 are kept OFF condition.
4. **Output voltage $0V_{dc}$:** S_1 , S_5 switches are kept ON condition and S_2 , S_3 , S_4 are kept OFF condition.
5. **Output voltage $-V_{dc}$:** S_1 , S_2 switches are kept ON condition and S_3 , S_4 , S_5 are kept OFF condition.
6. **Output Voltage $-2V_{dc}$:** S_1 , S_3 switches are kept ON condition and S_2 , S_4 , S_5 are kept OFF condition.
7. **Output Voltage $-3V_{dc}$:** S_1 , S_4 switches are kept ON condition and S_2 , S_3 , S_5 are kept OFF condition

III. MODULATION STRATEGIES FOR MULTILEVEL INVERTER

Various modulation strategies are available for multilevel inverters. They are generally classified as pulse width modulation, fundamental switching and space vector strategies. Space vector and fundamental switching strategies are very complicated for higher number of levels so, the disposed PWM carrier based switching strategy is preferred. For an m -level inverter, $(m-1)$ carriers with the same frequency f_c and variable amplitude A_c are used.

The frequency ratio m_f as follows:

$$m_f = f_c / f_m$$

The amplitude modulation m_a as follows:

$$m_a = 2A_m / (m-1)A_c$$

Where

m_f - frequency modulation

m_a - amplitude modulation

f_c - Amplitude of carrier

f_m - Amplitude of reference

In this work various PWM strategies used to generate firing pulses for a chosen inverter. These technique provides small rippled current and less harmonics in output voltage and can be easily expanded to any level. The sine wave and Trapezoidal are used as references.

A) Phase Disposition PWM strategy:

In this method six carriers above and below zero reference line are in same phase with all carriers are same amplitude. The carrier arrangement for seven level inverter using PDPWM with sine and trapezoidal references are shown in Fig 2 and 3 respectively.

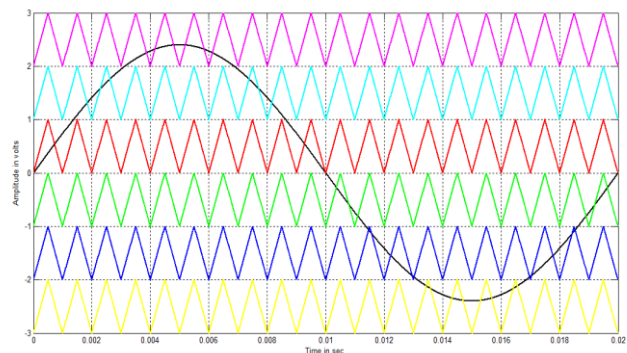


Fig 2: Carrier arrangement for PDPWM strategy with sine reference ($m_a=0.8$ and $m_f=20$)

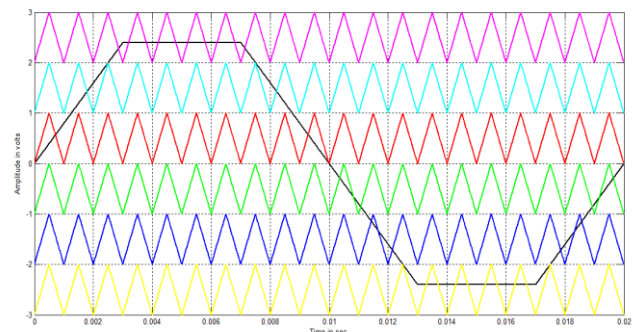


Fig 3: Carrier arrangement for PDPWM strategy with Trapezoidal reference ($m_a=0.8$ and $m_f=20$)

B) Phase Opposition Disposition PWM Strategy:

In this strategy, the carriers are same amplitude and frequency, but all the carriers above the zero reference are in phase and below the zero reference carriers also in phase but they are 180 degree phase shifted with respect to above reference. The carrier arrangement for seven level inverter using PODPWM with sine and trapezoidal references are shown in Fig 4 and 5 respectively.

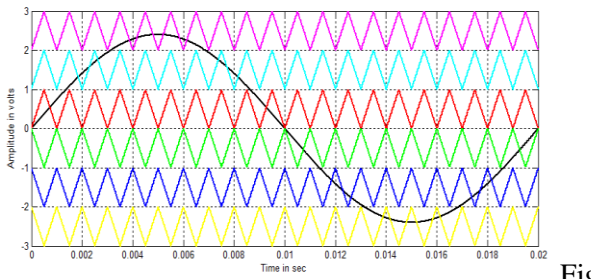


Fig 4: Carrier arrangement for PODPWM strategy with sine reference ($m_a=0.8$ and $m_f=20$)

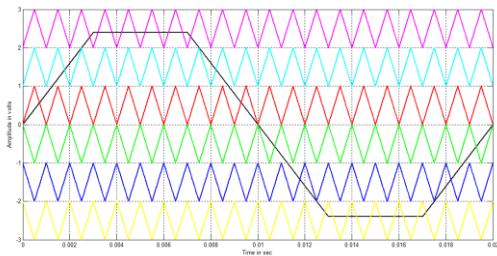


Fig 5: Carrier arrangement for PODPWM strategy with Trapezoidal reference ($m_a=0.8$ and $m_f=20$)

C) Alternate Phase Opposition Disposition PWM Strategy:

In this alternate phase opposition disposition strategy, carriers are same amplitude and frequency than each carrier is phase shifted by 180 degrees with the previous one. The carrier arrangement for seven level inverter using APODPWM with sine and trapezoidal references are shown in Fig 6 and 7 respectively.

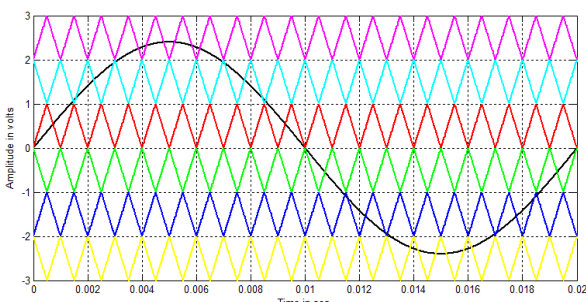


Fig 6: Carrier arrangement for APODPWM strategy with sine reference ($m_a=0.8$ and $m_f=20$)

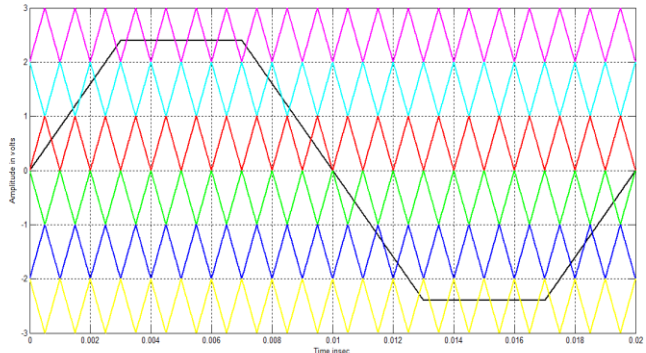


Fig 7: Carrier arrangement for APODPWM strategy with Trapezoidal reference ($m_a=0.8$ and $m_f=20$)

IV. SIMULATION RESULTS

The single phase symmetrical seven level inverter are modeled in MATLAB/SIMULINK using power system block set. Simulations are carried out for different values of modulation indices. Figure 8 shows the simulated output voltage generated by the PDPWM strategy with sine reference and its corresponding FFT plot is shown in Figure 9. Figure 10 shows the simulated output voltage generated by the PDPWM strategy with Trapezoidal reference and its corresponding FFT plot is shown in Figure 11. Figure 12 shows the simulated output voltage generated by the PODPWM strategy with sine reference and its corresponding FFT plot is shown in Figure 13. Figure 14 shows the simulated output voltage generated by the PODPWM strategy with Trapezoidal reference and its corresponding FFT plot is shown in Figure 15. Figure 16 shows the simulated output voltage generated by the APODPWM strategy with sine reference and its corresponding FFT plot is shown in Figure 17. Figure 18 shows the simulated output voltage generated by the APODPWM strategy with Trapezoidal reference and its corresponding FFT plot is shown in Figure 19. Figure 20, 21, 22 and 23 shows that %THD and V_{RMS} Comparison Chart for various PWM strategy. From “Figure 9” it is observed that PDPWM strategy with sine reference shows the 20th harmonic energy is dominant. From “Figure 11” it is observed that PDPWM strategy with Trapezoidal reference shows the 5th and 20th harmonic energies is dominant. From “Figure 13” it is observed that PODPWM strategy with sine reference shows the 9th, 15th and 19th harmonic energies is dominant. From “Figure 15” it is observed that PODPWM strategy with Trapezoidal reference shows the 3rd, 5th and 9th harmonic energies is dominant. From “Figure 17” it is

observed that APODPWM strategy with sine reference shows the 9th, 13rd, and 19th harmonic energies is dominant. From “Figure 19” it is observed that APODPWM strategy with Trapezoidal reference shows the 3rd, 5th, 11th, 13th, 15th and 19th harmonic energies is dominant. The corresponding values of %THD, and V_{RMS} are measured using their values are shown in Table 2 to 5 respectively. % DF for the chosen strategies are calculated using their values are shown in Table 6 and 7. The following parameter values are used for MATLAB simulation: Resistive load = 100ohms, $V_{dc} = 100V$.

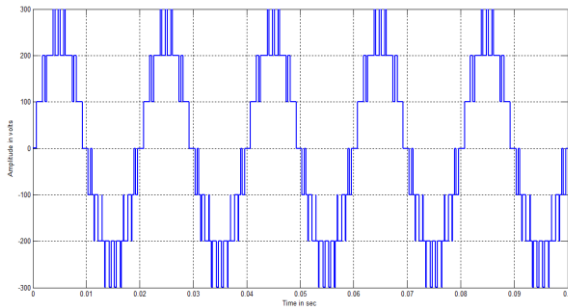


Fig 8: output voltage generated by PDPWM strategy with Sine reference

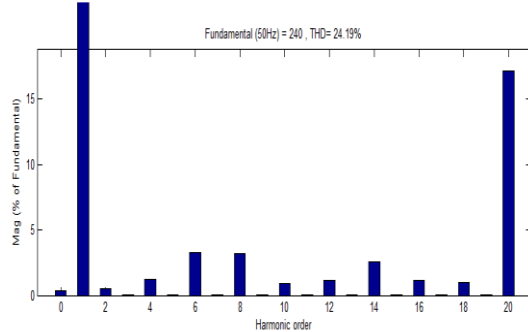


Fig 9: FFT plot for output voltage of PDPWM strategy with Sine reference

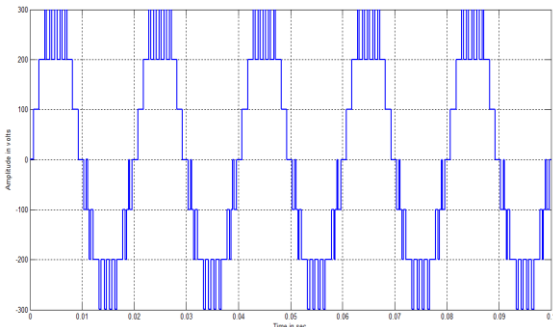


Fig 10: output voltage generated by PDPWM strategy with Trapezoidal reference

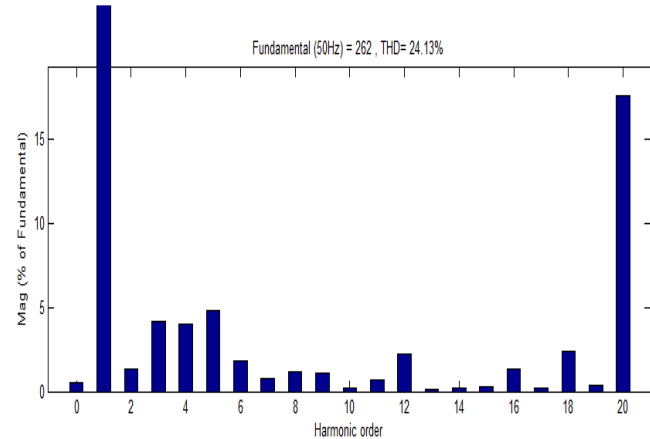


Fig 11: FFT plot for output voltage of PDPWM strategy with Trapezoidal reference

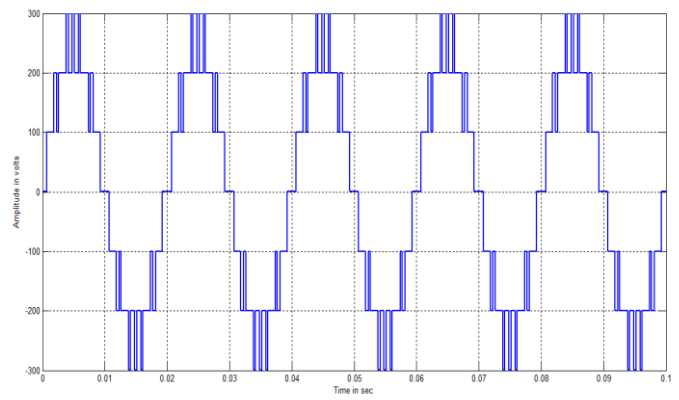


Fig 12: Output voltage generated by PODPWM strategy with Sine reference

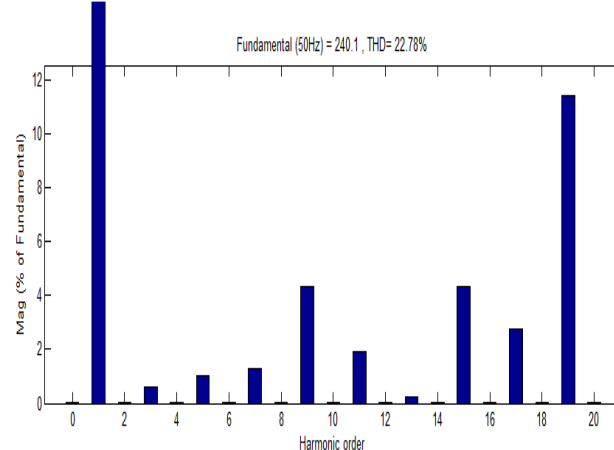


Fig 13: FFT plot for output voltage of PODPWM strategy with Sine reference

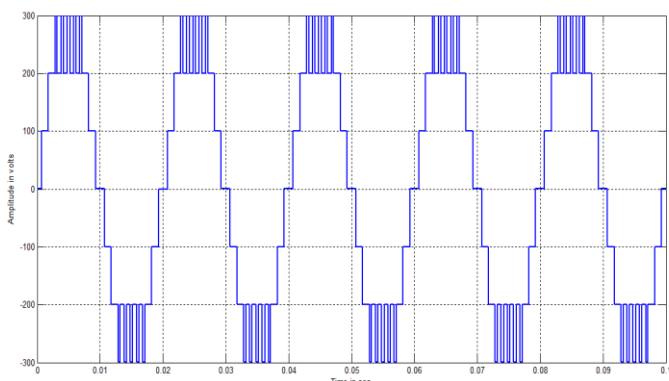


Fig 14: Output voltage generated by PODPWM strategy with Trapezoidal reference

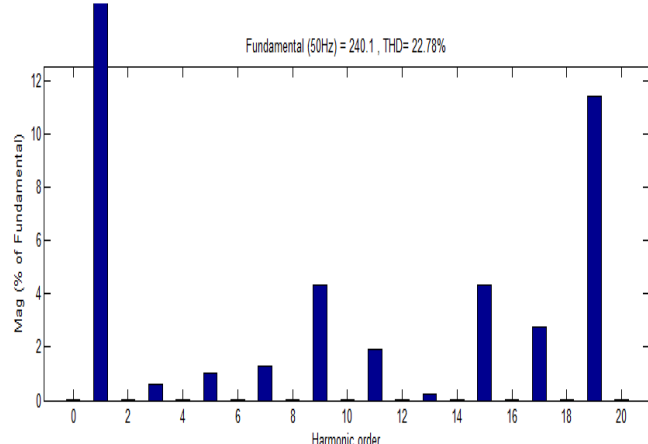


Fig 17: FFT plot for output voltage of APODPWM strategy with Sine reference

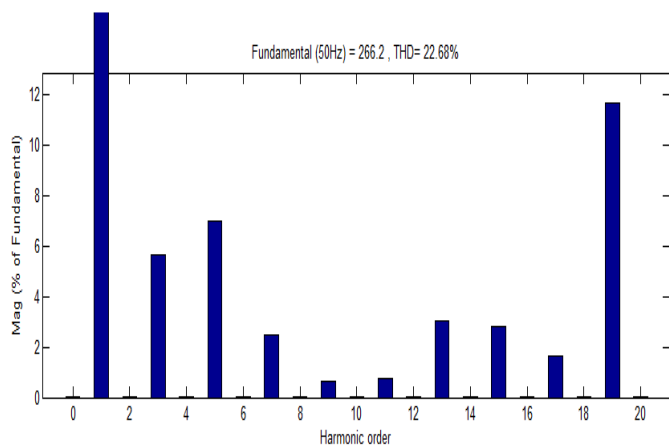


Fig 15: FFT plot for output voltage of PODPWM strategy with Trapezoidal reference

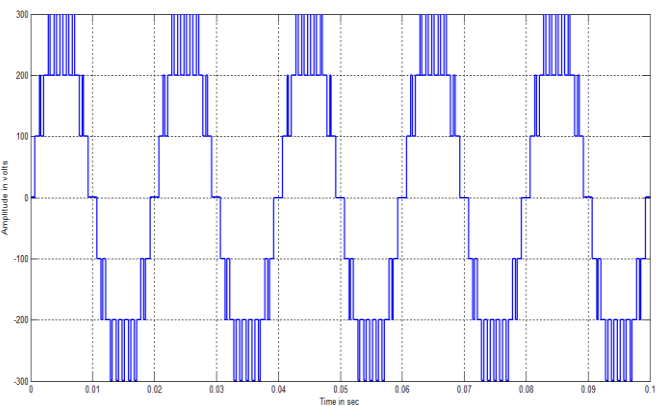


Fig 18: Output voltage generated by APOD PWM strategy with Trapezoidal reference

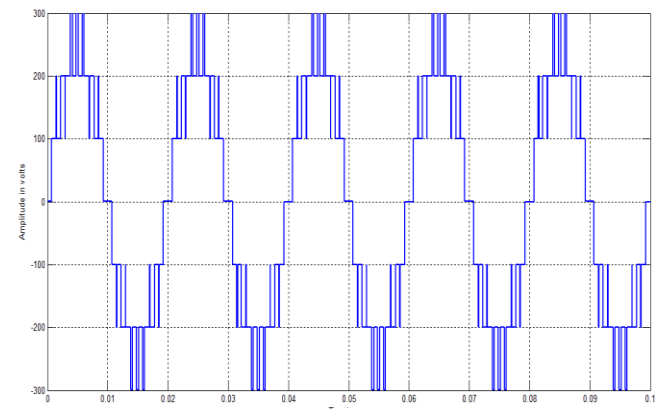


Fig 16: Output voltage generated by APODPWM strategy with Sine reference

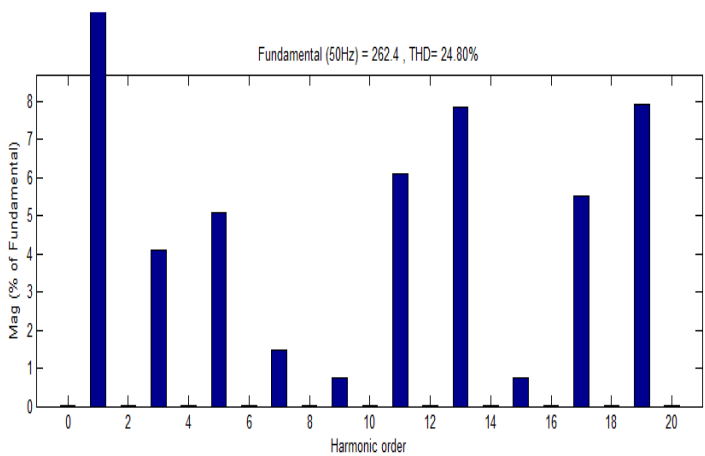


Fig 19: FFT plot for output voltage of APOD PWM strategy with Trapezoidal reference

TABLE 2: % THD comparison for Sine reference

m_a	PDPWM	PODPWM	APODPWM
1	17.88	15.97	18.64
0.95	20.22	18.43	21.04
0.9	22.47	22.14	22.38
0.85	23.64	22.50	22.34
0.8	24.19	22.78	22.30
0.75	23.94	22.52	22.46
0.7	24.82	24.19	22.36

TABLE 3: % THD comparison for Trapezoidal reference

m_a	PDPW M	PODP W M	APODP WM
1	12.54	12.49	12.60
0.9	18.28	16.7	18.10
0.9	21.74	19.67	21.62
0.8	23.69	21.6	23.87
0.8	24.13	22.68	24.80
0.7	24.74	23.98	24.19
0.7	23.6	22.88	21.16

TABLE 4: V_{RMS} comparison for Sine reference

m_a	PDPWM	PODPWM	APODPWM
1	212.1	299.7	299.9
0.95	201.5	286.8	284.9
0.9	190.9	270.9	269.9
0.85	180.3	254.5	255
0.8	169.7	240.1	240
0.75	159.1	227.8	225
0.7	148.5	209.9	209

TABLE 5: V_{RMS} comparison for Trapezoidal reference

m_a	PDPW M	PODPW M	APODP WM
1	232.4	226.8	230.5
0.9	220	216.8	219.1
0.9	208	207	207.9
0.8	196.8	197.8	197.8
0.8	185	188.3	188.3
0.7	173	175.7	175.7
0.7	162	163.7	163.7

TABLE 6: % Distortion Factor for Sine reference

m_a	PDPW M	PODPW M	APODPW M
1	0.6221	0.1725	0.0657
0.9	0.5234	0.1277	0.0653
0.9	0.3858	0.0987	0.0656
0.8	0.2469	0.0878	0.066
0.8	0.1905	0.1091	0.0652
0.7	0.218	0.1613	0.0635
0.7	0.1517	0.177	0.0629

TABLE 7: % Distortion Factor for Trapezoidal reference

m_a	PDPWM	PODPWM	APODPW M
1	0.9365	0.2780	0.4804
0.95	0.8732	0.3148	0.4772
0.9	0.7971	0.4060	0.4794
0.85	0.7183	0.5350	0.4900

0.8	0.5751	0.6886	0.5060
0.75	0.5751	0.6752	0.5270
0.7	0.5404	0.6668	0.5526

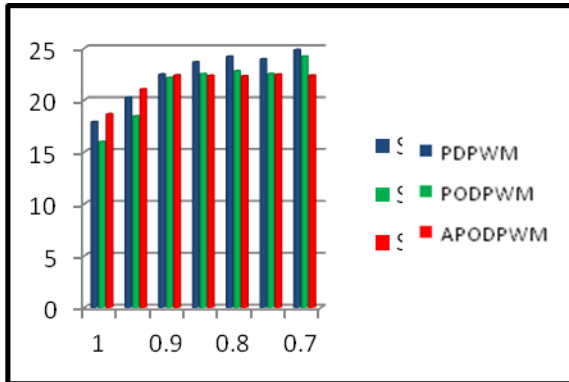


Fig 20: %THD Vs m_a for PWM Strategy with Sine Reference

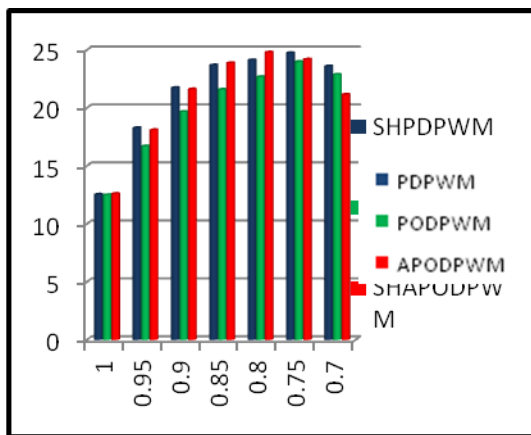


Fig 21: %THD Vs m_a for PWM Strategy with Trapezoidal Reference

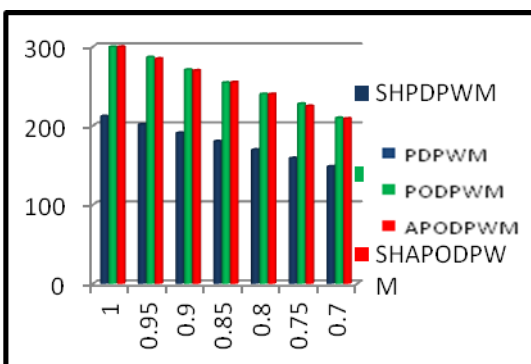


Fig 22: V_{RMS} Vs m_a for PWM Strategy with Sine reference

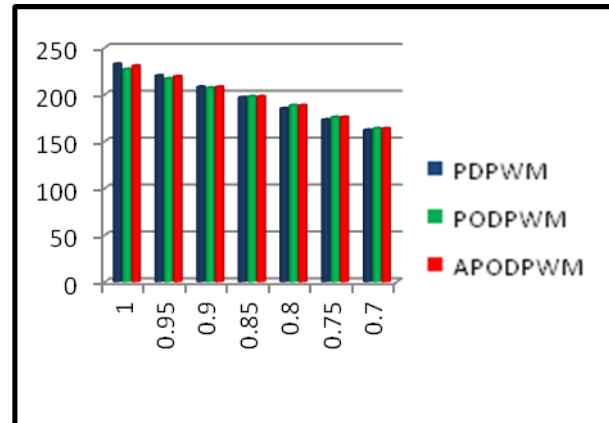


Fig 23: V_{RMS} Vs m_a for PWM Strategy with Trapezoidal reference

V. CONCLUSION

The various PWM techniques for new seven level multilevel inverter have been presented. The various functional parameters like %THD, V_{RMS}, and Distortion Factor have been computed and analyzed. It is found that the PODPWM strategy with trapezoidal reference provides relatively lower %THD, and APODPWM strategy with sine reference provides relatively higher V_{RMS} output voltage and better DC utilization.

VI. REFERENCES

- [1] R. Teodorescu, F. Beabjerg, J. K. Pedersen, E. Cengelci, S. Sulistijo, B. Woo, and P. Enjeti, "Multilevel converters — A survey," in *Proc. European Power Electronics Conf. (EPE'99)*, Lausanne, Switzerland, 1999.
- [2] Fang Zheng Peng, "A Generalized Multilevel Inverter Topology with Self Voltage Balancing," *IEEE Transactions On Industry Applications*, Vol. 37, No. 2, March/April 2001.
- [3] Jose Rodriguez, Jih-Sheng Lai and Fang Zheng Peng, "Multilevel Inverters: A Survey of Topologies, Controls, and Applications," *IEEE Transactions On Industrial Electronics*, Vol. 49, No. 4, August 2002.
- [4] Mariusz Malinowski, K. Gopakumar, JoseRodriguez and Marcelo A. Perez, "A Survey on Cascaded Multilevel Inverters," *IEEE Transactions On Industrial Electronics*, Vol.57, No.7, July 2010.
- [5] Gierr Waltrich and Ivo Barbi, "Three-Phase Cascaded Multilevel Inverter Using Power Cells With Two Inverter Legs in Series," *IEEE Transactions On Industrial Electronics*, Vol.57, No.8, August 2010.
- [6] Patricio Cortés, Alan Wilson, Samir Kouro, JoseRodriguez and Haitham Abu-Rub, "Model Predictive Control of Multilevel Cascaded H-Bridge Inverters," *IEEE Transactions On Industrial Electronics*, Vol.57, No.8, August 2010.

- [7] Jing Zhao,Xiangning He and Rongxiang Zhao, “A Novel PWM Control Method for Hybrid-Clamped Multilevel Inverters,” *IEEE Transactions On Industrial Electronics*, Vol.57, No.7, July 2010.
- [8] Nho-Van Nguyen, Bac-Xuan Nguyen, and Hong-Hee Lee, “An Optimized Discontinuous PWM Method to Minimize Switching Loss for Multilevel Inverters,” *IEEE Transactions On Industrial electronics*, Vol.58, No.9, September 2011.
- [9] Damoun Ahmadi, KeZou, CongLi, Yi Huang, and Jin Wang, “A Universal Selective Harmonic Elimination Method for High-Power Inverters,” *IEEE Transactions On Power Electronics*, Vol. 26, No. 10, October 2011.
- [10] Bernardo Cougo,Thierry Meynard and Guillaume Gateau, “Parallel Three-Phase Inverters: Optimal PWM Method for Flux Reduction in Intercell Transformers,” *IEEE Transactions On Power Electronics*, Vol. 26, No. 8, August 2011.
- [11] Soumitra Das and G. Narayanan, “Novel Switching Sequences for a Space-Vector-Modulated Three-Level Inverter,” *IEEE Transactions On Industrial Electronics*, Vol.59, No.3, March 2012.
- [12] Bernardo Cougo,Guillaume Gateau, Thierry Meynard, Malgorzata Bobrowska-Rafal, and Marc Cousineau, ”PD Modulation Scheme for Three-Phase Parallel Multilevel Inverters,” *IEEE Transactions On Industrial Electronics*, Vol.59, No.2, February 2012.
- [13] Pradyumn Chaturvedi,Shailendra Jain, and Pramod Agarwal, “Carrier-Based Neutral Point Potential Regulator With Reduced Switching Losses for Three-Level Diode-Clamped Inverter,” *IEEE Transactions On Industrial Electronics*, Vol.61, No.2, February 2014.
- [14] Ebrahim Babaei, Somayeh Alilu, and Sara Laali, “A New General Topology for Cascaded Multilevel Inverters With Reduced Number of Components Based on Developed H-Bridge,” *IEEE Transactions On Industrial Electronics*, Vol.61, No.8, August 2014.
- [15] Ammar Masaoud, HewWooi Ping, Saad Mekhilef, and Ayoub Suliman Taallah, “New Three-Phase Multilevel Inverter With Reduced Number of Power Electronic Components,” *IEEE Transactions On Power Electronics*, Vol. 29, No. 11, November 2014.

Congestion Management Based On Active Power Rescheduling Of Generator units using Bacterial Swarming algorithm

*N. Chidambararaj, ME, (Ph.D)
Research Scholar, Sathyabama University,
Chennai- 600119.
INDIA
mailto:chidha@gmail.com*

*Dr. K. Chitra
Professor,
Department of Electronics and Communication Engineering
VIT University- Chennai Campus,
Chennai-119. INDIA
chitra_kris@yahoo.co.in*

Abstract—In this paper, an efficient method has been proposed for transmission line over load alleviation in deregulated power system. Here the generators are selected based on their sensitivity to the congested line and the active power of the participating generators is rescheduled using Bacterial Swarming Algorithm (BSA) for relieving congestion. The algorithm is tested in IEEE 30-bus system and compared with the particle swarm optimization for its effectiveness and robustness in congestion management. It is observed that BSA algorithm minimizes the cost effectively when compared to the particle swarm optimization (PSO).

Keywords—*Congestion management, Deregulated market, Bacterial Swarming Algorithm, PSO, Generator Sensitivity.*

I. INTRODUCTION

In competitive markets, electricity price is regulated based on proposals offered by all market participant, these markets provide the possibility of exchanging energy between various participants. Electricity is a commodity with special features which should be considered when making laws. For example, it is difficult to save, in any case it has losses when transmitting and controlling the electricity flow requires using expensive equipment. Congestion is defined as the overloading of one or more transmission lines and/or transformers in the power system. In the deregulated electricity market, congestion occurs when the transmission system is unable to accommodate all of their desired transactions due to violation of MVA limit of transmission lines. In such market, most of the time, the transmission lines operate near to their stability limits as all market players try to maximize their profits from various transactions by fully utilizing transmission systems. R.D. Christie et al. [1] explained in detail the congestion management and felt that controlling the transmission system so that transfer limits are observed is perhaps the fundamental transmission management problem. In order to relieve congestion, one can either use FACTS devices [2], operate taps of a transformer, redispatch of generation [3] and curtailment of pool loads and/or bilateral contracts. In a deregulated environment, all the GENCOs and DISCOs plan their transactions ahead of time. But by the time of implementation of transactions there may be congestion in some of the transmission lines.

Hence, ISO has to relieve the congestion so that the system remains in secure state. ISO use mainly two types of techniques to relieve congestion and they are as follows:

- i) Cost free means:
 - a. Out-aging of congested lines.
 - b. Operation of transformer taps/phase shifters.
 - c. Operation of FACTS [2] devices particularly series devices.
- ii) Non-cost free means:
 - a. Re-dispatch of generation [3] in a manner different from the natural settling point of the market. Some generators back down while others increase their output. The effect of this is that generators no longer operate at equal incremental costs.
 - b. Curtailment of loads and the exercise of (non-cost-free) load interruption options.

R.S. Fang et al. [4] considered an open transmission dispatch environment in which pool and bilateral/multilateral dispatches coexist and proceeded to develop a congestion management strategy for this scenario. K.L. Lo et al. [5] presented congestion management techniques applied to various kinds of electricity markets. Ashwani Kumar et al. [6] reviewed extensively the literature for reporting several techniques of congestion management and informed that the congestion management is one of the major tasks performed by Independent System Operators (ISOs) to ensure the operation of transmission system within operating limits. In

the emerging electric power markets, the congestion management becomes extremely important and it can impose a barrier to the electricity trading. Ashwani Kumar et al. [7] proposed an efficient zonal congestion management approach using real and reactive power rescheduling based on AC Transmission Congestion Distribution factors considering optimal allocation of reactive power resources. The impact of optimal rescheduling of generators and capacitors has been demonstrated in congestion management. H.Y. Yamina and Shahidehpour [8] described a coordinating mechanism between generating companies and system operator for congestion management using Benders cuts. F. Capitanescu and Van Cutsem [9] proposed two approaches for a unified management of congestions due to voltage instability and thermal overload in a deregulated environment. J. Fu and Lamont [10] discussed a combined framework for service identification and congestion management while a new approach were applied to identify the

services of reactive support and real power loss for managing congestion using the upper bound cost minimization.

J. Kennedy and Eberhart [11] described the Particle Swarm Optimization(PSO) concept in terms of its precursors, briefly reviewing the stages of its development from social simulation to optimize and discussed application of the algorithm to the training of artificial neural network weights. Y. Shi [12] surveyed the research and development of PSO in five categories viz. algorithms, topology, parameters, hybrid PSO algorithms and applications. Y. Del Valle et al. [13] presented a detailed review of the PSO technique, the basic concepts and different structures and variants ,as well as its applications to power system optimization problems. Z.X. Chen et al. [14] introduced PSO for solving Optimal Power Flow (OPF) with which congestion management in pool market is practically implemented on IEEE 30 Bus system and proved that congestion relief using PSO is effective in comparison with Interior Point Method and Genetic Algorithm approach. J. Hazra and Sinha[15] proposed cost efficient generation rescheduling and/or load shedding approach for congestion management in transmission grids using Multi Objective Particle Swarm Optimization (MOPSO)method. K.M. Passino [16] explained in detail the biology and physics underlying the chemotactic (foraging) behaviour of Escherichia colibacteria that formulated Simple Bacterial Foraging (SBF) Optimization Algorithm for optimization process represented by the activity of social bacterial foraging. Janardan Nanda et al. [17] made a maiden attempt to examine and highlight the effective application of Bacterial Foraging algorithm to optimize several important parameters in Multi area Automatic Generation Control (AGC) of a thermal system and compared its performance to establish its superiority over Genetic Algorithm (GA) & classical methods. H. Vahedi et al. [18] proposed a novel Mixed Integer SBF algorithm for solving constrained OPF problem for practical applications.

It is observed that researchers have not attempted so far to dynamically adjust the run length vector of the BSA algorithm for optimal rescheduling of the active powers of the participating generators by relieve congestion in the congested line. Further, no attempt has been made so far to employ BSA algorithm for optimal rescheduling of active power of the select participating generators to relieve congestion in the congested line. To incorporate the innovativeness into congestion management, a new method of BSA algorithm is attempted for the first time to relieve congestion in the congested line by optimal rescheduling of active powers of the select participating generators instead of selecting all the generators to relieve congestion, in this paper it is proposed to select only those generators which are very sensitive for relieving congestion in transmission lines. This is done by the selection of participating generators using generator sensitivities to the power flow on congested lines. Further, it is proposed to solve congestion management problem by optimal rescheduling of active power of participating generators employing the BSA algorithm. Subsequently, BSA algorithm is compared with PSO algorithms to determine the best optimal solution for rescheduling the active power of participating generators to relieve the congestion.

In this paper static congestion management by optimal rescheduling of active power of the generators selected based on their sensitivities to the congested line is attempted by BSA algorithm for the first time and compared with the PSO. The main advantage of this approach of relieving congestion in the congested line is quite efficient as it is a non-cost free means technique. This paper illustrates the effectiveness of the proposed method on the congestion management problem considering IEEE30-bus system

II. CONGESTION MANAGEMENT TECHNIQUE

Congestion is defined as the overloading of one or more transmission lines and/or transformers in the power system. In the deregulated electricity market, congestion occurs when the transmission system is unable to accommodate all of their desired transactions due to violation of MVA limits of transmission lines.

Congestion may lead to rise in cost of electricity, tripping of overloaded lines and consequential tripping of other healthy lines. It may also create voltage stability related problems. It should be relieved to maintain power system stability and security, failing which results into system blackout with heavy loss of revenue. Various factors and phenomena cause congestion on transmission lines that inherent limitations of transmission network can be pointed as one of them which are divided into two major categories:

1. Physical limitations

2. System limitations

Thermal limitation of a transmission line or a transformer is among physical limitations of transmission network. Voltage limitation in a node, transient stability, dynamic stability, reliability and similar cases are also examples of system limitations of transmission network. Given the above limitations, many factors can be effective in the occurrence of congestion on transmission lines, such as energy consumption increase in point in the network, concurrent use of electrical appliances during peak hours and non-coordinated exchanges. Also the departure of a number of transmission lines or power generation units in a point in the network due to error or repairs makes more loading of network healthy lines and congestion on these lines. Hence, ISO has to relieve the congestion so that the system remains in a secure state. ISO mainly uses two types of techniques to relieve congestion. These are listed below.

i) Cost free means

- a. Out-aging of congested lines
- b. Operation of transformer taps/phase shifters
- c. Operation of FACTS [2] devices, particularly series devices

ii) Non-Cost free means

- a. Re-dispatching power generation [3] in a manner different from the natural settling point of the market. Some generators back down, while others increase their output. Consequently, generators no longer operate at equal incremental costs.
- b. Curtailment of loads and the exercise of (non-cost free) load interruption options.

III. GENERATOR SENSITIVITY

A change in real power flow in a transmission line k connected between bus i and bus j due to change in power generation by generator ‘ g ’ can be termed as generator sensitivity to congested line (GS).

$$GS_g = \frac{\Delta P_{ij}}{\Delta P_g} \quad (1)$$

Where,

ΔP_{ij} = change in the real power flow of the congested line.

ΔP_g = change in the real power generated by the generator.

IV. OBJECTIVE FUNCTION

The objective function of rescheduling real power generation using cost

Minimization is given by

$$C = \text{minimize } \sum_{g=1}^{N_g} C_g (\Delta P_g) \Delta P_g \quad (2)$$

Where,

$C_g(\Delta P_g)$ = incremental and decremental bids submitted by generators

ΔP_g = Unit change in real power adjustment at generator

N_g = Number of generators

Subject to

$$\sum_{g=1}^{N_g} ((GS_g) \Delta P_g) + PF_k^0 \leq PF_k^{\max} \quad (3)$$

Where $k=1, 2, 3 \dots N_l$ (4)

$$\Delta P_g^{\min} \leq \Delta P_g \leq \Delta P_g^{\max} \quad (5)$$

$$\Delta P_g^{\min} = P_g - P_g^{\min} \quad (6)$$

$$\Delta P_g^{\max} = P_g^{\max} - P_g \quad (7)$$

$$\sum_{g=1}^{N_g} \Delta P_g = 0 \quad (8)$$

Where $g=1, 2 \dots N_g$ (9)

PF_k^0 = power flow caused by all contracts requesting the transmission services.

PF_k^{\max} = line flow limit of the line connecting bus-i and bus j

N_l = number of transmission lines in the system.

V. BACTERIAL SWARMING ALGORITHM

Bacterial Foraging Algorithm (BFA) was first proposed by Kevin Passion in 2002, which was inspired by *Escherichia coli* chemotactic behavior. In order to speed up the convergence of BFA and utilize the cell-to-cell communication, BSA was developed incorporating the group information of bacteria [24]. The goal of BSA for multi-objective optimization is not only to guide the search towards the Pareto-optimal set but also to maintain population diversity in the set of non-dominated solutions by the application of mutation which will eliminate bacterium in the better way compared with elimination or dispersal used in Bacterial Foraging Algorithm. Hence BSA will converge faster. BSA is categorized into three processes: chemotaxis, simplified quorum sensing, and mutation.

The process of BSA for obtaining optimal generator rescheduling is given by the following steps.

Step 1: Prepare the input power system parameters (e.g. system topology, line and load specifications, generation limits, line flow limits, and cost coefficient parameters). An initial population of bacteria is set with random positions and an empty external Pareto-optimal set is created. A velocity vector is randomly set for the bacterium movement.

Step 2: At each position, run power flow for each particle and determine voltage magnitudes and phase angles at all the buses. Calculate the power flow in each transmission line of the system. Calculate the fitness values of each bacterium. After the evaluation of the fitness values, the non-dominated individuals are found and their fitness values are copied into the external Pareto set. Once the external Pareto set is updated, new non-dominated individuals are included and all dominated solutions are removed from the set.

Step 3: Calculate the random tumbling angle. With this position, new fitness function is calculated after performing load flow. The external Pareto set is updated each time when the bacterium moves to a new position. The fitness function and tumbling angle are calculated considering an n -dimensional search space. The i^{th} bacterium at the k^{th} tumble-run process, has a current position $X_i^k \in R^n$, a moving angle $\Phi_i^k = (\Phi_{i1}^k, \Phi_{i2}^k, \dots, \Phi_{i(n-1)}^k) \in R^{n-1}$ and a moving direction $D_i^k(\phi_i^k) = (d_{i1}^k, d_{i2}^k, \dots, d_{in}^k) \in R^n$.

The new direction of the run process is calculated from a new angle $\Phi_p^k + \Delta\Phi$.

$$\text{Step size, } \Delta\Phi = r_2 \theta_{\max}/2 \quad (10)$$

As there are specific bounds for bacterial position, new position is always checked for the limits. If the new position is outside bounds, it has been made to jump in to the limits with a random jump.

$$X_{p+1}^k(I) = X_p^k + r_{l\max} D_p^k (\Phi_p^k + \Delta\Phi) \quad (11)$$

The run step will continue till N_c , the total number of run steps.

$$X_{p+1}^k(h+1) = X_{p+1}^k(h) + r_{l\max} D_p^k (\Phi_p^k + \Delta\Phi) \quad (12)$$

where h represents the counter of the run steps ($h = 1$ to N_c).

Step 4: The velocity vector is updated with the random function. Bacterium position is changed with respect to the global best solution. Most individuals are attracted by the pheromone randomly. This is incorporated using gain parameter for the bacterium attraction. The new position is calculated as follows,

$$X_{p+1}^k = \delta \cdot (X_{best}^{k+1} - X_{p+1}^k) \quad (13)$$

where δ represents the gain parameter for the bacterial attraction, X_{best}^{k+1} is the position of global best solution in the $(k+1)^{\text{th}}$ optimization process and X_{p+1}^k indicates the position of the p^{th} bacterium after the tumble-run process. With the updated pareto optimal set at global best location X_{best}^{k+1} , the location of the Facts devices is determined as this set is fitted with the cost and severity indices at various bacterium position.

Step 5: As equation (13) makes dominant solutions to converge, it might result in premature convergence. To avoid this, mutation is applied on the remaining individuals to have population diversity. The mutation can be described as,

$$\Delta\Phi = r_2 \cdot \pi/2 \quad (14)$$

$$X_{p+1}^{k+1} = X_{p+1}^k + r_3 l_{range} D_{p+1}^{k+1} (\Phi_{p+1}^{k+1} + \Delta\Phi) \quad (15)$$

where $r_1, r_2, r_3 \in R_n$ is a normally distributed random number drawn from $N(0,1)$. This will cause the dominated sets of bacterium to move to the farthest distance and jump out of the bound.

Step 6: The best non-dominated solution after N_c steps is considered and the load flow is performed. A sensitivity based approach is considered to optimally reschedule the generation units.

This algorithm is applied to equation (2) considering IEEE 30 bus system (Fig.3) and the results are discussed in section 6.

V. RESULT AND DISCUSSION

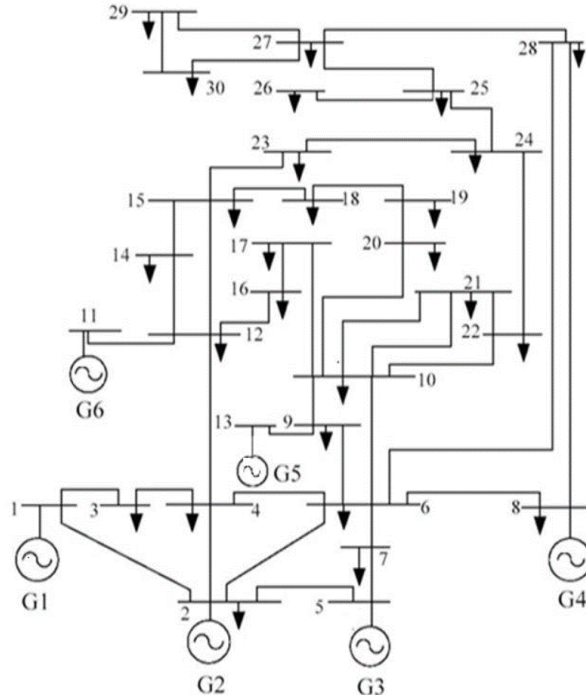


Fig.3. Single Line Diagram of IEEE 30 Bus System

The IEEE 30-bus system (Fig.3) consists of six generator buses and 24 load buses. Accordingly, the Generator Sensitivities are computed for the congested Line-26 for the system. Generators which are to participate in congestion management are to be selected depending on their sensitivities to the congested line. In this test system, it is observed that all the generators show strong influence on the congested line. This is perhaps the system is very small and generally very tightly connected electrically. All the generators are participating in congestion management and the evolutionary algorithms are employed to optimally reschedule the active power of the generators for relieving congestion in Line-26. Mostly, congestion is due to exceeding power flow limit of one or more lines and outage of some important elements.

For evaluating the performance of the proposed technique, the congestion occurred line is considered in between bus-10 and bus-17. This congestion is created by increasing the demand of load bus. In congested line, real power flow after congestion is 5.928 MW. After applying the congestion management technique, the congestion of the line is reduced as 5.48 MW gives in Table I. For the reason of optimal rescheduling of the real power generation of the generators, the congestion has to be

relieved. Then, the sensitivity of the generator is calculated after rescheduling real power by using the sensitivity equation. According to the sensitivity of generator, the generators which are to participate in congestion management can be analyzed. In this test system, it is observed that all the generators show strong influence on the congested line. This is perhaps the system is very small and generally very tightly connected electrically. The generator sensitivity chart of the proposed system after solving the transmission line congestion between bus 10 and 17 is illustrated in Fig.4.

TABLE I:REAL POWER FLOW OF CONGESTED LINE BEFORE AND AFTER CONGESTION MANAGEMENT.

Real power flow		Real power (MW) before congestion management	Real power (MW) after congestion management	
From bus	To bus		BSA	PSO [25]
10	17	5.928	5.782	5.9

TABLE II: Comparisons of cost of congestion management for IEEE 30-bus system

CM cost (Rs./MWh)	BSA	PSO [25]
Best	148.05	160.23
Worst	148.35	161.61
Mean	148.04	161.49

TABLE III :Active power generation before and after congestion management for IEEE 30-bus system

Generator number	Active power (MW) before congestion management (BCM)		Active power (MW) after congestion management (BCM)	
	BSA	PSO	BSA	PSO [25]
G ₁	184	185.046387	113.23	184.240386
G ₂	60.2	46.795654	22.734	46.632538
G ₅	38	19.102783	20.836	20.564745
G ₈	29.5	10	22.681	10
G ₁₁	26	10	10.356	10
G ₁₃	34	12	19.516	12

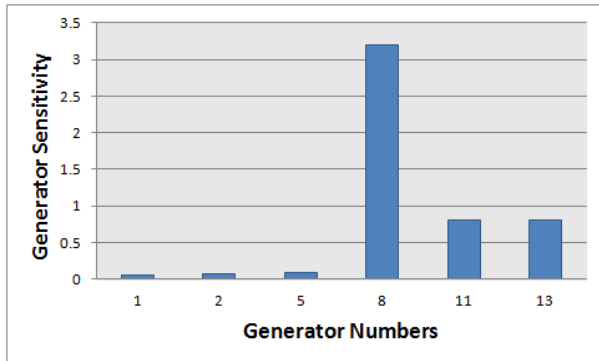


Figure 4: Generator sensitivity after solving congestion of line between bus 10 and 17.

The real power follow of the line (bus 10 and bus 17) of the proposed method is analyzed before managing congestion and after managing congestion. The analyzed values are compared with BSA algorithm and PSO algorithm [32] which gives in Table I. Then, the real power flow of the generator before and after managing congestion is analyzed. The real power generation by the 6 contributing generators before the congestion management and after the congestion management utilized is give in Table III. From the comparison of the cost of congestion we can conclude that the BSA Algorithm is lowest than the particle swarm optimization (Table II).

VI. CONCLUSION

In this work, Congestion management problem has been solved using optimal rescheduling of active powers of generators selected based on the generator sensitivity to the congested line, utilizing BSA Algorithm. Here rescheduling is done taking into consideration the minimization of cost and satisfying line flow limits. The results obtained by the BSA Algorithm are compared with PSO algorithms. This method is tested on IEEE 30-bus. The results show that BSA Algorithm is giving the best optimal solution in comparison with PSO algorithms with respect to cost and runtime for relieving congestion in the congested line.

REFERENCES

- [1]R.D.Christie,B.F.Wollenberg,I.Wangensteen, "Transmission management in the deregulated environment", *in Proc.IEEE* pp.170–194,"2000.
- [2]D.M.Vinod Kumar, Ch.Venkaiah, "Swarm intelligence based security constrained congestion management using SSSC", *in Proc. APPEEC*, 2009.
- [3]S. Dutta, S.P. Singh, "Optimal rescheduling of generators for congestion management based on particle swarm optimization", *IEEE Transactions on Power Systems*, vol.23, no.4, pp.1560–1569, 2008
- [4]R.S.Fang,A.K.David, "Transmission congestion management in an electricity market", *IEEE Transactions on Power System*, vol.14. no.3, pp. 877–883, 1999.
- [5]K.L. Lo, Y.S. Yuen, L.A. Snider, Congestion management in deregulated electricity markets, *in proc. IEEE International Conference on Electric Utility Deregulation and Restructuring and Power Technologies*, pp. 47–52.
- [6]Ashwani Kumar, S.C. Srivastava, S.N. Singh, "Congestion management in competitive power market", a bibliographical survey, *Electric Power Systems Research*, pp.153–164,2005.
- [7]Ashwani Kumar, S.C. Srivastava, S.N. Singh, " A zonal congestion management approach using real and reactive power rescheduling", *IEEE Transactions on Power Systems*, vol.19,no.1, pp.554–562,2004.
- [8]H.Y.Yamina, S.M. Shahidehpour, "Congestion management coordination in the deregulated power market, *Electric Power Systems Research*", pp.119–127,2003.
- [9]F.Capitanescu, T.VanCutsem, "A unified management of congestions due to voltage instability and thermal overload", *Electric Power Systems Research*, pp.1274–1283, 2007.
- [10]J. Fu, J.W. Lamont, A combined framework for service identification and congestion management, *IEEE Transactions on Power Systems*, vol.6,no.1, pp.56–61,2001.
- [11]J. Kennedy, R. Eberhart, "Particle swarm optimization", *in proc.IEEE*, pp. 1942–1948,1995.
- [12]Y. Shi, "Particle swarm optimization", *in proc. IEEE Neural Networks Society*, pp.8–13, 2004.
- [13]Y.del Valle, G.K. Venayagamoorthy, S. Mohagheghi, J.-C. Hernandez, R.G. Harley, "Particle swarm optimization: basic concepts, variants and applications in power systems", *IEEE Transactions on Evolutionary Computation*, vol.12, no.2,pp.171–195,2008.
- [14]Z.X.Chen, L.Z.Zhang, J.Shu, "Congestion management based on particle swarm optimization", *in Proc. IEEE The 7th International Power Engineering Conference*, pp. 1019–1023, 2005.,
- [15]J.Hazra,A.K.Sinha,"Congestion management using multiobjective particle swarm optimization",*IEEETransactions on Power Systems*, vol.22, no.4, pp.1726–1734,2007.
- [16]K.M.Passino,"Biomimicry of bacterial foraging for distributed optimization and control", *IEEE Control Systems Magazine*, pp. 52–67,2002.
- [17]Janardan Nanda, S. Mishra, Lalit Chandra Saikia, "Maiden application of bacterial foraging-based optimization technique in multiarea automatic generation control", *IEEE Transactions on Power Systems*, vol.24, no.2, 602–609,2009.
- [18]H.Vahedi, S.H.Hosseini, R. Noroozian, "Bacterial foraging algorithm for securityconstrained optimal power flow", *in Proc. of IEEE*, pp. 1–6,2010.
- [19] Yang Xin-She, and Deb Suash, "Cuckoo Search via Levy flights" *World Congress on Nature & Biologically Inspired Computing*, pp.210-214, 2009
- [20] Xin-She Yang, "Bat Algorithm and Cuckoo Search: A Tutorial", *Artificial Intelligence, Evolutionary Computing and Metaheuristics*, Vol.427, pp.421-434, 2013
- [21] Xin-She Yang, and Suash Deb, "Engineering optimisation by cuckoo search", *International Journal of Mathematical Modelling and Numerical Optimisation*, Vol.1, No.4, pp.330-343, 2010
- [22] Visalakshi, S., and Baskar, S., "Covariance matrix adapted evolution strategybased decentralised congestion management for multilateral transactions", *IET Generation, Transmission & Distribution*, Vol.4, No.3, pp.400-417, 2010.
- [23] Hadi Besharat, and Seyed Abbas Taher, "Congestion management by determining optimal location of TCSC in

deregulated power systems", *International Journal of Electrical Power & Energy Systems*, Vol.30, No.10, pp.563–568, December 2008

[24] S.Sakthivel, D.Mary, and S.Ramya, "Reactive Power Optimization and Voltage Stability Limit Improvement with TCSC Device through DE algorithm under Most Credible Contingency Condition", *International Journal of Scientific & Engineering Research*, Vol.3, No.5, pp.1-8, 2012

[25] S. Dutta, and S.P. Singh, "Optimal rescheduling of generators for congestion management based on particle swarm optimization", *IEEE Transactions on Power Systems*, Vol.23, No.4, pp.1560–1569, 2008



N. Chidambararaj was born in the year 1981. He completed his Diploma in Electrical and Electronics Engineering in the year 2000. He received his B.E degree in Electrical and Electronics Engineering in the year 2003 and proceeded with pursuing Masters in Power Systems Engineering and graduated in the year 2005. He is working as an Associate professor at St. Joseph's College of Engineering in the Department of Electrical and Electronics Engineering since 2005. He is 8 years of experience in the respective field. He is currently pursuing Ph.D in Sathyabama University. His subject of interest includes Power systems, Engineering Electromagnetics, Digital signal processing and Machine design and his core research is on deregulated power system.



Currently **Dr. K. Chitra** is working as a Professor, in the department of Electronics and communication Engineering at VIT Chennai Campus, Chennai. Dr. K. Chitra received her B.E. Degree in Electronics and communication Engineering from BharathiarUniversity, Coimbatore in 1990, M.E. Degree in Applied Electronics from Bharathiar University in 1992 and Ph.D. degree in Optical Communication from Anna University Chennai in 2008.

Dr. K.Chitra has spent her 22 years of experience in teaching and 2 years of industrial experience. Dr. K. Chitra has added 15 international publications to her credit. She has few funded projects from Government of India. Dr. K. Chitra's areas of interests include optical communication, optical networks, wireless sensor and computer networks, Biomedical Engineering and microwave Engineering.

DESIGN AND IMPLEMENTATION OF ANFIS CONTROLLER FOR SOLID OXIDE FUEL CELL SYSTEM

Selvaraj.V¹, Sivakumar.R²and Rajasekaran.G¹

1.PG Student, Department of EIE, St. Joseph's College of Engineering, Anna University,Chennai-600119, India.

2.Professor, Department of EIE, St. Joseph's College of Engineering, Anna University,Chennai-600119, India.

Corresponding Author Email: v.selvam1990@gmail.com or selvaraj.venni@gmail.com

ABSTRACT

In this paper, an attempt is made to control the output power of the Solid oxide fuel cell. A hybrid control of fuzzy and neural network system ANFIS (Adaptive Neuro Fuzzy Inference System) is proposed to the fuel cell. The ANFIS controller performance is compared with conventional PID controller and Fuzzy logic controller. The Simulation results shows that the performance indices like ISE, IAE, ITAE, peak overshoot and settling time of ANFIS controller have better response than other two controllers.

Keywords: ANFIS, SOFC, Fuzzy, PID controller, Tuning.

1. INTRODUCTION

Fuel cells generate the power directly through the electrochemical reaction between hydrogen and oxygen. The conversion of chemical energy into electrical energy is highly efficient and leaves only water and heat as the by-products, which is the main motivation for the increasing interest in this technology [6]. Resulting advantages of this technology are high efficiency, low emissions, and noiselessness (due to nonexistence of moving parts), and have the free adjustable ratio (50 kW to 3 MW) of electric and heat generation.

The basic components of a typical fuel cell include two electrodes, an anode and cathode where the chemical reactions take place. An electrolyte (membrane) is sandwiched between the two electrodes which allow the ions to cross over and it blocks the electrons. The membrane also allows the ions that are formed to cross-over to the other electrode, which happens because of the tendency of the charged particles migrating to the regions of lower electrochemical energy. The electrical energy is generated when the electrons flowing from the anode to the cathode through the external circuit. The end products of a fuel cell are heat and electricity, which make them suitable for Combined Heat and Power applications. The most widely used fuel in the

fuel cell is hydrogen and the oxidant is usually oxygen and the product of chemical reaction is water which is produced either at the cathode or at the anode depending on the type of fuel cell used. For SOFC, the electrochemical reaction employed is illustrated in Figure 1.

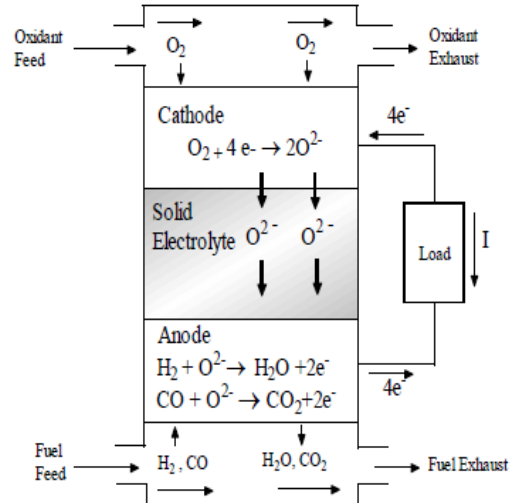


Figure 1: Basic Electrochemistry of an SOFC

2. PROBLEM FORMULATION

The various Physical and chemical equations are employed in the solid oxide fuel cell system. Modeling of SOFC is done by using the Nernst equation [3][8]. Using the system identification tool box, the Solid oxide fuel cell is modeled as the first order transfer function with dead time and then second order transfer function with dead time. Then these two transfer functions are compared with actual response and then the second order transfer function with dead time is retuned using trial and error method. The model of the SOFC at 100KW is given by:

$$G(S) = \frac{0.00005433}{s^2 + 0.01115s + 0.00005433} e^{-37s} \quad (1)$$

3. PID CONTROLLER

A Proportional–Integral–Derivative (PID) controller is a generic control loop feedback mechanism widely used in industrial control systems. A PID controller is the most widely used feedback controller. The controller compares the value of the output signal with a reference value and gives the control signal to the final control element. The implementation of PID control requires finding suitable values for the gain parameters K_p, K_i, and K_d. The equation of ideal PID controller is

$$u = K_p \left(e + \frac{1}{Ti} \int_0^t edt + Td \frac{de}{dt} \right) \quad (2)$$

According to Zeigler-Nichols frequency response tuning criteria,

K_p=0.6 Kcu,

T_i=Pu/2 and

T_d=Pu/8.

For the PID controller used, the values of tuning parameters obtained are

K_p=3.5775,

T_i=177.9655 and

T_d=44.4914.

The response of the Zeigler Nichols tuned three term controller of SOFC is shown below in figure 2.

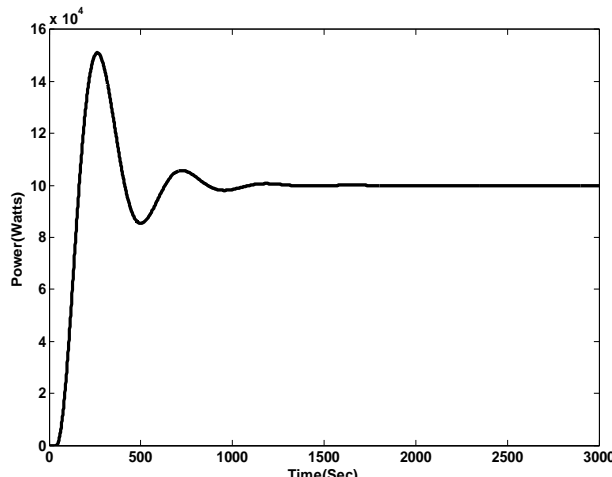


Figure 2: Response of PID controller

4. FUZZY LOGIC CONTROLLER

Fuzzy Logic Control has the advantage that it does not require an accurate mathematical model of the process. It uses the set of rules in a decision-making table and calculates an output based on the table.

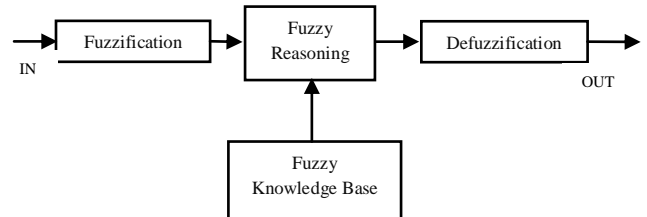


Figure 3: Architecture of fuzzy logic control

Figure 3 and 4 show a schematic diagram of a fuzzy control system. Input variables of the process go through the fuzzification interface and are converted to linguistic variables. Then, database and rule base having the decision-making logic are used to infer the fuzzy output. Finally, centroid defuzzification method used to converts the linguistic variables into the crisp variables to be sent out [13].

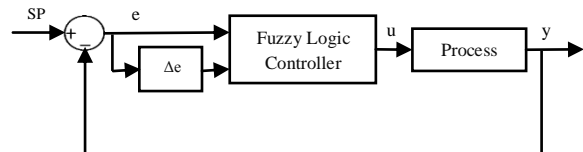


Figure 4: Block diagram of a FLC.

For finding the range of the universe of discourse of the input and output membership functions, the PID controller has been tuned using the conventional Zeigler Nichols method. From there, the range of the input as well as output membership functions has been found. In this paper we have considered different linguistic variables. The linguistic variables are assigned as: negative big (NB), negative medium (NM), negative small (NS), zero (ZO), positive small (PS), positive medium (PM) and positive big (PB). Designing efficient fuzzy rule base is the key to obtain satisfactory control performance for a particular operation. Control strategy and Classical analysis are incorporated in the rule base. The IF-THEN rule base of the fuzzy logic controller is shown in Table 1.

Table 1: IF-THEN rule base for Fuzzy Logic Controller

u(t)		e(t)						
		NB	NM	NS	ZO	PS	PM	PB
Δe(t)	NB	NB	NB	NB	NB	NM	NS	ZO
	NM	NB	NB	NB	NM	NS	ZO	PS
	NS	NB	NB	NM	NS	NS	PS	PS
	ZO	NB	NM	NS	ZO	ZO	PM	PM
	PS	NM	NS	ZO	PS	PS	PB	PB
	PM	NS	ZO	PS	PM	PM	PB	PB
	PB	ZO	PS	PM	PB	PB	PB	PB

The response of the fuzzy logic controller of SOFC is shown below in figure 5.

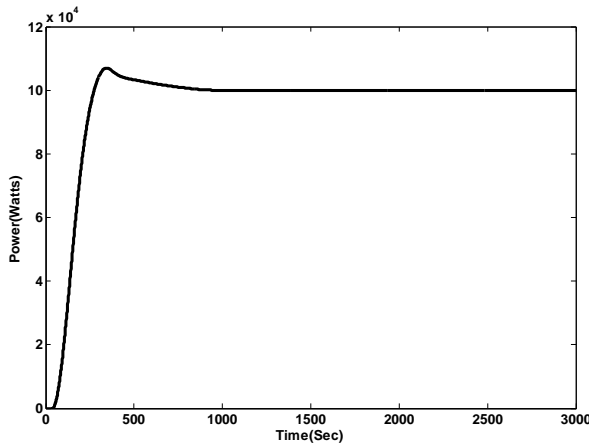


Figure 5: Response of FLC

5. ANFIS CONTROLLER

A typical structure of an ANFIS which is used is Sugeno fuzzy models consist of five layers that every layer has the node shown in Figure 6. There are two types of nodes that called the adaptive node (square symbol) and fixed node (circle symbol) as shown in Figure 6. The structure of Sugeno model has two inputs x_1 and x_2 and one output y [11]. For a first-order Sugeno fuzzy model [2][4], a common rule set with two fuzzy if-then rules is given below,
If x_1 is A_1 and x_2 is B_1 Then $y_1 = c_{11}x_1 + c_{12}x_2 + c_{10}$
If x_1 is A_2 and x_2 is B_2 Then $y_2 = c_{21}x_1 + c_{22}x_2 + c_{20}$
If α predicate for two roles are w_1 and w_2 , then can be determined the weight average, as in

$$y = \frac{w_1 y_1 + w_2 y_2}{w_1 + w_2} = \bar{w}_1 y_1 + \bar{w}_2 y_2 \quad (3)$$

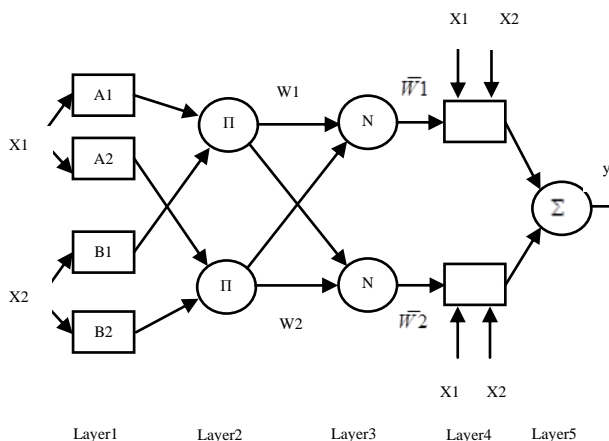


Figure 6: Structure of ANFIS

The function of every layer is:

Layer 1: Every node i in this layer is an adaptive node with a node activation function parameter. The output of every node is the membership function degrees which given by input membership function.

$$O_{1,f} = \mu_{A_i}(x_1) \quad \text{for } i=1,2 \text{ or} \quad (4)$$

$$O_{1,i} = \mu_{B_{i-2}}(x_2) \quad \text{for } i=3,4$$

Where x_1 or x_2 is the input to the node, A_i or B_{i-2} is the fuzzy set associated with this node and it is characterized by the shape of the membership function in this node. The parameters in this layer are referred to as premise (antecedent) parameters.

Layer 2: Every node in this layer is a fixed node denoted as π , which multiplies the incoming signals and output product.

$$O_{2,i} = W_i = \mu_{A_i}(x_1) \mu_{B_i}(x_2) \quad \text{for } i=1,2 \quad (5)$$

Each node output represents the firing strength (α predicate) of a rule. In general, any other T-norm that performs fuzzy AND can be used as the node function in this layer.

Layer 3: The circular node in this layer is denoted as N , the i^{th} node computes the ratio of the i^{th} rule's firing strength to the sum of all rule's firing strengths.

$$O_{3,i} = \bar{W}_i = \frac{W_i}{W_1 + W_2} \quad \text{for } i=1,2 \quad (6)$$

The output of this layer is called as normalized firing strengths.

Layer 4: Node i in this layer calculate the contribution of the i^{th} rule towards the model output with the following node function.

$$O_{4,i} = \bar{W}_i f_i = \bar{W}_i (c_{i1}x_1 + c_{i2}x_2 + c_{i0}) \text{ for } i=1,2 \quad (7)$$

Where \bar{W}_i is a normalized firing strength from layer 3 and $\{C_{i1}, C_{i2}, C_{i0}\}$ is the parameter set of this node. The parameters in this layer are called as consequent parameters.

Layer 5: The node of this layer is a fixed node labeled Σ that computes the overall output as the summation of all incoming signals.

$$\text{Overall Output} = O_5 = \sum_i \bar{W}_i Y_i \quad (8)$$

6. DESIGN OF ANFIS CONTROLLER

The basic idea behind the design of neuro-adaptive learning techniques is very simple. These techniques give a method for the fuzzy modeling procedure to learn the information about data set to compute the membership function parameters that best allow the associated fuzzy inference system to track the given input output data [1][12]. ANFIS is a special type of neural network which combines the features of both

neural networks and fuzzy logic. ANFIS develops a Takagi Sugeno fuzzy inference system (FIS) with the help of an input output data set [7][9]. The Triangular type membership function is used as input membership function for control design. The inputs to the adaptive neuro fuzzy controller are the error (e) and the rate of change of error (de/dt). The input output data set has been taken from a PID controller tuned using conventional Ziegler Nichols method. This approach has been implemented using ANFIS editor in MATLAB. ANFIS can be trained using hybrid learning algorithm that consists of two steps such as feed forward pass and backward pass [10]. More specifically, in the feed forward pass of the hybrid learning algorithm, the node outputs propagate to the forward until layer 4 and consequent parameters are identified by the least squares method. In the backward pass, the error signal goes to the backward and the premise parameters are updated by gradient descent. The ANFIS model structure is a two input single output feed-forward structure having three hidden layers [5]. The response of the ANFIS controller for SOFC is shown in the below figure 7.

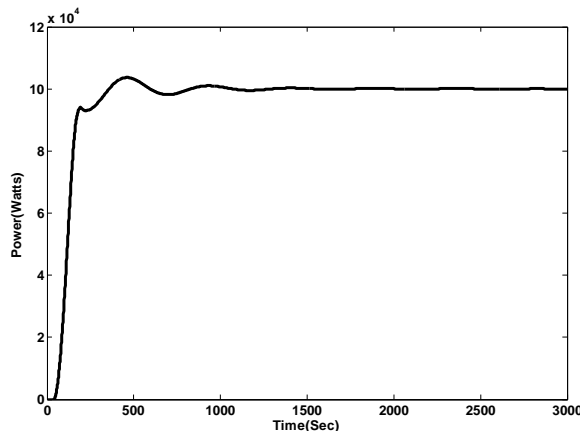


Figure 7: Response of the ANFIS controller

7. RESULTS AND DISCUSSION

The Simulink models of the different controllers are developed and simulated using MATLAB software. To test the robustness of the different controllers, power demand of 100KW is chosen. Figure 9; represent the variation of power while using ANFIS controller, PID controller and Fuzzy logic controller respectively. The results show that ANFIS controller gives the best control performance and then it minimizes the ISE, IAE and ITAE. The ANFIS controller response is compared with conventional ZN tuned PID controller and fuzzy logic controller. From the figure 9, we can determine the response of ANFIS controller is better than other two controllers.

The performance indices ISE, IAE and ITAE of all three controllers are listed in Table 2.

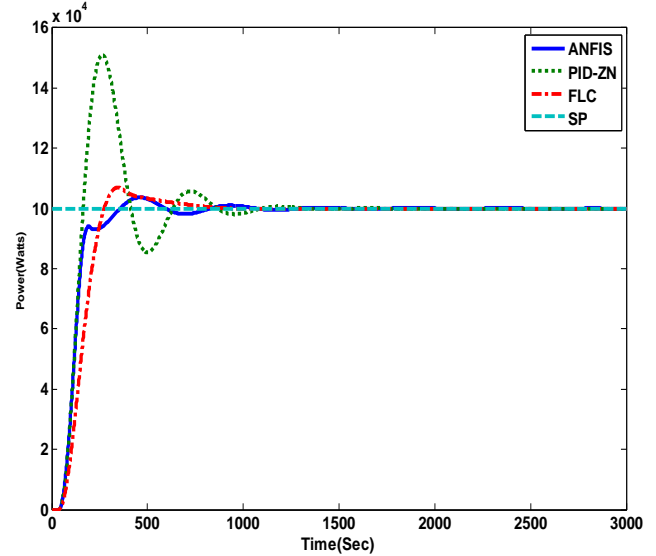


Figure 9: Response of the three controllers

Table 2: Performance Analysis

S.No	M _p	T _s	IAE	ISE	ITAE
ZN-PID	0.5104	2455	2.242E+07	1.301E+12	4.912E+09
FLC	0.0698	980	1.724E+07	1.238E+12	2.181E+09
ANFIS	0.0367	1600	1.375E+07	9.788E+11	1.838E+09

8. CONCLUSION

In this paper, an intelligent technique Adaptive Neuro Fuzzy Inference System (ANFIS) controller is used for control the power of SOFC. From the simulation study, it is observed that the ANFIS controller produce good response over power control of SOFC. Also, it results in minimum Error and better set point tracking.

REFERENCE

- [1] Fernandez de Canete, J., 2000, "An Adaptive Neuro-Fuzzy Approach to Control a Distillation Column, International Journal of Neural Computing and Applications", 211-217.
- [2] Hidayat, PH.Sasongko, Sarjiya and Suharyanto, 2011, "Modeling and Simulation of Adaptive Neuro Fuzzy Inference Systems (ANFIS) for Speed Control of Brushless DC Motor", Proc. CITEE 2011, Yogyakarta, paper E-4-1.

[3] James Larminie and Andrew Dicks, “Fuel Cell Systems Explained”, Second Edition, John Wiley & Sons Ltd, The Atrium, Southern Gate, Chichester, January 2003.

[4] Jang, J.S.R., Sun C.T., and Mizutani, E., 1997, “Neuro-Fuzzy and Soft Computing, Prentice-Hall International Inc”, USA.

[5] Mon, Y.J., Lin, C.M., and Rudas, I.J., 2013, “ANFIS-based Wireless Sensor Network (WSN) Applications for Air Conditioner Control”, Acta Polytechnica Hungarica, Vol. 10, No. 3, pp. 5-16.

[6] Morgantown, W., “Fuel Cell Handbook” 6th Edition, EG&G Technical Services, Virginia, November 2002. [Online]. Available: <http://www.rwth-aachen.de/lbz/linksframe.html>.

[7] Nedjah, N., and Mourelle, L., 2007, “Studies in Fuzziness and Soft Computing”, Germany, Springer Verlag, 2007.

[8] Selvaraj.V., Sivakumar.R and Raja Sekaran.G, 2014, “Modeling and Simulation of Solid Oxide Fuel Cell System”, International Journal of Innovative Science, Engineering & Technology, Volume 1, Issue 9.

[9] Shing, J., and Jang, R., 1993 “ANFIS: Adaptive Network Based Fuzzy Inference System”, IEEE Transactions on Systems, Man, and Cybernetics, Vol. 23, No. 3.

[10] Sivakumar, R., and Balu, K., 2010 “ANFIS based Distillation Column Control”, IJCA Special Issue on Evolutionary Computation for Optimization Techniques, ECOT, pp. 67-73.

[11] Sivakumar, R., Muthu, H., and Siddhardhan, R., 2014 “Design of ANFIS Controller for Quadruple-Tank Interacting System”, International Journal of Engineering Research and Applications, Vol. 4, Issue 4(Version 5), pp.152-157.

[12] Sivakumar, R., Sahana, C., and Savitha, P.A., 2012 “Design of ANFIS based Estimation and Control for MIMO Systems”, International Journal of Engineering Research and Applications, Vol. 2, Issue 3, pp.2803-2809.

[13] Rahul Malhotra and Rajinder Sodhi, 2011, “Boiler Flow Control Using PID and Fuzzy Logic Controller”, IJCSET, Volume 1, Issue 6, pp.315-319.

DESIGN AND IMPLEMENTATION OF WATER PUMPING SYSTEM USING SEPIC CONVERTER

Ms.V.Keerthana, A V Vigneswaran, M Vijay Nishanth, Mohana Krishnan M,

St.Joseph's College of Engineering Chennai-119

Dr.T.D.Sudhakar, Associate Professor, St. Joseph's College of Engineering Chennai-119

t.d.sudhakar@gmail.com

ABSTRACT: The aim of the proposed work is to utilize a sepic converter in the control mechanism of water pumping system. A PV panel feeds energy to the load through sepic converter. The sepic converter has its input and output voltage of same polarity and is capable of operating in both boost and buck modes to give the required magnitude of voltage. The sepic converter is modelled using MATLAB/SIMULINK and simulations are done to show characteristics of current and voltage. The hardware of the sepic converter is constructed and implemented for the pumping application.

KEYWORD: Renewable energy, PV panel, SEPIC converter.

I INTRODUCTION

The demand for solar energy is increasing rapidly along with the population. Also the natural sources are getting depleted which leads to emission of green-house gases. Hence to reduce the adverse effects of nature and to meet the day-to-day demands we are switching to renewable energy sources. The PV energy generates electricity from solar radiation and at present represents one of the Renewable energy sources emerging technologies due to the continuous cost reduction and technological progress. The PV technology is implemented along with a converter technology for obtaining better results for the pumping operation[1]. By using the solar energy to power agricultural or house hold water pumping systems is that to increased water requirements for live-stock irrigation tend to coincide with seasonal increasing of solar energy. If we properly designed these PV systems can result in long term cost savings and smaller environmental foot print compare to conventional systems[2]. In the proposed work, we have designed a water pumping using the dc-dc sepic converter topology which increases the voltage level and feeds it to the pump. There are various converter topologies available such as boost, buck, buck-boost, cuk and sepic. The sepic converter is implemented in this paper since it has the advantage of giving output with a positive

polarity when connected with a proper load connected to it. The block diagram of the proposed system is shown in figure 1.

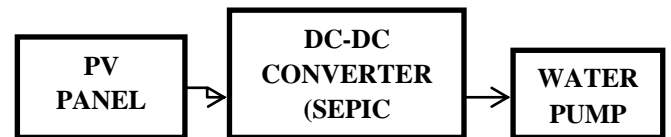


Fig:1 Block diagram of the proposed work

II PROPOSED SYSTEM

The proposed system consists of a PV module for giving input to the sepic converter. The output of the converter is obtained and utilized for the pumping application. The block diagram of the proposed system is shown in the below figure 1.

III MODELLING OF SEPIC DC-DC CONVERTER

SEPIC refers to “Single Ended Primary Inductor Converter”. SEPIC is a type of DC-DC converter that has an output voltage to be greater than, less than, or equal to that at its input. The output of the SEPIC converter is controlled by the duty cycle of the control transistor. It is similar to a normal buck-boost converter. One of the main features of the converter is the polarity of the input and output voltages are same. The circuit diagram of a sepic converter is shown in the figure 2.

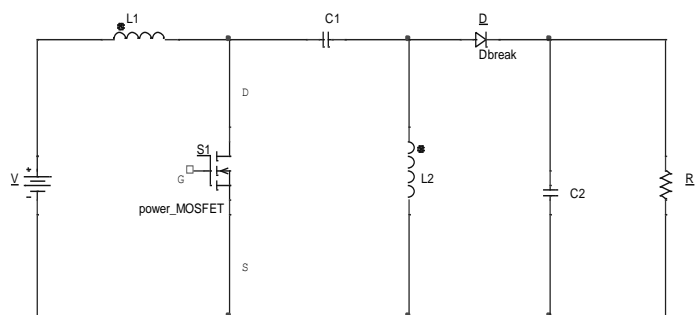


Fig:2 Circuit diagram of sepic converter

The output voltage of the sepic converter is given as

$$V_{out} = (V_{in} \times k) / (1 - k)$$

DESIGN CALCULATION

The sepic converter is designed based on the following parameters:

Step 1: Duty cycle calculation

$$k = V_{out} / (V_{in} + V_{out})$$

Step 2: inductor selection

The peak to peak ripple current is assumed as 20%. The ripple current flowing through the inductors L_1 and L_2 is same and calculated as

$$\Delta I_L = I_{out} \times (V_{out} / V_{in}) \times 20\%$$

And the inductance for L_1 and L_2 is:

$$L_1 = L_2 = L = (V_{in} \times k) / (\Delta I_L \times f_{sw})$$

Step 3: Output capacitor selection

$$C_{out} = (I_{out} \times k) / (V_{ripple} \times 0.5 \times f_{sw})$$

Where V_{ripple} is the peak-to-peak ripple, 2% of the output voltage,

f_{sw} is the switching frequency.

Step 4: Input capacitor selection

$$C_{in} = C_{out}/10$$

IV SEPIC CONVERTER DESIGN

A sepic converter is designed based on the specifications given below:

Input voltage, V_{in} = 12V

Output voltage, V_{out} = 24V

Output current, I_{out} = $V_{out}/R = 24/10 = 2.4A$

Input current, I_{in} = $(V_{out} \times I_{out}) / V_{in}$

$$I_{in} = (24 \times 2.4) / 12 = 4.8A$$

Switching frequency, $f_{sw} = 25$ kHz

Step 1: Duty cycle calculation

$$k = V_{out} / (V_{in} + V_{out}) = 24 / (12 + 24) = 0.67$$

Step 2: Inductor selection

The input inductor L_1 ripple current is:

$$\Delta I_L = I_{out} \times (V_{out} / V_{in}) \times 20\% = (2.4 \times (24 / 12)) / 20\% = 0.96 A$$

And the inductance for L_1 and L_2 is: $L_1 = L_2 = L = (V_{in} \times k) / (\Delta I_L \times f_{sw}) = (12 \times 0.67) / (0.96 \times 25000) = 335 \times 10^{-6} H$

Step 3: Output capacitor selection

$$C_{out} = (I_{out} \times k) / (V_{ripple} \times 0.5 \times f_{sw})$$

$$= (2.4 \times 0.67) / (0.2 \times 24 \times 0.5 \times 25000) = 26.8 \times 10^{-6} F$$

Step 4: Input capacitor selection

$$C_{in} = C_{out}/10 = (26.8 \times 10^{-6}) / 10 = 2.68 \times 10^{-6} F$$

V SIMULATION RESULTS

The below section describes the modeling and simulation of the sepic converter using MATLAB/SIMULINK. The simulation diagram of the sepic converter is shown in the figure3.

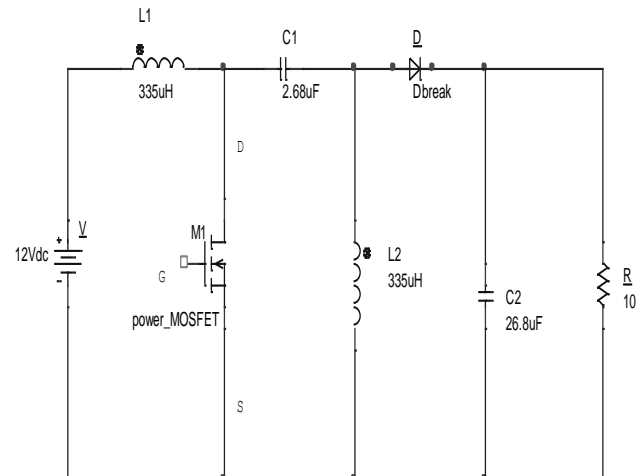


Fig:3 Simulation diagram of sepic converter

An input voltage of 12V dc supply is given as input to the sepic converter. The converter consists of a high frequency switch, MOSFET. A pulse generator with a time period of 40 μs gives gate signals to turn on the MOSFET. The switch turns on and the sepic converter produces an output with positive polarity. The waveforms obtained from the sepic converter are as follows.

Diode Rectifier Output

The output of the diode rectifier is shown in the figure 4.

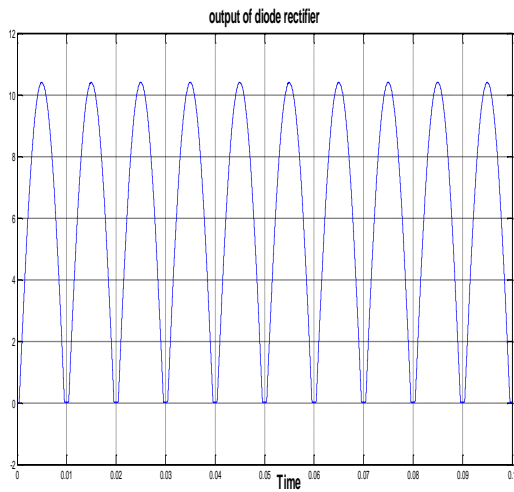


Fig:4 output of diode rectifier

Current waveforms

An input current of 4.8 A and an output current of 2.4 A are the currents obtained from the sepic converter. The waveform of the input and output currents are shown in figure 5.

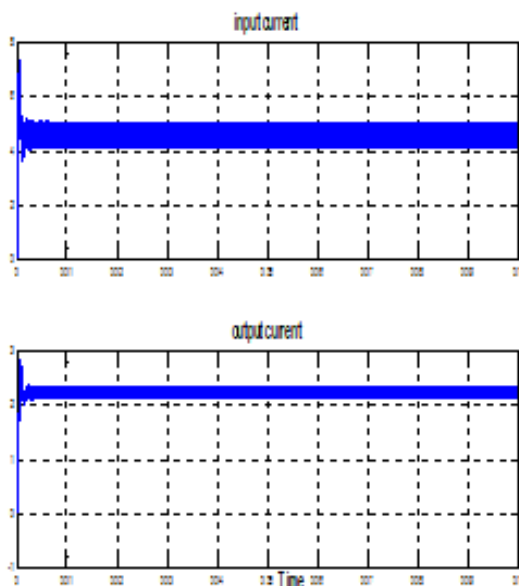


Fig:5 Input and Output currents.

Voltage waveforms

With a 12V dc input supply, the waveform of the output voltage is obtained from the sepic converter as shown in the figure 6.

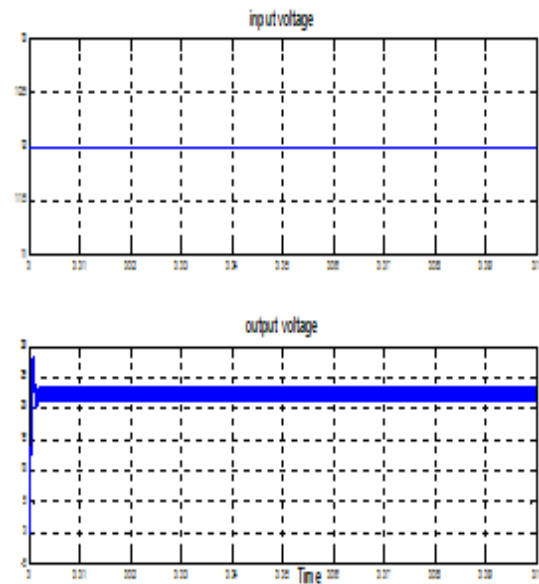


Fig:6 Input and Output voltages.

The inductor values and the capacitor values applied in the converter are calculated theoretically. Hence for a given dc supply voltage of 12V with a duty cycle of 67%, the output voltage is boosted and obtained as 23.43V.

VI. HARDWARE IMPLEMENTATION

The sepic converter is designed and implemented as shown below in the figure 7.

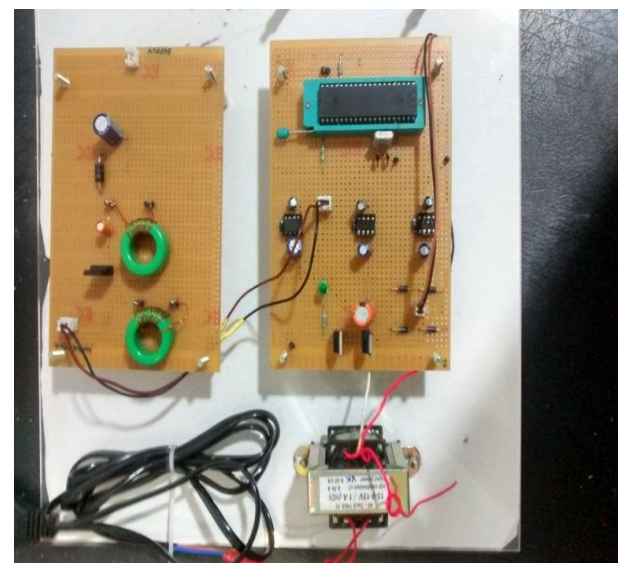


Fig:7 Hardware implementation

VII CONCLUSION

The model of the sepic converter has been simulated in MATLAB/SIMULINK software and the hardware is also implemented. The sepic

converter has been discussed for the pumping application. The advantage of the sepic converter over the conventional methods is that it has input and output voltages are of same polarity and required magnitude of voltage is obtained. The output of the sepic converter is then applied for the pumping application with a proper load connected to it. Hence with a sepic converter the pumping is done efficiently and the results have presented.

Systems”, IEEE Transactions on Industrial Electronics, Vol. 56, No. 11, November 2009, pp 4399 – 4406

[8] Elke Lorenz, Johannes Hurka, Detlev Heinemann and Hans Georg Beyer, “Irradiance Forecasting for the Power Prediction of Grid-Connected Photovoltaic Systems”, IEEE Journal of Selected Topics in Applied Earth Observations and Remote Sensing, Vol. 2, No. 1, March 2009, pp 2 – 10

VIII REFERENCE

- [1] Design and implementation of solar powered water pumping system P. Nisha, St.Joseph's College of Engineering, Ramani Kalpathi, Professor, St.Joseph's College of Engineering.
- [2] Design and simulation of SEPIC Topology Based Solar Water pumping and lightning system, 1B.Sanjay Raju, 2V.Lavanya, 1PG scholar, School of Electrical Engineering, VIT University, Chennai, India 2Assistant Professor (Sr.), School of Electrical Engineering, VIT University, Chennai
- [3] Billy M. T. Ho and Henry Shu-Hung Chung, “An Integrated Inverter with Maximum Power Tracking for Grid-Connected PV Systems”, IEEE Transactions on Power Electronics, Vol. 20, No. 4, JULY 2005, pp 953 – 962
- [4] Bo Yang, Wuhua Li, Yi Zhao and Xiangning He, “Design and Analysis of a Grid-Connected Photovoltaic Power System”, IEEE Transactions on Power Electronics, Vol. 25, No. 4, April 2010, pp 992 – 1000
- [5] David M.Whaley, Gurhan Ertasgin, Wen L. Soong, Nesimi Ertugrul, James Darbyshire, Hooman Dehbonei and Chem V. Nayar, “Investigation of a Low-Cost Grid-Connected Inverter for Small-Scale Wind Turbines Based on a Consatnt-Current Source PM Generator”, IEEE IECON 2006 – 32nd Annual Conference on Industrial Electronics, pp 4297 – 4302
- [6] Eduardo Román, Ricardo Alonso, Pedro Ibañez, Sabino Elorduizapatarietxe and Damián Goitia, “Intelligent PV Module for Grid-Connected PV Systems”, IEEE Transactions on Industrial Electronics, Vol. 53, No. 4, August 2006, pp 1066 – 1073
- [7] Elena Villanueva, Pablo Correa, José Rodríguez and Mario Pacas, “Control of a Single-Phase Cascaded H-Bridge Multilevel Inverter for Grid-Connected Photovoltaic

Energy Management System For Hybrid Renewable Energy Sources using Adaptive Neural Network

R. Saravanapriyan,
PG Scholar Department of EEE,
K.S.Rangasamy College of Technology,
Tiruchengode, Namakkal, 7200779074
spriyan92@gmail.com.

S. Devi, M.E, (Ph.D),
Associate Professor, Department of EEE,
K.S.Rangasamy College of Technology,
Tiruchengode, Namakkal.

Abstract—Renewable energy sources play an important role in electrical energy generation. The drawbacks of Renewable energy sources have been overcome by the use of hybrid power generating unit. A typical hybrid renewable energy system (HRES) combines several renewable energy sources such as wind turbine (WT) and photovoltaic (PV) panels as primary energy sources and an energy storage system (ESS) based on fuel cell and battery. All of the energy sources are connected together to a central dc bus by means of power converters. This paper includes a supervisory control called adaptive neural network which determines the power that must be generated by/stored in the fuel cell and battery, taking into account the control demand by the grid, the offered power, the hydrogen reservoir point and the state-of-charge (SOC) of the battery. The proposed EMS is compared with classical EMS composed of state based supervisory control system based on states and inverter control system based on PI controller. Dynamic simulation results of the proposed EMS demonstrate the better performance than the classical EMS

Keywords—Adaptive neural network, energy management system, energy storage system, renewable power sources, mixture system

I. INTRODUCTION

A typical HRES configuration combines several renewable energy sources, such as wind turbine (WT) and photovoltaic (PV) panels, with ESS. The renewable sources are used as primary energy sources, which are generating whenever there is wind or solar radiation. However, because the sun irradiance and the wind speed are uncontrollable parameters, a support energy source is needed to increase the degree of controllability and operability of the HRES. Traditionally, this function is performed by an ESS such as battery and hydrogen system (i.e., FC, electrolyzer and hydrogen storage tank). These ESS are considered to be an effective solution to balance the generation and demand supporting the renewable energy deficit when necessary, and storing the primary energy excess when possible.

All renewable sources and ESS are connected together to a central dc bus by means of power converters. These converters are designed to deliver energy from the energy sources, ensuring stable, sustainable and reliable operation. In grid-connected mode, dc–dc and ac–dc power converters interface the renewable sources and ESS to a dc bus, while dc–ac voltage source inverters are in charge of delivering the active and reactive power to the grid.

HRES presents two-level control architecture. In the highest level, the supervisory control system is responsible for determining the reference power that must be generated

by/stored in the ESS. The lowest level is in charge of controlling the converters associated with the renewable sources and ESS, so that the energy sources work as required by the supervisory control system. Most of the studies about HRES control architectures consider standalone operation in isolated sites due to the advances in renewable energy technologies and power electronic converters, which are used to convert the unregulated power generated from the renewable sources into useful power at the load end.

Classical and intelligent control techniques have been applied to the control system of stand-alone HRES. Classical control techniques (i.e., based on state machine controllers or PI controllers) require exact mathematical model of the system and are very sensitive to parameter variations. Intelligent control techniques such as artificial neural networks, fuzzy logic, or neuro-fuzzy are more efficient and robust than classical techniques, since they do not require an exact model of the system and improve the dynamic behavior of the system.

This paper presents a new adaptive neural network-based EMS for a HRES composed of renewable energies, hydrogen and battery, and an adaptive neural network-based control for the three-phase inverter, which connects the HRES to grid. The main novelties of this paper are: 1) the application of adaptive neural network to the supervisory control system of a grid-connected HRES in order to determine the power that must be generated by/stored in the ESS (hydrogen and battery), taking into account the control demand by the grid, the offered power, the hydrogen tank level and the battery SOC and 2) the application of adaptive neural network to the three-phase inverter in order to properly control the power delivery to grid by using the active and reactive power as control variables. It is organized as follows. Section II describes the grid-connected hybrid system under study. Section III describes the classical EMS used to evaluate the performance of the Adaptive neural network based EMS. Simulation results are presented in section IV. Finally, Section V establishes the conclusions derived from this work.

II. GRID-CONNECTED HYBRID SYSTEM

Fig. 1 shows the grid-connected hybrid system under study in this work, which is composed of WT and PV panels (renewable and primary energy sources) and hydrogen subsystem and battery (ESS). All of them use dc–dc power converters in order to connect them to a central dc bus. The whole system is connected to a grid by a three-phase inverter.

In this system, the renewable sources are generating whenever there is wind or solar radiation. When possible, renewable energy is stored in the battery and/or in the form of hydrogen by using the electrolyzer, and this stored energy is recovered to support the renewable production when necessary.

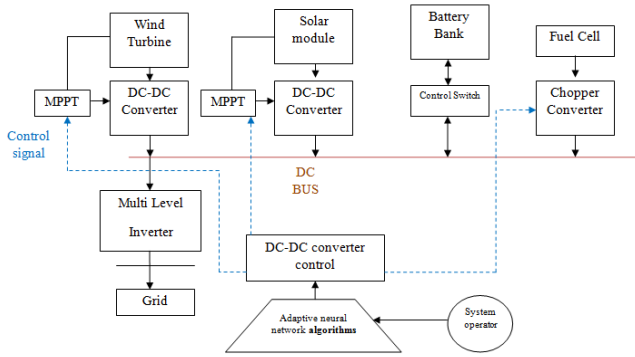


Fig. 1 Grid-connected hybrid system

A dynamic model of this grid-connected hybrid system is implemented in a MATLAB/Simulink environment, as described below.

A. Wind Turbine

The WT presents a rated power of 1.5 kW. It presents a two blade turbine coupled to a three-phase permanent magnet synchronous generator (PMSG). This WT is represented by a model with the following subsystems: turbine and generation system. The turbine model expresses the mechanical power extracted from the wind, which is a function of the wind speed and the blade tip speed ratio, as defined by the actuator disk theory.

The generation system is composed of a three-phase PMSG, ac–dc converter, and dc–dc converter, which are represented by models included in SimPowerSystems [1]. The electrical and mechanical parts of the PMSG are represented by a secondorder state-space model. The ac–dc and dc–dc converters are modeled by average-value equivalent models. The dc–dc power converter, which connects the WT to the hybrid system dc bus, is controlled by a torque reference-based maximum power point tracking (MPPT) control in order to extract the maximum available power from the WT. This MPPT control maintains the operating point of the WT on its maximum power coefficient for any wind speeds in the below-rated wind speed region, modifying the duty cycle of the WT dc–dc converter, which produces a variation of its rotational speed. Furthermore, the WT generation system incorporates a braking resistor at the dc bus, in which the power excess with above nominal winds is dissipated to assure WT rated power.

B. PV Panels

The PV system presents nine 0.180-kW PV panels, with a total rating of 1.6kW. Asingle-diode model, which is composed of a current source and a parallel diode (representing the ideal PV cell) with two resistances (series and parallel resistances), is used to represent each PV panel.

This model presents suitable accuracy [1], and the parameters are easy to find in the commercial datasheets [7], which makes it perfect for the simulation of PV devices with power converters. A dc–dc power converter controlled by a MPPT controller adapts the PV output voltage to the dc bus voltage. The MPPT controller generates the duty cycle of the PV converter to move the PV voltage to the voltage that corresponds to the maximum power point (MPP). In this work, the MPP voltage is defined as proportional to the PV open-circuit voltage [11]. Thus, a fractional open-circuit voltage algorithm is used as MPPT algorithm to generate the duty cycle of the controller due to its simplicity.

C. Hydrogen Subsystem

The hydrogen subsystem is composed of 0.48-kWPEM electrolyzer, 2280-liter hydrogen tank, and 1.2-kW PEM FC. PEM electrolyzer and PEM FC are highly efficient units that are suitable for autonomous and distribution operation [5].

The PEM electrolyzer uses electrical energy to produce hydrogen from water. It is modeled by a resistance, in which the power needed to produce hydrogen is consumed. Faraday's law is used to calculate the hydrogen produced depending on the electrical current in the resistance [4]. The hydrogen produced by the electrolyzer is stored in the hydrogen tank. In the hydrogen tank model, the hydrogen available in the tank is obtained from the rate of incoming and outgoing hydrogen, taking into account the ideal gas equation [2]. The PEM FC uses the hydrogen available in the tank in order to produce electrical energy. It is modelled by a reduced model of the complete model detailed in [10].

The validity of the reduced model was demonstrated in [8], where both the reduced and complete models were compared, showing similar responses, but with a considerable reduction of the computational time for the first one. Several control strategies for FC vehicles [2]–[5] were evaluated by using this reduced model. In this reduced model, the FC voltage depends on the cell voltage and number of cells [1], [5]. The cell voltage is determined as a function of the current density, temperature, and water, and hydrogen and oxygen partial pressures. The compressor, which controls the air flow in the cathode to keep constant the oxygen excess ratio, is represented by a first-order system. Finally, an ideal air cooler and humidifier are considered in the FC model [4].

D. Batteries

The hybrid system uses a 14.48-kWh lead-acid battery. This type of battery is usually the least expensive storage battery for any application, while still providing good performance and life characteristics [4]. This battery is modeled by a conflict in series with a variable voltage source [5].

E. DC–DC Converters

Each energy source of the hybrid system provides a variable voltage, which depends on the current demand, at different ranges. Therefore, it uses a pulse-width modulated

(PWM) dc–dc converter [6] to transfer the output power to the central dc bus. The output voltage of the WT rectifier is higher than the dc bus voltage. Thus, the WT plus rectifier system is connected to the dc bus by using a buck-type unidirectional converter. The connection of PV, FC, and electrolyzer to the dc bus is performed by using boost-type unidirectional converters. The PV and FC converters transfer power from the source to the dc bus, since both sources terminal voltages are lower than the dc bus voltage. The electrolyzer converter transfers power from the dc bus to the electrolyzer, whose terminal voltage is higher than the dc bus voltage. The battery uses a bidirectional converter, which allows the power flow from the battery to the dc bus (boost-type) and vice versa (buck-type). Each dc–dc converter is modeled by using the two-quadrant chopper model included in SimPowerSystems [9]. In this model, the chopper is represented by a simplified version of the converter containing an average-value equivalent model.

F. Inverter

A three-phase IGBT inverter connects the dc bus of the hybrid system to grid. This inverter is represented by the model developed in [3]. In this model, the snubber capacitor is eliminated, so that only the snubber resistance is taken into account. Furthermore, the forward voltages of the IGBTs and diodes are considered null. The inverter is PWM to produce the three-phase 50-Hz sinusoidal voltage. It uses adaptive neural network switching and controls the active and reactive power, as will be shown below.

III. CLASSICAL ENERGY MANAGEMENT SYSTEM OF THE HYBRID SYSTEM

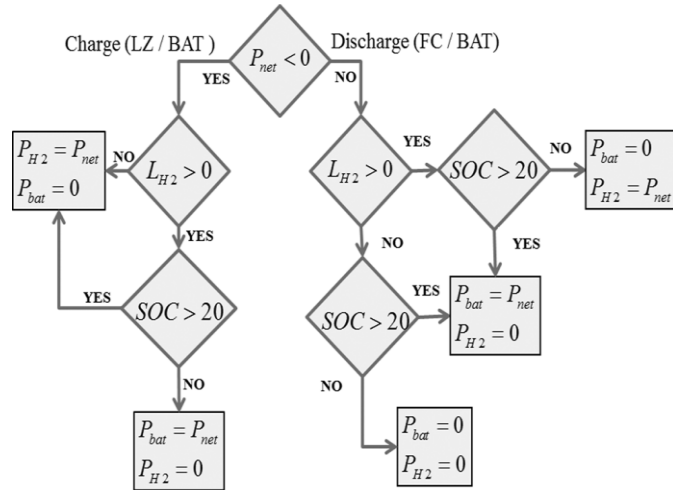


Fig. 2 Scheme of the supervisory control system based on states

Here, the classical EMS used to test the performance of the proposed Adaptive neural network control system is described. The classical EMS is composed of state-based supervisory control system based on states and inverter control system based on PI controllers.

The supervisory control system uses the control scheme shown in Fig. 2 in order to determine the power generated by/stored in the hydrogen and battery, taking into account the power demanded by the grid, the available power, the hydrogen tank level and the battery SOC.

IV. SIMULATION RESULTS

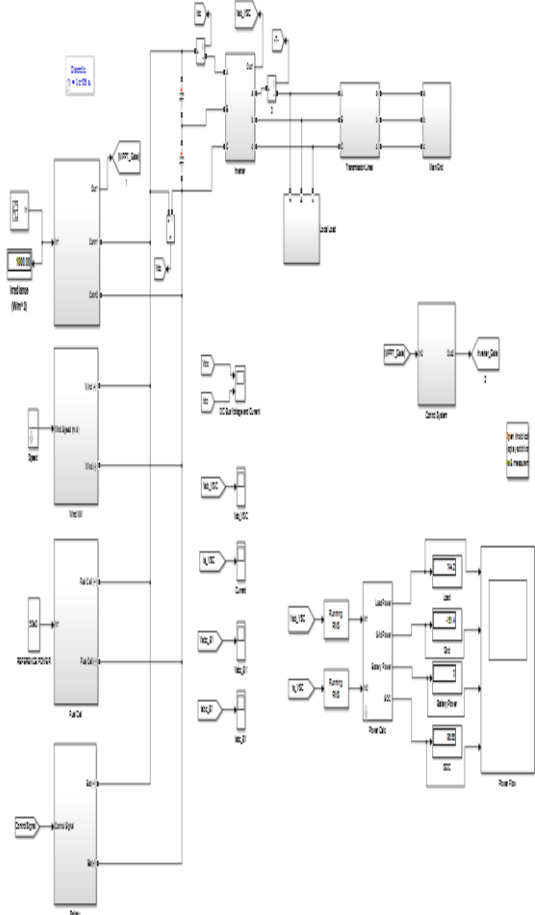


Fig. 3 Simulation Model in MATLAB/Simulink

Fig. 3 presents the power demanded by the network and the power of each energy source during 20 s. As mentioned previously, the renewable sources are generating the maximum available power. During the first 10 s, the renewable power (PV and WT power) is higher than the power demanded by the grid. In this case, the power excess is stored in the battery and used in the electrolyzer to produce hydrogen. From the second 10 s, the power demanded by the grid increases, and it becomes higher than the renewable power. Then, the FC and battery generate extra power to satisfy the demanded power.

Table I Presents the results (i.e., battery, hydrogen system, and hybrid system efficiencies and the energy injected into grid) obtained by each control during the first simulation. Analyzing the results, it can be concluded that the Adaptive neural network control achieves higher battery and hybrid system efficiencies, and it is capable of injecting more energy into grid than the classical control. It shows in detail the

dynamic behaviour of the supervisory controls and inverter control systems.

The implemented EMS is based on a predictive controller, which generates the FC and battery reference currents to provide the power demanded by the tramway, meeting the battery and SC SOC constrains (i.e., keeping their SOC between a specific range) and ordering the operation of the braking resistor, when necessary, during regenerative braking[4].

TABLE I. SUMMARY OF RESULTS OBTAINED IN THE SIMULATION

Parameters	Efficiency
PV panels (%)	95
Wind Turbine, η_{HS} (%)	67
Fuel cell, η_{H2} (%)	39
Battery, η_{bat} (%)	76
Energy injected, E_{inv}^{inj} (kWh)	5490 kWh

A. Charging condition

Fig. 4 presents load is off. The power flow through grid and battery. Here the battery is charging mode.

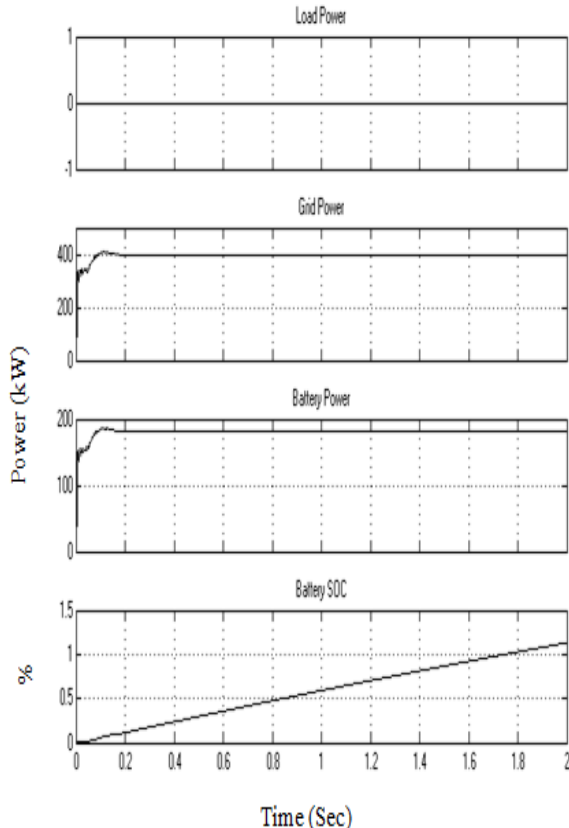


Fig. 4 Power flow in Load, Grid, Battery Power and State of Charge

B. Discharging situation

Fig. 5 presents load is on. The power flow through load only. Here the battery is discharging mode.

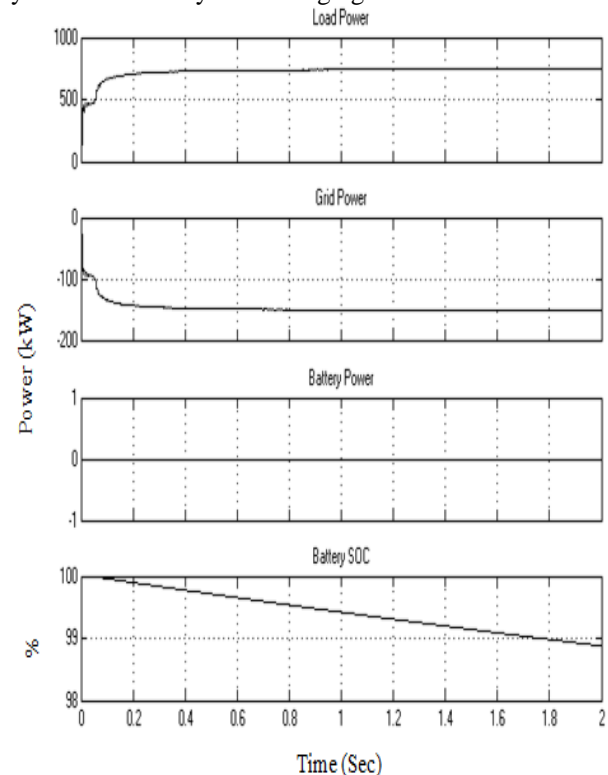


Fig. 5 Power flow in Load, Grid, Battery Power and State of Charge

V. CONCLUSION

The renewable energy sources operate at the Maximum Power Point, independently of the Energy Management System (EMS). Therefore, the EMS is responsible for managing the operation of the ESS (battery and hydrogen system), taking into account the power demanded by the grid, the available renewable power, and the available ESS power (battery SOC and hydrogen tank level). Once determined which ESS has to absorb/generate the power excess/deficit, the appropriate control of the dc-dc converter associated to the battery and hydrogen system allows the ESS to achieve the operation required by the EMS, maintaining constant the dc bus voltage. On the other hand, in coordination with the EMS, the three phase inverter is controlled by a Adaptive neural network-based controller in order to regulate the active and reactive power that the hybrid system is required to deliver with the grid.

REFERENCES

- [1] Chunhua Liu, Xiaodong Zhang, "An Efficient Wind–Photovoltaic Hybrid Generation System using Doubly Excited Permanent-Magnet Brushless Machine", IEEE Trans. Ind. Electron., vol. 57, no. 3, pp.831-839, 2013.

- [2] F. Kennel, D. Görges, and S. Liu, “Energy management for smart grids with electric vehicles based on hierarchical MPC,” IEEE Trans. Ind. Inf., vol. 9, no. 3, pp. 1528–1537, Aug. 2013.
- [3] F.González-Espín, I. Patrao, E. Figueres, and G.Garcerá, “An adaptive digital control technique for improved performance of grid connected inverters,” IEEE Trans. Ind. Inf., vol. 9, no. 2, pp. 708–718, May 2013.
- [4] J. P. Torreglosa, P. García, L.M. Fernández, and F. Jurado, “Predictive control for the energy management of a fuel cell-battery-super capacitor tramway,” IEEE Trans. Ind. Inf., vol. 10, no. 1, pp. 276–285, Feb. 2014.
- [5] L. Valverde, F. Rosa, and C. Bordons, “Design, planning and management of a hydrogen-based microgrid,” IEEE Trans. Ind. Inf., vol. 9, no. 3, pp. 1398–1404, Aug. 2013.
- [6] M. P. Kazmierkowski, M. Jasinski, and G.Wrona, “DSP-based control of grid-connected power converters operating under grid distortions,” IEEE Trans. Ind. Inf., vol. 7, no. 2, pp. 204–211, May 2011.
- [7] M. Singh and A. Chandra, “Real-time implementation of ANFIS control for renewable interfacing inverter in 3P4W distribution network,” IEEE Trans. Ind. Electron., vol. 60, no. 1, pp. 121–128, Jan. 2013.
- [8] P. Siano, C. Cecati, H. Yu, and J. Kolbusz, “Real time operation of smart grids via FCN networks and optimal power flow,” IEEE Trans. Ind. Inf., vol. 8, no. 4, pp. 944–952, Nov. 2012.
- [9] S. Dasgupta, S. N. Mohan, S. K. Sahoo, and S. K. Panda, “A plug and play operational approach for implementation of an autonomous microgrid system,” IEEE Trans. Ind. Inf., vol. 8, no. 3, pp. 615–629, Aug. 2012.
- [10] S. N. Bhaskara and B. H. Chowdhury, “Microgrids – A review of modeling, control, protection, simulation and future potential,” in Proc. IEEE Power and Energy Soc. Gen. Meeting, 2012, pp. 1–7.
- [11] Z. Nie, X. Xiao, R. McMahon, P. Clifton, Y. Wu, and S. Shao, “Emulation and control methods for direct drive linear wave energy converters,” IEEE Trans. Ind. Inf., vol. 9, no. 2, pp. 790–798, May 2013.
- [12] Ghareeb, A.T. and Mohammed,O.A., “ Wavelet-adaptive ANN forecaster for renewable energy sources for continuous supply in microgrid applications,” IEEE Trans. Power and Energy Society General Meeting (PES),, vol. 10, no. 1, pp. 1 – 5, Jul. 2013.
- [13] Xiang Li and Chien Chern Cheah, “ Adaptive Neural Network Control of Robot Based on a Unified Objective Bound,” IEEE Trans. Control Systems., vol. 22 , no. 3, pp. 1032 – 1043, Jan. 2014.
- [14] Xusheng Lei and Pei Lu, “ The Adaptive Radial Basis Function Neural Network for Small Rotary-Wing Unmanned Aircraf,” IEEE Trans. Ind. Electronics., vol. 61, no. 9, pp. 4808 – 4815, Jun. 2014.
- [15] Zhen Zhao, Wei He and Shuzhi Sam Ge, “Adaptive Neural Network Control of a Fully Actuated Marine Surface Vessel With Multiple Output Constraints,” IEEE Trans. Control Systems., vol. 22, no. 4, pp. 1536 – 1543, Jul. 2014.
- [16] Juntao Fei and Zhe Wang, “Adaptive control of active power filter using RBF neuralnetwork,” IEEE Trans. Mechatronics and automation., pp. 767 – 772, Feb. 2013.
- [17] Yang, S. and Dingwei Wang, “Constraint satisfaction adaptive neural network and heuristics combined approaches for generalized job-shop scheduling,” IEEE Trans. Neural Network., vol. 11, no. 2, pp. 474 - 486 , Jul. 2000.
- [18] Zhen Zhao and Wei He ; Shuzhi Sam Ge, “Adaptive Neural Network Control of a Fully Actuated Marine Surface Vessel With Multiple Output Constraints,” IEEE Trans. Control Systems., vol. 22, no. 4, pp. 1536 – 1543, Jul. 2014.
- [19] Wen-Shyong Yu, “ Adaptive neural network tracking control of robotic systems,” IEEE Trans. Neural Network., pp. 1 – 8, May. 2012.
- [20] Tso, S.K. and Lin, N.L., “ Adaptive neural network controller for robot manipulator systems,” IEEE Trans. Neural Network., vol. 5, pp. 2320 – 2325, Jan. 1995.

A Grid Connected Solar Energy System using LQR based P&O MPPT Algorithm

I.Felice Browni¹, J.Arun Venkatesh²

¹PG Scholar, Department of EEE, Velammal Engineering College, Chennai.

²Assistant Professor, Department of EEE, KCG College of Technology, Chennai.

Abstract—The energy requirement for the modern era is continuously increasing. The supply and demand are not met. The conventional plants such as coal based or nuclear based are almost depleted and are not safe for the environment and the atmosphere. The renewable energy sources are now replacing the conventional energy sources. But interconnecting the existing grid with the renewable energy source is a problem which requires a control strategy to integrate them. This paper proposes the maximum power tracking from solar and connecting it to the grid using abc to dq0 transformation control strategy. The LQR based P&O is used for maximum power point tracking and the abc to dq0 transformation is used to generate the pulses for the inverter through which grid connection is achieved.

Keywords— *Linear Quadratic Regulator (LQR), Perturb and Observe algorithm, Solar array, Solar cell, Voltage source converter (VSC)*

I. INTRODUCTION

Access to quality, reliable and affordable energy is critical for promoting economic and social development in rural areas. Due to increased standards in people's living and growth population and rapid development in industrialization etc., the energy demand has been increased at a faster rate and hence the gap between generation and demand has considerably increased. Distributed Generation (DG) is the power generation from sources available at the distribution end which are generally renewable energy sources. Usage of DG is increasing since distributed energy systems with renewable sources have achieved great potential in providing reliable and continuous power to the rural areas where grid power is unreliable and not continuous. The increasing demand in the electrical energy and the focus on environmental protection has pushed us to concentrate mainly on developing renewable energy sources which is completely harmless to environment. United Nations is planning 50% of total energy from renewable sources by 2050, Europe 20% by 2020 and India 10% by 2012. Renewable energy source (RES) integrated at distribution level is termed as distributed generation (DG). The utility is concerned about the issues created due to the high penetration level of intermittent RES in distribution systems as it may pose a threat to network in terms of stability, voltage regulation and power-quality (PQ) issues. Therefore for grid integration the DG systems are required to comply with strict technical and regulatory frameworks to ensure safe,

reliable and efficient operation of overall network. With the advancement in power electronics and digital control technology, the DG systems can now be actively controlled to enhance the system operation. However, the extensive use of power electronics based equipment and non-linear loads at PCC generate harmonic currents, which may deteriorate the quality of power. But at the same time achieving maximum possible power from RES is also an issue. In this paper solar energy is used in interconnection with the grid and the MPPT is used to get maximum possible power from solar.

II. ENERGY SOURCES

A. Energy Sources

Natural resources such as oil, coal, or the sun, which can be used to provide power for light, heat, machines, etc. We are committed to the development of clean and renewable energy sources.

The world's energy resources can be divided into fossil fuel, nuclear fuel and renewable resources. Based on long-term availability the energy resources are classified as,

- Non-renewable energy resources.
- Renewable energy resources.

B. Non Renewable Energy

A non-renewable energy source is a source that does not restore itself at significant rate for sustainable economic extraction in meaningful human time-frames. An example is carbon-based, organic fuel. The organic material when subjected to changes with the aid of heat and pressure becomes a fuel such as oil or gas.

Disadvantages of Non-renewable Energy Resources

- Fossil fuels generate pollution. These pollutants degrade the environment, cause health hazards. Mainly carbon dioxide which causes global warming.
- Coal a petrochemical is used as raw material for chemical, pharmaceutical and paint industries. In long-term it is desirable to conserve coal for future needs.
- The waste materials in nuclear plants has radioactivity quotients of dangerous levels, it remains above the safe limit for long period and is health hazard.

- Possibility of accidental leakage of radioactive material from reactor is another safety issue.
- Non-renewable sources will finish up one day.
- Conventional sources are not sufficient to meet the growing demand.

Due to these reasons it has become necessary to identify non-conventional or renewable resources to reduce too much dependence on conventional or non-renewable resources. India is the only country having a full-fledged ministry devoted especially to developing new and renewable energy sources.

C. Maintaining the Integrity of the Specifications

A renewable energy source is natural source that can replenish in due time compared to the usage, either through biological reproduction or other naturally recurring processes. Renewable resources are a part of Earth's natural environment and the largest components of its ecosphere.

Advantages of Renewable energy

- It acts as a solution to the energy problem for the stabilization of carbon dioxide emissions and other greenhouse gases. Replaces energy generation plants which use conventional sources lead to a reduction in the emission of pollutants such as sulphur and nitrogen oxides which cause acid rain.
- Domestic sources of energy and contribute to increasing energy independence and society of energy supply at the national level.
- Geographically dispersed leading to the decentralization of the energy system making it possible for energy needs to be met at a local and regional level reducing losses from energy transmission.
- They provide opportunities for rational use of energy sources because they cover wide range of energy needs.
- Low operating costs which are not influenced by fluctuations in the international economy and especially in prices for conventional fuels.

16% of global energy consumption presently comes from renewable resources, 10% of energy from traditional biomass used for heating, and 3.4% from hydroelectricity. New renewable account for another 3% and are increasing rapidly. National renewable energy markets are projected to continue to grow strongly in the coming decade and beyond.

Renewable energy sources all over wide geographical areas in contrast to other energy sources which are concentrated in a limited number of countries to particular areas. Rapid deployment of renewable energy and energy efficiency is resulting in significant energy security, climate change mitigation, and economic benefits. In international public opinion surveys there is strong support for promoting renewable sources such as solar power and wind power. While many renewable energy projects are large-scale, renewable

technologies are also suited to rural and remote areas and developing countries.

III. MAXIMUM POWER POINT TRACKING

Maximum Power Point tracking is a technique that is used to get maximum possible power from one or more photovoltaic (PV) devices. Solar cells have a complex relationship between solar irradiation, temperature and total resistance that produces non-linear output efficiency which can be analyzed based on I-V curve. It is MPPT system to sample the output of the cells and apply the proper resistance load to obtain maximum power for any given environmental conditions. MPP (Maximum power point) is the product of the MPP voltage (V_{mpp}) and MPP current (I_{mpp}). MPPT devices are typically used in electric power system that provides voltage or current conversion, filtering, and regulation for various loads such as power grids, batteries, or motors.

A. Perturb and Observe Algorithm

In this method the controller adjusts the voltage by a small amount from the array and measures power; if the power increases, further adjustments in that direction are tried until power no longer increases. This is perturb and observe method which is most common, this method results in oscillations of power output. It is referred as hill climbing method, because it depends on the rise of the curve of power against voltage below the maximum power point, and the fall above that point. Perturb and observe is the most commonly used MPPT method due to its ease of implementation. Perturb and observe method may result in top-level efficiency, provided that a proper predictive and adaptive hill climbing strategy is adopted. The flowchart is shown in fig 1.

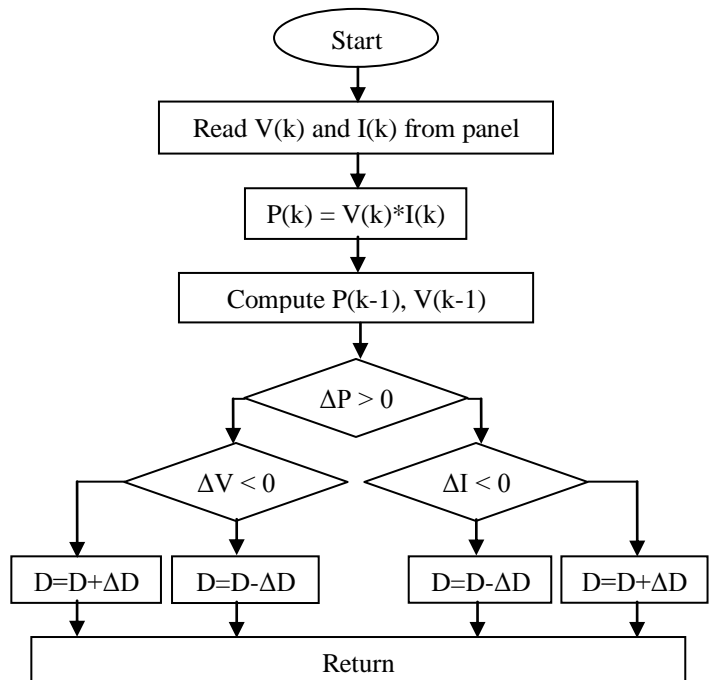


Fig 1 Flowchart of perturb and observe algorithm

IV. LINEAR QUADRATIC REGULATOR

The term “linear quadratic” refers to the linear system dynamics and the quadratic cost function. LQR design is based on the selection of feedback gain such that the cost function J is minimized. This ensures that the gain selection is optimal for the cost function specified. For LQR design the system need to be described by state space model:

$$\dot{x} = Ax + Bu \quad \text{---(1)}$$

$$y = Cx + Du \quad \text{---(2)}$$

The performance index is defined as,

$$J = \int_0^{\infty} (x^T Q x + u^T R u) dt \quad \text{---(3)}$$

where, Q and R are the weight matrices. Q is positive definite or positive semi-definite real symmetric matrix and R is positive definite symmetric matrix. The feedback control function limits to a linear function so that,

$$u = -Kx \quad \text{---(4)}$$

where K is given by,

$$K = R^{-1} B^T P \quad \text{---(5)}$$

and P can be determined by solving the continuous time algebraic *Riccati* equation

$$A^T P + P A - P B R^{-1} B^T P + Q = 0 \quad \text{---(6)}$$

V. SIMUALTION RESULTS

The simulation for the test system is done by MATLAB / Simulink. The test system is shown in fig. 2 and the solar boost converter is shown in fig 3. The P&O controller is shown in fig 4. The simulation is done for a test system with a solar panel as source and the output of solar is given to a boost converter which is supplying the load. The solar array is connected to the boost converter which is controlled by LQR based P&O MPPT algorithm. The boost converter output is given to the inverter where the pulses are provided by using a PWM pulse generator. The inverter output is connected in shunt to the grid which supplies the load. The output from the boost converter is shown in fig 5 and the load voltage and current waveforms after connecting the solar panel with the grid is shown in fig 6.

The simulation is carried out for the test system using solar cell to form solar panel which has the following ratings as mentioned in table 1.

TABLE I. SIMULATION DATAS

	Parameter	Value
Solar Cell	Short Circuit Current, ISC	7.34 A
	Open Circuit Voltage, VOC	0.6 V
	Irradiance, Ir	1000 W/m ²
Solar Array	10 x Solar Cells	10 x 6 = 6 V
Solar Panel	5 x Solar Aray	5 x 6 = 30 V

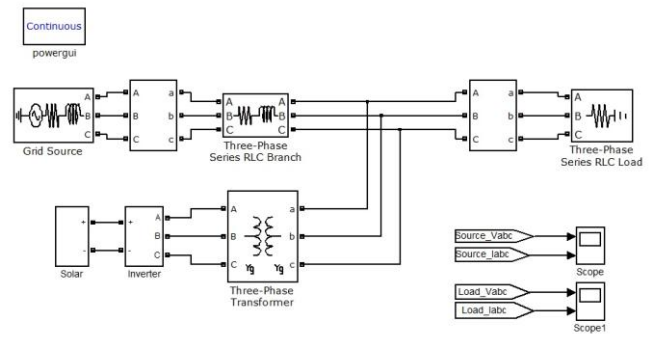


Fig 2 Simulation diagram for Test System

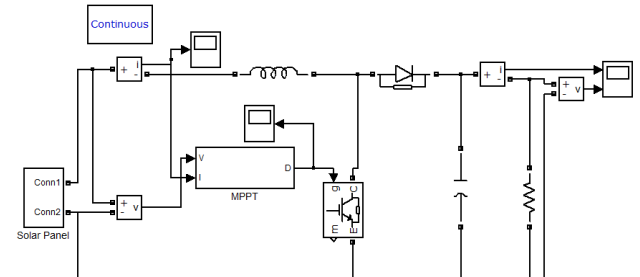


Fig 3 Simulation diagram for Solar Boost Converter

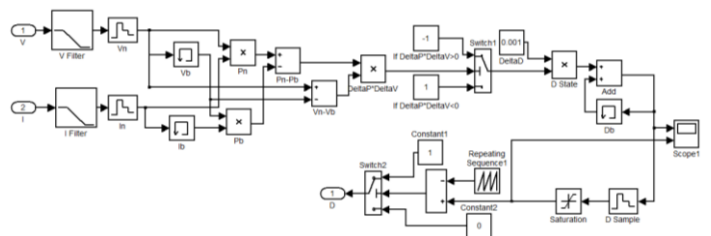


Fig 4 Simulation Diagram P&O Algorithm Controller

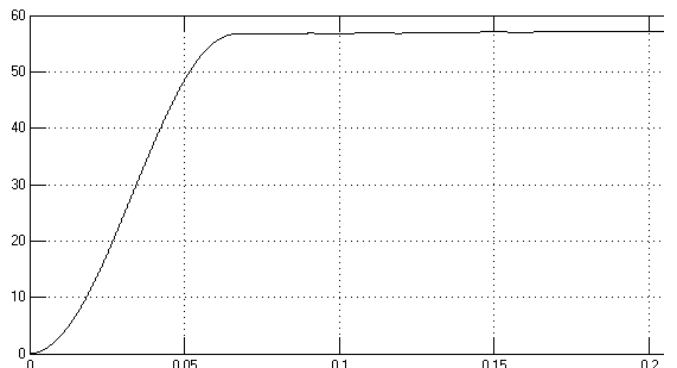


Fig 5 Boost Converter Output

The load voltage is plotted for per unit value with a base value of 415 V. The voltage in the system is obtained to be 0.99 pu.

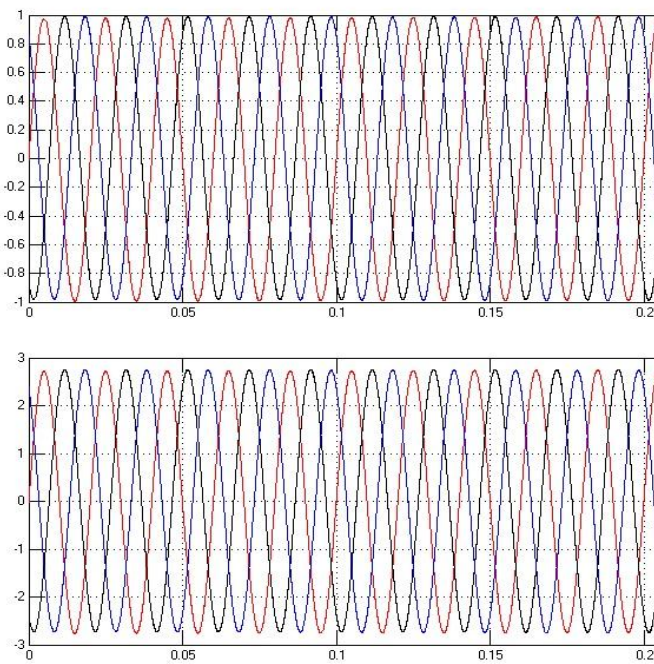


Fig 6 Load Voltage and Current waveforms

VI. CONCLUSION

The linear quadratic regulator based maximum power point tracking for the solar energy system is proposed with grid interconnected system. The proposed controller has the advantage that cost function has been taken into consideration depending on various parameters such as current, temperature, irradiance which gives the maximum power point. The linear quadratic controller has been proposed for perturb and observe algorithm for maximum power point tracking. The simulation is carried out for test system using MATLAB/ Simulink. The Linear quadratic regulator has the advantage of the system with robust and stable. The system has less settling time and reduced steady state error. The system can be modified by using optimization algorithms in which the MPP can be achieved with higher efficiency and advantages.

REFERENCES

- [1] D.S.Karanjkar, S.Chatterji, Amod Kumar, "Design and Implementation of a Linear Quadratic Regulator Based Maximum Power Point Tracker for Solar Photo-Voltaic System", International Journal of Hybrid Information Technology, January Vol.7, No.1 (2014), pp.167-182.
- [2] Sathish Kumar Kollimalla, Student Member, IEEE, and Mahesh Kumar Mishra, Senior Member, IEEE, "Variable Perturbation Size Adaptive P&O MPPT Algorithm for Sudden Changes in Irradiance", IEEE Transactions on Sustainable Energy, vol. 5, no. 3, July 2014
- [3] Sathish Kumar Kollimalla, Mahesh Kumar Mishra, "A Novel Adaptive P&O MPPT Algorithm Considering Sudden Changes in the Irradiance", IEEE Transactions on Energy Conversion, vol. 29, no. 3, September 2014, pp.602-610.
- [4] Patrizio Manganiello, Mattia Ricco, Giovanni Petrone, Member, IEEE, Eric Monmasson, Senior Member, IEEE, and Giovanni Spagnuolo, Senior Member, IEEE, "Optimization of Perturbative PV MPPT Methods Through Online System Identification", IEEE Transactions on Industrial Electronics, vol. 61, no. 12, December 2014.
- [5] Mohammed A. Elgendi, Bashar Zahawi, Senior Member, IEEE, and David J. Atkinson, "Assessment of the Incremental Conductance Maximum Power Point Tracking Algorithm", IEEE Transactions on Sustainable Energy, vol.4,no.1,January 2013.
- [6] Dezso Sera, Member, IEEE, Laszlo Mathe, Member, IEEE, Tamas Kerekes, Member, IEEE, Sergiu Viorel Spataru, Student Member, IEEE, and Remus Teodorescu, Fellow, IEEE, "On the Perturb-and-Observe and Incremental Conductance MPPT Methods for PV Systems", IEEE Journal of Photovoltaics, vol. 3, no. 3, July 2013.
- [7] Mohammed A. Elgendi, Bashar Zahawi, Senior Member, IEEE, and David J. Atkinson, "Assessment of Perturb and Observe MPPT Algorithm Implementation Techniques for PV Pumping Applications", IEEE Transactions on Sustainable Energy, vol.3,no.1,January 2012.
- [8] Giovanni Petrone, Giovanni Spagnuolo, Massimo Vitelli, "A Multivariable Perturb-and-Observe Maximum Power Point Tracking Technique Applied to a Single-Stage Photovoltaic Inverter", IEEE Transactions on Industrial Electronics, vol. 58, no. 1, January 2011, pp.76-84
- [9] A. Dolara, R. Faranda, S. Leva, "Energy Comparison of Seven MPPT Techniques for PV Systems". Electromagnetic Analysis & Applications, 2009, 3: 152-162 doi:10.4236/jemaa.2009.13024 Published Online September 2009.
- [10] Nicola Femia, Giovanni Petrone, Giovanni Spagnuolo, Massimo Vitelli, "Optimization of Perturb and Observe Maximum Power Point Tracking Method", IEEE Transactions on Power Electronics, vol. 20, no. 4, July 2005, pp.963-973.

FUEL COST FUNCTION FOR ECONOMIC LOAD DISPATCH USING PARTICLE SWARM OPTIMIZATION ALGORITHM

¹KJ.Krishnanand, ²C.BASKARAN

1. PG Scholar- Department of Power Systems Engineering, St. Joseph's College of Engineering, Chennai-600119, India
 2. Associate Professor-Department of EEE, St. Joseph's College of Engineering, Chennai-600119, India
 E-mail:1 krishnankj34@gmail.com, 2 c.baskaran@rediffmail.com.

Abstract - The input–output characteristics of thermal power plants are affected by many factors such as the ambient operating temperature and aging of generating units. Thus, periodical estimation of fuel cost function is very crucial to improve the overall operational and economical practices. The higher the accuracy of the estimated coefficients of the cost function, the more accurate the results obtained from the economic dispatch and optimal power flow calculations. Different models that describe the input–output relationship of thermal units are considered, including the one that accounts for the valve loading point. The goal is to minimize the total estimation error such that the selected model follows the actual data measurements as closely as possible. Particle Swarm Optimization (PSO) is employed to minimize the error associated with the estimated parameters.

Keywords- Particle swarm optimization (PSO), Swarm intelligence. Economic dispatch,

1. INTRODUCTION

Economic load dispatch (ELD) is a constraint based optimization problem in power systems that have the objective of dividing the total power demand among the online participating generator economically while satisfying the essential constraints. The conventional methods include the lambda iteration methods [1, 2], base point and participation factors, etc. Among these methods lambda iteration is the most common method because of ease of implementation. The ELD is a non-convex optimization problem required rigorous efforts to solve by traditional methods. Moreover, evolutionary and behavioral random search algorithms such as genetic algorithm (GA) [3], particle swarm optimization (PSO) [4] have been implemented on the ELD problem. GAs does possess some weaknesses leading to larger computation time premature convergence [5]. This paper proposes PSO as an optimization technique to solve constraints based quadratic cost function with generator constraints and power loss. Algorithm is tested for three generator units system.

Particle swarm optimization was first introduced by Kennedy and Eberhart in the year 1995. It is an exciting new methodology in evolutionary computation and a population-based optimization tool like GA. PSO is motivated from the simulation of the behavior of social systems such as fish schooling and birds flocking. The PSO algorithm requires less memory

because of its inherent simplicity. PSO is similar to the other evolutionary algorithms in that the system is

Initialized with a population of random solutions, called particle (swarm), flies in the d-dimension problem space with a velocity, which is dynamically adjusted according to the flying experiences of its own and colleagues. Swarms collect information from each other through an array constructed by their positions using the velocity of particles. Position and velocity are both updated by using guidance from particles' own experience and experience of neighbors. The position and velocity vectors of the ith particle of a d-dimensional search space can be represented as
 $X_i = (x_{i1}, x_{i2}, \dots, x_{id})$ and $V_i = (v_{i1}, v_{i2}, \dots, v_{id})$, respectively.

The first step consists in selecting individuals for reproduction. This selection is done randomly with a probability depending on the relative fitness of the individuals so that best ones are often chosen for reproduction than poor ones.

In the second step, offspring are bred by the selected individuals. For generating new chromosomes, the algorithm can use both recombination and mutation. Then the fitness of the new chromosomes is evaluated.

2. MODELLING OF FUEL-COST FUNCTION

The modelling of fuel-cost function consists of two smooth and non-smooth functions

1.In this case , the fuel cost curve for a thermal generating unit(i) as a function of the MW output power can be modelled by a polynomial function in an idealized form as:

$$F_i(P_{ti}) = a_{0i} + \sum_{j=1}^L a_{ij} P_{ti}^j + r_i \quad i = 1, 2, \dots, N$$

Where,

F_i is the fuel cost function of the ith generating unit.

P_{ti} Is the power generated by the ith thermal generating unit

2. In large steam turbine generating units, the input–output characteristics are neither always smooth nor differentiable everywhere. Large steam turbine generating units tend to have a number of steam admission valves that are opened in sequence to obtain an ever increasing output of the unit. In general, the valve point effects produce ripple, such as heat rate curve. The number of ripples is proportional to the degree of non-convexity in the shape of the objective function, and it increases the difficulty of detecting the global solution. In this situation, the fuel-cost function is

modelled by adding a sinusoid term to compute the optimal scheduling of the generators with and without considering the losses for the given network system

ECONOMIC DISPATCH

Economic dispatch means optimum allocation of Generators to each station to minimize the fuel costs for The power system. Economic load dispatch problem is allocating loads to plants for minimum cost while meeting the constraints. It is formulated as an optimization problem of minimizing the total fuel cost of all committed plant while meeting the demand and losses .The variants of the problems are numerous which model the objective and the constraints in different ways. The basic economic dispatch problem can described mathematically as a minimization of Problem of minimizing the total fuel cost of all committed plants subject to the constraints.

Minimize P_i

$F_i P$ is the fuel cost equation of the ‘i’th plant. It is the variation of fuel cost (\$ or Rs) with generated power (MW).Normally it is expressed as continuous quadratic equation. 2 min max

The total generation should meet the total demand and transmission loss. The transmission loss can be determined form either Bmn coefficients or power flow.

NEED FOR ECONOMIC DISPATCH

The purpose of Economic dispatch or optimal dispatch is to reduce fuel costs for the power systems. By economic load scheduling, the total fuel cost must be minimum and at the same time the total demand and losses at any instant must be met by the generation.

ECONOMIC DISPATCH WITHOUT LOSSES

Consider a system of N – generating units connected to a single bus bar serving a received electrical load P_{load} .

(1)The input of each unit, F_i represents the cost rate (Rs. /Hr.). The output of each unit P_i is the electrical power generated by that particular unit.

(2)The total cost rate (F_T) subject to the constraint that the sum of the output powers must equal the reactive load.

(3)Objective Function: Min

Where

$$F_i = \alpha_i + \beta_i P_i + \gamma_i P_i^2$$

Subject to two constraints - Equality constraints
Inequality constraints

ECONOMIC DISPATCH WITH LOSSES

Consider a system of N – generating units connected to a single bus bar serving a received electrical load P_{load} . The input of each unit, F_i represents the cost rate (Rs./Hr.). The output of each unit P_i is the electrical power generated by that particular unit. The total cost rate (F_T)

subject to the constraint that the sum of the output powers must equal the reactive load.

Objective function is,

$$\text{Min } F_T = \sum_{i=1}^N F_i(P_i)$$

Subjected to the following constraints

Equality Constraint,

Where,

$$F_T = \sum_{i=1}^N F_i(P_i)$$

$$F_T = F_1 + F_2 + \dots + F_N$$

N--- Number of generating units

Here the transmission losses are neglected

In equality constraint

$$P_{i,min} \leq P_i \leq P_{i,max}$$

$P_{i,min}$ - Minimum Power generation from plant i

$P_{i,max}$ - Maximum Power generation from plant i

Let

$$\Phi = P_{LOAD} - \sum_{i=1}^N P_i = 0$$

By making use of Lagrangian multiplier the auxiliary function is obtained as

$$L = F_T + \lambda \phi$$

Where λ – Lagrangian multiplier

WITH LOSS

$$P_{LOAD} + P_{LOSS} - \sum_{i=1}^N P_i$$

Where N – number of generating units

P_{LOAD} – Total load of the system

P_{LOSS} – Total network losses of the system

In equality constraint

$$P_{i,min} \leq P_i \leq P_{i,max}$$

$P_{i,min}$ - Minimum Power generation from plant i

$P_{i,max}$ - Maximum Power generation from plant i

The Lagrangian function was formulated by adding the constraints to the objective function by using Lagrangian multiplier and is given below,

Let,

$$\Phi = P_{LOAD} + P_{LOSS} - \sum_{i=1}^N P_i$$

P_{LOSS} - is the total system loss

Making use of the Lagrangian multiplier the auxiliary function is

$$L = F_T + \lambda \phi$$

$$L = F_T + \lambda (P_{LOAD} + P_{LOSS} - \sum_{i=1}^N P_i)$$

$$\frac{\partial L}{\partial P_i} = (\frac{\partial F_i}{\partial P_i}) + \lambda ((\frac{\partial P_{LOAD}}{\partial P_i}) + (\frac{\partial P_{LOSS}}{\partial P_i}) + \sum_{i=1}^N \frac{\partial P_i}{\partial P_i}) = 0$$

$$(\frac{\partial F_i}{\partial P_i}) + \lambda (0 + (\frac{\partial P_{LOSS}}{\partial P_i}) - 1) = 0$$

$$(\frac{\partial F_i}{\partial P_i}) + \lambda (\frac{\partial P_{LOSS}}{\partial P_i}) = \lambda ----- \text{co-ordination equation}$$

$(\frac{\partial P_{LOSS}}{\partial P_i})$ = Incremental Transmission loss at plant ‘i’

λ = Incremental production cost (Rs/Mph)

$$\lambda = P_{LOAD} + (\sum_{i=1}^N (\beta_i / 2\gamma_i)) / (\sum_{i=1}^N (1/2 \gamma_i))$$

Find the value of power output of all the generators by using the formula given below

$$P_i = (\lambda - \beta_i) / (2\gamma_i)$$

3. PARTICLE SWARM OPTIMIZATION (PSO)

Particle swarm optimization was first introduced by Kennedy and Eberhart in the year 1995. It is an exciting new methodology in evolutionary computation and a population-based optimization tool like GA. PSO is motivated from the simulation of the behavior of social systems such as fish schooling and birds flocking. The PSO algorithm requires less memory because of its inherent simplicity. PSO is similar to the other evolutionary algorithms in that the system is initialized with a population of random solutions, call particle (swarm), flies in the d-dimension problem space with a velocity, which is dynamically adjusted according to the flying experiences of its own and colleagues. Swarms collect information from each other through an array constructed by their positions using the velocity of particles. Position and velocity are both updated by using guidance from particles' own experience and experience of neighbors.

The position and velocity vectors of the i^{th} particle of a d -dimensional search space can be represented as

$X_i = (x_{i1}, x_{i2}, \dots, x_{id})$ and $V_i = (v_{i1}, v_{i2}, \dots, v_{id})$, respectively. On the basis of the value of the evaluation function, the best previous position of a particle is recorded and represented as

P best $i = (p_{i1}, p_{i2}, \dots, p_{id})$. If the g^{th} particle is the best among all particles in the group so far, it is represented as

$$P \text{ best } g = G\text{-best} = (p_{g1}, p_{g2}, \dots, p_{gd}).$$

The particle tries to modify its position using the current velocity and the distance from p best and g best. The modified velocity and position of each particle for fitness evaluation in the next, that is, $(k+1)^{th}$ iteration, are calculated using following equations:

$$\begin{aligned} V_{id}(k+1) &= [W * v_{id} + c_1 * R_{id} * (P \text{ best } id - x_{id}) \\ &+ c_2 * R_{id} * (G \text{ best } gd - x_{id})] \end{aligned}$$

$$X_{id}(k+1) = x_{id} + v_{id}(k+1)$$

Here W is the inertia weight parameter which controls the global and local exploration capabilities of the particle. c_1 and c_2 are cognitive and social coefficients, respectively, and R_{id} , R_{id} are random numbers between 0 and 1. c_1 pulls the particles towards local best position and c_2 pulls towards the global best position. Usually these parameters are selected in the range of 0 to 4. In the procedure of the particle swarm paradigm, the value of maximum allowed particle velocity V_{max} determines the resolution, or fitness, with which regions are to be searched between the present position and the target position. If V_{max} is too high, particles may fly past good solutions. If V_{max} is too small, particles may not explore sufficiently beyond local solutions. Thus, the system parameter V_{max} has the beneficial effect of preventing explosion and scales the exploration of the particle search.

Optimization problems are widely encountered in various fields in science and technology. Sometimes such problems can be very complex due to the actual and

practical nature of the objective function or the model constraints. Most of power system optimization problems have complex and nonlinear characteristics with heavy equality and inequality constraints.

Recently, as an alternative to the conventional mathematical approaches, the heuristic optimization techniques such as genetic algorithms (GAs), Tabu search, simulated annealing, and particle swarm optimization (PSO) are considered as realistic and powerful solution schemes to obtain the global or quasi-global optimums (K. Y. Lee et al., 2002).

This chapter would introduce an educational simulator for the PSO algorithm. The purpose of this simulator is to provide the undergraduate students with a simple and useable tool for. In some cases the modern power generating units are valve operated and multiple fuels can be used in these units depending on power levels required.

5. PROBLEM FORMULATIONS

The objective of ED is to minimize the total generation costs of a power system over an appropriate period (usually one hour), while function considered in this paper can be represented as follows: The Let C_i mean the cost, expressed for example in dollars per hour, of producing energy in the generator unit I .

The total controllable system production cost therefore will be

(1).The generated real power P_{Gi} accounts for the major influence on C_i . The individual real generation are raised by increasing the prime mover torques, and this requires a cost of increased expenditure of fuel. The reactive generations do not have any measurable influence on C_i because they are controlled by controlling by field current. The individual production cost C_i of generators unit I is therefore for all practical purposes a function only of P_{Gi} , and for the overall controllable production cost

(2)When the cost function C can be written as a sum of terms where each term depends only upon the scheduled combined units for each specific period of operation operating zones.

The data matrix should have 5 columns of fuel cost coefficients and plant limits.

- 1.a (\$/MW²)
- 2. b \$/MW
- 3. c (\$)
- 4.lower limit(MW)
- 5.Upper limit(MW)

This Example system is taken from the book Power System Analysis by Prof Haadi Sadaat no. of rows denote the no of plants (n)

The generating cost of such fossil fired units are represented by piece-wise quadratic cost function. Such types of cost function are called hybrid cost function. The notations used for representing the cost of i^{th} unit for k^{th} fuel used is as indicated below (It is assumed that m is the number of generating units and f is the number of fuels which can be used):

- i) P_{min} is the minimum power generation limit of i^{th} unit with fuel 1.
- ii) P_1 is the maximum power generation limit of i^{th} unit with fuel 1.
- iii) P_{f1} is the minimum power generation limit of i^{th} unit with fuel f .

- iv) P_{\max} is the maximum power generation limit of i^{th} unit with fuel f .
- v) Subscript i indicates generating unit number and subscript k indicates type of fuel.
- vi) a_{ik} , b_{ik} and c_{ik} are cost curve coefficients of i^{th} generating unit with fuel k .
- v) $\text{cost}(P_i)$ is the hybrid cost function of i^{th} unit.

$$\begin{aligned} & a_{i1} + b_{i1}P_{i1} + c_{i1}P_{i12} \\ & P_{\min} \leq P_{i1} \leq P_{i1} \text{ for fuel } (1) \\ & a_{i2} + b_{i2}P_{i2} + c_{i2}P_{i22} \\ & \text{Cost}(P_i) = P_{i1} \leq P_{i2} \leq P_{i2} \text{ for fuel } (2) \end{aligned}$$

$$\begin{aligned} & a_{ik} + b_{ik}P_{ik} + c_{ik}P_{ik2} \\ & P_{k-1} \leq P_{ik} \leq P_k \text{ for fuel } (k) \quad (7) \end{aligned}$$

$a_{if} + b_{if}P_{if} + c_{if}P_{if2}$
 $P_{f-1} \leq P_{if} \leq P_{\max}$ for fuel (f)
 Let the total power demand of the area is P_D . Then the power balance equation assuming lossless transmission line

$$\sum_{i=1}^m P_{ik} - P_D = 0 \quad (8)$$

Total power generation cost to meet the load demand is given by

$$J = \sum \text{cost}(P_i)$$

"Given the hybrid cost characteristics and inequality constraints for each fuel used in generation for each unit as represented by equation (7) and the power balance (equality constraints) represented by equation (8), it is required to find power generation of each unit and type of fuel for each unit to meet the total power demand such that the total cost of generation given by equation (9) is minimum." It is attempted to solve this problem using PSO technique as discussed in next section

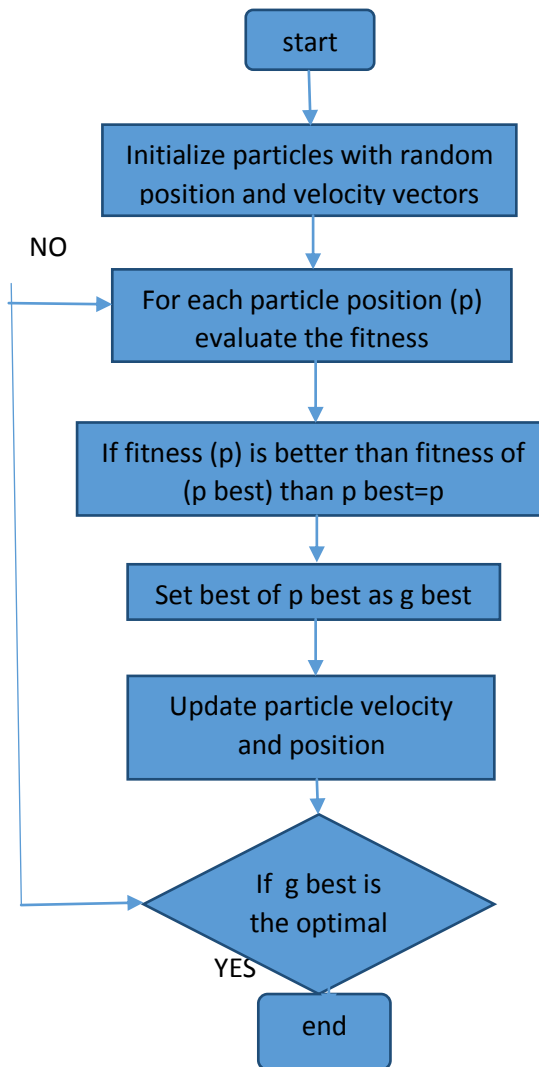
6. SOLUTION PROCEDURE

The optimization problem for an interconnected multiple area power system is stated in the previous section. There are a number of methods exists for solution of such problems using analytical methods such as linear programming, nonlinear programming, gradient method, integer programming and so on, and heuristic methods such as GA, ANN, and others. In this section we will try to solve this problem using PSO and its variants. It is a heuristic iterative method revolving around two equations velocity (distance) and position updating given by the two equations (1) & (2). Sometime the method may land up with "Explosion". To prevent Explosion some variations of PSO are there as discussed in previous section as given in equations (3) & (4) and (5) & (6). The details of solution procedure are given below.

Initialization

To start the iteration process initialization of individual particle position and velocity is necessary. At first a population is selected i.e. the number of particles n in the population will have. Then each particle's position is selected randomly wide spread in the search space such that it does not violate the constraints represented by equations (7) & (8) for i^{th} particle as $X_i = (X_{i1}, X_{i2}, \dots, X_{im})$ in m dimensional space where m is the number of variables. In this case m is the number of generating units and the generation cost depends on f number of fuels that can be used for each unit. The initial

velocity of i^{th} particle $V_i = (V_{i1}, V_{i2}, \dots, V_{im})$ is created. Keeping in view that the velocity components chosen must satisfy the inequality constraints i.e. they should lie within the maximum and minimum velocity limit ($-V_{i\min} < V_{id} < V_{i\max}$) where
 $V_{i\max} = (X_{id\max} - X_{id\min})/N$ (10)
 $V_{i\min} = -V_{i\max}$ (11)
 where N is iteration number and suffix d is the dimension.



The initial value of p_{best} of individual i is set as the initial position of individual i i.e. initial value of p_{best} is same as the initial value of position. The initial value of g_{best} is obtained by finding the fitness function of all the particles and select the particle which has optimum value. Updating the Position and Velocity of Particles In order to modify the position of each particle, it is necessary to calculate the velocity of each particle in the next stage (iteration / generation).The velocity is modified first using equation (2) or its variants equation (3) or (5). Then the position is modified using (1). The modified position of each individual particle may not satisfy the equality and inequality constraints equations (8) and (7) respectively.

If the position of particles crosses its limiting value (generation is beyond its limits i.e. less then minimum value or more then maximum value), it is adjusted first

satisfying inequality constraint equation (7) as shown below in equation (12).

$$X_{idk} + V_{idk} \text{ if } X_{idk \min} < X_{idk} + V_{idk} < X_{id \max}$$

$$X_{idk+1} = X_{id \ min} \text{ if } X_{idk} + V_{idk+1} < X_{id \ min} \quad (12)$$

$$X_{id \ max} \text{ if } X_{idk} + V_{idk+1} > X_{id \ max}$$

In addition to the inequality constraints as in (7), the equality constraint given by (8) has to be satisfied for implementing the PSO algorithm in each iteration. To satisfy the equality constraints a heuristic method is proposed as given below.

i) Find the sum of the variables of a particle (sum of generations of each machine in this case).

ii) Compare it with the equality constraint and find the difference.

iii) The difference is divided by the number of variables and then adds this value to each element of the particle.

iv) Repeat (i) to (iii) till it is satisfied or remains within certain limit. Updating pbest and gbest

The pbest i of each individual particle at each iteration k+1 is updated as follows:

$$Pbest_{idk+1} = X_{idk+1} \text{ if } J_{ik+1} < J_{ik} \quad (13)$$

$$Pbest_{idk+1} = pbest_{idk} \text{ if } J_{ik+1} > J_{ik} \quad (14)$$

Where, J_{ik} is the objective function / fitness function evaluated at the position of individual particle at iteration k , X_{idk+1} is the position of the particle i at iteration k+1 pbest idk+1 is the best position of the individual particle i until iteration k+1.

Equation (13) & (14) compares the pbest of every individual particle with its current fitness value. If the new position value of an individual particle has better performance then the current pbest i, the pbest i is replaced by new position. If the new position has lower performance then the current pbest value remains unchanged. The gbest the global best position at iteration k+1 is set as the best evaluated position among all pbest i (among all particles).

The Stopping Criterion The proposed iterative method is terminated if the iteration approaches a predefined criterion, usually a sufficient good fitness or if it reaches the maximum number of iterations as defined. At the end when the optimum value of the problem is reached, all the particles will have the same value of Pbest as the value of gbest .

The problem stated in previous section can be solved using PSO method as explained in this section. Normally this method gives solutions to all types of problems it may be linear, continuous, discontinuous or nonlinear problems. In the next section the method is explained by taking an example and simulation is done by using MATLAB software.

The complete solution procedure step-wise is present as below:

Steps for solution:

(i) Find out the dimensions of the problem which is equal to the number of generating units.

(ii) Choose the population i.e. the number of particles.

(iii) Initialize the position of the swarm keeping in view of the constraints (equality and inequality)

(iv) Select the minimum and maximum velocity limit of the particles.

(v) Initialize the velocity of the swarm keeping in view of the velocity limit.

(vi) Select the initial value of Pbest as the initial value of the position of the swarm.

(vii) Find the fitness function of each particle and then find Gbest , which is the minimum of all particles.

(viii) Update the velocity using equation (2).

(ix) Test for velocity limit.

(x) Update the position using equation (1).

(xi) Test for equality and inequality constraints for position.

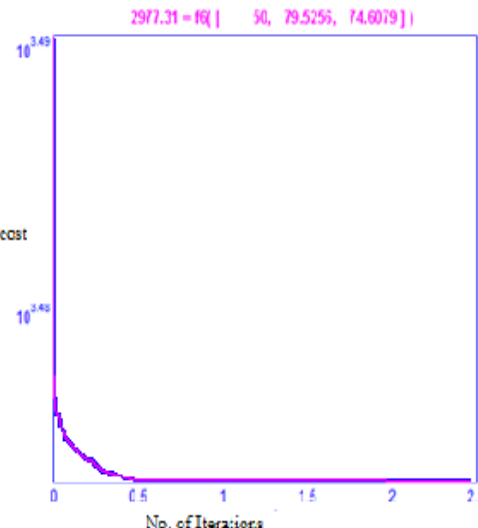
(xii) Find the fitness function.

(xiii) Find Pbest using equation (13 & 14).

(xiv) Find Gbest .

(xv) Test for the termination of iteration process if satisfied stop the iterations, otherwise go to step (viii).

6. SIMULATION RESULT



7. CONCLUSIONS

This paper presents a new approach to address practical ED issues. Power crisis is one of the major issues of concern all over the world today. The production is not enough to meet the demands of consumers. Under these circumstances the power system should be efficient in Economic Load Dispatch which minimizes the total generating cost. This paper presents a new approach to address practical ED issues. A new approach to the solution of ED using Particle Swarm Optimization has been proposed, and proven by a systematic simulation processes. Through the proposed coding scheme, constraints of ED problems can be effectively released during the search process, therefore, the solution quality, as well as the calculation time, is greatly improved. The proposed approach has been demonstrated by three unit system and proven to have superior features, including high quality solutions, stable convergence characteristics, and good computational efficiency. The generation limits and the demand are considered for practical use in the

proposed method. The encouraging simulation results showed that the proposed method is capable of obtaining more efficient, higher quality solutions for ED problems.

8. REFERENCES

- [1]A. J. Wood and B. F. Wollenberg, *Power Generation, Operation and Control* New York: Wiley, 1984.
- [2] C. L. Chen and C. L. Wang, "Branch-and-bound scheduling for thermal generating units," *IEEE Trans. Energy Convers.* vol. 8, no. 2, pp. 184–189, Jun. 1993.
- [3] K. Y. Lee *et al.*, "Fuel cost minimize at ion for both real- and reactive power dispatches," *Proc. Inst. Elect. Eng., Gen., Trans. Distribute.* vol. 131, no. 3, pp. 85–93, 1984
- [4] Selvakumar I, Dhanushkodi K, Jaya Kumar J, Kumar Charlie Paul C, "Particle Swarm optimization solution to emission and economic dispatch problem", in Conf. Convergent Technologies for Asia-Pacific Region (TENCON-2003), vol.1, pp 435-439.
- [5] Zhao B, Jia Yi Cao, "Multiple objective particle swarm optimization technique for economic load dispatch", Journal of Zhejiang University SCIENCE, 2005 vol-6, pp420-439.
- [6] Park JB, Lee KS, Shin JR, Lee KY., "A particle swarm optimization for economic Dispatch with non-smooth cost functions", IEEE Transaction of Power System; Feb 2005; vol-20, pp34–42.
- [7] Umayal SP, Kamraj N, "Stochastic multi objective short term hydro thermal Scheduling using particle swarm optimization", In: Proceedings of the IEEE Indic on conference; 2005, pp 497–501
- [8] Bo Z, Guo C, Cao Y., "Dynamic economic dispatch in electricity market using Particle swarm optimization Algorithm", In: Proceedings of the 5th world Congress on intelligent control and automation; 2004, pp. 5050–5054.
- [9]In 1995, Eberhart and Kennedy suggested a PSO based on the analogy of swarm of bird and school of fish (J. Kennedy *et al.*, 1995). The PSO mimics the behavior of individuals in a swarm to maximize the survival of the species. In PSO, each individual makes his decision using his own experience together with other individuals' experiences (H. Yoshida *et al.*, 2000).
- [10]The algorithm, which is based on a metaphor of social interaction, searches a space by adjusting the trajectories of moving points in a multidimensional space. The individual particles are drawn stochastically toward the present velocity of each individual, their own previous best performance, and the best previous performance of their neighbors (M. Clerc *et al.*, 2002).
- [11]The practical economic dispatch (ED) problems with valve-point and multi-fuel effects are represented as a non-smooth optimization problem with equality and inequality constraints, and this makes the problem of finding the global optimum difficult. Over the past few Decades, in order to solve this problem, many salient methods have been proposed such as a hierarchical

numerical method (C. E. Lin *et al.*, 1984), dynamic programming (A. J. Wood *et al.*, 1984)

[12] evolutionary programming (Y. M. Park *et al.*, 1998; H. T. Yang *et al.*, 1996; N.Sinba *et al.*, 2003), Tabu search (W. M. Lin *et al.*, 2002), neural network approaches (J. H.Park *et al.*, 1993; K. Y. Lee *et al.*, 1998), differential evolution (L. S. Coelho *et al.*, 2006), particle swarm optimization (J. B. Park *et al.*, 2005; T. A. A. Victoire *et al.*, 2004; T. A. A.Victoire *et al.*, 2005), and genetic algorithm (D. C. Walters *et al.*, 1993).

HIGH EFFICIENT CURRENT CONTROLLED CONVERTER FOR SRM

A.Vivek¹, M R Ancelin Geo²

^avivekarokiya@gmail.com ,ancelingeo@gmail.com

¹P.G Scholar, Department of Electrical and Electronics Engineering, St. Joseph's College of Engineering, Affiliated to Anna University, Chennai-60119.

²P.G Scholar, Department of Electrical and Electronics Engineering, Jeppiaar Engineering College, Affiliated to Anna University, Chennai-60119.

ABSTRACT:

Switched reluctance motor has many types of converters to control its operation. Each and every converter has its own advantages and disadvantages. This paper proposes a current controlled converter with angle control method. The proposed converter has front end switch that controls the current of the phase winding of SRM that reduces the switching loss thereby increases the efficiency of the converter. Also this paper compares the proposed converter with some existing converters such as Classical converter, R-Dump converter, Suppression Resistor converter and Modified C-dump converter. The tabulated results defines the proposed converter has higher efficiency when compared to other existing converters.

Keywords— Switched Reluctance Motor (SRM), Current Source Converter, Torque.

I.INTRODUCTION

The cost of the DC motor is less but it has some limitations to work under high temperature and the generation of copper loss in the rotor resistance leads to affect the efficiency of the motor. On the other hand Permanent Magnet motors has high efficiency but the cost of the motors are high due to the rare earth magnet present in it and it could not operate under high temperature because of the presence of magnet in the rotor part that starts to demagnetize. To attain high efficiency and low cost drive system, SRM is preferred. SRM has many positives that is it can operate under high temperature because it does not have permanent magnet, windings in its rotor and it can rotate at high speed when compared to other motors. SRM has several phase windings which is independent of one another and this makes the SRM as a highly reliable one. But it has some limitations like acoustic noise, torque ripples and vibration. SRM is singly excited doubly salient electric motor that has winding in the stator part alone and not in the rotor part. The number of stator and rotor poles would not be equal because if the number of stator and rotor poles are equal, the rotor poles locked with the stator poles when excitation given causes the

rotor being in the state of producing no initial torque and no further rotation happens in the rotor side. The rotor always tries to get aligned in the minimum reluctance position by rotating along with the rotating magnetic field which is created by the excitation of the stator. Thus the movement of the rotor can be controlled by the excitation given to the phase winding. The excitation to the phase winding can be controlled with the help of converters. By controlling the duty cycle and switching frequency of the switches of the converter, the rotor speed of the motor can be controlled

II.SRM MODELLING

The model of the SRM has to be done only in operational region because the parameters are changing continuously and mathematical model is not consistent over a wide region [4]. The SRM phase voltage equation can be given by

$$V = iR + \frac{d\lambda}{dt} \quad (1)$$

Where, V is the voltage of the DC bus, i is the instantaneous phase current, λ is the flux linkage and R is the resistance of the phase winding. The flux linkage can be given as

$$\lambda = Li \quad (2)$$

By equation (2), equation (1) can be written as

$$V = iR + \frac{d(Li)}{dt} \quad (3)$$

The equation (3) can be expanded as

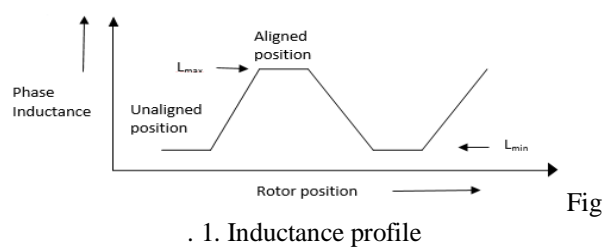
$$V = iR + L \frac{di}{dt} + im\omega \quad (4)$$

Where $m = \frac{dL}{d\theta}$ is the slope represents the inductance change with rotor position, ω is the speed of the rotor, $im\omega$ is the back emf that is generated by the motor action. The plot of phase inductance profile with

angular position is shown in Fig. 1. During the rising inductance region equation (5) defines the variation of inductance with rotor position.

$$L(\theta) = L_u + m\theta \quad (5)$$

Where θ is the angular position of the rotor, $L(\theta)$ is the instantaneous phase inductance. The back emf which is generated by the motor action depends on the sign of slope of the inductance. A positive and useful torque is generated by positive slope which generates positive back emf [6].



The instantaneous torque is proportional to the square of the current and it can be given as:

$$T = \frac{1}{2} i^2 \frac{dL}{d\theta} \quad (6)$$

Because of the current square proportionality the direction of the torque is independent of the polarity of the current flow in the coil. Hence it can be concluded that the sign of the slope of inductance decides the motoring action and the torque.

III. Drive of SRM

SRM needs high performance drive system because it is not a self-commutated motor. The SRM drive consists of a commutation module with a rotor position sensor for sensing the relative position of the rotor which provides the commutation signal for the converter and a converter to deliver controlled power [2]. The SRM drive system is shown in the figure. 2

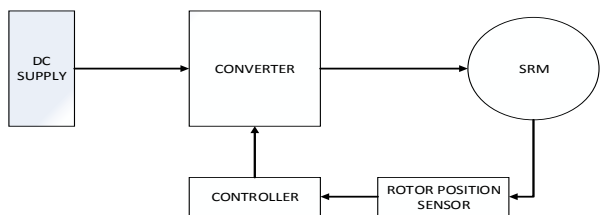


Fig. 2. The SRM drive system

IV. EXISTING CONVERTERS:

A. CLASSICAL CONVERTER:

In order to have a fast built-up of the excitation current, high switching voltage is required; the asymmetric bridge converter is used. Fig.3.1, shows the asymmetric bridge converter for 3-phase SRM drive. The unipolar switching strategy can be achieved by that converter which consists of two power switches and two diodes per phase. In each phase, the upper switch is used to perform the PWM switching control, while the lower one is used in charge of commutation. Each phase can be controlled independently. The three current modes of operation, defined as magnetization, freewheeling, and demagnetization mode.

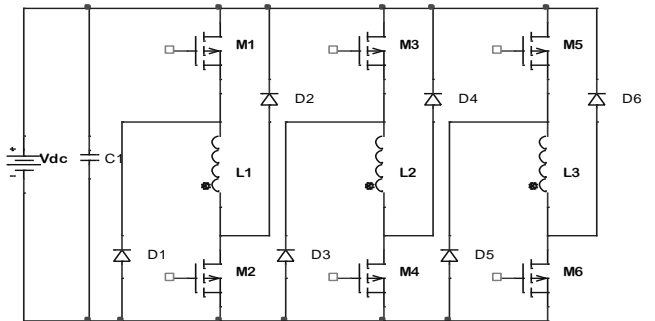


Fig.3.1 Classical converter

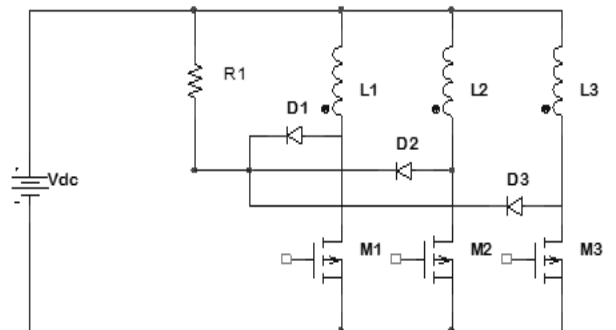


Fig.3.2 Suppression converter

The benefit of using unipolar switching strategy is to obtain less current ripple and a better frequency response in the inner current control loop of the drive system. With the asymmetric converter, the SRM is usually controlled by either current control or voltage control. The main advantage of current control over voltage control is that the phase current can be controlled precisely, which means that torque is properly controlled and the reduction of torque ripple or noise is possible. In the SRM drive system, the current reference value is enforced with a current feedback loop where it is compared with the phase current. At that time the phase diodes complete the path through the dc source. The disadvantages are; one switch is always in the current conduction path, thus increasing the losses in the converter and requiring a larger heat sink for cooling. This would further reduce the system efficiency. Two devices are always in series with the

motor winding, which increases the conduction loss, size of the drive as well as cost increases because three switches and three diodes are used for 3-ph SRM drive.

B.SUPPRESSION RESISTOR CONVERTER:

The complete circuit of the suppression resistor topology is shown in Fig. Since all the switches share a common point, only one power supply is necessary for all the gate drive circuits. When the switch M1 gets turned on, the phase winding starts to magnetize. When the switch M2 gets turned off, demagnetization takes place quick demagnetization takes place because of the suppression resistor and the power dissipated in the suppression resistor leads to affect the efficiency of the converter. But the cost of the converter is too low compared to all the converters.

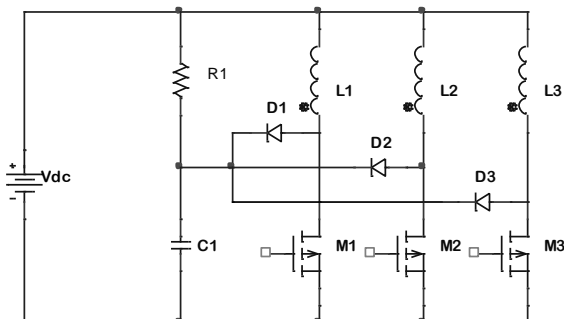


Fig.3.3.R-Dump converter

C.R-DUMP CONVERTER:

The R-dump converter type is shown in Fig. 3.3. It is one of the configurations which have one switch and one diode per phase. When the switch M1 is turned off, the current freewheels through diode D1, charging C1, and later flows through the external resistor R. This resistor partially dissipates the energy stored in the energized phase.

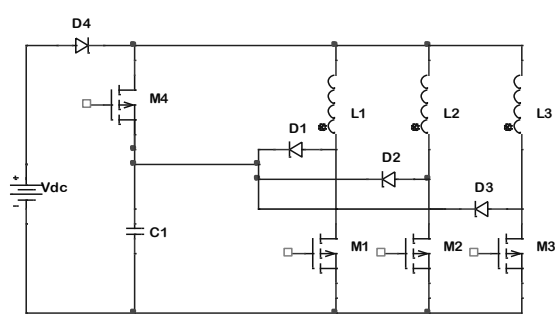


Fig.3.4. Modified C-Dump converter

If the current comes under the negative slope region of the phase inductance, negative torque will be generated, decreasing the average motoring torque. This converter has the disadvantage that the current in any of phases

will take longer to extinguish compared to recharging the source and also the energy is dissipated in a resistor; thus reducing the overall efficiency of the motor drive

D.MODIFIED C-DUMP CONVERTER:

For energizing of the phase winding L1, switch M1 is turned on. When the current of phase winding L1 exceeds a set value, M1 is turned off, then C1 will be charged shown in the fig.3.4. When the voltage of the capacitor C1 exceeds the dc source voltage, M1 conducts and current takes the path of machine phase, diode D1, and M1. When the current in phase A has to be commutated, M1 is turned off without turning on M4 which enables the transfer of the energy from the machine partially to C1 and partially for power conversion in the machine. The energy accumulated in C1 during commutation of phase L1, is used for faster current rise at the time of initiating the current in the next phase. Alternatively, the energy could be used in the latter during rising phase inductance for good current and torque control. The limitations in this converter are; only motoring operation is possible, switching of M4 is very much higher than that of phase switches, control coordination between the freewheeling switch and main phase switches during commutation with overlapping phase currents restricts control flexibility

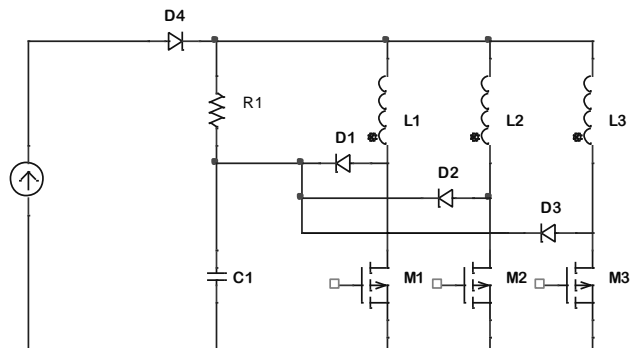


Fig.4.1Proposed Converter

V.PROPOSED CONVERTER:

Generally the gating pulse is generated by the current controller which gets feedback signal from the rotor position sensor. In conventional converters the switches of the phase winding has to switch at very high frequency. But in the proposed converter no need of continuous switching to maintain the current constant in the phase winding because current can be controlled with the help of CSI front end. The proposed converter is shown in the figure 4.1. There are 3 switches M1, M2, M3 for the excitation of the phase windings L1, L2, L3. D1, D2, D3 are the diodes which are used for the demagnetization of the phase windings L1, L2, L3. C1 is the dump capacitor used for the

demagnetising purpose of the phase winding. R1 is the low value resistor that creates path for the capacitor discharge. L4 and M4 is needed to control the current within the allowable limit. The switch L4 gets switched at very high frequency with low duty cycle to control the current flow across the phase winding.

VI.MODES OF OPERATION

Considering the DC supply along with M4 and L4 as current source and the circuit of the proposed converter can be redrawn as the given as the figure 4.2.

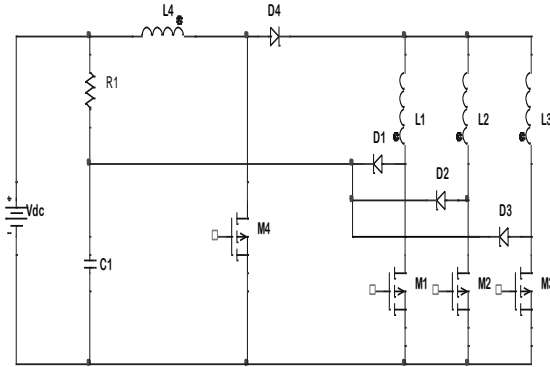


Fig.4.2 Considering current source

A.MODE 1:

Consider M1 is turned on, M3 is just turned off and M2 is in off condition. Initial current is already high due to the current source and this makes low current rising time in the Phase winding L1. The capacitor C1 is in discharging condition, discharges through the resistor for the quick excitation of the next phase. The demagnetization of the phase winding L3 happens through the diode D3 which is in forward biased condition allows the current to the low value resistor R1. The mode 1 can be represented as fig 5.1

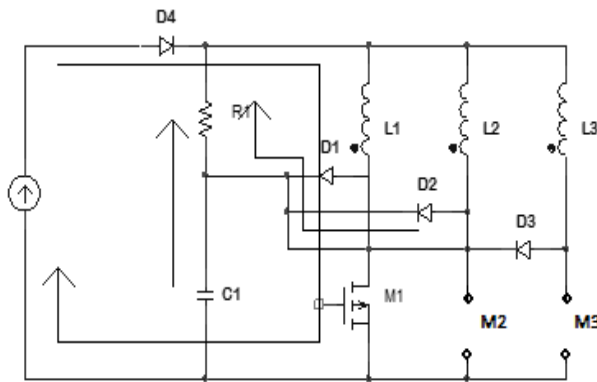


Fig.5.1. Mode 1

B.MODE 2:

Consider M1 is now turned off and Demagnetization of the phase winding L1 happens in

this time through Diode D1. This can be represented in the fig 5.2.The Diode D1 gets forward biased and allows the current to the dump capacitor. The capacitor gets charged in very quick time because of the demagnetizing current of the phase winding L1

C.MODE 3:

The demagnetization of the phase winding continues in this mode also. The capacitor gets discharged in this mode through the low value resistor R1. Since the capacitor voltage is greater than the DC bus voltage, a negative voltage is applied across the phase winding. Therefore, the phase current decreases. When the phase current reaches the minimum current set, mode 1 repeats. At turn-off time, the converter operates in mode 2 until the phase current reaches zero. This can be given as fig 5.3

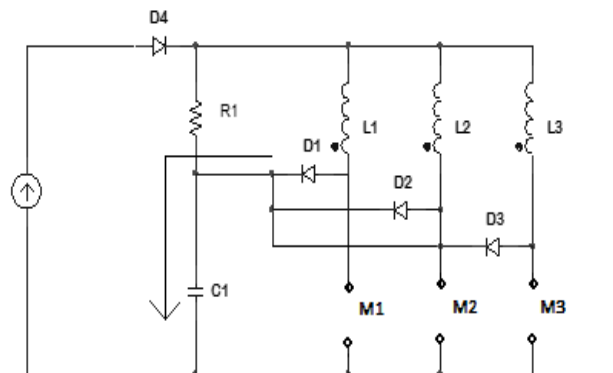


Fig.5.2 Mode 2

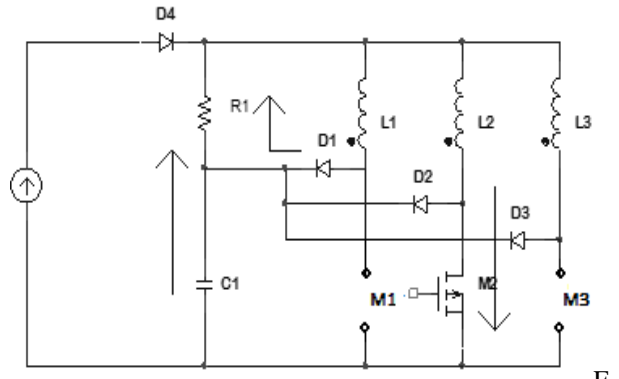


Fig.5.3 Mode 3

D.FORMULAE:

$$\text{Switching loss} = ((V_{in} * I_{out})/2) * (T_{rise} + T_{fall}) * f_{sw}$$

Where,

V_{in} = Input voltage of the converter, I_{out} =Output current of the converter, T_{rise} = Rise Time, T_{fall} = Fall time

f_{sw} = Switching frequency

Conduction loss= $I^2 R$ Where, R = resistance of the switch

Diode loss= $0.7 * \text{area/time}$

Efficiency= $((I/P \text{ power-Losses})/I/P) * 100$

VII.TABULATION

Features	Proposed converter	Suppression resistor converter	Modified C-dump converter	R-Dump converter	Classical converter
Phase Independence	Partial	complete	partial	Partial	complete
Freewheeling	Allowed	allowed	allowed	Allowed	allowed
No. of switches	4	3	4	3	6
Performance	Very good	fair	very good	Fair	very good
Efficiency %	75.8	58.083	68.64	58.33	66.03
Control	Complex	simple	complex	Simple	simple
Efficiency	High	Low	Medium	Low	Medium
Energy	Within the phase winding	Dissipated	Within the phase winding	Dissipated	Back to the source

XIII.SIMULATION OF PROPOSED CONVERTER:

In the simulation of the proposed converter, there is no need of relay block or taking the current as feedback. The required current for the phase winding can be fixed with the help of controlling turn on and turn off angle of the switches. So the position of rotor of the SRM can be sensed by the RPS that generates pulse can be directly send to the gate of the switch of the phase winding. The MATLAB model of the proposed converter is shown in the figure 8.1

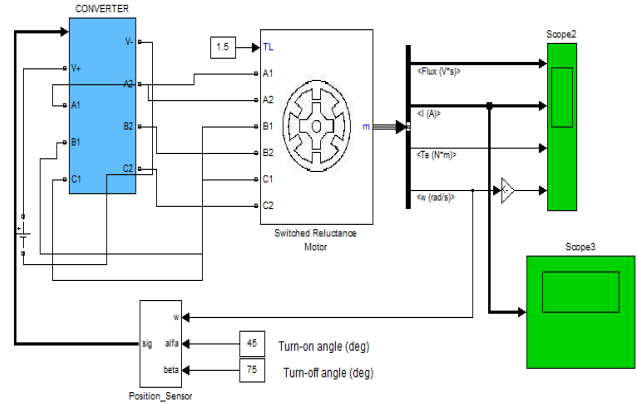


Fig.8.1 MATLAB model for proposed converter

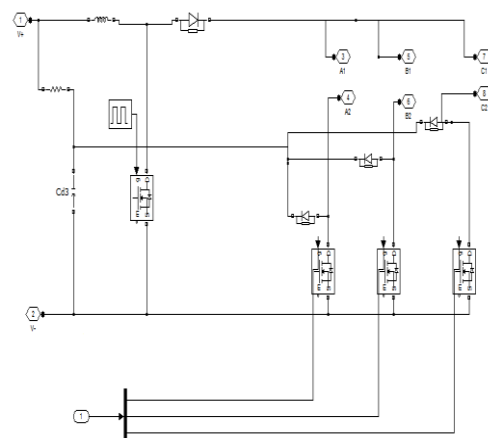


Fig.8.2 Converter part

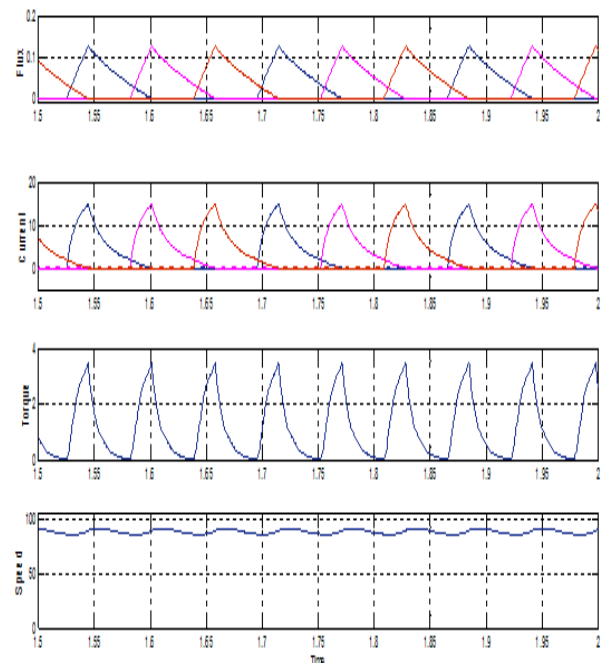


Fig.8.3 Simulation output of the proposed converter

From the simulation result fig 8.3, it is concluded that there is less current ripples when compared to the other converters to realize fast di/dt and small current ripple at the phase winding.it is possible to reduce the number of switching, the square current wave form can increase the effective current and it can also instantaneously shift the current conductive phase without the excessive current. These makes the converter to conclude as high efficient when compared to all other converters. Current control can be done by controlling the turn on and turn off angles of the switches along with the front end switch in the converter with respect to the load torque

For Load torque=1,Conduction angle<11

Average current in phase 1(A)	Turn On angle(α)	Turn off angle(β)	Conduction angle(in degrees)
2.621	55	65	10
2.513	56	65	9
2.273	57	65	8
2.173	58	65	7
1.878	59	65	6

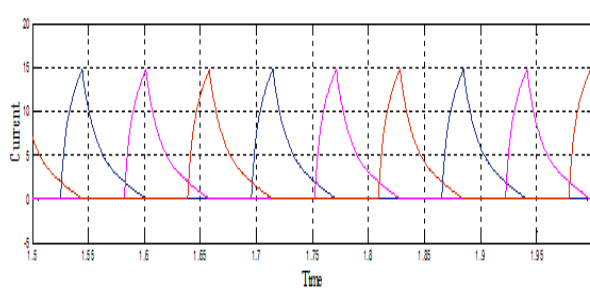
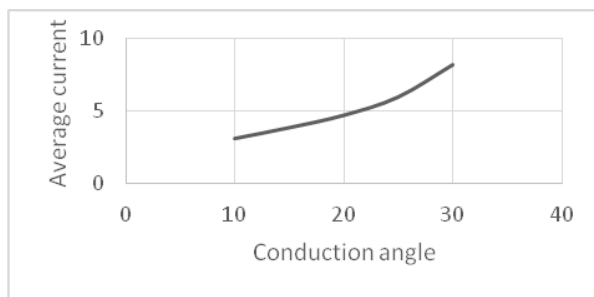


Fig. 8.4.Current waveform

Fig 8.4 shows the current waveform of the proposed converter. To maintain the average current of 2 A in the phase winding for load torque of 1 the turn on and turn off of angle has to be 55 and 65 degrees.Hence the simulation results shows there is no need to implement hysteresis control to maintain constant current, because of this there is no continuous switching hence switching losses are minimized when compared to other existing converters

IX.RESULT:

Hence with the help of the tabulation and simulation results,it is shown that proposed converter has high efficiency and less ripples when compared to the other existing converters that are discussed above. In order to reduce the losses and increase the life time of the converter, the angle control method is discussed. The conduction angle tabulation part shows that the current of the phase winding can be controlled by controlling of the conduction angle.

REFERENCES

- [1] Yolanda Vidal, Leonardo Acho, and FrancescPozo, Robust Control of an Electronic Throttle System Via Switched Chattering Control: Benchmark Experiments: Submitted to IFAC Workshop on Engine and Power train Control, Simulation and Modeling Paris, France (2009).
- [2] Tomohiro Takahashi, Takanori Nagai and KanAkatsu, High Efficiency SRM drive using a Current Source Inverter: Submitted to International Future Energy Electronics Conference, Taiwan (2013).
- [3] T. Nagai, G. Ando, K. Akatsu, Consideration of CSI drive for SRM compared with VSI drive , Power Electronics and Motion Control Conference , Harbin, China (2012) 1087- 1094.
- [4] Abhinav A. Kalamdani, A Novel Solution for Variable Speed Operations of Switched Reluctance Motors, In Proceedings of 13th IEEE Bangalore Section National Symposium on Power Systems, Bangalore, India (2010) 26-27.
- [5] Hiroki Ishikawa, Daohong Wang, and HaruoNaitoh ,A New Switched Reluctance Motor Drive Circuit for Torque Ripple Reduction, Power Conversion Conference, Osaka (2002) 683-688.
- [6] Samia M. Mahmoud, Mohsen Z. El-Sherif, and Emad S. Abdel-Aliem, “Studying Different Types of Power Converters Fed Switched Reluctance Motor” International Journal of Electronics and Electrical Engineering 1 (4) (2013) 281-290.

IMPLEMENTATION OF SINGLE PHASE MATRIX CONVERTER

M.Rajarajan¹, Dr.T.D. Sudhakar², Dr. N. C. Lenin³

1M.E Power system engineering, St. Joseph's college of Engineering, Chennai-119,

2 Associate Professor, St. Joseph's college of Engineering, Chennai-119,

3 Associate professor, Department of E.E.E., Vellore institute of Technology, Chennai,

Corresponding Author Email: er.rajarajan@yahoo.com

Abstract: A single phase matrix converter is implemented and tested with resistive(R) load. The development of force commutated cyclo-converter is termed as "matrix converter". The main advantage of the matrix converter is the elimination of DC link and it is presented in conventional cyclo-converter. A single phase matrix converter topology is designed as frequency changer. A single phase matrix converter has been tested with resistive load. Finally, the analysed converter is tested with a 50 ohms resistive load.

Index terms: Single phase matrix converter (SPMC), Bi-directional switches, pulse generator, sinusoidal pulse width modulation (SPWM),

I INTRODUCTION

The first principle of a matrix converter was published in 1976 by Gyugyi and Pelly. In 1980, the Matrix Converter concept is introduced by Venturini and Alessina in the mathematics form. The single phase matrix converter has proposed to reduce the DC link in the inverter circuit was done by Ziogas and Blaabjerg. All published studies have dealt with three-phase circuit topologies. The Single-phase matrix converter was first realised by Zuckerberg [1]. Divya ahirrao, et.al, proposed about single phase matrix converter performs a function such as frequency changer, rectifier, inverter and chopper [2]. The ac to ac power conversion technique using static circuits can be categorized into two basic schemes i.e. indirect ac / ac power frequency conversion scheme and direct ac/ac power frequency conversion scheme. As the name implies that indirect power conversion scheme consists of two or more stages for convert the ac into desired ac, which also requires dc link. While direct conversion scheme includes single stage ac/ ac power frequency conversion [3].

Basically there are two types of cyclo-converter i.e. Naturally Commutated Cyclo-converter (NCC) and Forced Commutated Cyclo-converter (FCC) [4, 5]. As compared to indirect dc link converter, naturally commutated cyclo-converter has advantages of

lower conduction and commutation losses, due to which it has more compact design and bidirectional power flow capability. It has also some disadvantages i.e. low output frequency upper limit, lower input/output voltage transfer ratio, poor power factor and large number of thyristors, which requires complex control. Due to these restrictions, NCC are restricted up to low speed and high power reversible AC drives. Many NCC limitations can be overcome with FCC by using semiconductor devices with self-turn off capability so it is possible to implement control algorithms, which uses high switching frequency allows output frequency to be higher than input frequency, input power factor as well as input/output voltage transfer ratio must be improved. As compared with indirect ac / ac conversion scheme as well as cyclo-convertisers, matrix converter is capable to perform frequency conversion with sinusoidal output voltages and currents at desired output frequency and it also allows bi-directional power flow [6, 7].

II SINGLE PHASE MATRIX CONVERTER

A single phase matrix converter is defined as input power at a frequency to output power at different frequency. It is a development of force commutated cyclo-converter called matrix converter. Matrix converter is classified in to direct matrix converter and in-direct matrix converter. Direct matrix converter was implemented in this work. It requires bi-directional switches such as IGBT and MOSFET. Figure 2 shows the connection of eight switches of single phase matrix converter. It can be arranged in four units. Each unit has two switches connected in anti-parallel. Forward switches are designated as S1a, S2a, S3a, and S4a. Reverse switches are designated as S1b, S2b, S3b, S4b. It has four modes of operation. Phase delay is important of each switches because, it decides the operation of single phase matrix converter at different frequencies. The phase delay was given by pulse generator and sinusoidal pulse width modulation technique.

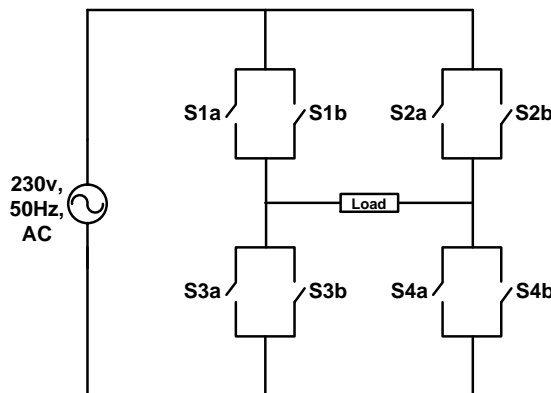


Figure 1. Single phase matrix converter topology

In mode 1, S1a and S4a are switched on and it conducts forward biased [ref fig 2]. In that current form a loop from positive to negative side. This mode is called as positive half-cycle mode.

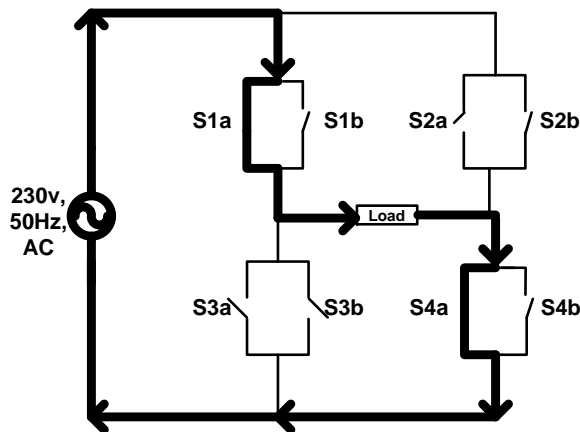


Figure 2. Mode 1 operation of single phase matrix converter
In mode 2, S2a and S3a are switched on and it conducts forward biased [ref fig 3]. In that current form a loop from positive to negative side. This mode is called as positive half-cycle mode.

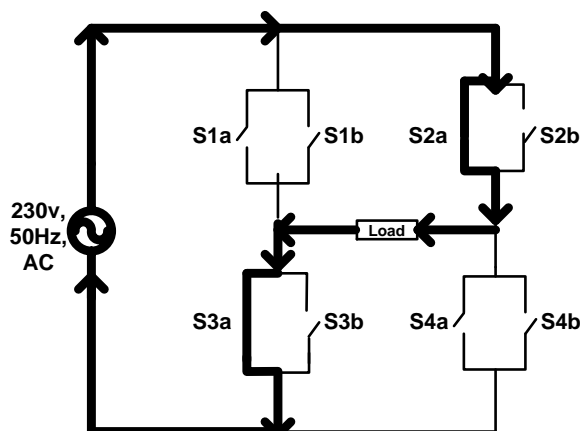


Figure 3. Mode 2 operation of single phase matrix converter

In mode 3, S4b and S1b are switched on and it conducts reverse biased [ref fig 4]. In that current

form a loop from negative to positive side. This mode is called as negative half-cycle mode.

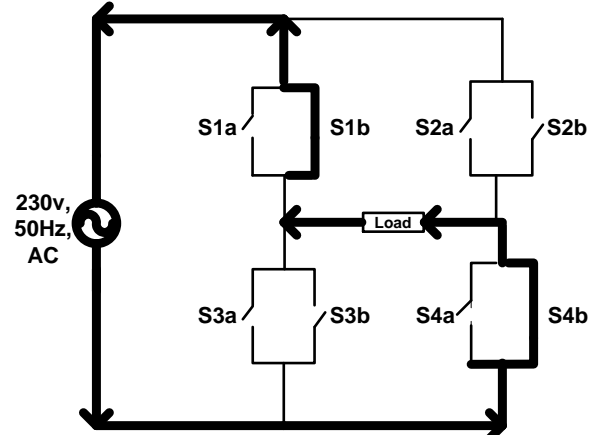


Figure 4. Mode 3 operation of single phase matrix converter
In mode 4, S3b and S2b are switched on and it conducts reverse biased [ref fig 5]. In that current form a loop from negative to positive side. This mode is called as negative half-cycle mode

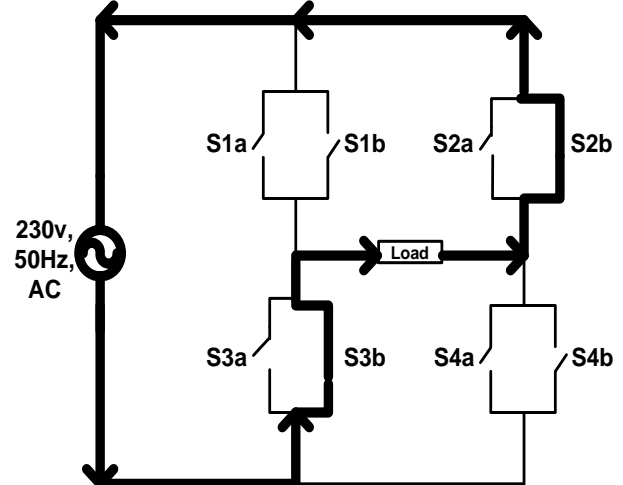


Figure 5. Mode 4 operation of single phase matrix converter

As an example for 230v, 50Hz AC supply to 230v, 50Hz AC supply. It is a direct AC-AC frequency conversion. During positive half-cycle S1a, S4a conducts at a period of 0 to π . This is called positive half-cycle mode. During negative half-cycle S1b, S4b conducts at a period of π to 2π . This is called negative half cycle mode. By using these modes, 50Hz frequency was generated [ref fig 6]. It is possible to attain 25Hz from 50Hz and 100Hz from 50Hz by switching operation.

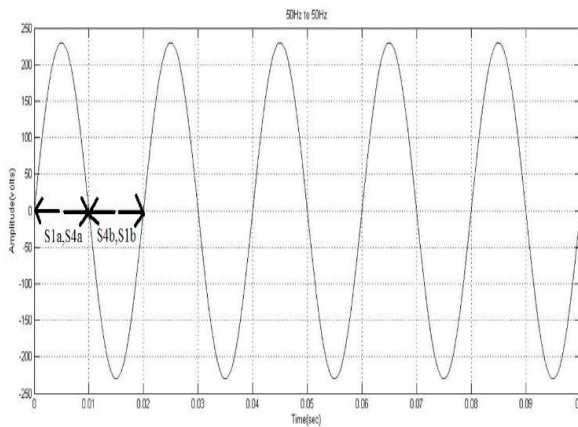


Figure 6. Conversion from 50Hz to 50Hz

III PERFORMANCE PREDICTION

The entire converter is modelled in a simulation platform [ref fig 7]. Three different analysis are carried out. These simulation describes, input at 230v, 50Hz frequency it converts in to output at 230v, 50Hz frequency without the help of DC link. In this resistive load (50 ohms) was used. The switching frequency of this case is 0.02 sec. Here two modes of operation takes place that is positive half-cycle and negative half-cycle mode. Many pulse generators are available such as pwm techniques, space vector modulation etc. In below simulation sinusoidal pulse width modulation and pulse generator was used to give the phase delay. Pulse generators provide a gate signal to S1a and S4b switch. Sinusoidal pulse width modulation provide a gate signal to S1b and S4a switch. During positive half-cycle s1a, s4a conduct from 0 to π . During negative half-cycle s1b, s4b conduct from π to 2π . By using these modes and switching sequence, single phase matrix converter works as direct frequency conversion. By using these modes and switching sequence, single phase matrix converter works step up and step down frequency conversion. The switching sequence are shown in table I.

TABLE: 1 SWITCHING STRATEGY OF SINGLE PHASE MATRIX CONVERTER AS AC-AC CONVERTER

Input frequency	Switching sequence	Designed frequency & Switching period		
		25Hz	50Hz	1000Hz
50Hz	S1a,S4a	0 to π	0 to π	0 to $\frac{\pi}{2}$
	S2a,S3a	2 π to 3 π	-	$\frac{\pi}{2}$ to π
	S3b,S2b	π to 2 π	-	π to $\frac{3\pi}{2}$
	S4b,S1b	3 π to 4 π	π to 2 π	$\frac{3\pi}{2}$ to 2 π

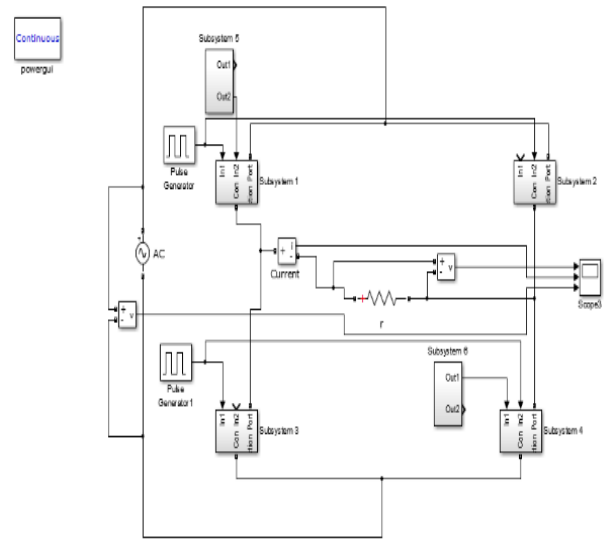


Figure 7. Simulation of single phase matrix converter tested with R-load

In Figure 8 depicts the sub-system having bi-directional switches and the switches S1a and S1b are connected in anti-parallel. The pulse generator to trigger the switch is depicted in fig 9.

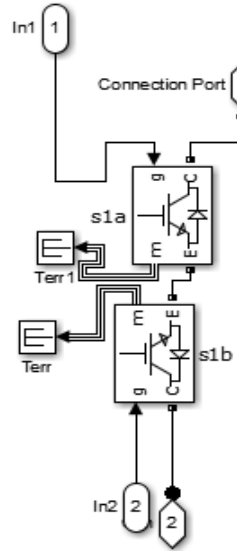


Figure 8. Arrangement of switches in subsystem

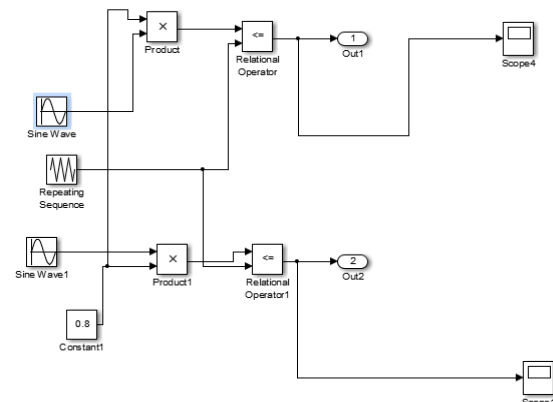
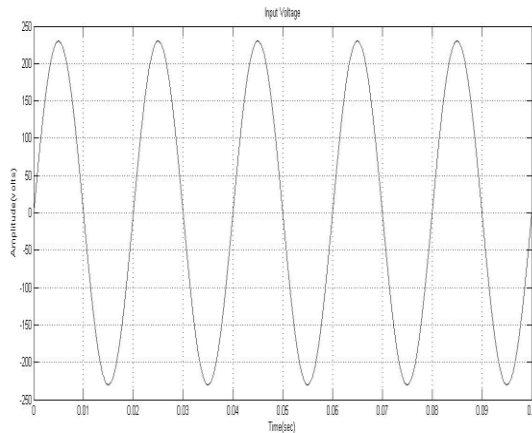
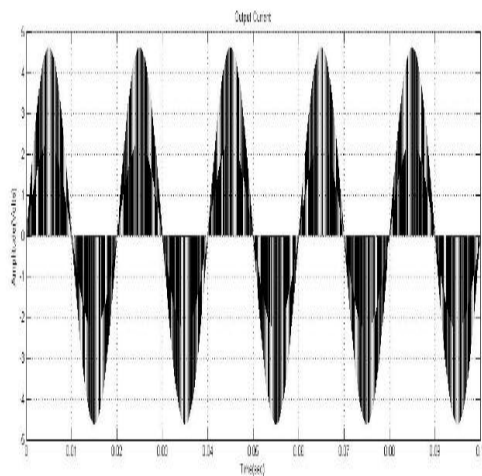


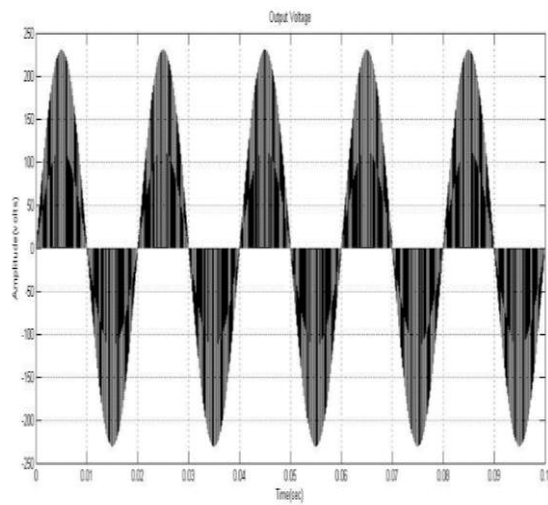
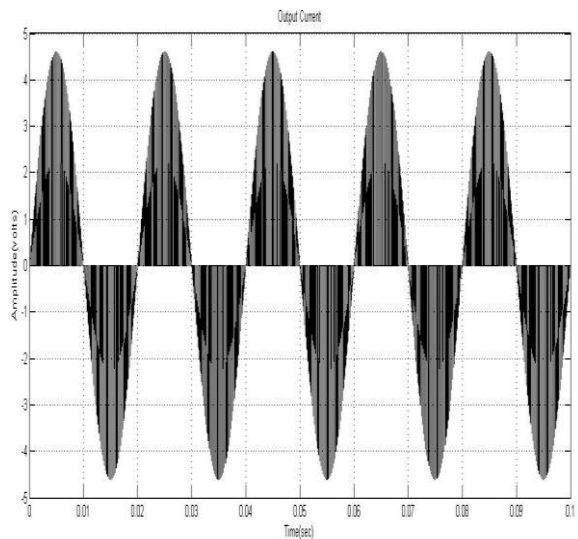
Figure 9. Pulse Generation

V RESULTS AND DISCUSSIONS

In figure 10 depicts the input voltage of the single phase matrix converter. It is 230v, 50Hz AC supply. In fig 11 depicts the input current of the single phase matrix converter. It is 4.6A.

**Figure 10. Input Voltage at 50Hz****Figure 11 Input Current at 50Hz**

In fig 12 depicts the output voltage of the single phase matrix converter. It is 230v, 50Hz AC supply. In fig 13 depicts the output current of the single phase matrix converter. It is 4.6A.

**Figure 12 Output Voltage at 50Hz****Figure 13 Output Current at 50Hz**

V HARDWARE IMPLEMENTATION

AC voltage of 230V is fed to the power supply circuit comprising ICs 7805 and 7812 to obtain required DC output voltages. The 5V DC output voltage obtained from regulator IC 7805 is given to the controller circuit and 12V DC output voltage obtained from regulator IC 7812 is given to the driver circuit. The control circuit comprising of PIC16F877A decides the sequence of pulses to be given to the switches in the power circuit. The driver circuit isolates the input from the output and amplifies the pulses to the required level. The power circuit is an arrangement of eight MOSFET switches (IRF840) with an input AC supply (230V/12V). The gate terminals of the switches are triggered according to the output frequency requirements.

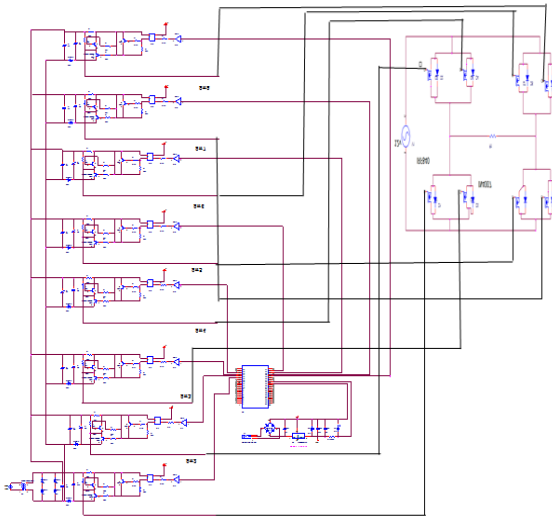


Figure 14. Hardware circuit of single phase matrix converter at 50Hz



Figure 15. Hardware implementation of single phase matrix converter at 50Hz

A single phase matrix converter miniature was implemented using above design. It was designed for 50Hz-50Hz frequency conversion. It was depicted in fig 15.

VI CONCLUSION

A single phase matrix converter has been simulated using MATLAB/SIMULINK and tested with an R-load (50 ohms). The results are verified with the practical case. Although simulation results show that the output voltage is equal to the input voltage (because of ideal case) but in practice the output voltage is always less than the input voltage as experimented from the hardware results.

VII REFERENCES

- [1] A. Zuckerberger, D. Weinstock, and A. Alexandrovitz, "Single-phase Matrix Converter", IEEE Proc.-Electr. Power Appl., vol. 144, No. 4, pp. 235-240., July 1997.

[2] Divya Ahirrao, Bhagyashrigaware, and et.al, "Analysis of single phase matrix converter" Int. Journal of Engineering Research and Applications ISSN: 2248-9622, Vol.4, Issue 3(Version 1), pp.856-861, sept 2014.

[3] L. Hasegawa, T. Takashita, "PWM Strategy of Voltage Harmonics for Matrix Converters", IEEE Proceedings, pp. 668-673.-673 July 2010.

[4] Ebubekir Erdem, Yetkin Tatar, Sedat Sunter, "Effects of Input Filter on Stability of Matrix Converter Using Venturini Modulation Algorithm", International Symposium on Power Electronics, Electrical Drives, Automation and Motion, pp. 1344-1349, Jan 2010.

[5] C. Klumper, P. Nilesan, I. Boldea, F. Blaabjerg, "New steps toward a low-cost power electronic building for matrix converters", In Conf. Rec IEEE-IAS Annu. Meeting, Vol. 3, Rome, Italy, pp. 1964-1971, Oct. 8-12, 2000.

[6] A. Alesina, M. Venturini, "Analysis and Design of optimum amplitude nine switch direct AC-AC converters", IEEE Trans. Power electron. Vol. 4, pp. 101-112, Jan 1989.

[10] P. Ziogas, S. Khan, M. Rashid, "Some improved force commutated cyclo-converters structures", IEEE Trans. Ind Application, Vol. IA-21, pp. 1242-1253, Sept/Oct. 1985.

Load Based Pricing in Demand Side Management through Ant Colony Optimization

N.Ayswarya,
PG Scholar, Department of EEE,
K. S. Rangasamy College of Technology,
Tiruchengode, Namakkal, 9566717459
ayswaryanagu@gmail.com

S.Devi, M.E., (Ph.D)
Associate Professor, Department of EEE,
K.S.Rangasamy College of Technology,
Tiruchengode, Namakkal.
Tiruchengode, India

Abstract-To meet the fast growing demand of energy, smart techniques need to be adopted that are in compliance with the environment and energy conservation. An autonomous demand-side energy management is implemented to modify the electricity consumption pattern. In this paper, an important tool called load factor is discussed. Load factors are an important simplification of electrical energy use data and depend on the ratio of average demand to peak demand. The operating time of different labs and cost are analysed and it is optimized through ant colony. Simulation results shows that the proposed approach can maximize load factor.

Keywords—Demand Side Management (DSM), Ant Colony Optimization (ACO), load factor.

I. INTRODUCTION

In the fabric of liberalized electricity market, there is a need for sustainable environment with adoption and implementation of energy efficient resources. Evolution of smart grid has provided a breakthrough in the existing power system in order to maintain a reliable, uninterrupted and secure infrastructure. However, in order to keep pace with the modern challenges of meeting dynamic electricity demand, techniques like advancement in automation, data communication and distributed generation have been effectively deployed to accommodate suppliers and consumers from a wide range of scenarios, to anticipate and respond to changing operating conditions with greater economic efficiency and energy usage. Demand side management (DSM) proves advantageous and economically viable for strategically and intelligently influencing the load instead of investing money on setting up a new power generating unit [2].

DSM is nothing but actions carried out by the utility on the customer's premises that help manage the customer's electrical usage to modify energy use patterns including electricity demand timing or amount of demand and to encourage actions by the customer to modify the electrical usage to meet some goal, usually a reduction in electricity cost. DSM primarily includes different pricing methods adopted by utilities to ensure efficient network utilization. Different pricing methods commonly used by utilities are: flat-rate method, TOU (time of use) method and load based methods. Time of use tariffs and flat rates techniques are used less as they may not necessarily cut down the peak of energy usage but would adversely create a steep rise in off-peak hours. Consequently, demand response programs were introduced which are based on load based pricing instead of time base, i.e., electricity tariffs vary proportionally to the power system load as specified in the desired function.

It does not necessarily reduce energy consumption but influences the consumption pattern [9]. Appropriate load shifting becomes a cause of major concern as PHEVs (plug-in hybrid electric vehicles) come into picture due to their high charging rate. They acts as a significant load on existing distribution system, deteriorating the load factor accordingly and thus causing degradation of power quality, fluctuation in system frequency and voltage, sufficient loss to the utility and consumer and thereby creating imbalance in the power distribution system.

In order to maintain a balance between demand and supply to certain extent, dynamic load control (DLC) strategy was adopted [2], where in accordance to the contractual arrangement, the utility can remotely control the operations on certain priority-specified household appliances. Consumer privacy is considered bottle-neck for this method.

With limitations of other pricing methods and improvements in smart metering technologies, load-based pricing are becoming more popular and imperative. Different pricing methods have been studied in literature. For instance, day ahead pricing method is adopted to provide assistance to retail providers or DISCOMs (DIStribution COMpanies) [4]. Locational-pricing method, take into account use-of-system charges and connection charges [4]. Other methods use price-prediction filters to achieve both lesser cost and better peak-to-average ratio [1].

Here data were taken from college and load factor is analyzed for electrical block. Individual power consumption of four different labs along with cost function is calculated and optimized through ant colony (ACO) and finally an improvement in load factor is attained. The rest of the paper is organized as follows. System model used for problem formulation is presented in Section II. Section III Load Factor Maximization. Simulation results are presented in Section IV. The paper is concluded along with future works in Section V.

II SYSTEM MODEL

Load factor of consumer is defined as ratio of average energy consumption over a period to peak energy consumption of consumer in that period. Electrical energy supply cost is largely depended on load factor. Higher the value of load factor lower will be the overall cost per unit generated. In order to find the peak consumption, readings were noted for every one hour and it is analyzed. The load data of one block and the power consumption of individual lab is given in TABLE I and II.

TABLE I. LOAD DATA

HOUR	CURRENT in AMPERE				
	MON	TUE	WED	THU	FRI
9.00 AM	20	29	25	30	18
10.30 AM	41	33	57	54	38
11.30 AM	54	43	53	52	58
12.30 PM	41	48	35	53	55
1.30 PM	45	35	62	38	59
2.30 PM	59	47	78	60	60
3.30 PM	63	68	85	79	67

TABLE II POWER CONSUMPTION/DAY

NAME OF THE LAB	POWER in KW									
	MON		TUE		WED		THU		FRI	
	FN	AN	FN	AN	FN	AN	FN	AN	FN	AN
MAC	3.3	4.6	3.2	4.8	3.2	4.6	3.3	4.6	3.3	4.6
PE	-	3.8	3.8	-	3.8	3.8	3.8	3.8	3.8	3.8
M & I	-	-	2.6	-	2.6	-	2.6	2.6	2.6	2.6
EDC	2.5	2.5	2.5	2.5	-	-	-	2.5	2.5	-

From the load data, the load factor can be calculated based on the following formula.

$$\text{Average Consumption} = \frac{\sum_{i=1}^{1=N} \sum_{h=1}^{h=T} (wih) * th}{\sum_{j=1}^{j=T} tj} \quad (1)$$

$$\text{Load Factor} = \frac{\text{Average Consumption}}{E_{\max}} \quad (2)$$

Here w_i^h = load of the i_{th} lab in h_{th} time interval

t_h = h_{th} time interval

No of lab = 04

Time interval = 2.30 hr.

By applying equations 1 and 2, average consumption and load factor can be calculated. The load factor for the individual day is given below.

Average Consumption = 3.4 kW

Peak Consumption = 4.6 kW

Load factor = 73%

Therefore the load factor for Monday is 73% and for Tuesday, Thursday, Friday is 71% and for Wednesday is 77%.

III LOAD FACTOR MAXIMIZATION

The objective of optimization problem is load factor maximization. Load factor maximization objective can be written as

$$\max \frac{\left(\sum_{i=1}^{i=N} \sum_{h=1}^{h=T} (wih) * th \right)}{\left(\max(wih * th) \right) \left(\sum_{j=1}^{j=T} tj \right)}$$

Load factor can be maximized by reducing the peak consumption. From the load data, it is clear that the peak consumption is during at noon hours. The labs which are operating at noon period can be shifted to morning hours. By shifting, we can achieve a constant load profile and maximum load factor. The power and the corresponding cost for individual lab is given in TABLE III.

TABLE III. POWER CONSUMPTION/MONTH

NAME OF THE LAB	UNITS CONSUMED/MONTH	RUPEES/MONTH
AC MAC	160	1040
PE	124	806
M&I	64	416
EDC	60	390
OTHER LAB	140	910

After the operating time of lab, load factor is maximized. The calculation is given below.

Average Consumption = 2.52 kW

Peak Consumption = 3.32 kW

Load factor = 77%

Load factor after shifting the lab is 77% for Monday , 76% for Tuesday and 79% for Wednesday, Thursday and Friday. The comparison table is given in TABLE IV.

TABLE IV. COMPARISON OF LOAD FACTOR

DAY	LOAD FACTOR BEFORE SHIFTING	LOAD FACTOR AFTER SHIFTING
MONDAY	73%	77%
TUESDAY	72%	76%
WEDNESDAY	77%	79%
THURSDAY	71%	79%
FRIDAY	71%	79%

IV SIMULATION RESULTS

The load data which is given in table I is examined to find out the peak consumption. The graph is shown in figure.

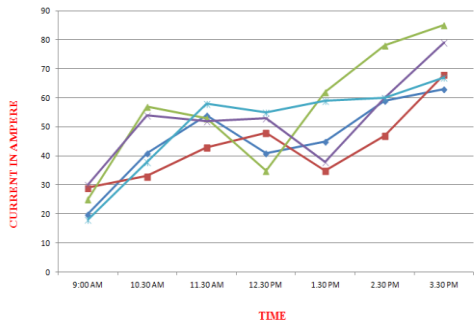


Fig. 1. Load Profile

Figure 1 shows load profile of one particular block. Here minimum power consumption at 9.00 AM and maximum consumption at 3.30 PM. It is mainly due to lab which is running at afternoon hours. It can be shifted to morning hours to make the load profile constant. Load factor before shifting the operating time of lab is given in figure 2.

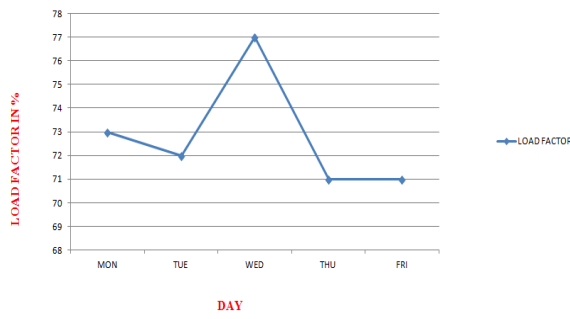


Fig. 2. Load Factor before Shifting

Load factor before shifting the operating time of lab is given in figure 2. X axis represents day and Y axis represents the load factor. Load factor after shifting is given in figure 3.

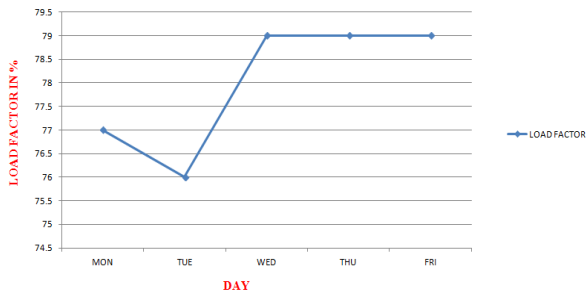


Fig. 3. Load Factor after Shifting

Figure 3 shows the load factor after shifting the operating time of lab. There is an increase in % of load factor for Wednesday, Thursday and Friday. The comparison graph is shown in figure 4.

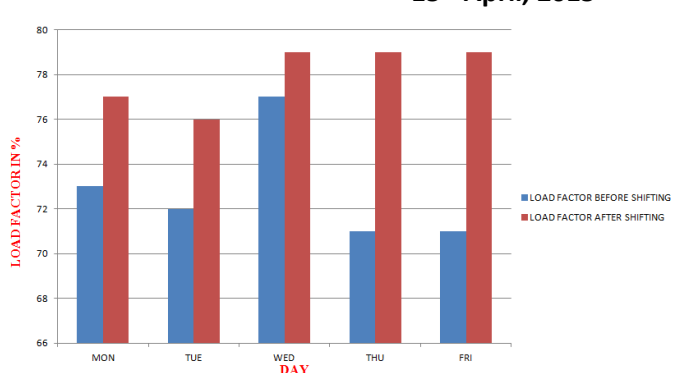


Fig .4. Comparison of Load factor

Load factor comparison before shifting and after shifting is given in figure 4. Red line represents the actual load factor and blue line represents after changing the operating time. It is clearly evident that the load factor is maximized by reducing the peak consumption. Load factor of individual day is increased and it leads to improvement in overall load factor.

V CONCLUSION

Demand Side Management (DSM) is a portfolio of measures to improve the energy system at the side of consumption. It ranges from improving energy efficiency by using better materials, over smart energy tariffs with incentives for certain consumption patterns. This paper presents a new approach to ensure improvement of overall load factor. Here Energy management method is proposed and is implemented in electrical block to improve the load factor and thus it is achieved.

REFERENCES

- [1] Amir-Hamed Mohsenian-Rad, and Alberto Leon Garcia, (2010) "Optimal Residential Load Control With Price Prediction in Real-Time Electricity Pricing Environments", IEEE Transactions on Smart Grid, Vol. 1,no. 2, pp.120-133.
- [2] Amir-Hamed Mohsenian-Rad, Vincent W. S. Wong, Juri Jatskevich, Robert Schober, and Alberto Leon-Garcia,(2010) "Autonomous Demand-Side Management Based on Game-Theoretic Energy Consumption Scheduling for the Future Smart Grid" IEEE Transactions On Smart Grid, Vol. 1, no. 3, pp.320-331.
- [3] Badri Ramanathan, and Vijay Vittal, (2008)"A Framework for Evaluation of Advanced Direct Load Control With Minimum Disruption", IEEE Transactions on Power Systems,Vol. 23,no. 4,pp.1681-1688.
- [4] Christine Brandstatt, Gert Brunekreeft, and Nele Friedrichsen, (2011) "Locational signals to reduce network investments in smart distribution grids", Elsevier,pp.244-254.
- [5] Gomes.A, C. H. Antunes, and A. G. Martins,(2007) "A Multiple Objective Approach to Direct Load Control Using an Interactive Evolutionary Algorithm", IEEE Transactions On Power Systems, Vol. 22, no. 3, pp.1004-1011.
- [6] Kittipong Methaprayoon, Wei-Jen Lee, Sothaya Rasmiddatta, James R. Liao, and Richard J. Ross,(2007) "Multistage Artificial Neural Network Short-Term Load Forecasting Engine With Front-End Weather Forecast", IEEE Transactions On Industry Applications, Vol. 43, no. 6, pp.1410-1416.

- [7] Leehter Yao, Wen-Chi Chang, and Rong-Liang Yen,(2005) “An Iterative Deepening Genetic Algorithm for Scheduling of Direct Load Control”, IEEE Transactions on Power Systems, Vol. 20, no. 3, pp.1414-1421.
- [8] Meysam Doostizadeh, and Hassan Ghasemi,(2012) “A day-ahead electricity pricing model based on smart metering and demand-side management”, Elsevier, pp.221-230.
- [9] Peter Palensky, and Dietmar Dietrich,(2011) “Demand Side Management: Demand Response, Intelligent Energy Systems, and Smart Loads”, IEEE Transactions on Industrial Informatics, Vol. 7, no. 3, pp.381-388.
- [10] Wolfgang Granzer, Fritz Praus, and Wolfgang Kastner,(2010) “Security in Building Automation Systems”, IEEE Transactions on Industrial Electronics, Vol. 57, no. 11, pp.3622-3630.

MAXIMUM POWER TRACKING IN SOLAR SYSTEM IN UNCERTAIN ENVIRONMENT USING ROBUST OPTIMIZATION

K.Dinesh., PG Scholar

*Department of Electrical and Electronics Engineering
KSR College of Technology
Tiruchengode, India, 9787628890
kdineshshankar@gmail.com*

D.Sri Vidhya, M.E., Assistant Professor

*Department of Electrical and Electronics Engineering
KSR College of Technology
Tiruchengode, India
vidhayasriramesh@gmail.com*

Abstract—The renewable energy sources are the future power source for power generation sources but the sudden changes in environment changes are uncertain so the power generation varies. To avoid the generation changes due to nonlinear weather condition, the peak operating condition of its primary energy source by the mean of a Maximum Power Point Tracking (MPPT) to extract the maximum power. Therefore MPPT controller is necessary for uncertain weather in order to improve the output power. Several MPPT power-converters and different types of control techniques have been considered in the past. This paper mainly considers the MPPT power-converter control algorithm which is robust optimization to track the maximum power point in PV panel. The proposed method has been evaluated by simulation using MATLAB under different insolation, or sunlight concentration levels. The obtained result demonstrates the effectiveness of the proposed technique and its capability for practical and efficient tracking of maximum power.

Index Terms— Maximum Power Point Tracking (MPPT), Photovoltaic (PV), Robust Optimization

I. INTRODUCTION

The term distributed generation refers to the production of electricity near the load. The distributed Generation resources are renewable energies and cogeneration (simultaneous production of heat and electricity). Fossil fuels continue to be depleted, and their use has been instrumental to climate change, a problem that grows more austere each year. Renewable energy is energy from natural resources such as wind, sunlight, tides, waves,

geothermal heat and biomass. A photovoltaic (PV) power generation system, which uses a renewable resource, has been extensively used in emergency facilities and in generating electricity for mass use. Due to hurried growth in the semiconductor and power electronics techniques, PV energy is of growing interest in electrical power applications. It is important to operate PV energy exchange systems near the maximum power point to increase the output efficiency of PV arrays. Therefore, many techniques have been developed to provide utmost PV power. Some researchers control photovoltaic features to match load conditions. Some systems use an online maximum power point tracking (MPPT) algorithm to obtain the maximum power point. An MPPT method often used is the perturbation and observation method because the method is easy to implement. However, oscillation is unavoidable. The incremental conductance method is used to avoid oscillation by comparing the incremental and instantaneous conductance of the PV array, but the implemented circuit is more complex. FLC have the advantages of working with imprecise inputs, not needing an accurate mathematical model and handling nonlinearity. Therefore, FLC-based MPPT method performs well under varying weather conditions. Conventionally, PV energy conversion systems are composed of a dc/dc converter, a dc/ac inverter, batteries, and a center-tapped output transformer. By controlling the duty cycle, the designed controller can match the load to the PV array under various atmospheric conditions. By applying the proposed approach to a small-scale PV conversion system, the tests show the computational efficiency and a reduction in tracking time.

II. TRACKING OF MAXIMUM POWER POINT

Given the high cost and limited efficiency of photovoltaic systems, it is highly desirable that strategies for maximum power point tracking (MPPT) be implemented that allow the PV array to deliver near maximum power. The operating point (V_{mpp} , I_{mpp}) at which maximum power is obtained changes substantially with varying temperature and irradiance conditions, which can vary drastically in a typical day making it imperative for the MPP tracking strategy to be able to keep up with rapidly changing atmospheric conditions.

A. Effects of Changing Irradiance and Temperature on MPP

Changing irradiance has a major effect on PV current, but a relatively more subtle effect on voltage. The change in PV short-circuit current I_{sc} is modeled simply as

$$I_{sc}(G) = I_{sc} \times (G/G_{STC}) \quad (1)$$

Where G is the irradiance and G_{STC} is the irradiance at standard test conditions, defined as 1000W/m^2 of irradiance and a temperature of 298K . The relation between open-circuit voltage, V_{oc} , and G is slightly more complex and can be obtained. V_{oc} and V_{MPP} are far less sensitive to irradiance changes than I_{sc} and I_{MPP} respectively. The effects of temperature and irradiance changing simultaneously can result in an exacerbated level of shifting of the maximum power point.

B. Methods for MPP Tracking

MPP tracking methods vary from extremely simple implementations that fix module voltage at a certain proportion of the PV open-circuit voltage to more elaborate methods using Robust PID controllers. It must be noted that the high cost of PV power coupled with the limited efficiency, as mentioned earlier, makes it crucial that the maximum power be eked out of any PV-based setup, rendering a number of existing strategies for MPP tracking suboptimal. Perturb and Observe (P&O) is the most commonly used method in commercial MPP trackers. Despite its simplicity, perturb and observe algorithm is extremely competitive when compared to other algorithms, and can provide nearly as much efficiency for MPP tracking as the slightly more complex method of Incremental Conductance. However, as will be seen below, the basic P&O strategy suffers from high oscillations due to fast changing environmental conditions.

III. PROPOSED MPPT ALGORITHM

The power of PV panel depends on voltage and current. The voltage varies depending on variable weather conditions. So a Solar charge controller is necessary to increase the efficiency of PV panel. PWM is one of the two key algorithms used in photovoltaic solar battery chargers, the other being MPPT. Drawback of this technique is the power drawn by the load is not constant but rather discontinuous. Problem of PWM is overcome by MPPT, which is capable of tracking higher voltage and down converting to a lower voltage. An MPPT method affords better response and is able to produce optimum electrical power under changing weather conditions. MPPT makes adjustments in the charge or voltage for the higher output of the panels. Since optimum array voltage is non-linearly related to solar insolation, the linear approximation techniques are not suitable. Under these circumstances, the Robust PID controller provides viable solution for the online estimation for different insolation.

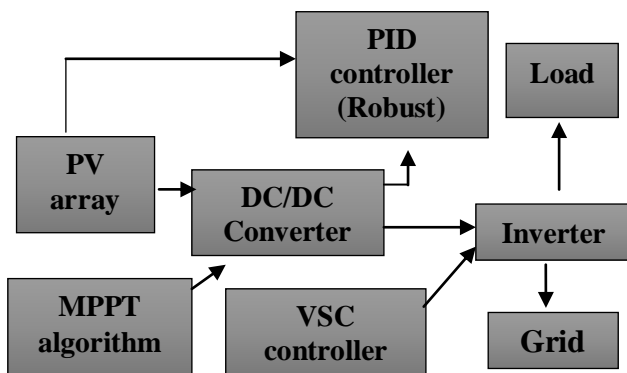
A. Robust PID controller

The Robust Optimization is the method of technique to optimize the maximum efficiency in the uncertainty in environment. The sun radiation is unpredictable so the PV panel voltage generation will change. The system output is always oscillated so the grid connected system is affected seriously. To avoid the oscillation MPPT controller is used. The generated output is specified to the boost converter to step up the input voltage. In uncertain whether condition the generated output voltage oscillation is reduced by the Robust PID controller. The maximum and minimum value of voltage is given as reference values. Then reference voltage is compared to the getting voltage and error signal is generated, then error is given as input to the signal generator. So the controller always control the boost converter depends on error value. The output is maintained constant.

IV. BLOCK DIAGRAM

The power generated from PV array using maximum power point optimization technique. The maximum power can be generated by controlling the dc-dc converter. The output of converter is given to inverter to change dc to ac and supplied to local loads. The grid voltage and current can be taken as reference and given to voltage source controller to produce signals to control the inverter voltage in case to synchronize with the grid. PID controller is to

calculate the error signals and makes the error zero to interconnect with the grid.



V. SIMULATION RESULTS

The PV array can always obtain the maximum output power from the PV during different irradiance levels. The output power of the PV is more than the demand of the islanded mode; the excess power is transferred to the main grid. At the same time, the utility grid also provides power to the ac loads.

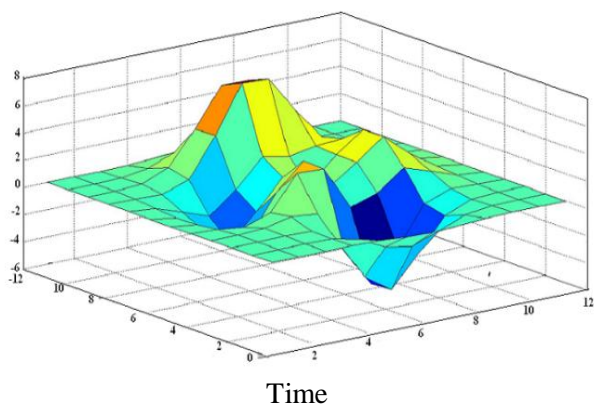


Fig 1 Tracking Time of MPP

It shows that the tracking time is between 5ms-12ms and it is more efficient than the conventional methods. The tracking time can be calculated by time taken for the 100 lines of program to complete compiling.

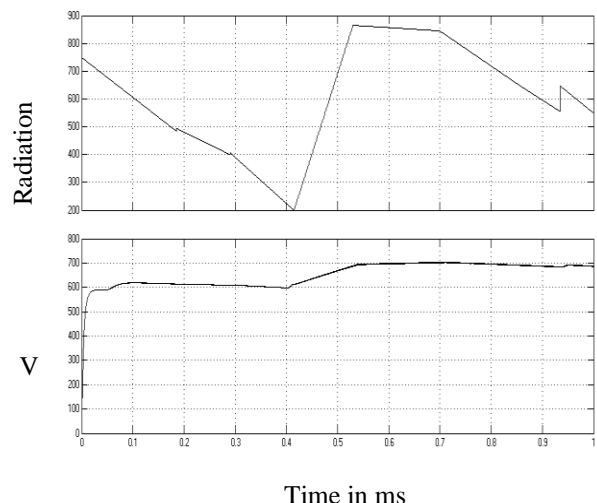


Fig 2 pv1 voltage and current at 1000 irradiance level,
pv1 power at 1000 irradiance level

Fig 2 pv1 voltage and current at 1000 irradiance level, pv1 power at 1000 irradiance level. From the above figure of PV voltage and current graph at 1000 irradiance the voltage obtained is 320 volts and current is 200 amps and hence the power obtained is 40KW.

VI. CONCLUSION

Robust PID controller is proposed for tracking maximum power from the PV array. It integrates the multiple power sources thus enhancing the reliability of power supply. Under stable and varying atmospheric conditions, the proposed technique reduces the tracking time (5ms-12ms) to less than that required by traditional methods. The grid synchronized system stability is the main part of power system stability. So the grid synchronized PV system operated under various radiation condition the output is maintained constant.

REFERENCES

- [1] Aymen Chaouachi, Rashad M. Kamel, Ken Nagasaka,(2010)“ Microgrid Efficiency enhancement based on neuro-fuzzy Mppt control for photovoltaic generator”, IEEE Transactions.
- [2] Jia-Wei Huang, Chun-Liang Liu, Rong Ceng Leou, Yi-Hua Liu,(2011)“ Design and Implementation of a FLC-Based MPPT Technique for Photovoltaic Systems”, IEEE Transactions.
- [3] Himanshu Kumar, and Dr. R.K. Tripathi,(2012)“ Simulation of Variable Incremental Conductance

- Method with Direct Control Method Using Boost Converter”, IEEE Transactions.
- [4] Hiroaki Kakigano, Yushi Miura, and Toshifumi Ise,(2010)“ Low-Voltage Bipolar-Type DC Microgrid for Super High Quality Distribution”, IEEE Transactions on Power Electronics, vol. 25, no. 12, December 2010.
- [5] Lian ,J. H. Jhang, and I. S. Tian,(2014)“ A Maximum Power Point Tracking Method Based on Perturb-and-Observe Combined With Particle Swarm Optimization”, IEEE Journal of Photo Voltaics, vol. 4, no. 2.
- [6] Liang-Rui Chen ,Chih-Hui Tsai, Yuan-Li Lin, and Yen-Shin Lai,(2010) “A Biological Swarm Chasing Algorithm for Tracking the PV Maximum Power Point”, IEEE transactions on Energy Conversion, vol. 25, no. 2.
- [7] A. Mellit, A. Hadj Arab, N. Khorissi, and H. Salhi,(2007) “An ANFIS-based Forecasting for Solar Radiation Data from Sunshine Duration and Ambient Temperature”, IEEE transactions.
- [8] Paloma Sodhi, Dhruv Kapoor, Mahesh S. Illindala,(2012) “An Enhanced MPPT Strategy for a Grid-Connected PV Station under Rapidly Varying Environmental Conditions”, IEEE International Conference on Power Electronics, Drives and Energy systems.
- [9] Piegari, Rizzo,(2010)“ Adaptive perturb and observe algorithm for photovoltaic maximum power point tracking”, IET Renew. Power Generation., Vol. 4, Iss. 4, pp. 317–328 317 doi: 10.1049/iet-rpg.2009.0006
- [10] Swagatam Das, Arijit Biswas, Sambarta Dasgupta, and Ajith Abraham,“ Bacterial Foraging Optimization Algorithm: Theoretical Foundations, Analysis, and Applications”.
- [11] Yuansheng Xiong, Suxiang Qian, Jianming Xu,(2012) “Single-phase grid-connected photovoltaic system based on boost inverter”, IEEE Transactions.

Minimization of Load Forecast Uncertainty for Reliable Supply

C Arunachalam¹, V Uma²

¹arunachalam622@gmail.com²umafuji2007@gmail.com

¹PG Scholar, Department of Electrical and Electronics Engineering, St.Joseph's College of Engineering, Affiliated to Anna University, Chennai – 600119.

²Associate Professor, Department of Electrical and Electronics Engineering, St.joseph's College of Engineering, Affiliated to Anna University, Chennai – 600119.

ABSTRACT:

Load forecasting is a technique used to predict the future electrical power demand. If power generation is not enough to fulfil the demand, there would be irregular supply to consumer and in case of excess generation, leads to wastage of electrical power. The load prediction period may be a month or few years for the medium and long term forecast and an hour or few day for short term forecast. The medium term and long term forecast is used to determine the capacity of power plant, transmission system or distribution system which is need in future, also maybe for further expansion of power plant. The short term forecast is used to predict next hour or next day load. The load has two patterns, weekday and weekend-day pattern. Here Neural Network technique is used to minimize the load forecast uncertainty. Inputs to the ANN is past load data, weather information and seasonality, and output of ANN is forecasted load for given day. This paper presents a study of short-term hourly load forecasting using Artificial Neural Networks (ANNs). To demonstrate the effectiveness of the proposed approach, publicly available data from the isone website has been taken to forecast the hourly load. With the help of ANN we minimized the Mean Absolute Percentage Error.

INTRODUCTION:

Electrical energy is an essential for the industrial and development of any country. It is generated centrally in large and transmitted economically over long distances. Electrical energy is conserved at every step in the process of Generation, Transmission, Distribution and utilization of electrical energy. The electrical utility industry is probably the largest and most complex industry in the world and hence very complex and challenging problems to be handled by power engineering. Electrical load forecasting is an important tool used to ensure that the energy supplied by utilities meets the loads plus the energy lost in the system. To this end, a staff of trained person is needed to carry out this specialized function. Load forecasting is always defined as art of predicting the future demand in particular system, for a certain period of time ahead. These predictions may be an hour or as much as 20 years into the future for planning purposes. It is well known that the electric load is a dynamic one and does not have a precise value from one hour to another. Load forecasting is classified into three major categories. They are long-term forecasting, medium-term forecasting, short-term forecasting [1].

CONVENTIONAL METHODS OF LOAD FORECASTING:

In the past few years, many approaches for load forecasting have been proposed. These can generally be classified into four categories, i.e., time series approach, linear and nonlinear regression approach, and neural network approach [1]-[4]. As we know, the power consumption of each country heavily depends on its economic structure, life style, geographical characteristics, and so on, therefore, no prediction technique can be claimed as the best method in the area of power forecasting. But neural network has been widely applied in this area based on its powerful nonlinear modeling capability and portability for utility companies in different locations.

TIME SERIES MODEL - The most fundamental time series models are auto-regressive model (AR) and auto-regressive moving average model (ARMA). In AR model, the desired forecasting load value is generally expressed as a linear combination of n previous load values and a noise term. In the ARMA model, the forecasting load value is generally expressed as a linear combination of n previous load values and m previous noise terms. However, the weather information is not taken into account in most of AR and ARMA models. These models may have some problems when there is a sudden change in weather.

REGRESSION MODEL - The designing procedure of a regression model is to express the forecasting load as a function of its influencing factors, such as weather data, previous load values and so on. If the desired forecasting load is denoted as by $y(k)$, then a linear model can be expressed as

$$y(k) = \sum_{i=1}^m a_i x_i(k) + \omega(k) \quad (1)$$

Where a_i - regression co-efficient, $x_i(k)$ - input variable considered in the regression model and $\omega(k)$ - noise term.

In general, the designing procedure and the form of non-linear regression models are much complex than linear ones. Moreover, heavy statistical analysis for model identification and parameter estimation is needed in the designing process.

EFFECTIVE METHOD -Neural networks, with their remarkable ability to derive meaning from complicated or imprecise data, can be used to extract patterns and detect trends that are too complex to be noticed by either humans or other computer techniques. A trained neural network can be thought of as an "expert" in the category of information it has been given to analyze. Other advantages include: Adaptive learning - An ability to learn how to do tasks based on the data given for training or initial experience, Self-Organization - An ANN can

create its own organization or representation of the information it receives during learning time, Real Time Operation - ANN computations may be carried out in parallel, and special hardware devices are being designed and manufactured which take advantage of this capability.

ARTIFICIAL NEURAL NETWORK:

Artificial neural network has been motivated right from its inception by the recognition that the human brain computes in an entirely different way from the conventional digital computer. The brain is a nonlinear, parallel information processing system and highly complex. Its structural constituents are organized by neurons, so as to perform certain computations faster than the fastest digital computer. The brain routinely accomplishes perceptual recognition tasks. A neural network is a massively parallel distributed processor made up of simple processing units, which has a natural propensity for storing experimental knowledge and making it available for use. It looks like the brain in two respects, Knowledge is obtained by the network from its environment through a learning process, Interneuron connection strengths, called synaptic weights, are used to store the acquired knowledge.

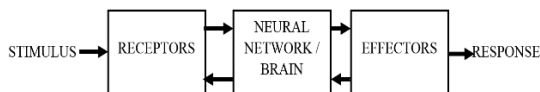


Fig 1: Block Diagram of Human Nervous System.

The human nervous system can be broken down into three stages. The receptors collect information from the environment. The effectors generate interactions with the environment e.g. activate muscles. The flow of activation/information is represented by arrows. There is a hierarchy of interwoven levels of organization: molecules and ions, synapses, neuronal microcircuits, neurons, dendritic trees, local circuits, inter-regional circuits, central nervous system. There are approximately 10 billion neurons in the human cortex. Each and every biological neuron is connected to several thousands of other neurons. Operating speed of biological neurons is measured in milliseconds. The most of neurons encode their activations or outputs as a series of brief electrical pulses. The neuron's cell body process the incoming activations and converts into output activations. The neuron nucleus contains the genetic material in the form of DNA. This exists in most types of cells. Dendrites are fibres which emanate from the cell body and provide the receptive zones that receive activation from other neurons. Axons are acting as transmission lines that send activation to other neurons. The junctions that allow signal transmission between axons and dendrites are called synapses. The process of transmission is carried by diffusion of chemicals called neurotransmitters across the synaptic cleft.

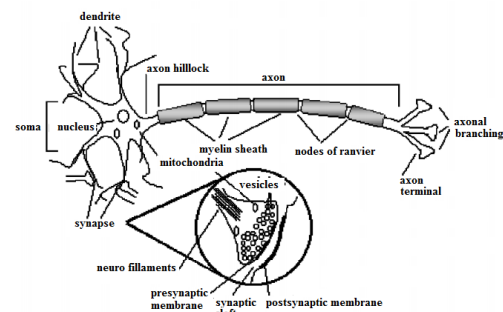


Fig 2: Schematic Diagram of a Biological Neuron

MATHEMATICAL MODEL OF A NEURON:

A neuron is an information processing unit that is fundamental to the operation of a neural network. The weight of an artificial neuron may lie in a range that includes negative as well as positive values. Three basic elements of the neuron model are: A set of weights, which is characterized by a strength of its own. Signal x_j connected to neuron k is multiplied by the weight w_{kj} . An adder for summing the input signals, weighted by the respective weights of the neuron. An activation function for limiting the amplitude of the output of a neuron is also referred to as squashing function which squashes the amplitude range of the output signal to some finite value.

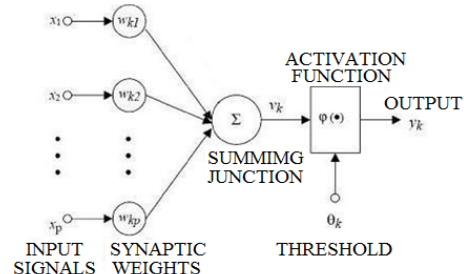


Fig 3: Model of an ANN

Therefore,

$$v_k = \sum_{j=1}^p w_{kj} x_j \quad (2)$$

$$y_k = \varphi(v_k + \theta_k) \quad (3)$$

There are three basic classes of network architectures, SINGLE-LAYER FEEDFORWARD NETWORKS: In a layered neural network the neurons are organized in the form of layers. In this network, we have an input layer of source nodes x_i and x_j , that projects onto an output layer of neurons y , but not vice versa. This network is strictly a Feedforward type. In single-layer network, there is only one output and input layer. Input layer is not counted as a layer since no mathematical calculations take place at this layer.

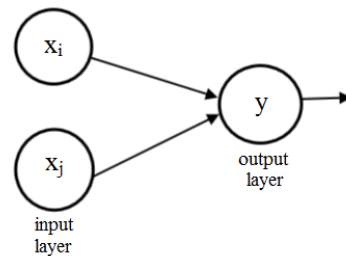


Fig 4: Single-layer Feedforward Network

MULTI-LAYER FEEDFORWARD NETWORKS: The second class of a Feedforward neural network distinguishes itself by the presence of one or more hidden layers $f_x(z)$, where computational nodes are correspondingly called hidden neurons. The function of hidden neuron is to intervene between the external input and the network output in some useful manner. By adding more hidden layers, the network is enabled to extract higher order stats. In the first layer input signal is applied to the neurons. The output signal of first layer is used as inputs to the second layer, and so on for the rest of the network.

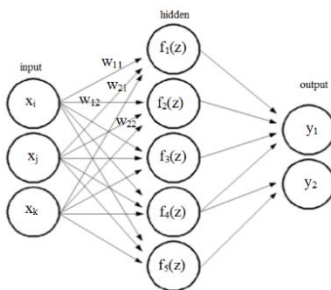


Fig 5: Multi-layer Feedforward Network

RECURRENT NETWORKS: A recurrent neural network has at least one feedback loop and may consist of a single layer of neurons with each neuron feeding its output signal back to the inputs of all the other neurons. Here self-feedback refers to a situation where the output of a neuron is fed back into its own input. The presence of feedback loops has a profound impact on the learning capability of the network and on its performance.

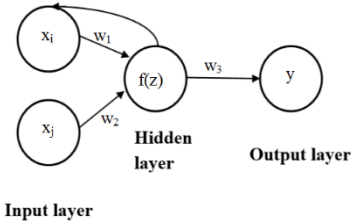


Fig 6: Recurrent Network

In learning process, we mean a procedure for modifying the weights and biases of a network. Purpose of learning rule is to train the network to perform some task. They are classified into three broad categories.

Supervised learning: The learning rule is provided with a set of training data of proper network behavior. As the inputs are applied to the network, outputs are compared to the targets. The learning rule is used to adjust the weights and biases of the network in order to move the network outputs closer to the targets.

Reinforcement learning: It is similar to supervised learning, but instead of providing correct output for each network input, the algorithm is only provide a grade. Here grade is a measure of the network performance over some sequence of inputs.

Unsupervised learning: The weights and biases are modified in response to network inputs only, no target outputs available. Most of the algorithms perform some kind of clustering operation. They learn to group the input patterns into a finite number of classes.

BACK PROPAGATION ALGORITHM

Multiple layer perceptron have been applied successfully to solve some difficult diverse problems by training them in a supervised manner with a highly popular algorithm known as the error back-propagation algorithm. And it is based on the error-correction learning rule. It may be

viewed as a generalization of an equally popular adaptive filtering algorithm- the least mean square (LMS) algorithm. Error back-propagation learning consists of two passes through the different layers of the network: forward pass and backward pass. In forward pass, an input vector is applied to the nodes of the network and its effect propagates through the network layer by layer. After that, a set of outputs is produced as the actual response of the network. During the forward pass the weights of the networks are all fixed. During the backward pass, the weights are all adjusted in accordance with an error correction rule. The network's actual response is subtracted from a desired response to produce an error signal and it is propagated backward through the network, opposite to the direction of synaptic connections. The weights are adjusted to make the actual response of the network move closer to the desired response [3].

The model of each neuron in the network includes a nonlinear activation function. The sigmoid function is commonly used which is defined by the logistic function:

$$y = \frac{1}{1 + \exp(-x)}$$

(4)

Another commonly used function is hyperbolic tangent.

$$y = \frac{1 - \exp(-x)}{1 + \exp(-x)}$$

(5)

The presence of nonlinearities is important because the input- output relation of the network could be reduced to that of single layer perceptron [5].

The network contains one or more layers of hidden neurons that are not part of the input or output of the network. These hidden neurons makes the network to learn complex tasks. The network exhibits a high degree of connectivity. A change in the connectivity of the network requires a change in the population of their weights. To illustrate the process a three layer neural network with two inputs and one output was taken, which is shown in the picture below,

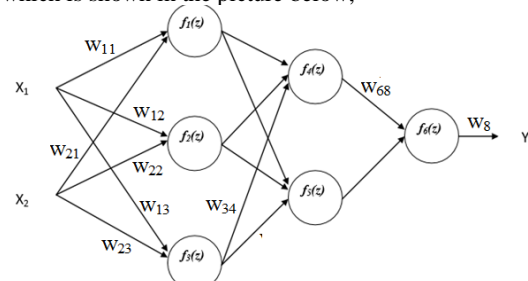


Fig 7: Three Layer Neural Network with Two Inputs and Single Output

Signal z is adder output signal, and $y = f(z)$ is output signal of nonlinear element. The training data set consists of input signals (x_1 and x_2) assigned with corresponding target (desired output) y' . The network training is an iterative process. In each iteration weights coefficients of nodes are modified using new data from training data set. Symbols w_{mn} represent weights of connections between output of neuron m and input of neuron n in the next layer. Symbols y_n represents output signal of neuron n .

$$y_1 = f_1(w_{11}x_1 + w_{21}x_2)$$

(6)

$$y_2 = f_2(w_{12}x_1 + w_{22}x_2) \quad (7)$$

$$y_3 = f_3(w_{13}x_1 + w_{23}x_2) \quad (8)$$

$$y_4 = f_4(w_{14}y_1 + w_{24}y_2 + w_{34}y_3) \quad (9)$$

$$y_5 = f_5(w_{15}y_1 + w_{25}y_2 + w_{35}y_3) \quad (10)$$

$$y_6 = f_6(w_{46}y_4 + w_{56}y_5) \quad (11)$$

The desired output value (the target), which is located in training data set. The difference is called error signal δ of output layer neuron.

$$\delta = y - y_d$$

$$\delta_1 = w_{14} \delta_4 + w_{15} \delta_5 \quad (12)$$

$$\delta_2 = w_{24} \delta_4 + w_{25} \delta_5 \quad (13)$$

$$\delta_3 = w_{34} \delta_4 + w_{35} \delta_5 \quad (14)$$

$$\delta_4 = w_{46} \delta \quad (15)$$

$$\delta_5 = w_{56} \delta \quad (16)$$

$$(17)$$

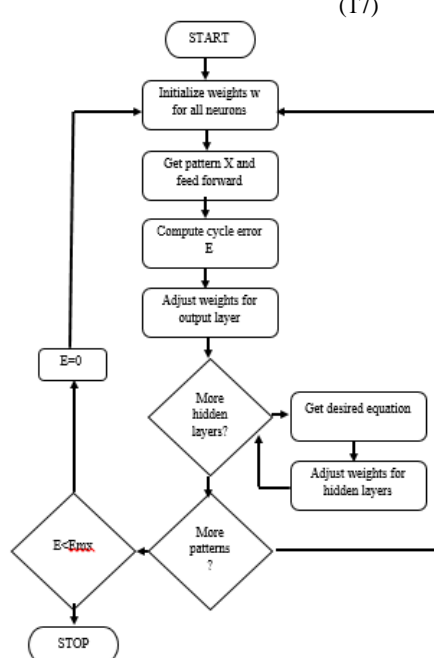


Fig 8: Flow Chart of Back Propagation Algorithm

When the error signal for each neuron is computed, the weights coefficients of each neuron input node may be modified. In formulas below $df(z)/dz$ represents derivative of neuron activation function.

The correction $w_{ij}(n)$ applied to the weight connecting neuron j to neuron i is defined by the delta rule:

Weight correction = learning rate parameter*local gradient*i/p signal of neuron i

$$\Delta w_{ij}(n) = \eta \cdot \delta_i(n) \cdot y_j(n) \quad (18)$$

The local gradient $\delta_i(n)$ depends on whether neuron i is an output node or a hidden node:

If neuron i is output node, $\delta_i(n)$ equals the product of the derivative $df_i(z)/dz$ and the error signal $e_i(n)$, both of which are associated with neuron i.

If neuron j is a hidden node, $\delta_i(n)$ equals the product of the associated derivative $df_i(z)/dz$ and the weighted sum of the δ s computed for the neurons in the next hidden or output layer that are connected to neuron j. Figure 5.2 shows the flow chart of Back Propagation Algorithm [1].

IMPLEMENTATION OF LOADRECASTING

In this paper load forecasting is achieved in two ways namely regression method and ANN method. Regression method is the conventional one and its accuracy will be low. To overcome this problem ANN is used to achieve high accuracy in prediction of future demand and minimize the error percent.

REGRESSION MODEL describe the relationship between a dependent variable y, and independent variable X. Dependent variable is also called the response variable. Independent variables are also called predictor or explanatory variables. Continuous predictor variables might be called covariates, meanwhile categorical predictor variables might be also referred to as factors. The matrix X, of observations on predictor variables is usually called the design matrix [6].

X is the input matrix, which contains dry bulb, dew point, hour, weekday, is working day, previous week same hour load, previous day same hour load, previous 24 hour load. Obtained from previous data set. Y is the target matrix, which contains system load for respective hour. Rgress process is carried out between Y and X in MATLAB using the command “[b,bint,r]=regress(Y,X)”. It returns a vector R of residuals. Mean absolute percent error is calculated, $mape=nanmean(abs(r./Y)*100)$

IMPLEMENTATION OF ANN USING MATLAB: In MATLAB nftool launches the neural network fitting wizard and leads solving a fitting problem using a two-layer feed-forward network trained with Levenberg-Marquardt. In fitting problems, neural network is to map between a data set of numeric inputs and a set of numeric targets. The Neural Fitting app (Fig 9) will help to select data, create and train a network, and then evaluate its performance using mean square error and regression analysis.



Fig 9: Neural Fitting Tool in MATLAB

A two-layer feed-forward network with sigmoid hidden neurons and linear output neurons, can fit multi-dimensional mapping problems. The network will be trained with Levenberg-Marquardt back-propagation algorithm, unless there is not enough memory, in which case scaled conjugate gradient back-propagation will be used.

1. The input and output data should be created in the workspace from previous data set.
2. After creating the input and output data, it can able to import into neural fitting tool. Shown in below figure.

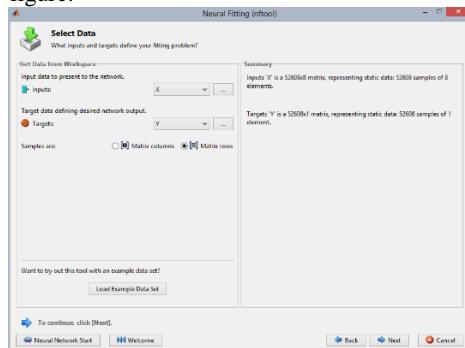


Fig 10: Import data into nftool

3. Training validation and testing percentage can be set according to the need. Here training was set to 70%, Validation was 15% and Testing was 15%. Which is shown in Fig 11

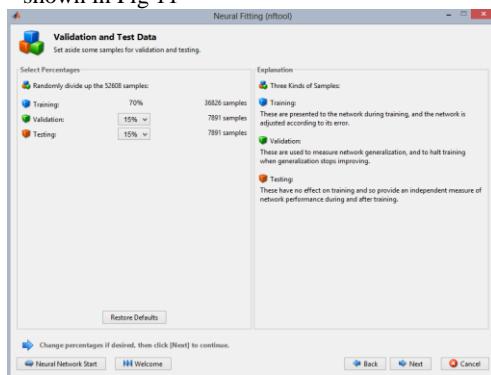
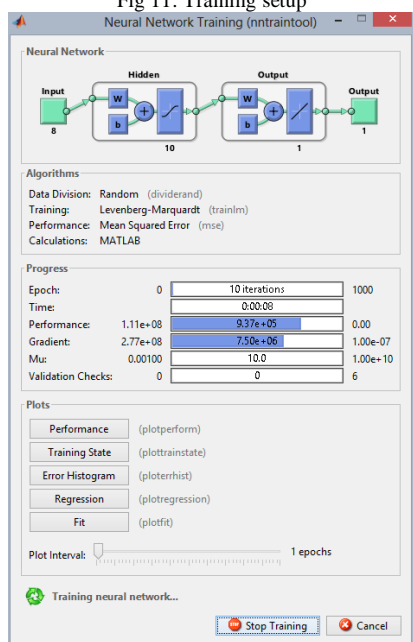


Fig 11: Training setup



- Fig 12: Train State
4. The number of neurons in the fitting network's hidden layer is to be defined.
 5. After selecting the hidden layer, training should be started.
 6. During training process, the train state, fit and regression is shown with performance. Shown in Fig 10

OUTPUT

REGRESS METHOD: X is the input matrix, which contains dry bulb, dew point, hour, weekday, is working day, previous week same hour load, previous day same hour load, previous 24 hour load. Obtained from previous data set. Y is the target matrix, which contains system load for respective hour. Regress process is carried out between Y and X in MATLAB using the command “[b,bint,r]=regress(Y,X)”.

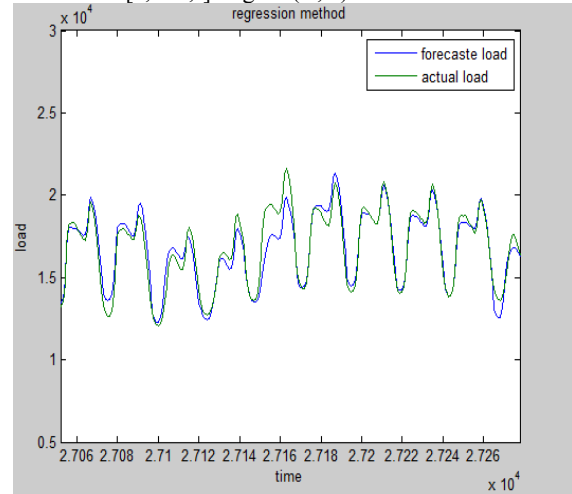


Fig 13: Actual Load vs Forecasted Load

It returns a vector r of residuals. Mean absolute percent error is calculated by, $mape = \text{nanmean}(\text{abs}(r./Y*100))$

$$\begin{aligned} \text{i.e. } & [b] = \text{regress}(Y, X); \\ & Y_{\text{pred}} = X * b; \\ & mape = \text{nanmean}(\text{abs}(r./Y*100)) \\ & mape = 4.665\% \end{aligned}$$

ANN METHOD: After training the neural network, the forecast program is executed, result were obtained is shown below.

>> LoadScriptNN

Mean Absolute Percent Error (MAPE): 2.01%

Mean Absolute Error (MAE): 297.31 MWh

Daily Peak MAPE: 1.99%

>>

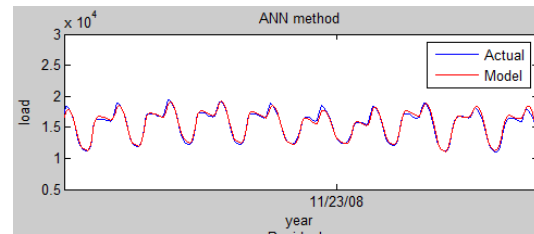


Fig 14: Actual Load vs Predicted Load

COMPARISON: Therefore future demand is predicted and its error percent is calculated by comparing with the actual load. In regress method and ANN this is computed, compare to regress, ANN gives better result.

Table 7.1 Comparison between Regress and ANN Method

	MAP E	GRAPH
REGRESSION METHOD	4.665 %	
ANN METHOD	2.01%	

OBSERVATION: No prediction technique can be claimed as best method in the area of power forecasting, because the power consumption of each country heavily depends on its economic structure, culture, life style, geographical location and so on. Even though, the power forecasting using neural network gives the accurate model of future power demand.

CONCLUSION:

Prediction of future power demand is achieved using Artificial Neural Network and it is compared to the regress method. An adaptive training algorithm based on Levenberg-Marquardt Algorithms is used in this paper. Thus in this way the Neural Network will replace

the conventional regress method and hence real time operation of forecasting is possible.

REFERENCES:

- [1] K. Y. Lee, Y. T. Cha, and J. H. Park. Short-term load forecasting using an artificial neural network. Transactions on Power Systems, Vol. 7. No. 1, February 1992.
- [2] Wiktor Charytoniuk, and Mo-Shing Chen. Very short-term load forecasting using artificial neural networks. IEEE transactions on power systems, vol. is. no.1, February 2010.
- [3] Wiktor Charytoniuk, E. Don Box, Wei-Jen Lee, Mo-Shing Chen, Paul Kotas, and Peter Van Olinda. Neural-network-based demand forecasting in a deregulated environment. IEEE transactions on industry applications, VOL. 36, NO. 3, MAY/JUNE 2000.
- [4] Tomonobu Senju, Hitoshi Takara, Katsumi Uezato, and Toshihisa Funabashi. One-hour-ahead load forecasting using neural network. IEEE transactions on power systems, VOL. 17, NO. 1, FEBRUARY 2002.
- [5] Titti Saksornchai, Wei-Jen Lee, Kittipong Methaprayoon, James R. Liao, and Richard J. Ross. Improve the unit commitment scheduling by using the neural-network-based sort-term load forecasting. IEEE transactions on industry applications, VOL. 41, NO. 1, January/February 2005
- [6] Kyung-Bin Song, Seong-Kwan Ha, Jung-Wook Park, Dong-Jin Kweon, and Kyu-Ho Kim. Hybrid load forecasting method with analysis of temperature sensitivities. IEEE transactions on power systems, VOL. 21, NO. 2, MAY 2006.

Enhance the Performance of Hierarchical Control in Microgrid Application

T. Vidya,

PG Scholar, Department of EEE,
K.S.Rangasamy College of Technology,
Tiruchengode, Namakkal, 9965263946.
viduthangaraj@gmail.com.

P. Aravindan, M.E., (Ph.D.),

Associate Professor, Department of EEE,
K.S.Rangasamy College of Technology,
Tiruchengode, Namakkal.
paravindan@rediffmail.com

Abstract— Voltage Source Inverters (VSIs) which are connected in parallel composed of Microgrids (MGs). The steps towards the stability of these MGs have been rewarded in this paper. For this reasonableness, this system is assured of two control levels using hierarchical control scheme for the parallel operated VSI system. The primary control enfolds the droop method pursues the virtual impedance loops. The secondary control which embraces the unified phase shift modulation technique renovates the frequency and amplitude deviations twisted by the droop method. This technique regulates the phase and magnitude of voltage which can be resolute based on zero crossings of the voltage and also accessible for connecting the MG to the main grid. Simulation results are provided not only to be acquainted with the good frequency as well as enhancing the voltage amplitude which enhances the stability of the Microgrid (MG) control system.

Keywords— Voltage Source Inverters (VSIs), Distributed Generation System (DGS), droop method, virtual impedance concepts, hierarchical control, Microgrid (MG), Unified Phase Shift Modulation (UPSM) Technique.

I. INTRODUCTION

With the raise of small scale industries curiosity in Microgrids (MGs) is hastily escalating predominantly. Novel power electronic equipment will preside over the electrical grid in the next decades because of smart grid system. Consistently Voltage Source Inverters (VSIs) are worn as interface of power electronics; consequently, the formation of MG can be achieved by controlling the parallel operated VSIs has been analysed in the last few years [1]–[9]. With the augmentation of power electronic based microgrids, the hierarchical control systems are predictable, which are capable to contrive both in Island mode and grid connected mode.

Distributed Generation Systems (DGS) is hastily escalating due to the facts that larger power plants are economically unfeasible in many regions because of increasing system, fuel costs and stricter environmental regulations. These DGS are often connected to the utility grid or Microgrid through a power electronic interface converter. Microgrid is a local grid consisting of generation, transmission system and dispersed loads which may operate in grid connected or islanded mode. The DC source worn out at this juncture is solar panel and fossil fuel to augment the better economic as well as eco-friendly environmental fact.

An interconnected network for delivering electricity from suppliers to consumers is called electrical grid. It is composed of generating stations that produce electrical power, high voltage transmission lines that carry power from distant sources to demand centers and distribution lines that connect

individual customers. Power stations may be located near a fuel source, at a dam site or to take advantage of renewable energy sources, and are often located away from heavily populated areas. They are usually quite large to take advantage of the economies of scale. The electric power which is generated is stepped up to a higher voltage at which it connects to the transmission network. The transmission network will move the power long distances, sometimes across international boundaries, until it reaches its wholesale customer.

The virtual impedance loop have been developed to augment the consistency and performances of the droop controlled VSIs, providing to the inverters with harmonic power sharing, hot swap operation, etc [10]. The focal predicament to be completed in such mechanism is the frequency control of the system. Nevertheless, voltage stability and synchronization issues are additionally of the essence to get done adequate suppleness to manoeuvre in both mode.

It is an analogy to the predictable droop method is not suitable when the paralleled system must donate to nonlinear loads because the control units should take into account harmonic currents as well as to equilibrium active and reactive power. When sharing nonlinear loads, harmonic current sharing techniques have been projected to avoid the circulating deformation power. It is mandatory to concern for communication systems to propel information among the DG units to utilize such a category of multilevel control algorithm[17]–[20]. In order to perk up the negative aspects of droop controlled VSIs, some implications were made by combination of low-bandwidth communications with average power sharing, droop control and extra harmonic compensation control loops [18], [19].

It is vital to first synchronize the MG to the main grid, in the case of shifting from islanded operation to grid connected operation. Thus, a distributed synchronization control loop is inevitable [1]. A static transfer switch attaches the MG to the grid or to an MG cluster after reached the synchronization. At the point of common coupling, it is obligatory to control the active and reactive power flows after the transfer process between grid connected and islanded mode is refined. Boon over this system is if one inverter trips, another can competent to distribute the supply to the non linear load, the system will still stay behind stable [21]. These all specifics emphasize the consistency and the excellent performance of the MG control system.

The multilevel inverter can operate at both fundamental switching frequencies that are higher switching frequency and lower switching frequency. It should be noted that the lower switching frequency means lower switching loss

and higher efficiency is achieved. Selective harmonic elimination technique along with the multi-level topology results the total harmonic distortion becomes low in the output waveform without using any filter circuit.

Two inverters are warned to provide the uninterrupted supply to the load. Among the various types of inverters diode clamped inverters are preferable since it is plausible to weaken the stress on other electrical devices and afford the multiple voltage level. This inverter is to amalgamate a near sinusoidal voltage from abundant levels of dc voltage. As number of levels increases, the synthesized output waveform has more steps which provide a staircase wave that approaches a desired waveform and also the harmonic distortion of the output wave decreases.

The main concept of this inverter is to use diodes and afford the multiple voltage levels through the series connection of different phases to the capacitor banks. This type of inverters provides the high efficiency because the fundamental frequency worn for all the switching devices and it is an uncomplicated method of the back to back power shift systems. The degree of control or stability of the r.m.s voltage at the load frequently specified in relation to other parameters such as input voltage changes, load changes or temperature changes.

The frequency trip settings may be adjusted according to local standards. Some utilities may want larger DG to remain connected to a much lower frequency to help with system stability issues following loss of a major generating plant or a tie-line. In order to maintain the stability of frequency, control modulation methods are implemented. This modulation technique provides faster transmission of signals and also makes the system to attain the stable frequency and voltage amplitude of the Microgrid control system.

This paper is organized as follows. In Section II illustrate the primary control includes the droop method and virtual impedance concepts. Section III suggests the secondary control for frequency and voltage amplitude restoration using Unified Phase Shift Modulation(UPSM) technique. Section IV clarifies the simulation results. Finally, Section VI depicts the conclusion of this paper.

II. PRIMARY CONTROL

The control projected for the parallel operated VSI system is based on the droop control framework, which is composed of the voltage and current control loops, the virtual impedance loop and the droop control strategy. This control level is employed to regulate the frequency and amplitude of the voltage reference endow with the inner current and voltage control loops. The reference voltage V_{ref} , frequency and amplitude will be controlled by the droop functions, generated in abc and transformed to $\alpha\beta$ coordinates using the well-known Clarke transformation and also, currents and voltages

15th April, 2015

are transformed. The above theory can be integrated in VSIs using the P/Q droop method as pursues,

$$\omega = \omega^* - G_p(s).(P - P^*) \quad (1)$$

$$E = E^* - G_Q(s).(Q - Q^*) \quad (2)$$

Where ω and E specifies the reference output voltage of the frequency and amplitude, ω^* and E^* corresponds to their references, P and Q are the active and reactive power, P^* and Q^* are their references, and $G_p(S)$ and $G_Q(S)$ are their subsequent transfer functions.

A. Droop Control and Virtual Impedance Loop

For parallel connected inverters, the droop method compiled of subtracting relative parts of the output standard active and reactive powers from the frequency and amplitude of each section for imitate the virtual inertias. This control is a cooperative control to share active and the reactive power. These control modules have been applied for paralleled inverters with UPS systems to evade mutual control wires while obtaining good power sharing [4].

This control method is frequently used in this level to emulate physical behaviors that makes the system stable and more damped and also to avoid circulating currents among the converters without using any critical communication between them. The main initiative of this control level is to mimic the behavior of a synchronous generator, which reduces the frequency at the active power increases. With the subsequent correlation [16], this method computes P and Q in the $\alpha\beta$ -coordinates from power block computation as,

$$p = v_{ca} i_{oa} + v_{cb} i_{ob} \quad (3)$$

$$q = v_{cb} i_{oa} - v_{ca} i_{ob} \quad (4)$$

With p and q corresponds the instantaneous active and reactive powers and $i_{o\alpha\beta}$ and $V_{c\alpha\beta}$ represents the output current and the capacitor voltage correspondingly. The execution of the droop control and the virtual output impedance is shown in fig.2. This virtual impedance control loop is to follow physical output impedance. This virtual output impedance has trifling power losses contrary with physical impedance and also it is probable to execute resistance exclusive of efficiency losses. The block diagram of two VSIs forming an MG is shown in fig.1. The virtual impedance loop can be expressed in $\alpha\beta$ coordinates [14] as,

$$v_{va} = R_v i_{oa} + \omega L_v i_{ob} \quad (5)$$

$$v_{vb} = R_v i_{ob} - \omega L_v i_{oa} \quad (6)$$

Where L_v and R_v specifies the virtual inductance and resistance value and $i_{o\alpha\beta}$ and $V_{v\alpha\beta}$ specifies the output current and voltage in the $\alpha\beta$ frame correspondingly. The droop characteristic therefore allows multiple units to share load without the units fighting each other to control the load. It shifts up the droop function to restore the initial frequency of the inverters using an integrator to avoid frequency deviation.

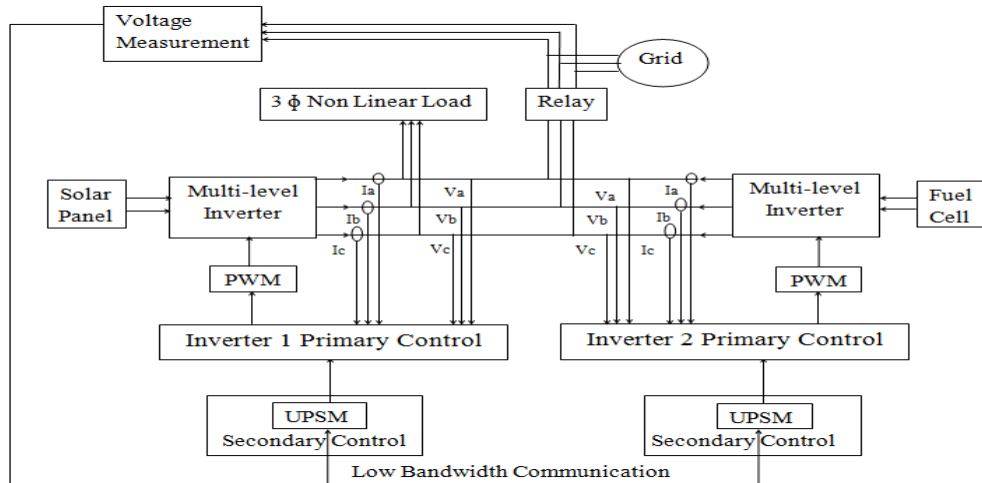
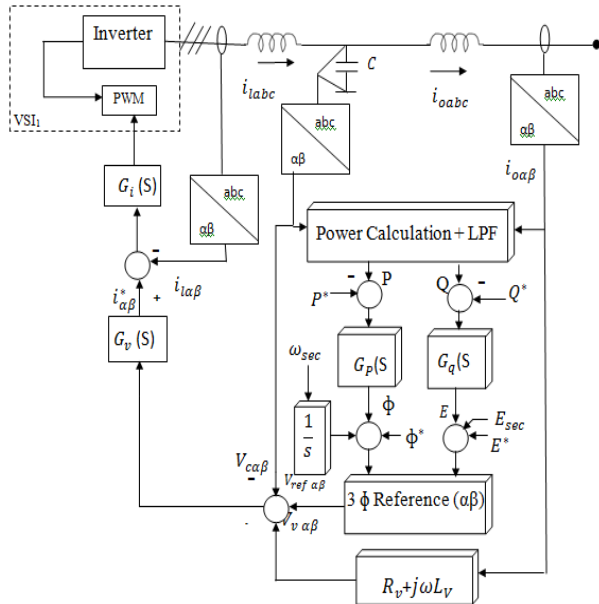


Fig.1. Block Diagram of Two VSIs forming an MG.

Fig.2. Block Diagram of the Droop Control and the Virtual Output Impedance in $\alpha\beta$ Co-ordinates.

III. SECONDARY CONTROL USING UPSM

A secondary control is probable to reimburse for the frequency and amplitude deviations as well as for eradicate any steady state error pioneered by the droop control and virtual impedance method [15], [16]. This control is also called Automatic Generation Control (AGC), the use of frequency data is appropriate for low bandwidth communications as an alternative of using phase or time domain information, which would be crucial for critical high speed communication. This control allows the synchronization of the renewable agent with the utility grid for grid connected power system with deduction of the computational requirement. For synchronizing all the VSI of the MG using the $\alpha\beta$ components of the grid and the VSI voltage variables V_{gap} and V_{cap} , a coordinated synchronization process is

indispensable. After the synchronization of both voltages, presume that

$$v_{g\beta} v_{ca} - v_{g\alpha} v_{c\beta} = 0 \quad (7)$$

where x represents the average value of the variable x with the

grid frequency. Thus, the above affiliation can be derived using the subsequent PLL structure with orthogonal product, a low pass filter and a PI controller. The secondary be in charge of be supposed to exact the frequency deviation contained by the tolerable limit with enchanting the grid constraint [22].

A. Proposed UPSM

The new modulation technique called unified phase shift modulation technique is projected which can autonomously standardize the phase and magnitude of the voltage. The controllers of phase and magnitude incorporated by the proposed modulation can accomplish optimized output synchronization which can be resolute based on the zero crossings of the voltage. This technique is easily relevant for parallel operation of inverters. The unified PSM contains various amplifiers, comparators and more logic gates than the symmetrical PSM. When grid failure occurs, this technique can probable to acquire the reference voltage which accomplish the fast renovation of frequency and the voltage amplitude of the microgrid. A novel modulation circuit called as unified PSM is proposed to solve these issues so that output discrepancy is minimized and optimized synchronization is achieved. This technique achieves the faster transmission of signals results in reducing the raising time of the system, thus enhances the stability of the frequency.

B. Frequency Restoration

A model has been proposed to investigate the stability of the system and also to regulate the parameters of the frequency secondary control as shown in Fig 3. It allocates for regulating the control parameters of the secondary control and also to cram the inadequacy of the communication delay. It composes

the droop control of the system, the simplified PLL first order transfer function worn to extort the frequency of the MG and the secondary control G_f sec(s), pursued by a delay G_d sec(s) for the communication lines.

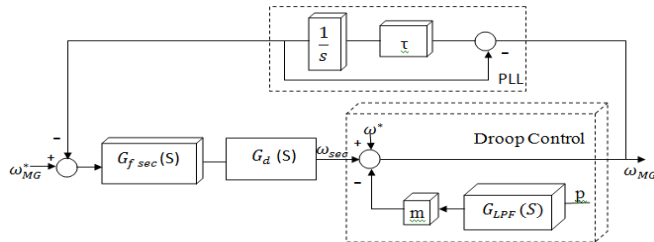


Fig.3. Block Diagram of the Frequency Secondary Control

C. Amplitude Restoration

The parallel process has been applied for designing the voltage secondary controller and also for obtaining the closed loop voltage dynamic model. Fig.4 represents the block diagram of the amplitude secondary control. Using an external centralized controller, this control will be implemented, in order to renovate the deviations twisted by the primary control.

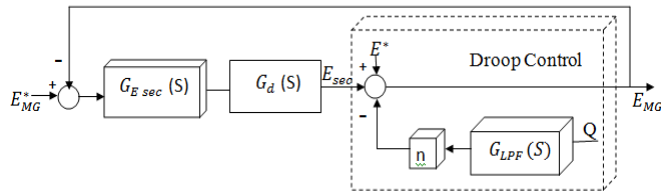


Fig.4. Block Diagram of the Amplitude Secondary Control

IV. SIMULATION RESULTS

Some simulation results from a 3 ϕ inverter MG are accessible. If the generated power is in excess with the nonlinear load, it should be afforded to the main grid else it should be acquired from the main grid. In secondary control, the grid voltage and the frequency can be compared using low bandwidth communication with the reference voltage of primary control. The inverters values are altered with grid values for any deviation. When grid failure occurs, this technique can probable to acquire the reference voltage with reference generator which accomplish the fast renovation of frequency and the voltage amplitude of the microgrid using UPSM technique. The selected control parameters and the data are listed in Table1for simulation.

Table 1 Simulation Parameters

S.No	Simulation parameters	Values
1	Nominal DC source voltage	500 V
2	Solar Panel	100 KW
3	Fuel cell	50 KW
4	DC source current rating	200 A
5	Inverter voltage	440 V
6	Inverter current rating	100A
7	Frequency	50 Hz

8	Nonlinear load	140 KW
9	Grid Load	30 MW

At initial, both inverters were coupled and provided supply to the nonlinear load. The output voltage of both inverters is 440V. Afterward, at $t=0.2$ s, the voltage (amplitude) of inverter 2 gets unbalanced which can be controlled by inverter 1. At $t=0.96$ s, some interruption occurs in inverter 1, it gets detached from the MG, i.e., it gets turned off; its voltage value is 0V. The inverter 2 is supplying all the required power, the output voltage of inverter 2 is 440V. The output voltage for inverter 1 and 2 are shown in Fig.5, with blue and pink color specifies the output voltage of inverter 1 and 2 correspondingly.

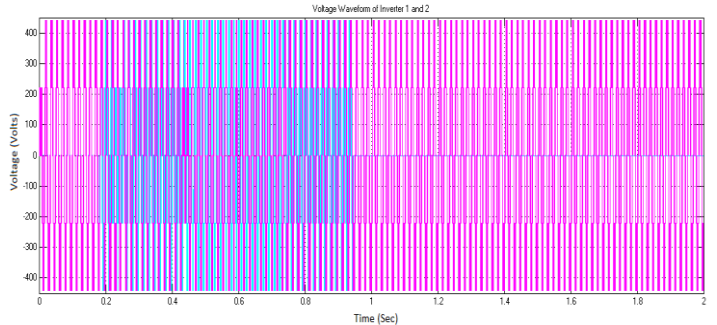


Fig.5. Output Voltage Waveform of Inverter 1 and Inverter 2

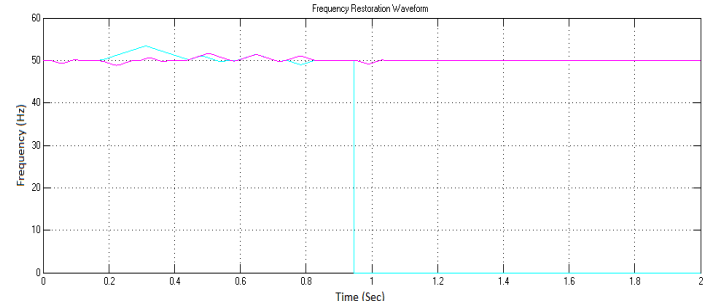


Fig.6. Frequency Restoration of Inverter 1 and Inverter 2

The frequency and amplitude renovation action done by the secondary control using UPSM are shown in Fig.5 and 6 respectively. At preliminary by $t=0.2$ s, the frequency gets deviated and it regains to normal frequency after 0.2s. Again at $t=0.5$ s, the frequency gets unbalanced and it regains to normal frequency after 0.05s followed by deviation at 0.76s and also regained at 0.8s. At $t=0.96$ s, some interruption occurs in inverter 1, it gets detached from the MG, i.e., it gets turned off; the first inverter frequency accomplishes 0Hz and the frequency of inverter 2 sustained in the similar value. Thus the system attains the faster stability by decreasing the raising time.

V. CONCLUSION

This paper proposes the hierarchical control for MGs based parallel connected three phase VSI. This control configuration was prearranged of two control levels. The primary control composed of the droop control method and the virtual impedance concepts. Pursued by this, the confined centralized

controller known as the secondary control is responsible for power sharing with the intention of renovating the frequency and amplitude deviations twisted by the above control methods using Unified Phase Shift Modulation (UPSM) Technique. This secondary control achieves the faster stability by decreasing the raising time. The different levels of control have been replicated and the closed loop system dynamics has been investigated. Simulation results have revealed the excellent concert and augment the consistency of the MG control system.

REFERENCES

- [1] J. C. Vasquez, J. M. Guerrero, J. Miret, M. Castilla and L. G. de Vicuna, "Hierarchical control of intelligent microgrids," IEEE Ind. Electron. Mag., vol. 4, no. 4, pp. 23–29, Dec. 2010.
- [2] T. C. Green and M. Prodanovic, "Control of inverter-based microgrids," Elect. Power Syst. Res., vol. 77, no. 9, pp. 1204–1213, Jul. 2007.
- [3] N. Pogaku, M. Prodanovic and T. C. Green, "Modeling, analysis and testing of autonomous operation of an inverter-based microgrid," IEEE Trans. Power Electron., vol. 22, no. 2, pp. 613–625, Mar. 2007.
- [4] R. Teodorescu, F. Blaabjerg, M. Liserre and P. C. Loh, "Proportional–resonant controllers and filters for grid-connected voltage source converters," Proc. Inst. Elect. Eng. Elect. Power Appl., vol. 153, no. 5, pp. 750–762, Sep. 2006.
- [5] M. B. Delghavi and A. Yazdani, "An adaptive feedforward compensation for stability enhancement in droop-controlled inverter-based microgrids," IEEE Trans. Power Del., vol. 26, no. 3, pp. 1764–1773, Jul. 2011.
- [6] C. K. Sao and P. W. Lehn, "Control and power management of converter fed microgrids," IEEE Trans. Power Syst., vol. 23, no. 3, pp. 1088–1098, Aug. 2008.
- [7] E. Barklund, N. Pogaku, M. Prodanovic, C. Hernandez Aramburo and T. C. Green, "Energy management in autonomous microgrid using stability-constrained droop control of inverters," IEEE Trans. Power Electron., vol. 23, no. 5, pp. 2346–2352, Sep. 2008.
- [8] R. Majumder, A. Ghosh, G. Ledwich and F. Zare, "Angle droop versus frequency droop in a voltage source converter based autonomous microgrid," in Proc. PES, 2009, pp. 1–8.
- [9] F. Katiraei and M. R. Iravani, "Power management strategies for a microgrid with multiple distributed generation units," IEEE Trans. Power Syst., vol. 21, no. 4, pp. 1821–1831, Nov. 2006.
- [10] J. M. Guerrero, J. C. Vasquez, J. Matas, M. Castilla and L. G. de Vicuna, "Control strategy for flexible microgrid based on parallel line-interactive UPS systems," IEEE Trans. Ind. Electron., vol. 56, no. 3, pp. 726–736, Mar. 2009.
- [11] P. L. Villeneuve, "Concerns generated by islanding," IEEE Power Energy Mag., vol. 2, no. 3, pp. 49–53, May/Jun. 2004.
- [12] M. C. Chandorkar, D. M. Divan and R. Adapa, "Control of parallel connected inverters in standalone AC supply systems," IEEE Trans. Ind. Appl., vol. 29, no. 1, pp. 136–143, Jan./Feb. 1993.
- [13] J. M. Guerrero, J. C. Vasquez, J. Matas, L. Garcia de Vicuna and M. Castilla, "Hierarchical control of droop-controlled AC and DC microgrids—A general approach towards standardization," IEEE Trans. Ind. Electron., vol. 58, no. 1, pp. 158–172, Jan. 2011.
- [14] J. He and Y. Lee, "Analysis and design of interfacing inverter output virtual impedance in a low voltage microgrid," in Proc. IEEE ECCE Conf., 2002, pp. 2857–2864.
- [15] H. Matthias and S. Helmut, "Control of a three phase inverter feeding an unbalanced load and operating in parallel with other power sources," in Proc. EPE-PEMC Conf., 2002, pp. 1–10.
- [16] E. Hoff and T. Skjellnes, "Paralleled three-phase inverters," in Proc. NORPIE Conf., 2004, pp. 1–6.
- [17] A. Hasanzadeh, O. C. Onar, H. Mokhtari and A. Khaligh, "A proportional–resonant controller-based wireless control strategy with a reduced number of sensors for parallel-operated UPSs," IEEE Trans. Power Del., vol. 25, no. 1, pp. 468–478, Jan. 2010.
- [18] M. N. Marwali and A. Keyhani, "Control of distributed generation systems—Part I: Voltages and currents control," IEEE Trans. Power Electron., vol. 19, no. 6, pp. 1541–1550, Nov. 2004.
- [19] M. N. Marwali, J. Jin-Woo and A. Keyhani, "Control of distributed generation systems—Part II: Load sharing control," IEEE Trans. Power Electron., vol. 19, no. 6, pp. 1551–1561, Nov. 2004.
- [20] J. A. P. Lopes, C. L. Moreira and A. G. Madureira, "Defining control strategies for microgrids islanded operation," IEEE Trans. Power Syst., vol. 21, no. 2, pp. 916–924, May 2006.
- [21] M. B. Delghavi and A. Yazdani, "Islanded-mode control of electronically coupled distributed-resource units under unbalanced and nonlinear load conditions," IEEE Trans. Power Del., vol. 26, no. 2, pp. 661–673, Apr. 2011.
- [22] UCTE, Technical Paper—Definition of a Set of Requirements to Generating Units, 2008.
- [23] Junfeng Liu, K. W. E. Cheng and Jun Zeng, "A Unified Phase-Shift Modulation for Optimized Synchronization of Parallel Resonant Inverters in High Frequency Power System," IEEE Transactions on Industrial Electronics, vol. 61, no. 7, pp. 3232–3247, July 2014.
- [24] Juan C. Vasquez, Josep M. Guerrero, Mehdi Savaghebi, Joaquin Eloy-Garcia, and Remus Teodorescu, "Modeling, Analysis and Design of Stationary Reference Frame Droop Controlled Parallel Three-Phase Voltage Source Inverters," IEEE Trans. on Industrial Electronics, vol. 60, no. 4, pp. 1271–1280, April 2013.

Optimal placement of Distribution Generator to maximize the net savings of the Distribution network

Mr.A.Apthi Joshva ¹, Mr.J.Subash Kumar ², Dr.M.Ramesh babu³ and Dr.S.Arunchalam⁴

^aapthi2626@gmail.com, ^bsubashkumarjsk@gmail.com, ^crameshbabum@stjosephs.ac.in and

^dmailto:arunchalam@gmail.com.

^{1,2}PG Scholar, Power Systems Engineering St. Joseph's College of Engineering Chennai, India-600119

³Professor- Dept. of EEE, St. Joseph's College of Engineering Chennai, India-600119

⁴Associate Professor-Dept. of EEE, St. Joseph's College of Engineering Chennai, India-6000119

ABSTRACT:

The Power system distribution network is constantly being faced with an integration of Distributed generators and the ever-growing load demand. The losses in the distribution network is high compare to transmission. This problem can be solved by optimal placement of Distributed generators due to which KW losses are minimized and net savingcan be maximised. This proposed work adopts Sensitivity analysis as a methodical technique, used to reduce the search space and to arrive at an accurate solution for recognizing the placement of DG. This paper also investigates the voltage support and loss reduction in distribution systems with the integration of Distributed generator.

INTRODUCTION:

The Power distribution system is the final stage in delivery of electric power; it carries power from the transmission system to consumers. Distribution networks are radial in structure. Radial Distribution Network (RDN) has distributed loads like industrial, commercial, domestic, etc., The Load profile of the network will fluctuate from time to time and causes imbalance power flow in the line which may lead to voltage collapse on account of low voltages. When there is a more active power loss in the Distribution network, the voltage in the buses may violate the constraint of line. This can affect the quality of power supply and the stability of the network. This problem has to be solved by optimally locating the Distributed generator at different candidate buses of RDN.

In order to evaluate the power distribution system performance and the effectiveness of proposed modifications at the planning stage, it is necessary to carry out the load flow analysis of the system repeatedly. Power flow analysis is a basic and necessary tool for any electrical system under

steady state condition to determine the exact electrical performance after DG incorporation. Load flow analysis is also employed for planning, optimization and stability studies of the distribution network.

DISTRIBUTION LOAD FLOW ANALYSIS:

Load Flow studies are performed on Power Systems to find the state and control variables. The voltage magnitudes and angles are considered as the state variables. The Load Flow analysis becomes a vital part of the power System network to find the system conditions for the different contingency conditions.

In the proposed work radial distribution power flow algorithm is used for load flow analysis in Complex mode including voltage controlled buses explained in [2].The element incidence matrix is formed by deriving relationship between the branch powers and bus powers. The power flow equations are written in terms of a recursive linear equations. From these equations the bus voltages and branch currents are obtained in terms of complex numbers. The implementation of this algorithm is simple and it can be extended to include the distributed generators for any complex networks. A matrix based data handling is used in this algorithm.

The equations for a radial distribution system are derived as a specified complex bus powers and the bus voltages. Power flowing from bus 'i' to bus 'j' is specified as S_{ij} .

$$S_{ij} = P_{ij} + iQ_{ij} \quad (1)$$

The basis for the proposed method is that branch currents can be expressed in terms of bus currents and N-1 lines only present in N bus radial distribution network. The bus current of node j is derived as linear equation from an element ij connected between nodes 'i' and 'j'.

$$I_j = I_{ij} - \sum I_{jk(j)} \quad (2)$$

At node j the set of k(j) nodes are connected. The non-singular square matrix is derived by relationship between bus currents and branch currents.

$$I_{bus} = K \cdot I_{branch} \quad (3)$$

$$I_{branch} = K^{-1} I_{bus} \quad (4)$$

The matrix K is incidence matrix.

FORMULATION OF PROPOSED METHOD:

- 1) Complex power S_{ij} is formed by adding real and reactive power.
- 2) Then form the Zbus (Z_{ij}) matrix and Ybus (Y_{ij}) matrix.
- 3) Built the bus incidence matrix K
 - I. K matrix is diagonal matrix and its size is $(n-1)$ where n is the total number of buses in network.
 - II. Main diagonal of the matrix is 1 representing it as starting line of bus and receiving end is taken as -1.
- 4) Take the inverse of K matrix.
- 5) Multiply the complex power with inverse matrix and form element PQ.
- 6) Form the R_{ij} by multiplying conjugate of Z with complex power.

$$R_{ij} = S_{ij} Z_{ij}^* \quad (6)$$

The Fig. 2 shows the representation of 2 nodes in a distribution line. Where V_i is sending end voltage and V_j is receiving end voltage.

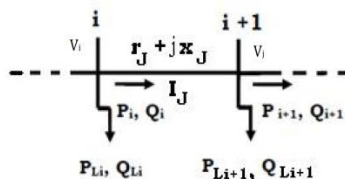


Fig 2. Representation of 2 nodes in Distribution system

- 7) The bus voltage and branch current are calculated from R_{ij} using the below formula.

$$V_j = V_i - \frac{R_{ij}}{V_i} \quad (7)$$

8) The bus voltage and current are calculated iteratively by updating values obtained in previous iteration by forward and backward sweep method.

- 9) Then the Line losses are calculated by multiplying line current with the line resistance.

$$TL_{loss} = I_{ij} * \text{line resistance} \quad (8)$$

- 10) Total system losses are calculated using

$$S_{branch}^{receiving} = S_{branch}^{sending} - TL_{loss} \quad (9)$$

DISTRIBUTION LOAD FLOW ANALYSIS WITH DISTRIBUTED GENERATOR:

Integrating DG in distribution load flow analysis is challenging to every power engineers. In the proposed work a simplified approach is used to integrate the DG for the distribution load flow algorithm.

The PV Generator will inject only the real power P_i so the injected real power is subtracted with the real power load already present in the bus and then the load flow analysis is carried out.

$$\text{Real power} = -P_i$$

$$S_{ij} = (P_{ij} - P_i) + iQ_{ij} \quad (10)$$

Whereas in our calculation we have taken the output of Distributed Generators as a negative load in calculation. By using this method the load flow analysis along with DG is easily calculated and the method is implemented in IEEE12, 28,30,33,69 and 119 bus test systems and the results are discussed below.

SENSITIVITY ANALYSIS:

Sensitivity analysis is considered in order to reduce the search space and to find an accurate solution for recognizing the locality. The sensitivity analysis is a methodical technique for finding the location of DG with maximum influence on the system active power losses. Sensitivity analysis is carried out to find the Loss Sensitivity Factor which is important to recognize the candidate bus for DG placement. LSF is able to predict which bus will have the biggest loss reduction when a Distribution Generator is placed. Therefore, the most sensitive buses can act as candidate buses for the placement of Distribution Generator. The search space for the optimization problem has been reduced by estimating these candidate buses. As only few

buses can be candidate buses for compensation, the installation cost of DG can also be cut shorted.

Let us consider $(r + jx)$ as impedance of the line and a load of $P_{eff_j} + Q_{eff_j}$ connected between (i) and (j) buses. P_{eff_j} and Q_{eff_j} are the active and Reactive power beyond the receiving end bus. KW loss in the line is given by I^2R losses, which can also be expressed as,

$$P_{mn(loss)} = \frac{[P_n]^2 + [Q_n]^2}{[V_m]^2} * R_{mn} \quad (11)$$

Similarly the reactive power loss of the line can be given as

$$Q_{mn(loss)} = \frac{[P_n]^2 + [Q_n]^2}{[V_m]^2} * X_{mn} \quad (12)$$

Where

P_{eff_j} = total active power supplied beyond the bus j.

Q_{eff_j} = total reactive power supplied beyond the bus j.

Now the loss sensitivity factor can be calculated as

$$\frac{\partial P_{lineloss_j}}{\partial Q_{eff_j}} = \frac{2 * Q_{eff_j} * r_{ij}}{(v_j)^2} \quad (13)$$

$$\frac{\partial P_{lineloss_j}}{\partial Q_{eff_j}} = \frac{2 * Q_{eff_j} * X_{ij}}{(v_j)^2} \quad (14)$$

ALGORITHM FOR SENSITIVITY ANALYSIS:

STEP 1: Loss sensitivity factor has to be calculated for all buses

$$LSF = \frac{\partial P_{LOSS}}{\partial Q} \quad (15)$$

STEP 2: All buses are arranged from higher to lower order based on Loss sensitivity factor

STEP 3: Calculate the Normalised bus voltage magnitude of all the buses.

$$\text{Norm}(i) = \frac{V[i]}{0.95} \quad (16)$$

STEP 4: The candidate bus for DG placement is selected based on buses whose Norm

$$(i) \frac{V[i]}{0.95} \text{ is less than } 1.01.$$

RESULT AND ANALYSIS:

The method is tested on 12-bus, 28-bus, 30-bus, 33-bus, 69-bus and 119-bus radial distribution systems to find the optimal placement and size of Distribution generators. The sizing and placement are tabulated in Table1.

Table 1: DG sizing and placement

Test bus System	Size of Distribution Generator (MW)	Placement of Distribution Generator
12 Bus System	0.04661	9
28 Bus System	0.370	8
30 Bus System	5.7553	21
33 Bus System	2.5106	6
69 Bus System	1.5660	61
119 Bus System	1.000, 3.000	29,64

EFFECT OF INCLUDING DG FOR LOSS MINIMIZATION:

The effect of DG for loss minimization in the network was calculated by load flow analysis method and results were tabulated in Table 2 which shows that due to integration of distribution generators the total losses of the system will get reduced.

Table 2: Effect of DG for loss minimization

Test bus System	Total System Losses Without DG(MW)	Total System Losses With DG(MW)
12 Bus	0.0207	0.0169
28 Bus	0.6869	0.4135
30 Bus	0.88	0.35
33 Bus	0.2110	0.1393
69 Bus	0.2250	0.08658
119 Bus	1.5412	1.2815

TOTAL COST REDUCTION AFTER DG:

The effect of including DG maximises the cost of saving was calculated and results were tabulated in Table 3 which shows that due to integration of distribution generators the total cost of power will get reduced.

Table3: Effect of DG for loss minimization

Test bus System	Total cost of Losses Without DG(MW)	Total cost of Losses after DG(MW)
12 Bus	5645.21	3968.39
28 Bus	28554.35	22877.82
30 Bus	33449.21	26828.37
33 Bus	37543.67	32987.98
69 Bus	41237.39	36872.21
119 Bus	82336.45	69364.65

CONCLUSION:

This work proposed the optimal placement and sizing of Distribution Generator so as to minimize the total system loss and maximize the net saving. The DG placement in a Distribution network is a discontinuous solution problem with discrete variable and objective of finding the best location for locating the DG of optimal rating in Distribution network such that the outcome yields maximum percentage of cost saved with improved voltage profile. The proposed work is implemented in IEEE test bus systems and the results obtained shows that DG integration leads to reduction of system loss, maximize the saving and improve the system voltage profile.

REFERENCE:

- [1] A. Appa Rao¹, M. Win Babu², K.S. Linga Murthy, "Forward Sweeping Method for Solving Radial Distribution Networks," International Journal of Advanced Research in Electrical, Electronics and Instrumentation Engineering Vol. 2, Issue 9, Sep 2013.
- [2] RM SalomanDanaraj, Shankarappa F Kodad, Tulsi Ram Das, "An algorithm for radial distribution power flow in Complex mode including voltage controlled buses," Indian Journal of Science and Technology Vol.1 no. 2, Dec 2007.
- [3] JanakaEkanayake, KithsiriLiyanage, JianzhongWu, Akihiko Yokoyama, Nick Jenkins, "Smart Grid Technology and Applications," A John Wiley & Sons, Ltd., Publication.
- [4] Sun, H.; Nikovski, D.; Ohno, T.; Takano, T.; Kojima. Y., "A Fast and Robust Load Flow Method for Distribution Systems with Distributed," Mitsubishi Electric Research Laboratories Tr2011-070, Sep 2011.
- [5] M. Abbagana, G. A. Bakare, I. Mustapha, "Optimal placement and sizing of a distributed generator in a power distribution system using differential evolution," International Journal of Research in Engineering, IT and Social Sciences Vol. 2 no. 4, Apr 2012.
- [6] A.KartikeyaSarma, K.Mahammad Rafi, "Optimal Selection of Capacitors for Radial Distribution Systems Using Plant Growth Simulation Algorithm" International Journal of Advanced Science and Technology Vol. 30, May 2011.
- [7] KrischonmeBhumkittipich and WeerachaiPhuangpornpitak, "Optimal Placement and Sizing of Distributed Generation for Power Loss Reduction using Particle Swarm Optimization," science Direct 10th Eco-Energy and

Materials Science and Engineering (EMSES), 2012.

[8] M. M. Aman, G. B. Jasmon, K. H. Solangi, A. H. A. Bakar, and H. Mokhlis, "Optimum Simultaneous DG and Capacitor Placement on the Basis of Minimization of Power Losses," International Journal of Computer and Electrical Engineering, Vol. 5, Issue 5, Oct 2013.

[9] F.J. Ruiz-Rodriguez, J.C. Hernández, F. Jurado, "Probabilistic load flow for radial distribution networks with photovoltaic generators," IET Renew. Power Gener., Vol. 6, Issue 2, pp. 110–121, 2012.

[10] UlasEminoglu, M.HakanHocaoglu, "A New PV-Node Modelling for the Distribution System Power Flow Algorithm," International Journal of Distributed Energy Resources, Vol. 6 no.1, pp. 1-17, 2010.

[11] K. Zou, A. P. Agalgaonkar, K. Muttaqi, S. Perera& N. Browne, "Support of distribution system using distributed wind and PV systems," in AUPEC'09: Proceedings of the 19th Australasian Universities Power Engineering Conference, pp. 1-6, 2009.

[12] Wencong Su, Member, IEEE, Jianhui Wang, Senior Member, IEEE, and Jaehyung Roh, Member, IEEE, "Stochastic Energy Scheduling in Microgrids With Intermittent Renewable Energy Resources," IEEE Transactions On Smart Grid, Vol. 5 no. 4, Jul 2014.

[13] Y.Mohamedshuaib, M.Suryakalavathi, C.ChristoberAsirRajan "Optimal capacitor placement in radial distribution system using gravitational search algorithm" science direct electric power and energy system 64(2015) 384-397.

Performance Analysis On Multi Carrier Trapezoidal PWM Strategies For Symmetrical Multilevel Inverter

Venkataraman.K¹, Jayaprakash.C²

¹Assistant Professor,Dept of EEE, Arunai Engineering College,Tiruvannamalai, Tamilnadu, India

²PG Scolar, Arunai Engineering College,Tiruvannamalai, Tamilnadu, India

c.jayaprakash0007@gmail.com

Abstract— This paper intends about the performance analysis of novel seven level symmetric inverter with reduced switch count. A new Multi Carrier Combined Disposition Pulse Width Modulation (MCCDPWM) strategies are proposed to trigger the switches with trapezoidal reference wave. Performance parameters like Total Harmonic Distortion (THD), Fundamental V_{RMS} (V_{RMS}), Crest Factor(CF), Distortion Factor(DF) is analyzed by applying newly proposed modulation strategies for various modulation indices using MATLAB-SIMULINK.

Keywords – MCCDPWM, THD, CF, DF, V_{RMS}

I.INTRODUCTION

Multilevel inverters are constructed by the arranging power electronic switches and DC sources in order to get synthesize desired output voltage in terms of several level. They are mostly employed in power conversion applications such as motor drives and utility sectors. Interconnection of devices for splitting DC sources amends the voltage handling capacity of these inverters for specified power devices [1] [2]. Manjrekar and Venkataraman [3] ascertained about new topologies and modulation strategies for multilevel inverters to reduce control complexity and to overcome voltage balancing problems. Variety of modulation strategies for multilevel inverters has been proposed for industrial applications. Mostly it employs carrier-based pulse width modulation scheme [4] [5]. McGrath and Holmes [6] analyzed about multi carrier based PWM strategies in which gating signals in each level is generated when a modulating signal is compared with multiple triangular Carriers. Radan et al [7] discussed the carrier-based PWM methods for multi-level inverters to have flexible control over output voltages generated. Yi-Hung Liao and Ching-Ming Lai [8] proposed a newly-constructed simplified single-phase multi string multilevel inverter employed in distributed energy resources which focus on conversion efficiency with lower electromagnetic interference. Ehsan Najafi and Abdul Halim Mohamed Yatim [9] designed a new multilevel inverter topology with reduced device counts which remedied the voltage balancing problems.

Satheeyamoorthy[10] proposed a new topology of cascaded hybrid multilevel inverter with series connected sub multilevel inverter blocks to reduce computational time, control simplicity by employing Genetic Algorithm technique. Krishna Kumar Gupta and Shailendra Jain [11] suggested a novel multilevel inverter which intends to reduce switch counts and accompanied by switched DC sources.

II.NOVEL MULTILEVEL INVERTER

Over a few decades, multilevel inverter has found wide spectrum of growth and advancement in their topologies made by various research individuals. Three basic type of multilevel inverter has made course for their evolution in structure. Ebrahim Babaei et al [12] proposed generalized cascaded multilevel inverters with reduced switching devices on the basis of Developed H-Bridge. This novel seven level inverter consists six switches which comprises of submultilevel blocks and polarity reversal units. The conventional inverter needs $2(m-1)$ switches where m represents the number of level of the inverter. For this configuration switch count decreases furthers as the number of levels has been increased. Fig 1. shows circuit configuration for novel multilevel inverter.

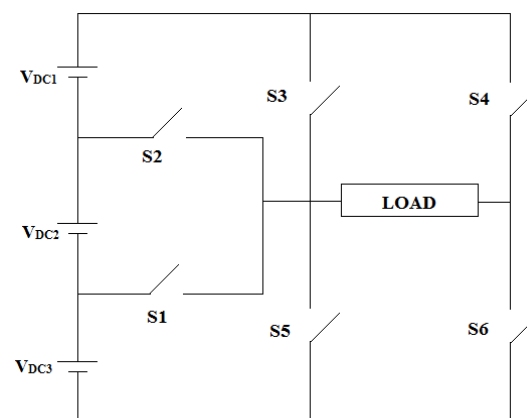


Fig. 1
Novel multi level inverter topology

The number of output levels of voltage generated can be given by:

$$m=2n+1$$

Where n is the number of DC source

Operations of novel inverter to generate Seven level output voltage as follows:

- 1) **Output voltage $3V_{DC}$:** Switch S3 and S6 were turned ON.
- 2) **Output voltage $2V_{DC}$:** The switch S2 and H bridge switch S6 were turned ON.
- 3) **Output voltage V_{DC} :** The switch S1 and H bridge switch S6 were turned ON.
- 4) **Zero output:** The switches S3 and S4 are ON, short-circuiting the load.
- 5) **Output voltage $-V_{DC}$:** The H Bridge switch S4 and switch S2 were turned ON.
- 6) **Output voltage $-2V_{DC}$:** The switch S4 and switch S1 were turned ON.
- 7) **Output voltage $-3V_{DC}$:** H Bridge switch S4 and S5 were turned ON.

III. MODULATION STRATEGIES FOR MULTILEVEL INVERTER

Optimized output voltage can be achieved by implementing various modulation strategies. Among different modulation strategies carrier based techniques are mostly used due to their control flexibility. Newly proposed modulation scheme is similar to that of carrier disposition modulation strategy. In this scheme different combination of Phase disposition and Alternate Phase opposition strategy has been taken into consideration to have combined merits of both strategies and to improve the performances. It has been defined as Multi carrier combined disposition strategy and classified into (MCCDPWM- A, B, C, D).

The amplitude modulation index is specified as " m_a ".

$$m_a = 2 A_m / (m-1) A_c$$

Where A_m - Amplitude of reference

A_c - Amplitude of carrier

Frequency ratio $m_f = f_c / f_m$

Where

f_c - frequency of carrier wave

f_m - frequency of reference wave

Gating signal is produced by comparing carriers with Trapezoidal reference which is shown below from Fig.2-.5.

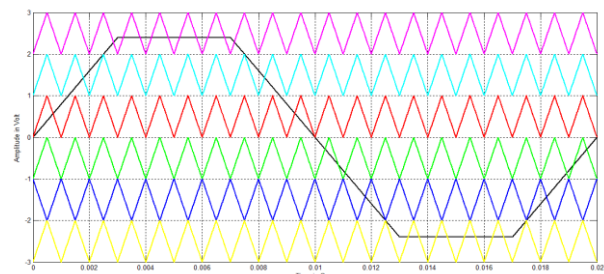


Fig. 2 Carrier arrangement for MCCDPWM-A Strategy
($m_a = 0.8, m_f = 20$)

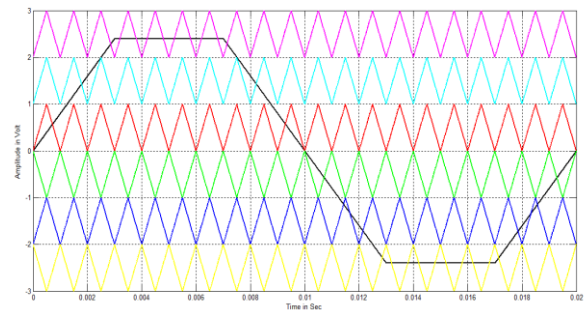


Fig. 3 Carrier arrangement for MCCDPWM-B Strategy
($m_a = 0.8, m_f = 20$)

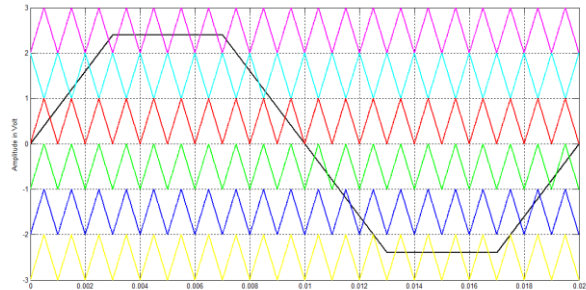


Fig. 4 Carrier arrangement for MCCDPWM-C Strategy
($m_a = 0.8, m_f = 20$)

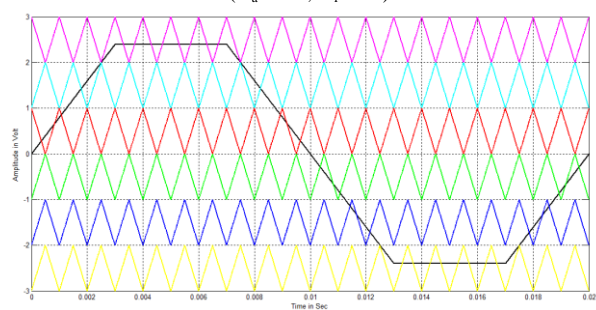


Fig. 5 Carrier arrangement for MCCDPWM-D Strategy
($m_a = 0.8, m_f = 20$)

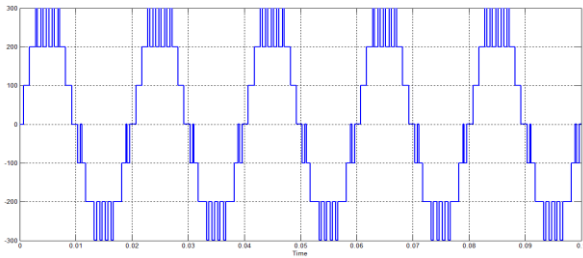


Fig. 6 Output voltage generated by MCCDPWM-A strategy

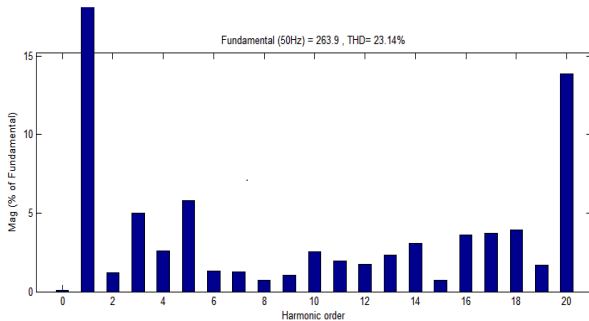


Fig. 7 FFT Plot for output voltage of MCCDPWM-A Strategy

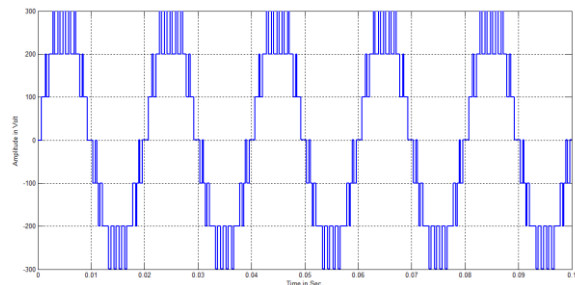


Fig. 10 Output voltage generated by MCCDPWM-C strategy

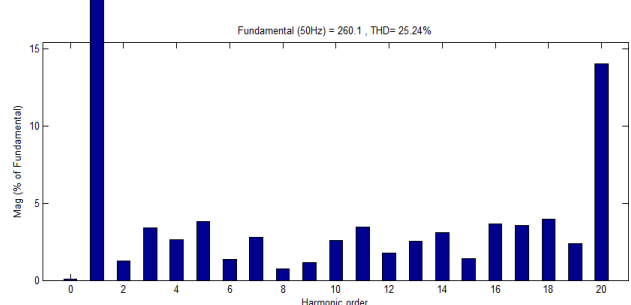


Fig. 11 FFT Plot for output voltage of MCCDPWM-C Strategy

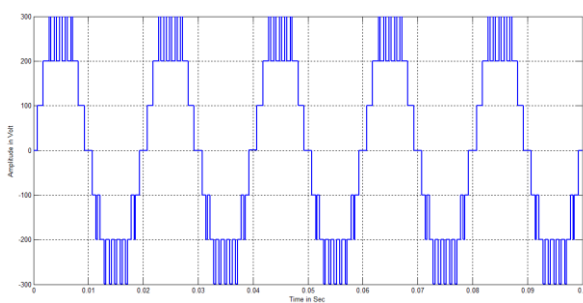


Fig. 8 Output voltage generated by MCCDPWM-B strategy

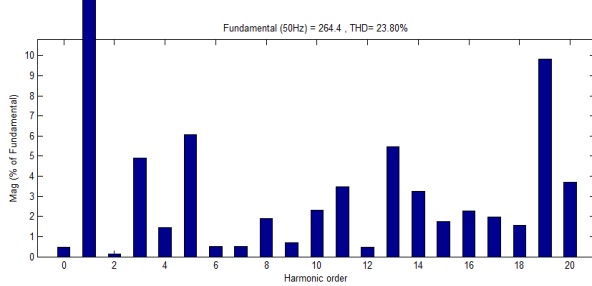


Fig. 9 FFT Plot for output voltage of MCCDPWM-B Strategy

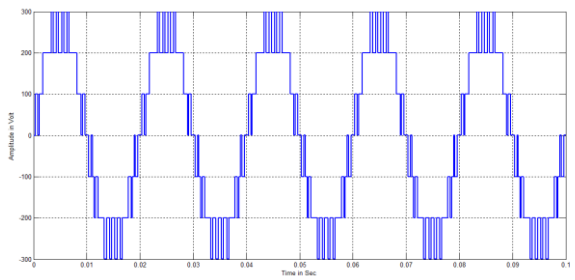


Fig. 12 Output voltage generated by MCCDPWM-D strategy

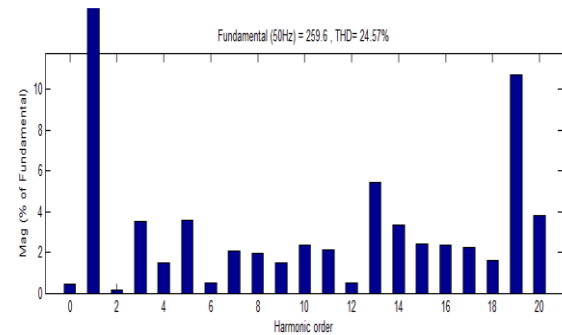


Fig. 13 FFT Plot for output voltage of MCCDPWM-D Strategy

IV. PERFORMANCE PARAMETERS OF INVERTERS

The outputs of practical inverters may be resolved into fundamental and harmonic components. Performance of an inverter is usually evaluated in terms of the following parameters:

1. Harmonic Factor of n^{th} harmonic

The harmonic factor is a measure of contribution of the individual harmonic in the output voltage of an inverter. It is defined as the ratio of the RMS voltage of n^{th} harmonic component V_n in the output to the RMS value of fundamental

$$\text{component } V_1 \cdot HF_n = \frac{V_n}{V_1}$$

2. Total Harmonic Distortion

THD is a measure of closeness in shape between a waveform and its fundamental component and is defined as

$$THD = \frac{1}{V_1} \sqrt{\sum_{n=2,3,\dots}^{\infty} V_n^2}$$

3. Distortion factor

Distortion factor indicates the amount of harmonics that remains in the output voltage after it has been subjected to second order attenuation (i.e. divided by n^2). It is defined as

$$DF = \frac{1}{V_1} \sqrt{\sum_{n=2,3,\dots}^{\infty} \left[\frac{V_n}{n^2} \right]^2}$$

4. Lowest Order Harmonic

The LOH is that harmonic component whose frequency is closest to the fundamental and its amplitude is greater than or equal to 3% of the fundamental component. Higher the frequency of LOH, lower will be the distortion in the output.

5. Crest Factor

CF is a measure of peak input current $I_{s(\text{peak})}$ as compared with its RMS value I_s . CF is often of interest to specify the peak current ratings of devices and components. The CF of the input current is defined by

$$CF = \frac{I_{s(\text{peak})}}{I_s}$$

These performance parameters has been simulated and tabulated for various proposed modulation strategies.

V.SIMULATION RESULTS

The simulation results were carried out in MATLAB / SIMULINK. Simulations were accomplished for various values of m_a ranging from 0.7 to 1. Fig. 6, 8, 10, and 12 represents the output voltage waveform generated for various MCCDPWM scheme such as (MCCDPWM-A, B, C, D) and its

corresponding FFT plot for the proposed modulation strategy were shown in Fig 7, 9, 11 and 13 . From “Fig.7” it has been detected that 3rd, 4th, 5th, 10th, 11th, 13th, 14th, 16th, 17th, 18th and 20th harmonic energy are dominant for MCCDPWM-A scheme. From ‘Fig. 9’ it has been noticed that 3rd, 5th, 10th, 11th, 13th, 14th, 16th, 17th, 19th, and 20th harmonics energy are dominant for utilizing trapezoidal reference, using MCCDPWM-B strategy. For MCCDPWM –C scheme it has been found that 3rd, 4th, 5th, 7th, 10th, 11th, 13th, 14th, 16th, 17th, 18th, 19th and 20th harmonics are high from “Fig. 11”. From “Fig. 13” it has been noticed that 3rd, 5th, 7th, 10th, 11th, 13th, 14th, 15th, 16th, 17th, 19th and 20th harmonics are dominant. The following parameter values are used for simulation: $V_{dc} = 100V$, Resistive load = 100ohms.

TABLE I
%THD COMPARISON BETWEEN DIFFERENT MODULATION STRATEGIES

m_a	MCCD PWM-A	MCCD PWM-B	MCCD PWM-C	MCCD PWM-D
1	12.98	12.49	12.82	13.55
0.95	17.78	17.41	18.97	19.43
0.9	20.87	20.67	22.69	22.93
0.85	22.65	22.79	24.76	24.64
0.8	23.14	23.8	25.24	25.42
0.75	24.7	24.15	24.9	24.43
0.7	24.08	21.96	22.33	24.57

TABLE II
 V_{RMS} COMPARISON BETWEEN DIFFERENT MODULATION STRATEGIES

m_a	MCCD PWM-A	MCCD PWM-B	MCCD PWM-C	MCCD PWM-D
1	230.3	228.4	234.6	236.5
0.95	219.1	217.9	221.4	222.7
0.9	208.2	207.8	208.8	209.2
0.85	197.3	197.3	196.1	196.1
0.8	186.6	187	183.9	172.5
0.75	174.5	175.2	173.1	161.3
0.7	162.2	163.1	162.3	183.6

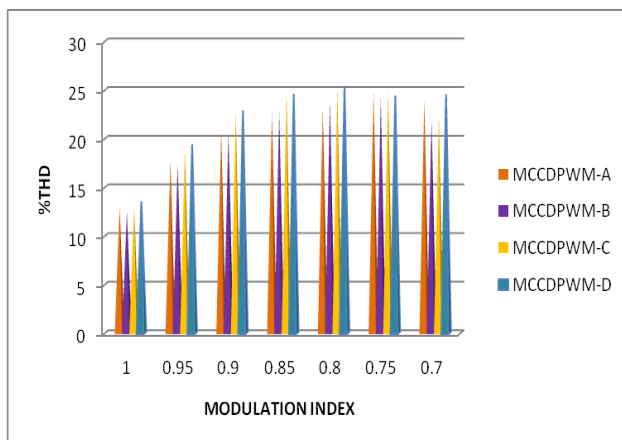
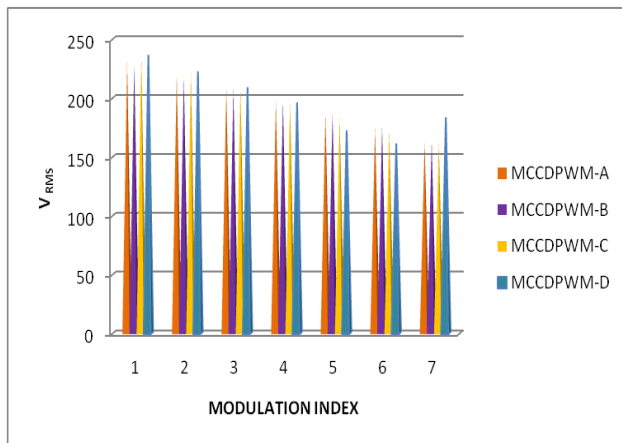
TABLE III
CREST FACTOR BETWEEN DIFFERENT MODULATION STRATEGIES

M_a	MCCD PWM-A	MCCD PWM-B	MCCD PWM-C	MCCD PWM-D
1	1.4142	1.4141	1.4138	1.4139
0.95	1.4144	1.4144	1.41463	1.414
0.9	1.4145	1.4109	1.4142	1.4144
0.85	1.414	1.414	1.414	1.4145

0.8	1.4142	1.4139	1.41435	1.4139
0.75	1.4143	1.4143	1.4147	1.4141
0.7	1.4136	1.4144	1.414	1.4139

TABLE IV
%DISTORTION FACTOR BETWEEN
DIFFERENT MODULATION STRATEGIES

M _a	MCCDPWM-A	MCCDPWM-B	MCCDPWM-C	MCCDPWM-D
1	0.6166	0.4426	0.8575	0.8163
0.95	0.6342	0.4452	0.7962	0.7314
0.9	0.6296	0.4811	0.709	0.6274
0.85	0.6477	0.206	0.6118	0.5137
0.8	0.6953	0.6069	0.5464	0.4331
0.75	0.6489	0.6117	0.5073	0.4277
0.7	0.584	0.6066	0.4883	0.4452

Fig.14 %THD Vs m_a for different modulation strategiesFig. 15 V_{RMS} Vs m_a for different modulation strategies

VI.CONCLUSION

Novel seven level symmetrical inverter was gated by implementing proposed Multi Carrier Combined Disposition scheme. The performance

parameters such as THD, V_{RMS}, for different modulation strategies were simulated and compared. From the simulation results Distortion factor, Crest factor was calculated and tabulated. From the simulation outcome we noticed that MCCDPWM-B strategy made lower harmonic distortion and MCCDPWM-D strategy renders higher V_{RMS} with better DC utilization.

VII.REFERENCES

- [1] Y. S. Kim, B. S. Seo, and D. S. Hyun, "A new N-level high voltage inversion system," in *Proc. IEEE IECON'93*, 1993, pp. 1252–1257.
- [2] F. Z. Peng, J. S. Lai, J. McKeever, and J. Vancoevering, "A multilevel voltage-source converter system with balanced DC voltages," in *Proc.IEEE PESC'95*, Atlanta, GA, 1995, pp. 1144–1150.
- [3] M. Manjrekar and G. Venkataraman, "Advanced topologies and modulation strategies for multilevel inverters," in *Conf. Rec. IEEE PESC 1996*, pp. 1013–1018.
- [4] Y. H. Lee, R. Y. Kim, and D. S. Hyun, "A novel PWM scheme for a three-level voltage source inverter with GTO thyristors," *IEEE Trans. Ind. Applicat.*, vol. 32, pp. 260–268, Mar./Apr. 1996.
- [5] L. M. Tolbert and T. G. Habetler, "Novel multilevel inverter carrier-based PWM method," *IEEE Trans. Ind. Appl.*, vol. 35, no. 5, Sep./Oct. 1999, pp. 1098–1107.
- [6] B. P. McGrath and D. G. Holmes, "Multicarrier PWM strategies for multilevel inverters," *IEEE Trans. Ind. Electron.*, vol. 49, no. 4, Aug. 2002,pp. 858–867.
- [7] A. Radan, A. H. Shahirinia, and M. Falahi, "Evaluation of carrier-based PWM methods for multi-level inverters," in *Proc. IEEE ISIE*, 2007, pp. 389–394.
- [8] Yi-Hung Liao, and Ching-Ming Lai, "Newly-Constructed Simplified Single-Phase Multistring Multilevel Inverter Topology for Distributed Energy Resources," *IEEE Trans. Power Electron.*, vol. 26, no. 9, Sept. 2011, pp.2386 -2390
- [9] Ehsan Najafi, and Abdul Halim Mohamed Yatim, "Design and Implementation of a New Multilevel Inverter Topology" *IEEE Trans. Power Electron.*, vol.59,no.11, Nov. 2012, pp.4148-4154
- [10] K. P. Satheyamoorthy, "New Topology of Cascaded Hybrid Multilevel Inverter," *International Journal of Advanced Technology in Engineering and Science* , Volume No.01, Issue No. 11, November 2013
- [11] Krishna Kumar Gupta and Shailendra Jain, "A Novel Multilevel Inverter Based on Switched DC Sources," *IEEE Trans.Indus. Elect.*, vol. 61, no. 7, July 2014 pp.3269-3278
- [12] Ebrahim Babaei, Somayeh Alilu, and Sara Laali, "A New General Topology for Cascaded Multilevel Inverters With Reduced Number of Components Based on Developed H-Bridge" *IEEE Trans.on Industrial Electronics*,vol. 61, no. 8, pp. 3932-3939, August 2014

PV BASED CASCADED SEPIC CONVERTER FOR BATTERY CHARGING

Nisha.V^{1,a*},Mr.R.Elanthirayan^{2,b}

¹St. Joseph's College of Engineering, Chennai-600119, Tamil Nadu, India

²St. Joseph's College of Engineering, Chennai-600119, Tamil Nadu, India
nishavaasu@gmail.com^a, ethirayan@gmail.com^b

Abstract—A Cascaded Sepic Converter [1] is implemented with a output sensing direct control method [2] to extract the maximum power from the sun using the MPPT (Maximum power point tracking) and is used for battery charging[3].Initially, the conventional sepic converter was primarily designed to provide a non pulsating input current, operating with both inductors in continuous current mode .The modified sepic Converter [1] is designed to operate as a dc-dc Converter and it can be viewed as a cascade of a modified boost Converter and a buck-boost Converter. The boost Converter operates in discontinuous current mode, while the buck-boost Converter operates in continuous current mode. The main novelty of the Cascaded Sepic Converter is the buffered input and output. This is mainly used for higher order system. The selection of the perturb& observe (P&O) [5] algorithm permits the use of output sensing direct control method which eliminates the output voltage and totally based on the theory of load matching. Perturb and Observe (P&O) algorithm is recommended because of its simplicity and ease of implementation.

Keywords: Cascaded Sepic Converter, Maximum Power Point Tracking(MPPT),Perturb& Observe(P&O), Load matching theory, Buffered input and output.

I INTRODUCTION

The Conventional sources of energy are rapidly depleting. Moreover the cost of energy is rising and therefore photovoltaic system is a promising alternative. They are abundant, pollution free, distributed throughout the earth and recyclable. The hindrance factor is its high installation cost and low conversion efficiency. Therefore our aim is to increase the efficiency and power output of the system. It is also required that constant voltage is supplied to the load irrespective of the variation in solar irradiance and temperature.

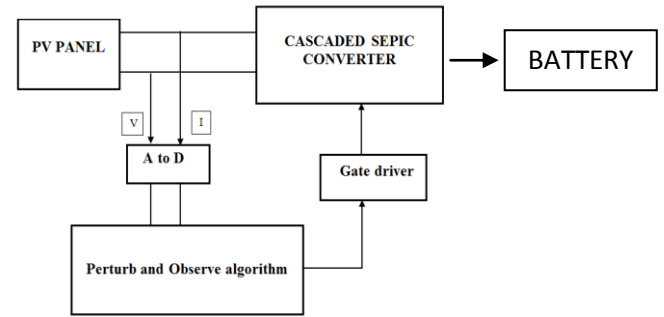


Fig.1. Block Diagram of The Proposed Scheme

PV arrays consist of parallel and series combination of PV cells that are used to generate electrical power depending upon the atmospheric conditions. So it is necessary to couple the PV array with a Cascaded Sepic Converter. Moreover our system is designed in such a way that with variation in load, the change in input voltage and power fed into the Converter follows the open circuit characteristics of the PV array. Our system can be used to supply constant stepped up voltage to dc loads using DC-DC Converter.

II PHOTO-VOLTAIC PANEL

Photovoltaic (PV) is the method of generating electrical power by converting solar radiation into direct current electricity using semiconductors that exhibit the photovoltaic effect.A photovoltaic cell is comprised of a P-N junction semiconductor material that produces current by the photovoltaic effect. Materials that are widely used for photovoltaic include mono crystalline silicon, polycrystalline silicon, amorphous silicon, cadmium telluride, and copper indium selenide. When light energy strikes the solar cell,electrons are let loose from the atoms in the semiconductor material. when the conductors are attached to the positive and negative sides, forming an electrical circuit, the electrons is obtained in the form of an electric current. The standard equivalent circuit of the PV cell is shown in Fig.1. This electricity can then be used to power a load. Due to the low voltage generated in a PV cell, several PV cells are

connected in series and in parallel to form a PV module for desired output. Due to the growing demand for renewable energy source, the manufacturing of solar cells and photovoltaic arrays has advanced considerably in recent years

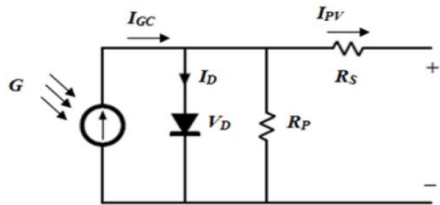


Fig.2.1 Equivalent Circuit of The PV Cell

$$I_{ph} = N_p I_{ph} - N_p I_S \left[\exp \left\{ \frac{q(R_s + I_{pv} R_s)}{N_e A k T} \right\} - 1 \right]$$

(1)

The output current from the PV cell is found by applying the Kirchhoff's current law on the equivalent circuit. Where I_{ph} is the photon current A is the ideality factor, k, the Boltzmann constant, q, the electron charge and T is the actual temperature. I_p is the photovoltaic current and N_p is the number of cells connected in parallel. I_s is the saturation current, In fact, the PV efficiency is sensitive to small change in R_s but insensitive to variation in R_{sh} .

III MAXIMUM POWER POINT TECHNIQUE PERTURB AND OBSERVE (P&O)ALGORITHM

The P&O method operates periodically incrementing or decrementing the output terminal voltage of the PV and comparing the power obtained in the current cycle with the power of the previous one (performs dP/dV). If the voltage varies and the power increases, the control system changes the operating point in that direction, otherwise change the operating point in the opposite direction. Once the direction for the change of voltage is known, the voltage is varied at a constant rate. This rate is a parameter that should be adjusted to allow the balance between faster response with less fluctuation in steady state. A modified version is obtained when the steps are changed according to the distance of the MPP, resulting in higher efficiency. This is an excellent method to reach the MPP and it is independently from the PV panel/manufacturer, although this method may suffer from fast changes in environmental conditions.

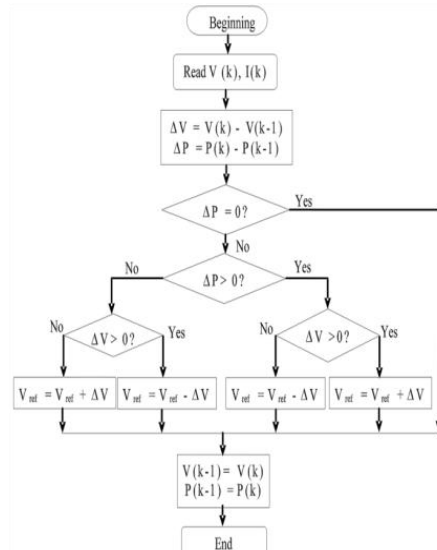


Fig.3.1 Flow Chart of P&O MPPT Method

IV CASCADED SEPIC CONVERTER

Single-ended primary-inductor Converter (SEPIC) is a type of DC-DC Converter allowing the electrical potential (voltage) at its output to be greater than, less than, or equal to that at its input; the output of the Sepic is controlled by the duty cycle of the control transistor.

The new topology is presented in figure In the following. The Converter may be viewed as a cascade of a modified boost Converter and a buck-boost Converter. The switches are turned on and off synchronously. The modified boost Converter operates in discontinuous current mode, while the buck-boost Converter operates in continuous current mode.

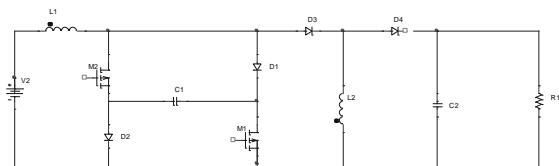


Fig.4.1 Circuit Diagram of Proposed Converter

The main novelty of the Cascaded Sepic Converter is the buffered input and output. By this property, any change in the input will not affect the output. This is mainly used for higher order system.

V. WORKING PRINCIPLE OF CASCADED SEPIC CONVERTER

Modes of Operation

Mode 1:

In mode 1, the switches S1 and S2 are turned ON. During this mode the diode d3 is forward biased the others are reverse biased. The current passes through the inductances and will discharge C1 to zero voltage. C2 discharges on the load resistor. In this mode the capacitor C1 gets charged from both the sides. The path in this mode is L-S1-C1-S2-Vs and Co-Ro sides mode is L-S1-C1-S2-Vs and Co-Ro.

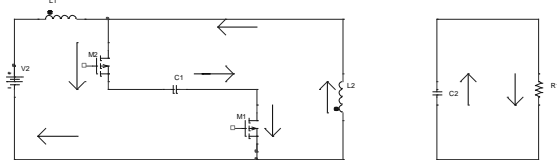


Fig.5.1 Mode 1 of Proposed Converter

$$V_{ll} = V_s + V_c$$

$$i_{L1} = (V_s + V_c)t/L$$

$$i_C = i_{L1} + i_{L2}$$

$$i_{L2} = V_c/L_2$$

Mode 2:

In this mode both the switches S1 and S2 are closed. Since both the switches are closed, the capacitor has to get discharged somewhere, so the path taken for discharging is C-D2-L2-D3-D1. Now at this time the inductor will have stored energy. So the current in the L is very high. Now this needs to get discharged so it flows from L-C-Ro(i.e) to the load. The current L2 freewheels through the diode D4.

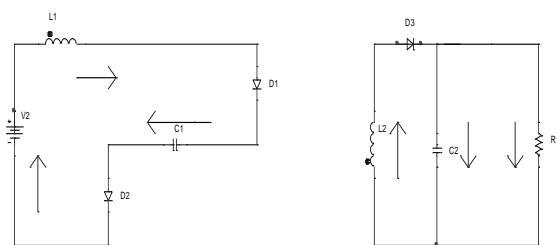


Fig.5.2 Mode 2 of Proposed Converter

$$V_{ll} = V_s - V_c$$

$$i_{L1} = (V_s - V_c)t/L$$

$$i_{L2} = i_{C0} + i_o$$

$$i_{L2} = C \left(\frac{d_{v0}}{dt} + \frac{V_0}{R_o} \right)$$

VI WORKING OF A BATTERY

The battery starts charging at the initial capacity level called the rated capacity of the battery. The nominal voltage represents the end of the linear zone of the discharge characteristics is assumed to be 12V. The initial State-Of-Charge (SOC) of the battery. 100% indicates a fully charged battery and 50% indicates an half charged battery. This parameter is used as an initial condition for the simulation and does not affect the discharge curve. We focus on the closed-loop techniques that communicate with the battery and terminate charge when certain responses occur. Lead acid charging acid charging uses a voltage-based algorithm that is similar to lithium-ion

A 2A current is maintained through a closed loop converter by sensing its current. The current can be varied by changing the shunt resistance value of the converter connected to the battery. The Ah of the battery is given to be 4Ah so in order to charge the battery fully, 2A current is made to flow through the battery for one-hour. Lead acid is sluggish and cannot be charged as quickly as other battery. Lead acid batteries should be charged in three stages, which are constant-current charge, topping charge and float charge

VII SIMULATION RESULTS

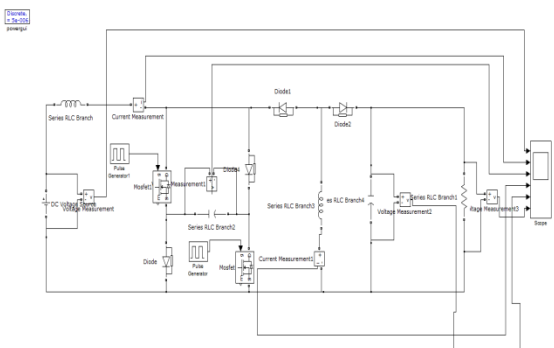


Fig 7.1 Simulation Diagram of Proposed Diagram

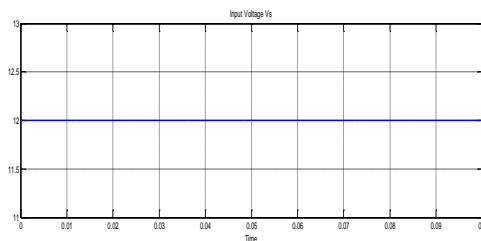
7.1 Input Voltage Waveform:

Fig 7.1 Simulation Output For Input Voltage

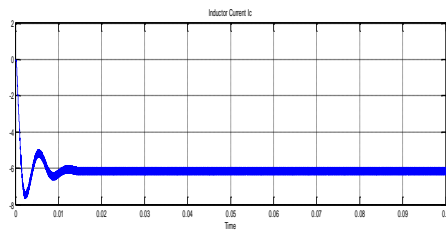
7.2 Current Flow Through L₁ Waveform

Fig 7.2 Simulation Output For Current In L1

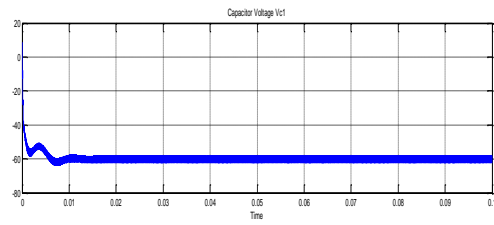
7.3 Capacitor Voltage Waveform(Vc1):

Fig 7.3 Simulation Output For Capacitor Voltage Vc1

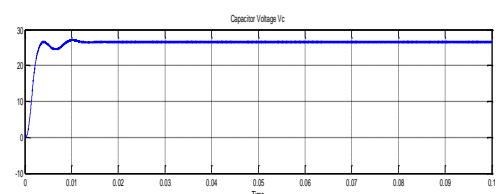
7.4 Capacitor Volatge Vc2 Waveform

Fig 7.4 Simulation Output For Capacitor Voltage Vc2

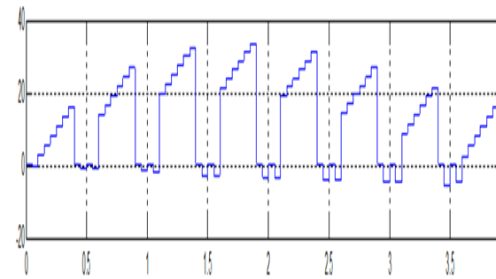
7.5 Inductor Current Waveform

Fig 7.5 Simulation Output For Inductor Current

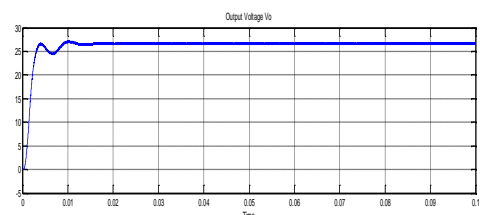
7.6 Output Voltage Waveform

Fig 7.6 Simulation Output For Output Voltage

VII CONCLUSION

From the simulation results, it is concluded that the performance of the proposed converter is high. In this paper presents a new topology of a SEPIC converter used as a higher order system in terms of stability characteristics. The modified sepic converter is designed to operate as dc-dc converter and it can be viewed as a cascade of a modified boost converter and a buck-boost converter. The boost converter operates in discontinuous current mode, while the buck-boost converter operates in continuous current mode. In the proposed converter the input and output is buffered. By this, any change in the input will not affect the output voltage. This makes the cascaded sepic converter as a higher order system.

VIII REFERENCES

- [1]Power Factor Correction Circuit with a New Modified SEPIC Converter, 24th International Spring Seminar on Electronics Technology May 5-9, 2001, Calimanesti-Caciulata, Romania
- [2]Azadeh Safari and SaadMekhilef, "Simulation and hardware implementation of incremental conductance MPPT with direct control method using Cuk converter," IEEE Trans. on Ind. Electron., vol. 58, no. 4, pp. 1154- 1161, April 2011
- [3]R.-J. Wai, W.-H.Wang, and C.-Y. Lin, "High-performance stand-alone photovoltaic generation system," IEEE Trans. Ind. Electron., vol. 55, no. 1, pp. 240-250, Jan. 2008
- [4] F. M. Gonzalez-Longatt, "Model of photovoltaic module in Matlab," in 2do congresoiberoamericano de estudiantes de ingenieriacute; aelectrica, electronic y computacion, ii cibelec, 2005, pp. 1-5.
- [5] A. K. Abdelsalam, A. M. Massoud, S. Ahmed, and P. N. Enjeti, "High performance adaptive perturb and observe MPPT technique for photovoltaic-based microgrids," IEEE Trans.Power Electron., vol. 26, no. 4, pp. 1010-1021, Apr. 2011.
- [6] F. M. Gonzalez-Longatt, "Model of photovoltaic module in Matlab," in 2do congresoiberoamericano de estudiantes de ingenieriacute; aelectrica, electronic y computacion, ii cibelec, 2005, pp. 1-5.
- [7] Y. H. Ji, D. Y. Jung, J. G. Kim, J. H. Kim, T. W. Lee, and C. Y. Won, "A real maximum power tracking method for mismatching compensation in PV array under partially shaded conditions," IEEE Trans. Power Electron., vol. 26, no. 4, pp. 1001-1009, Apr. 2011.
- [8] L. Zhang, W. G. Hurley, and W. H. Wolfle, "A new approach to achieve maximum power point tracking for PV system with a variable inductor," IEEE Trans. Power Electron. Vol. 26, no. 4, pp. 1031-1037, Apr. 2011.
- [9] L. Zhou, Y. Chen, and F. Jia, "New approach for MPPT control of photovoltaic system with mutative-scale dual-carrier chaotic search," IEEE Trans. Power Electron., vol. 26, no. 4, pp. 1038-1048, apr. 2011.
- [10] S. Chun and A. Kwasinski, "Analysis of classical root-finding methods applied to digital maximum power point tracking for sustainable photovoltaic energy generation," IEEE Trans. Power Electron.

Reconfiguration for loss reduction and Sensitivity Analysis for simultaneous optimal placement of FC banks and DG in radial distribution network

P. Amritta¹, M. RameshBabu²

^aamritta91@gmail.com, ^brameshbabudata@gmail.com

**¹PG Scholar, Department of Electrical and Electronics Engineering, St. Joseph's College of Engineering,
Affiliated to Anna University, Chennai-600119.**

**²Professor, Department of Electrical and Electronics Engineering, St. Joseph's College of Engineering,
Affiliated to Anna University, Chennai-600119.**

Abstract: This paper presents the network reconfiguration of the radial distribution system for voltage profile improvement and loss minimization. The process of changing the distribution system topology by altering the open or closed status of the switches is called as reconfiguration. In this paper the reconfiguration of the radial distribution system is formulated as a combinatorial optimization problem considering the various operational constraints with the optimal placement of DG and capacitor for power loss minimization. The proposed problem is solved by using Harmony Search Algorithm (HSA). The proposed problem formulation and solution using HSA is tested with an IEEE 33 bus radial distribution system and the results are compared and justified.

Index terms: Network reconfiguration, distributed generators, capacitors, harmony search algorithm, forward/reverse sweep algorithm.

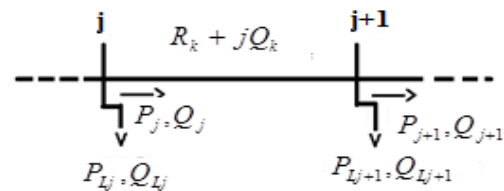
1. INTRODUCTION:

The distribution systems has several tie and sectionalizing switches. The initial status and positions of the switches determines configuration of the network. The distribution network is reconfigured by changing position of the switches through switching operation for several branches of the network in a radial distribution system [1]. The network reconfiguration to reduce the system loss was first proposed in [2]. An optimization method based on branch and bound optimization algorithm is used in [2] to determine the configuration of the network by minimizing the system losses. The branch and bound algorithm involves a major deal of power flow calculations and this inturn will increase the computational burden. Thus inorder to find a solution to this problem, various artificial intelligence algorithms are proposed and simultaneously used to solve the network reconfiguration problems. A Differential Evolution (DE) based method for solving network reconfiguration problem is proposed by Ching-Tzong Su and Chu-Sheng Lee [3]. The genetic algorithm and all the other mutation based evolutionary algorithms such as DE can generate new candidate solutions by the process of crossover

and mutation of the strings but the process of reconfiguration by using Genetic Algorithm (GA) and DE generates many infeasible solutions in which the radiality of the distribution system is violated [4]. Another widely used optimization tool known as Tabu search provides a good solution, but it does not show any good convergence property. The HSA algorithm which has been used in this paper to determine the optimal on/off configuration patterns of the switches for minimizing the system loss with subject to operating constraints overcomes all the above mentioned drawback and serves as an effective optimization tool. The effectiveness of this methodology has been emphasized through the practical application of the optimization technique to anIEEE 33-bus radial distribution system.

2. PROBLEM FORMULATION:

The distribution system reconfiguration is mainly aimed at finding the optimal configuration of the network with minimal power loss satisfying all the system constraints. The power flow method used in this method is a forward/reverse sweep algorithm [5] which is used to determine the power flow of a radial distribution system approximately. A two node radial distribution line is shown in Fig.1. Consider a branch 'k' that has been connected between two nodes 'j' and 'j+1'. The effective real (P_j) and reactive (Q_j) powers which are flowing through the branch 'k' between



node 'j' and 'j+1' can be calculated in the reverse direction from the last node and it is given as,

Fig1. A two node distribution system

$$P_j = P_{j+1} + r_j \frac{(P_{j+1}^2 + Q_{j+1}^2)}{V_{j+1}^2} \quad (1)$$

$$Q_j = Q_{j+1} + x_j \frac{(P_{j+1}^2 + Q_{j+1}^2)}{V_{j+1}^2} \quad (2)$$

The terms in equation described as follows,

$$P_{j+1} = P_{j+1} + P_{L_{j+1}} \text{ and } Q_{j+1} = Q_{j+1} + Q_{L_{j+1}}$$

P_{L_j} and Q_{L_j} are loads that are connected at node 'j'

$P_{L_{j+1}}$ and $Q_{L_{j+1}}$ are loads that are connected at node 'j+1'

P_{j+1} and Q_{j+1} are the effective active and reactive power flows from node 'j+1'

The magnitude and phase angle of the voltages for all the buses of the distribution system is given as,

$$V_{j+1} = \left[V_j^2 - 2(P_j r_k + Q_j x_k) + (r_k^2 + x_k^2) \frac{P_j^2 + Q_j^2}{V_j^2} \right]^{1/2} \quad (3)$$

$$\delta_{j+1} = \delta_j + \tan^{-1} \frac{(Q_j r_k - P_j x_k)}{[V_j^2 - (P_j r_k + Q_j x_k)]} \quad (4)$$

The total active power loss of the radial distribution network can be calculated as,

$$\text{Total } P_{\text{loss}} = \sum_{j=1}^{nb} r_j \frac{(P_j^2 + Q_j^2)}{V_j^2}$$

(5)The constraints to be satisfied are voltage profile of the system; the maximum current limit that can flow through the feeder and the radial structure of the distribution system. The objective function for the loss minimization of the distribution system is described as,

$$\begin{aligned} &\text{Minimize } f = \min(P_{T,\text{Loss}}) \\ &\text{Subjected to } V_{\min} \leq |V_j| \leq V_{\max} \\ &\quad |I_{j,j+1}| \leq |I_j| \leq |I_{j,j+1,\max}| \end{aligned} \quad (6)$$

Where,

$P_{T,\text{Loss}}$ is the total active power loss of the network.

V_{\min} is the minimum bus voltage

V_{\max} is the maximum bus voltage

$I_{j,j+1}$ is the current in the line section between the buses 'j' and 'j+1'

$I_{j,j+1,\max}$ is the maximum current limit of the line section between buses 'j' and 'j+1'

3. APPLICATION OF HSA ALGORITHM FOR THE RECONFIGURATION AND SENSITIVITY ANALYSIS OF A 33 BUS RADIAL DISTRIBUTION NETWORK:

The optimal configuration of the distribution network can be obtained by first generating all the possible radial structures of the given distribution network while considering the operating constraints and satisfying the objective function. In this paper, the HSA optimization is proven to be an effective approach[6] for the reconfiguration problem of the radial distribution network. The parameters of HSA used in this work is shown in Table1.

Step1: Initialise the HM matrix:

Initialize the Harmony Memory Size (HMS) and form the matrix of Harmony Memory (HM) composed of the combination of 1 to 32 sectionalizing switches HMS and the 5 tie line switches.

Initialise the HM matrix

HM = zeros(HMS,5) → Harmony Memory

HM(:,1:5) = randi([1,32],HMS,5)

(7)

Step2: Evaluation of the system's fitness:

The fitness function is calculated for each switching combination for both the HM matrix and INH memory matrix and the power loss is calculated for each combination of HM and INH matrix.

Step3: Improvised New Harmony Memory matrix:

The INH matrix is formed by making small changes to the existing Harmony Memory (HM) matrix by changing the combination of sectionalizing switch to be opened for each tie line switch to be closed by using the harmony search scheme by taking into account the Harmony Memory Considering Rate (HMCR) and the Pitch Adjusting Rate (PAR).

Table1. Parameters of the HSA

HMS	20
HMCR	0.85
PAR	0.3

Step4: Update the harmony memory:

The values of power loss generated for both the case i.e., the power loss for the matrix generated by HM and for the matrix generated by using INH matrix and the values are compared and the harmony memory is updated.

UpdateHarmony Memory:

```
for lp = 1:HMS
    if fitness_INH(lp) < fitness(lp)
        HM(lp,:) = INH(lp,:);
    end
end
```

Format of the Harmony Memory Matrix:

HM = [(1- 32 sectionalizing switches), HMS=20, tie line switch combination]

For example, parameters of HMC which has been given the value of 0.85 indicates that HSA will choose decision variable value from historically stored values in with 85% probability or from the entire possible range with 15% probability.

Step5: Continuous updation of the matrix until the iteration is reached:

After forming each possible switching combinations the program runs the load flow to find out the combination for which the losses are effectively minimized and the voltage profile has been improved. This is done by connecting two buses by a path in which the burden of the load is less.

Step6: Calculation of the expenditure before and after reconfiguration:

The power loss calculation for the 33 bus system is given as follows,

$$P_{loss(i)} = ((P_T(e_b))^2 + Q_T(e_b))^2 / abs(V_m(s_b))^2 * R(i) \quad (9)$$

The expenditure of loss for both the base case and the case after reconfiguration is calculated using the following equations used in coding,

$$\text{cost of } P_{loss} = k_p * P_{TLOSS} \quad (10)$$

$$\text{savings cost} = (\text{baseloss} - P_{TLOSS}) * k_p \quad (11)$$

It also gives the savings in cost of the expenditure after reconfiguration and it is calculated as the loss/Kw and is given as 168\$/Kw. Thus, the value of k_p is taken as 168\$ in the coding and the expenditure has been minimized after the performance of reconfiguration.

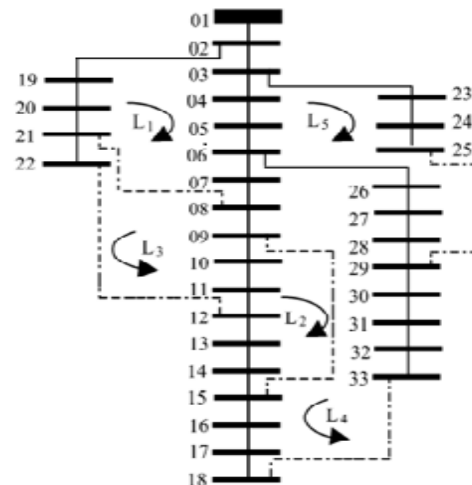
4. TEST RESULTS:

The proposed optimization technique is tested on a 33 bus radial distribution network and the obtained results proves its effectiveness. For all these systems, the substation voltages are considered to be 1 p.u., and all the tie and sectionalizing switches are to be considered as the

candidate switches for the reconfiguration problem. The optimization algorithm is developed in a computer with MATLAB software of version 2013 and the simulations are done in a system with Intel i3 core processor and 3 GB RAM.

TEST CASE:

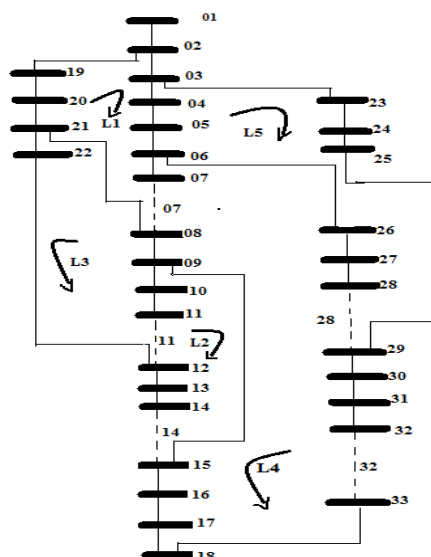
The test case considered in this section is a 33 bus radial distribution system as shown in the Fig.A1. The radial system consists of



5 tie line switches and 32 sectionalizing switches. The switches 33 to 37 are normally open switches while the switches 1 to 32 are switches which are normally closed. The total active and reactive power loads that has been connected on the system are 3715 KW and 2300 KVA.

Fig.2 Initial configuration

The Fig.2 with the initial configuration of the network before reconfiguration is shown in which the tie line switches 33,34,35,36 & 37 are



open and the initial power loss of the system before

reconfiguration is given as 199.102KW. The optimal topology of the radial network is provided in order to reduce the loss in power with relieving the overload on the feeders with less time consumption and more efficiency.

Fig.3 Optimal configuration

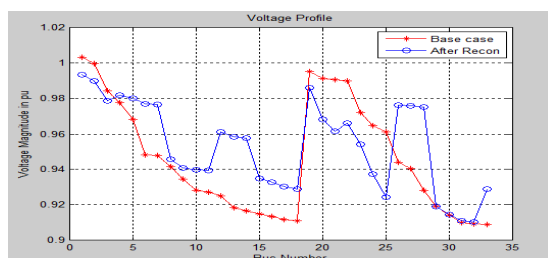
The optimal configuration of the 33 bus radial distribution network by reconfiguration using HSA algorithm is shown in the Fig.3 which shows that the tie lines switched out are 7,11,14,28 & 32 and for this switching combination the losses of the network has been reduced to 127.07KW.

Table2: Voltage magnitude profile – before and after reconfiguration

Bus No.	Voltage magnitude before reconfiguration (p.u.)	Voltage magnitude after reconfiguration (p.u.)
1	1.00334	0.99348
2	0.999673	0.989837
3	0.984357	0.978783
	0.977662	0.981914
5	0.968257	0.980158
6	0.94823	0.976851
7	0.947799	0.976606
8	0.941539	0.945705
9	0.934628	0.940907
10	0.928186	0.939661
11	0.927081	0.939563
12	0.925168	0.961107
13	0.918582	0.958283
14	0.916507	0.957578
5	0.91505	0.934886
16	0.913568	0.932931
17	0.911711	0.93024
18	0.911059	0.929109

19	0.995094	0.986021
20	0.991394	0.968266
21	0.990724	0.96143
22	0.990143	0.966198
23	0.971975	0.954296
24	0.964742	0.937423
25	0.961132	0.924314
26	0.944033	0.976183
27	0.940576	0.975883
28	0.928216	0.975341
29	0.919284	0.919111
30	0.914319	0.914498
31	0.910099	0.910953
32	0.909226	0.910294
33	0.908992	0.928773

The voltage profiles of the system before and after reconfiguration are shown in Fig.4 and the value of the magnitude of the voltage are shown in the Table2. The improvement in the voltage profile after the performance of the reconfiguration is an indication of relieving of the overload on feeders of the system.

**Fig.4 Voltage profile**

The status of the tie line switches for the base case and the switch numbers which has been opened as the tie lines after performing the reconfiguration using the HSA optimization are

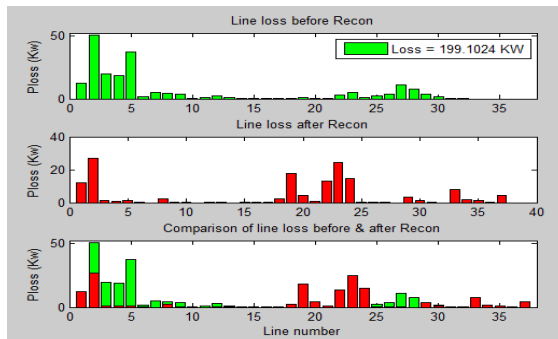


Fig.5 Power loss in 33 bus RDS

shown in Table3 and hence compares the network status for base case and after the performance of reconfiguration. The combination of the tie line switches to be opened after reconfiguration are selected in such a way that the losses has been reduced from 199.102KW from the base case loss to 127.07KW as shown in the Table3.

In Fig.5 the losses of the system before reconfiguration; the losses after the performance of reconfiguration and the comparison of both the losses at various lines are represented. A detailed comparison of the system losses before and after reconfiguration clearly depicts that the system losses has been reduced after reconfiguration using HSA optimization algorithm.

Table3: Simulation results of 33 bus radial distribution system for base case and after reconfiguration

Item	Initial configuration		Final configuration	
Status of tie line switches	33,34,35,36 & 37		Fuzzy adaptive EP[7]	6,14,9,32,37
			Proposed HSA algorithm (after 50 iterations)	7,11,14,28, & 32
Power loss(Kw)	Power loss before reconfiguration for base case (Kw)	199.10	Power loss after reconfiguration using FAEP(Kw) [7]	128.26
	Power loss after reconfiguration using proposed HSA (Kw)	127.07		
Minimum voltage(p.u.)	0.908992		0.910294	

Total expenditure (in \$)	33449.2	24062.6
Savings in loss after reconfiguration= \$ 9386.57		

The total expenditure of the loss before and after reconfiguration is also calculated in dollars and the cost of expenditure after reconfiguration is calculated as the loss/KW and is given as 168\$/KW and the savings in loss after reconfiguration has been effectively shown to be \$9386.57.

5. SENSITIVITY ANALYSIS FOR DG AND CAPACITOR PLACEMENT:

The loss sensitivity factor is used to determine the optimal placement of capacitors and distributed generators. This candidate node selection using the loss sensitivity calculation helps to reduce the search space for the optimal location of DG and capacitors in the radial distribution network. In this procedure a distribution line with an impedance $R+jX$ and a load of $P_{\text{eff}} + jQ_{\text{eff}}$ connected between 'L' and 'M' buses is considered as shown in Fig6.

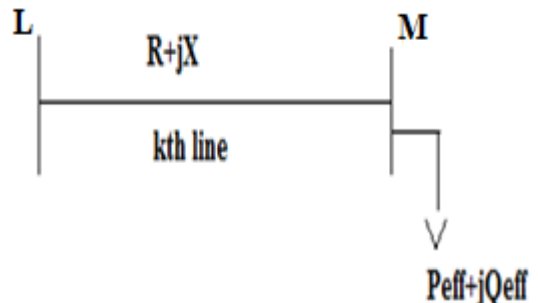


Fig.6 Schematic representation of a 2 bus distribution network

The Active power loss in the kth line is given by,

$$P_{\text{lineloss}}[L] = \frac{(P_{\text{eff}}^2[L] + Q_{\text{eff}}^2[M])R[k]}{(V[k])^2} \quad (12)$$

Where,

$P_{\text{eff}}[L]$ is the total effective active power supplied beyond the node 'L'.

$Q_{\text{eff}}[L]$ is the total effective reactive power supplied beyond the node 'L'.

Now the loss sensitivity factor can be obtained as,

$$\frac{\partial P_{lineloss}}{\partial Q_{eff}} = \frac{(2 * Q_{eff}[L] * R[k])}{(V[L])^2} \quad (13)$$

$$\frac{\partial Q_{lineloss}}{\partial Q_{eff}} = \frac{(2 * Q_{eff}[L] * X[k])}{(V[L])^2} \quad (14)$$

Table.4 Sensitive and non-sensitive buses of the 33 bus radial distribution system

Sensitive Buses	Non-sensitive Buses
06	02
28	03
29	04
30	05
09	19
13	20
10	21
08	22
27	23
31	24
26	25
14	26
07	
12	
17	
16	
15	
11	
32	
18	
33	
01	

Table.5 Optimal size and location of DG

DG LOCATION	DG SIZE IN KW
11	48
13	90.3759
31	86.1348

Table6. Candidate buses for capacitor location

CAPACITOR LOCATION	CAPACITOR SIZE IN KVAR
06	150
28	150
29	150

6. CANDIDATE NODE SELECTION USING LOSS SENSITIVITY FACTORS:

The Loss Sensitivity Factors ($\partial P_{lineloss}/\partial Q_{eff}$) are calculated from the base case load flows for all the lines of the given radial distribution system and the sensitive buses are arranged in the descending order of their sensitivity. The ‘end’ buses of the lines arranged in the descending order of the values ($\partial P_{lineloss}/\partial Q_{eff}$) is stored in a vector bus position represented as ‘bpos[i]’. The values of ($\partial P_{lineloss}/\partial Q_{eff}$) forms the ‘bpos[i]’ vector whose elements are arranged in the descending order of their values decides the sequence in which the buses are to be considered for compensation. The sequence in which the elements are arranged in the ‘bpos[i]’ is purely governed by the ($\partial P_{lineloss}/\partial Q_{eff}$) and hence the proposed ‘Loss Sensitive Coefficient’ factors become very powerful in the process of DG and capacitor placement.

Table7. System losses before and after DG and capacitor placement using sensitivity and optimization

OBSERVATIONS	RESULTS (KW)
BASE CASE LOSS WITHOUT DG AND CAPACITOR	199.102
LOSS AFTER DG AND CAPACITOR PLACEMENT	144.015
REDUCTION IN LOSS	55.087

The normalized voltage magnitudes ($norm[i] = V[i]/0.95$) are calculated by considering the base case voltage magnitudes at the buses of ‘bpos[i]’ vector. The buses for which the value of norm[i] vector is less than 1.01 are considered as the candidate buses for the optimal location of capacitors and DG’s. The location of the candidate buses for the placement are stored in the ‘rank bus’ vector. The ‘LossSensitivity factors’ is one of the important criterion to decide the sequence in which buses are to be considered for the siting of DGs and capacitors and the ‘norm[i]’ decides whether the buses needs Q-Compensation or not. For the buses whose $norm[i] > 1.01$ is healthy and these buses do not need compensation and will not be included in the ‘rank bus’ vector.

7. CONCLUSION:

In this work an effective meta-heuristic optimization algorithm based reconfiguration has been proposed for the power loss minimization and voltage profile improvement of the radial distribution network with simultaneous optimal allocation of DG and capacitors. The HSA optimization algorithm provides the optimal solution after a few number of power flow iterations with lesser computational time. Therefore, the proposed method can be effectively used in the real time applications when the reconfiguration of the larger distribution systems under widely loaded conditions are concerned. The objective function of the paper has been shown in which an HSA optimization technique has been efficiently used and it determines the optimal configuration and optimal allocation in the radial distribution systems which minimizes the overall distribution system power losses.

APPENDIX:

A1. IEEE 33 BUS RADIAL DISTRIBUTION SYSTEM:

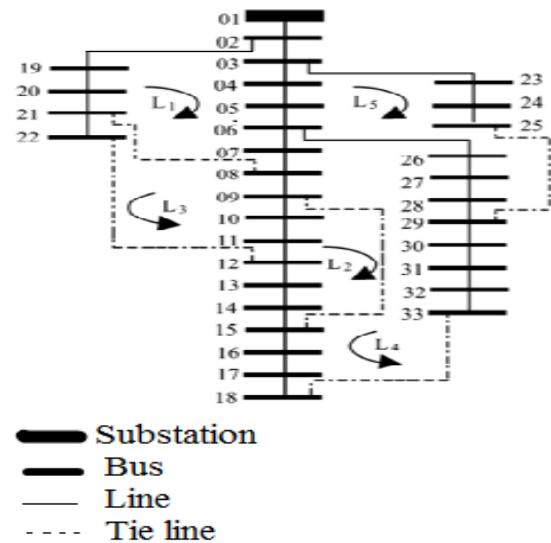


Fig.A1 Single line diagram of 33 bus radial distribution system

TableA1. Data for 33 bus test system

Line Number	Sending bus	Receiving bus	Resistance of the bus, Ω	Reactance of the bus, Ω	Receiving end load	
					Real power (KW)	Reactive power (KVAR)
1	1 Main SS	2	0.0922	0.0477	100	60

2	2	3	0.4930	0.2511	90	40
3	3	4	0.3660	0.1864	120	80
4	4	5	0.3811	0.1941	60	30
5	5	6	0.8190	0.7070	60	20
6	6	7	0.1872	0.6188	200	100
7	7	8	1.7114	1.2351	200	100
8	8	9	1.0300	0.7400	60	20
9	9	10	1.0400	0.7400	60	20
10	10	11	0.1966	0.0650	45	30
11	11	12	0.3744	0.1238	60	35
12	12	13	1.4680	1.1550	60	35
13	13	14	0.5416	0.7129	120	80
14	14	15	0.5910	0.5260	60	10
15	15	16	0.7463	0.5450	60	20
16	16	17	1.2890	1.7210	60	20
17	17	18	0.7320	0.5740	90	40
18	2	19	0.1640	0.1565	90	40
19	19	20	1.5042	1.3554	90	40
20	20	21	0.4095	0.4784	90	40
21	21	22	0.7089	0.9373	90	40
22	3	23	0.4512	0.3083	90	50
23	23	24	0.8980	0.7091	420	200
24	24	25	0.8960	0.7011	420	200
25	6	26	0.2030	0.1034	60	25
26	26	27	0.2842	0.1447	60	25
27	27	28	1.0590	0.9337	60	20
28	28	29	0.8042	0.7006	120	70
29	29	30	0.5075	0.2585	200	600
30	30	31	0.9744	0.9630	150	70
31	31	32	0.3105	0.3619	210	100
32	32	33	0.3410	0.5302	60	40

33*	21	8	0.0000	2.0000	0.0	0.0
34*	9	15	0.0000	2.0000	0.0	0.0
35*	12	22	0.0000	2.0000	0.0	0.0
36*	18	33	0.0000	0.5000	0.0	0.0
37*	25	29	0.0000	0.5000	0.0	0.0
* Tie line, Substation voltage-12.66kv						

REFERENCES:

- [1] Mesut E. Baran, et al., published “Network reconfiguration in distribution systems for loss reduction and the load balancing” in *IEEE Trans. on the power delivery*, vol.4, April 1989;
- [2] A. Merlin, et al.,“Search for a minimal loss operating spanning tree configuration in an urban power distribution system”; *5th Power System Computation Conference* held in U.K. in the year1975, pp. 1-18.
- [3] Ching-Tzong Su, IEEE Senior Member, et al., published “Network Reconfiguration of Distribution Systems Using Improved Mixed-Integer Hybrid Differential Evolution” in *IEEE Trans. on the power delivery*, vol.18 (July 2003).
- [4] K. Prasad, N.C. Sahoo, Member IEEE, et al., published “Optimal Reconfiguration of radial distribution system using fuzzy mutated genetic algorithm” in *IEEE transactions on power delivery* volume 20, April (2005).
- [5] Antonio Gomez Exposito and et al., published “Reliable load flow for the radial distribution networks” in the *IEEE Trans. on the power systems*, volume14 (August 1999).
- [6] Z.W. Geem, J.H. Kim, et al., presented a simulation in pp.60, Vol.76, 2001; “A new heuristic optimization algorithm: Harmony Search algorithm”.
- [7] B. Venkatesh, Member, IEEE, et al., published “Optimal Reconfiguration of Radial Distribution Systems to maximize the loadability” in *IEEE Trans. on the power systems*; vol.19, February 2004.
- [8] MA Junjie, Wang Yulong, LIU Yang, “Size and Location of DG in Distribution System Based on Immune Algorithm” in *2nd international conference on complexity science and information engineering, Systems Engineering Procedia* 4 (2012).
- [9] Komail Nekooei, Malihe M. Farsangi, Hossein Nezamabadi-Pour, and Kwang Y. Lee, Fellow, IEEE, “An improved multi-objective harmony search for optimal placement of DG’s in distribution systems” in *IEEE transactions on smart grid*, vol. 4, no. 1, march 2013.
- [10] Pushpendra Singh and Komal Arora, “Network reconfiguration and capacitor placement in distribution system with harmony search algorithm” in *Electrical and Electronics Engineering: An International Journal (ELEIJJ)* Vol.3, No 2, May 2014.

RESONANT BOOST CONVERTER FOR PV BASED PUMPING APPLICATION

P.Dhanwandhi^{1, a*}, ..R.Elanthirayan ^{2, b}

¹ PG Scholar, St. Joseph's College of Engineering, Chennai, India.

²Assistant Professor, St. Joseph's College of Engineering, Chennai, India.

[^a](mailto:a_dhanwandhi@gmail.com) [^b](mailto:b_etherayan@gmail.com), [^c](mailto:c_etherayan@gmail.com)

Abstract

This paper deals with the PV based pumping application by the use of resonant boost converter in order to enhance the efficiency and to reduce losses. In order to reduce the switching losses, the resonant inductor and capacitor is used thus arriving at the name resonant converter. The soft switching modality brought up for smooth transition of voltage through the IGBT are Zero Voltage Switching (ZVS).The maximum power point tracking technique is used to maximize the PV array output power irrespective of temperature, irradiation conditions and other electrical characteristics of the load. Use of microcontroller is implemented to modify the system as per the requirement and it ensures reliability.

Keywords: Resonant Boost Converter, soft switching, ZVS.

I. INTRODUCTION

Solar power is a renewable source of energy, which has become widely popular in modern times. It has obvious advantages over non-renewable energy sources, like the coal, oil and nuclear energy. The important advantages are sustainability, renewability and non-polluting, reliable and can produce energy anywhere that there is sunlight , hence its resources are not going to run out anytime. Other advantage is over other renewable energy sources, including wind and water power. Solar power is generated using solar panels, and does not need any mechanical parts, such as wind turbines They can also bring economic benefits to many regional areas that are located away from cities.

Increasing concern of global warming and the depletion of fossil fuel reserves, sustainable energy solutions are relied on to preserve the earth for the future generations. However, there is a drawback to solar power energy can only be produced when the sun is shining. To overcome this, usually solar panels are coupled with back up rechargeable batteries, which can store excess power generated during the day and use it to provide energy to systems when there is no sun shining. In this way solar power can be used to power houses and other large scale systems.

For this paper, the load to be connected only requires dc input, so, dc to dc conversion would be used to provide the correct power to the system from the power generated by the solar panel. The primary difficulty with the conventional boost converter is the hard switching of inductive currents which cause stress on the main switch and output diode. As the duty ratio increases, the switching and copper losses dramatically reduce efficiency of the converter. To overcome these difficulties a resonant boost converter that has soft switching technique to reduce losses and increase efficiency is used.

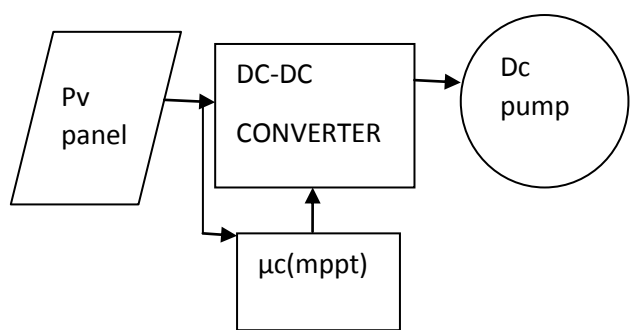


Fig.1. block diagram of the proposed scheme

The use of a maximum power point tracking technique Algorithm is necessary to extract as much power as possible from the solar when the irradiation and temperature changes. Microcontrollers are implemented which are intelligent chips. Hence the system can be modified as per the need of application and a converter is needed with high efficiency to transfer voltage from panel to DC load.

II. PHOTO-VOLTAIC PANEL

Photovoltaic (PV) is the method of generating electrical power by converting solar radiation into direct current electricity using semiconductors that exhibit the photovoltaic effect. A photovoltaic cell is comprised of a P-N junction semiconductor material that produces current by the photovoltaic effect. Materials that are widely used for photovoltaic include mono crystalline silicon, polycrystalline silicon, amorphous silicon, cadmium telluride, and copper indium selenide. When light energy strikes the solar cell, electrons are let loose from the atoms in the semiconductor material. When the conductors are attached to the positive and negative sides, forming an electrical circuit, the electrons are obtained in the form of an electric current. The standard equivalent circuit of the PV cell is shown in Fig.1. This electricity can then be used to power a load. Due to the low voltage generated in a PV cell, several PV cells are connected in series and in parallel to form a PV module for desired output. Due to the growing demand for renewable energy source, the manufacturing of solar cells and photovoltaic arrays has advanced considerably in recent years.

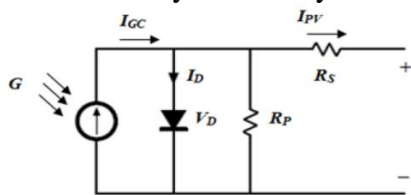


Fig.1.1 Equivalent circuit of the PV cell

$$I_{ph} = N_p I_{ph} - N_p I_s \left[\exp \left\{ \frac{q(R_s + I_{pv}R_s)}{N_s A k T} \right\} - 1 \right]$$

(1)

The output current from the PV cell is found by applying the Kirchhoff's current law on the equivalent circuit. Where I_{ph} is the photon current A is the ideality factor, k, the Boltzmann constant, q, the electron charge and T is the actual temperature. I_{pv} is the photovoltaic current and N_p is the number of cells connected in parallel. I_s is the saturation current, In fact, the PV efficiency is sensitive to small change in R_s but insensitive to variation in R_{sh} .

III. MAXIMUM POWER POINT TECHNIQUE PERTURB AND OBSERVE (P&O)ALGORITHM

The P&O method operates periodically incrementing or decrementing the output terminal voltage of the PV and comparing the power obtained in the current cycle with the power of the previous one (performs dP/dV). If the voltage varies and the power increases, the control system changes the operating point in that direction, otherwise change the operating point in the opposite direction. Once the direction for the change of voltage is known, the voltage is varied at a constant rate. This rate is a parameter that should be adjusted to allow the balance between faster response with less fluctuation in steady state. A modified version is obtained when the steps are changed according to the distance of the MPP, resulting in higher efficiency. This is an excellent method to reach the MPP and it is independently from the PV panel/manufacturer, although this method may suffer from fast changes in environmental conditions.

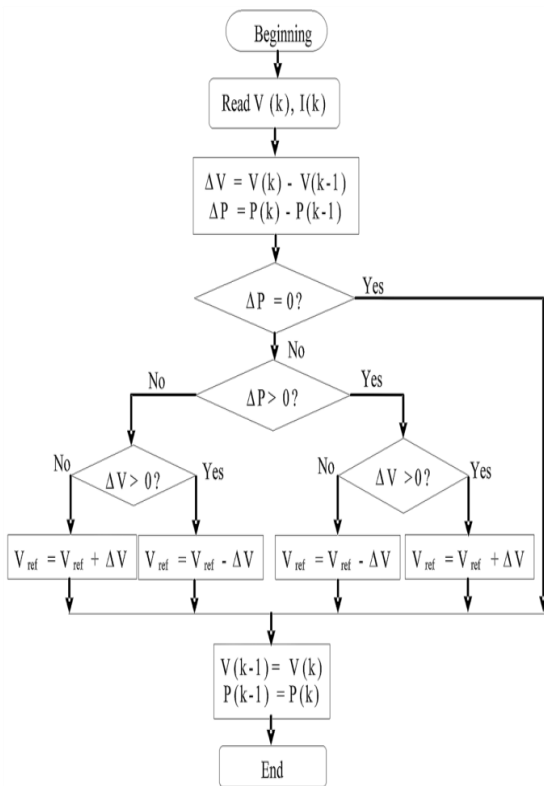


Fig.1.2 flow chart of P&O MPPT method

IV. RESONANT BOOST CONVERTER

To reduce the losses associated with hard switching, a converter operating in resonant mode was desired. By using an LC tank to create oscillatory voltage and current waveforms, resonant converters can achieve soft switching characteristics such as zero-voltage switching (ZVS)

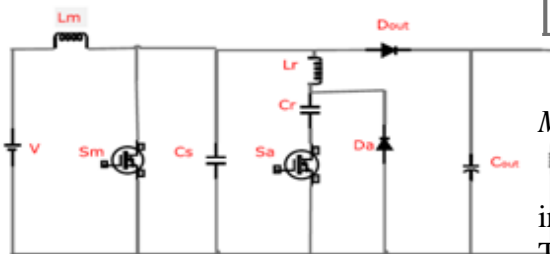


Fig 2. Resonant Boost Converter circuit

The above figure shows the circuit diagram of the proposed resonant boost converter. It consists of a main switch IGBT (Sm), auxiliary switch(Sa), Inductor L_m , auxiliary inductor L_r , Diodes Da & $Dout$, Capacitor C_s & auxiliary capacitor C_a and load

resistance R . The converter was appealing for its capability of providing high voltage gains independent of switch duty ratios, meanwhile having a low component count and a relatively simple topology

The conduction losses can be reduced by replacing the diode with a low resistance path provided by the IGBT. In order to reduce the switching losses, the auxiliary inductor and capacitor operate in resonance with each other, thus giving it the name resonant converter.

V. WORKING PRINCIPLE OF RESONANT BOOST CONVERTER

Mode 1

At t , the main switch Sm is turned off and auxiliary switch Sa is turned on with zero current switching. When the resonant inductor (L_r) resonates with the resonant capacitor(C_r),a resonant loop of $Lm-Lr-Cr-Sa-Vin$ is formed. The resonant capacitor is charged to $Vout$.If the current of Lm is equal to that of Lr ,mode 1 ends.

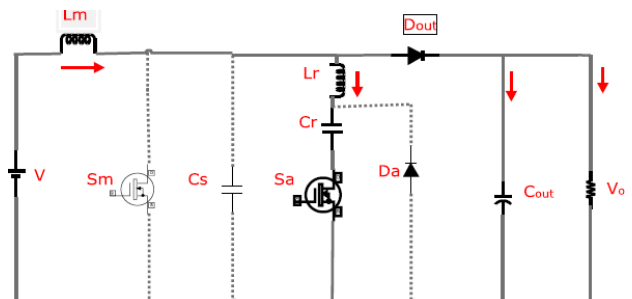


Fig 3. Equivalent circuit of model 1

Mode 2

The current through Lr continues to increase due to resonance between Lr and Cr . The charged in the snubber capacitor (C_s) starts to discharge and mode 2 ends when the voltage of Cr is to zero.

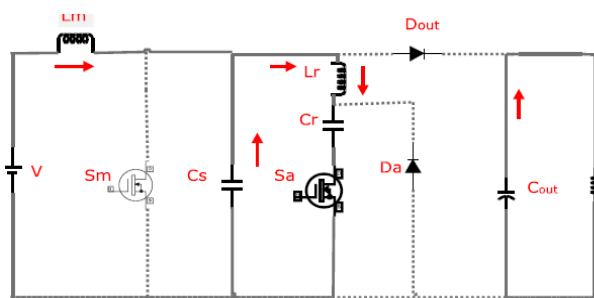


Fig4. Equivalent circuit of mode2

Mode 5

In this mode, the current flows through the auxiliary Diode Da instead of the anti-parallel diode of the auxiliary switch Sa. When Sm is turned OFF, this mode is ended.

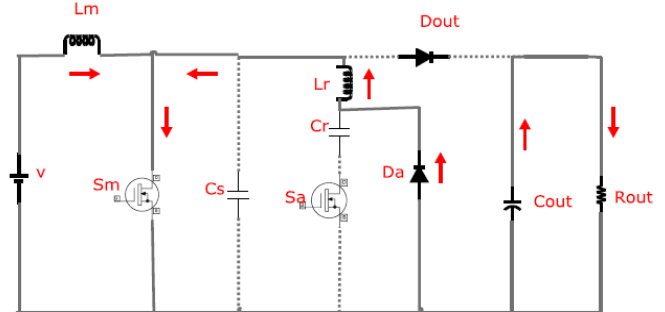


Fig6. Equivalent circuit of mode5

Mode 3

When the anti-parallel Diode Sm is turned ON, it makes voltage across the switch Sm to zero. When the main inductor current becomes equal to the resonant inductor current, this mode ends.

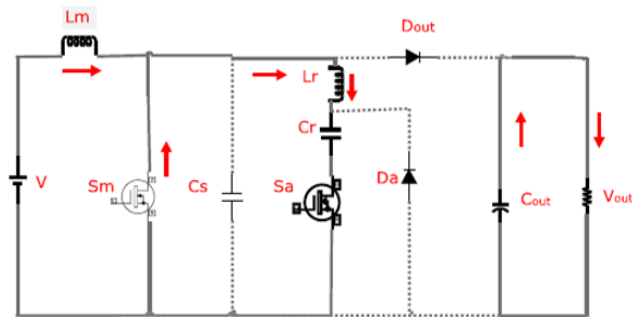


Fig 5. Equivalent circuit of mode3

Mode 4

In this mode, the current flows through the anti-parallel Diode of Sa. If the auxiliary switch Sa turns OFF in this interval, then it operate with ZVS. This mode ends when the resonant capacitor Cr discharges fully.

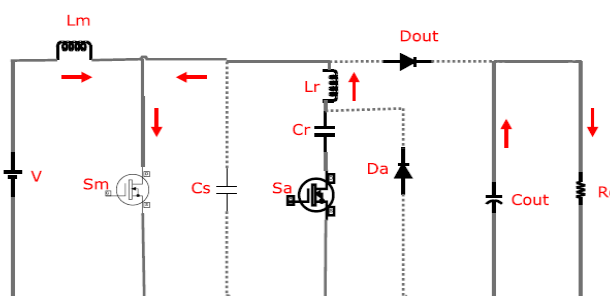


Fig6. Equivalent circuit of mode4

Mode 6

In this mode, all the switches are turned OFF. So the input current flows through the output diode Dout. This mode is ended with the turning ON of the auxiliary switch Sa.

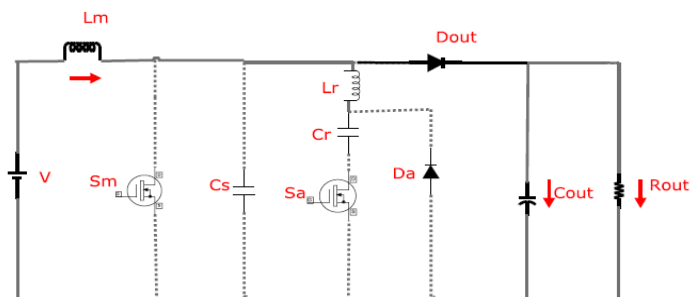


Fig7. Equivalent circuit of mode6

VI.**ODELLING OF PARAMETERS**

$$D = 1 - \frac{V_{in} * n}{V_{out}} \quad (1)$$

D= duty cycle

V_{in} = minimum input voltage

V_{out}= maximum output voltage

n= efficiency of the converter

M

$$V = L \frac{di}{dt} \quad (2)$$

$$L * \frac{di}{dt} = V_{in} * t_{on} \quad (3)$$

$$L * \frac{di}{dt} = V_{in} * D * T_s \quad (3a)$$

$$L * \frac{di}{dt} = V_{in} * (V_{out} - V_{in}) * \frac{1}{f_s} \quad (4)$$

V_{out}

$$\frac{L}{\Delta} = \frac{V_{in} * (V_{out} - V_{in}) * 1/f_s}{V_{out}} \quad (5)$$

$$I = (0.4 - 0.2) * I_{out} * V_{out} / V_{in} \quad (6)$$

$$F_s = 1/2\pi\sqrt{LC} \quad (7)$$

VII. DC PUMP

The DC submersible pump chosen here for its size and cost is the Kyocera SD 12-30 submersible solar pump. It is a diaphragm-type positive displacement pump equipped with a brushed permanent magnet DC motor and designed for use in standalone water delivery systems, especially for water delivery in remote locations. Flow rates up to 17.0L/min (4.5GPM) and heads up to 30.0m (100ft.) [39]. The typical daily output is between 2700L and 5000L. The rated maximum power consumption is 150W. It operates with a low voltage (12-30V DC), and its power requirement is as little as 35W [39]. The flow rate of water in positive displacement pumps is directly proportional to the speed of the pump motor, which is governed by the available driving voltage. DC submersible solar pump is connected with a single PV module with MPPT

VIII . SIMULATION RESULTS

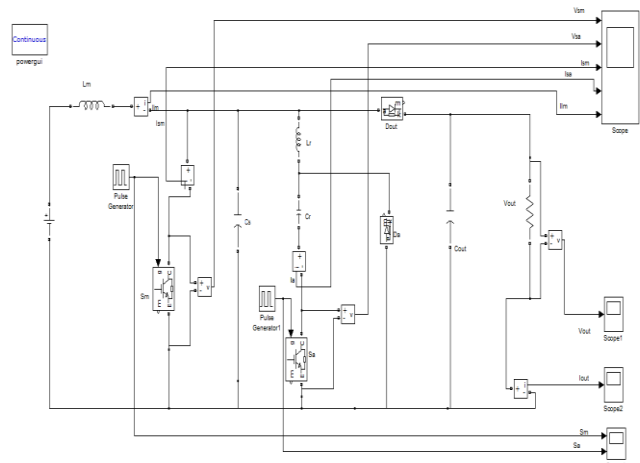


Fig.8 Simulink model of resonant boost converter

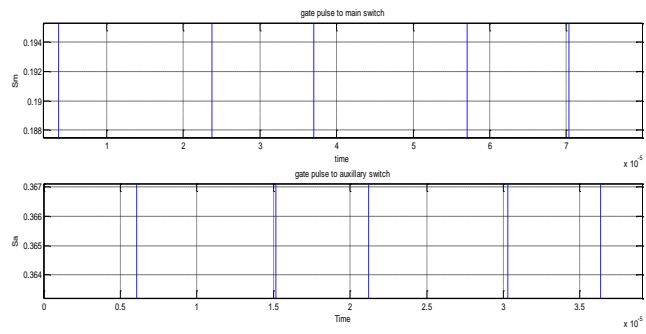


Fig.9 gate pulse of main and auxiliary switch

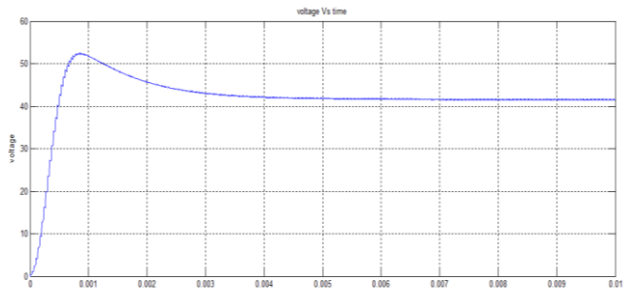


Fig.10.output voltage of resonant boost converter

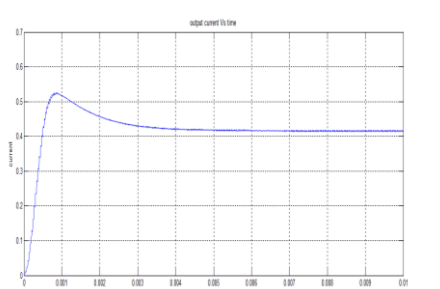


Fig.11 output current of resonant boost converter

VIII. CONCLUSION

A resonant boost converter using soft switching technique was designed and simulated for pumping application and to verify the proposed concept. The converter operation and analysis is presented in the respective chapters. The converter uses the resonant frequency and resonant inductor and capacitor to implement soft switching technique. A high voltage can be obtained by varying the duty cycle. Simulation of the proposed converter was carried out in MATLAB/simulink

IX. REFERENCE

- [1] “Photovoltaic Battery Charging System Based on PIC16F877A Microcontroller” Zaki Majeed AbduAllah, Omar Talal Mahmood, Ahmed M. T. Ibraheem AL-Naib.
- [2] Rashid M.H., “Power Electronics Circuits, Devices and Applications”, Prentice Hall India, Third Edition, New Delhi, 2004
- [3] The project is based on the paper “ design of maximum power point based PV charger” by Mr. S. K.Patil , Mr.D.K.Mahadik
- [4] a new mppt method for low power solar energy harvesting” Oscar López-Lapeña, Maria Teresa Penella, Student Member, IEEE, and Manel Gasulla, Member, IEEE.
- [5] “Current sensing for renewable energy” By Alex Latham, Systems Engineer, and Shaun Milano, Strategic Marketing Manager Allegro MicroSystems, LLC
- [6] N. Jain, P. K. Jain, and G. Joos, “A zero voltage transition boost converter employing a soft switching auxiliary circuit with reduced conduction losses,” IEEE Trans. Power Electron., vol. 19, no. 1, pp. 130–139.
- [7] H. Bodur and A. F. Bakan, “A new ZVT-ZCT-PWM DC-DC converter,” IEEE Trans. Power Electron., vol. 19, no. 3, pp. 676–684
- [8] J.-P. Lee, B.-D. Min, T.-J. Kim, D.-W. Yoo, and J.-Y. Yoo, “Design and control of novel topology for photovoltaic dc/dc converter with high efficiency under wide load ranges,” J. Power Electron., vol. 9, no. 2, pp. 300–307.
- [9] B.-D. Min, J.-P. Lee, and J.-H. Kim, “A novel grid-connected PV PCS with new high efficiency converter,” J. Power Electron., vol. 8, no. 4, pp. 309–316.
- [9] National Conference on Innovation & Challenges in Electrical & Electronics Engineering (NCICEEE'14) Vol. 3, Special Issue 1, February 2014.
- [10] A Newly Constructed Rectifier for Hybrid Wind-Solar Energy System C. Dinakaran Assistant Professor, Department of EEE, S.V.C.E.T, Chittoor, India G.Balasundaram Associate Professor, Department of EEE, S.V.C.E.T, Chittoor, India
- [11] Luo, Fang Lin. Advanced DC/DC converters / Fang Lin Luo and Hong Ye.
- [12] A Study on Maximum Power Point Tracking Algorithms for Photovoltaic Systems Ting-Chung Yu Yu-Cheng Lin Department of Electrical Engineering Lunghwa University of Science and Technology.
- [13] S.H. Park, G.R. Cha, Y.C. Jung and C.Y. Won, “Design and application for PV generation system using a soft switching boost converter with SARC,” IEEE Trans. On Industrial Electronics, vol. 57, no. 2, pp 515-522, February 2010.
- [14] S.H. Park, S.R. Park, J.S. Yu, Y.C. Jung and C.Y. Won, “Analysis and design of a soft switching boost converter with an H-bridge auxiliary resonant circuit,” IEEE Trans. on Power Electronics, vol. 25, no. 8, pp. 2142-2149, August 2010.
- [15] E.H. Kim and B.H. Kwon, “Zero-voltage-and zero current- switching full-bridge converter with secondary resonance,” IEEE Trans. on Industrial Electronics, vol. 57, no. 3, pp. 1017-1025, March 2010.
- [16] Charles J. McAtee, Jai P. Agrawal and Hassan Moghbelli, “A 100 watt power supply using ZVS boost converter,” Applied Power Electronics Conference and Exposition .

Security Constrained Unit Commitment Problem Based on Memetic Algorithm in Thermal-Wind Generation

K.S. Divya,

PG Scholar, Department of EEE,

*K.S.Rangasamy College of Technology,
Tiruchengode, Namakkal, 7418309432.*

k.s.divya73@gmail.com

Dr.T. Venkatesan,

Professor, Department of EEE,

*K.S.Rangasamy College of Technology,
Tiruchengode, Namakkal.*

pramoth99@yahoo.co.uk

Abstract— Promptly increasing the saturation level of renewable energy has executed new tasks to the operation of power systems. The Security Constrained Unit Commitment (SCUC) problem is subjected to the following operational constraints are power balance, generation limits, spinning reserve, minimum up/down time and adding a new constraint as frequency limit constraints. In this paper, the master problem involves deciding the unit commitment and production cost minimization & the sub problem performs to maintain the frequency limit without violation using the proposed method of Memetic Algorithm in IEEE six bus test system. The result indicates of proposed method that the unit is scheduled according to the demand and frequency is controlled within the limit in wind/thermal power generation into power systems for cost reduction.

Keywords— Security constrained unit commitment, frequency constraint, memetic algorithm.

I. INTRODUCTION

An unpredicted disturbance causing a bad fit during power supply in a power system, the system frequency starts deviating from the minimal value. In a real system, frequency drop caused by loss of generation or frequency fence caused by loss of load are of essential importance. Solving the time-domain equations describing power system dynamics would lead to different rotational speed for each generator during the transient period. For this reason, using the speed of a specific generator to represent system overall frequency condition is questionable. There have been many efforts to find the system average frequency path and avoiding the computationally expensive time-domain solutions, e.g., [1] and [2]. In these studies, an important assumption is made, which is to have a unique frequency variation throughout the system. Promptly increasing the penetration of renewable energies into the power systems has made the system operators meet new tasks in terms of maintaining power system security. In particular, wind power, as the leading source of renewables, has introduced many operational issues at high saturation levels.

The problem arising from integrating a large amount of wind generation originates from the incapability of widely used variable speed wind-turbine technologies in providing

inertial response and participation in frequency regulation in a similar way as the conventional synchronous generators. The problems of ensuring frequency response within an electricity market are studied in [3]. Two constraints are added to the problem of economic dispatch: one for limiting the rate of change of frequency and the other one for limiting the maximum frequency fall. However, the effect of each individual generator governor response cannot be seen in these constraints. Similarly, the offline calculation of the second constraint may need to be performed again if the system parameters change. The power flow and generators constraints are also left behind in [4]. These issues are addressed in the present study. The system frequency deviance after a contingency can be approximately derived based on static analysis. Governor load flow and inertia are the well-known static analysis of system frequency response [5]. Because of the intermittency and unpredictability of wind power generation, additional physical and economic operation constraints must be taken into consideration to reach a compromise between system security and total production cost. To provide coordination of wind and thermal generation scheduling, an HDP algorithm has been presented in this paper [6].

System spinning and operating reserves also suffer from high saturation level of irregular and unpredictable generation. The reserve requirement for system primary frequency response is studied and the frequency deviance considered is based on static analysis, similar to governor load flow, and no information about the system dynamics is retrievable from the simulations. More specifically, the scope of [7] is to find the best reserve for the generation units to ensure sufficient primary and tertiary reserves for the system after a contingency. Optimal reserve requirements for a system with large amount of wind generation are intended in [8] using stochastic optimization methods.

The study of several works on MAs (memetic algorithm), coming from different sources, with the purpose of designing a syntactical model for MAs [9]. A multi-objective memetic algorithm is then originally designed to solve EUCP. Within the MA, the global exploration is done by NSGA-II and the local exploitation by one local search strategy combined with

one local search operator which dynamically turns on/off the units at the boundaries of the generation schedules. The effectiveness of the proposed MA is demonstrated on a 10-unit system and a 100-unit system, with a time horizon of 24 hours [10]. The spinning reserve requirement is assumed to be 10% of the expected hourly peak load. The experiment is conducted with a population size of 250 using different crossover and mutation rates. For the result reported here, a crossover probability of 78% and a mutation rate of 15% were used, along with a stochastic remainder selection scheme for reproduction [11]. The results show that in every case examined the proposed MA converged to higher profit PBUC schedules than the genetic algorithm, the simulated annealing, and the Lagrangian relaxation method. Moreover, among all the considered metaheuristic optimization methods and for all the examined test systems, the proposed MA provides the highest success rate in finding the optimal solution. Furthermore, for large test systems with 60 units or more, the proposed MA constantly outperforms the LR, since the profit calculated even by the worst MA solution is always higher than the profit calculated by the LR method [12].

In this paper, the frequency control using Memetic algorithm is proposed which reports the problem of system-reduced inertia and primary frequency control due to high level of wind generation integration. Simplified system frequency response models are first derived and used to find analytical representation of system minimum frequency. The optimization problem is formulated and is solved using Memetic algorithm implemented.

II. SYSTEM FREQUENCY RESPONSE MODEL

The stability between the supplied and consumed power should be maintained during the power system operation to maintain synchronism. The smooth change in the load is met within day-ahead unit commitment and generators are scheduled to change their output power according to the load variation. Based on this approach for normal operation of power systems, the frequency is maintained within certain limits. Though, if a sudden disturbance happens, particularly in terms of large generation loss, the system will undergo a transient, as shown in Fig. 1. The main motivation of system frequency control is to help survive this transient period safely and rapidly.

In this paper, three stages in frequency transient phenomena are considered. The time duration of these stages varies from system to system, depending on the governor's control and system reserve. Right after the loss of generation, the frequency starts decreasing with a certain rate of decay, which can be found by the swing equation (1) of system equivalent single-machine representation.

$$\Delta P_m - \Delta P_e = M \frac{d\Delta\omega}{dt} + D\Delta\omega \quad (1)$$

Assuming that there is no change in the mechanical power of prime movers (2) in the very beginning of the incident ($\Delta P_m = 0$), load has no contribution in frequency response ($D = 0$), one will have

$$\frac{d\Delta\omega}{dt} = -\frac{\Delta P_e}{M} \quad (2)$$

Thus, the initial rate of decay of frequency mainly depends on the magnitude of the disturbance and the system equivalent inertia. The first stage in Fig.1 (Δt_1), which is mainly governed by M and ΔP_e , is referred to as system inertial response. The duration of this stage is usually a few seconds. After the first stage, the governor start to respond to the frequency fall, preventing it from further reduction. This stage, shown in Fig.1 as Δt_2 , is referred to as primary frequency control. The third stage in the frequency response begins when the governors cannot bring back the frequency to its original value (Δt_3 in Fig. 1). At this moment, the automatic generation control units participate in the frequency control and use their reserve to bring the frequency back. This stage is referred to as secondary frequency control.

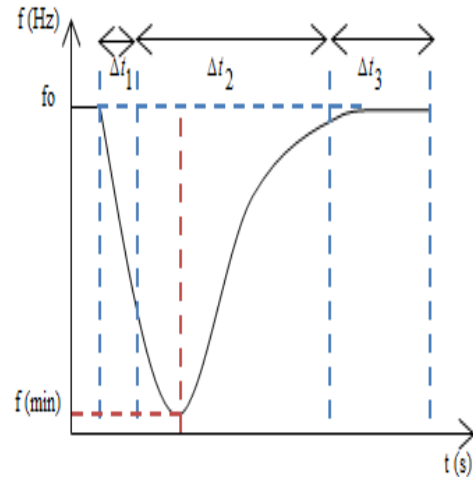


Fig. 1. Frequency Transient after Sudden Loss of Generation. Δt_1 : Inertial response; Δt_2 : Primary frequency control; Δt_3 :secondary control

A. Problem Formulation

The SCUC problem aims to determine the best dispatch for the generators in a system to minimize the production cost and at the same time, meet the system operational constraints.

The FCi is the cost function of the generator power output (3) at any time interval.

$$F(P_{TG}(i,t)) = a_i + b_i(P_{TG}(i,t)) + c_i(P_{TG}(i,t))^2 \quad (3)$$

where a_i, b_i, c_i represent unit cost coefficient, while $P_{TG}(i,t)$ is the i unit power output.

The overall production cost for i units and t hours (4) of thermal and wind units is the sum of these two costs.

$$TC = \sum_{t=1}^T \sum_{i=1}^{N_{TG}} [F(P_{TG}(i,t)) + SU_{TG}(i,t)] \\ + \sum_{t=1}^T \sum_{j=1}^{N_{WG}} [(P_{WG}(j,t) \cdot OCWG(j)) + FCWG(j)] \quad (4)$$

Following constraints in unit commitment problem

i. *Power balance constraint*

The total power generated must be equal to power demand PD and system losses PL(5).

$$\sum_{i=1}^{N_{TG}} P_{TG}(i,t) + \sum_{j=1}^{N_{WG}} P_{WG}(i,t) = P_D(t) + PL \quad (5)$$

ii. *Minimum up/down time constraints*

Once the unit gets turn on, it cannot be turn off immediately within the time period (6). Likewise, once the unit get turn off, it cannot turn on immediately within the time period (7).

$$[t_{ON,i}(t-1) - t_{ON,i}] = 0 \quad (6)$$

$$[t_{OFF,i}(t-1) - t_{OFF,i}] = 0 \quad (7)$$

iii. *Generation limit constraint*

Each generator must obey the minimum and maximum limit of each unit that is going to serve the purpose or to be committed (8).

$$P_{min}(t) \leq P_i(t) \leq P_{max}(t) \quad (8)$$

iv. *Frequency constraint*

The frequency limit is in the range of $\pm 0.5\%$ tolerance which is satisfied to reduce the violation.

$$F_{min} \leq F \leq F_{max} \quad (9)$$

v. *Total available wind generation*

The total available wind is calculated using the equation (10).

$$P_{WT}(t) = \sum_{j=1}^{NW} P_{Wj}(t) \quad (10)$$

vi. *Total actual wind generation limit*

The total actual wind generation should be in the limit by calculating in the equation (10).

$$0 \leq P_{WT}(t) \leq P_{*WT}(t) \quad (11)$$

III. PROPOSED ALGORITHM

A. Algorithm of Memetic Technique

Memetic algorithm is defined as the genetic algorithm(GA) with local search (neighbor parents). Meme is a cultural evolution which propagates from brain to brain via imitation. It can learn, change and adopt itself. It is fast and good convergence than GA to solve the optimization problem. The algorithm of proposed technique is as follows:

Step 1: Initialize the no. of population and apply local search to enhance the search capability for getting best optimization.

Step 2: Generate random vectors for each population with total number of rows and columns (generating units and hours) shown in Fig.2.

Step3: Check the constraints, if the constraints are not satisfied go to the previous step otherwise continue the steps.

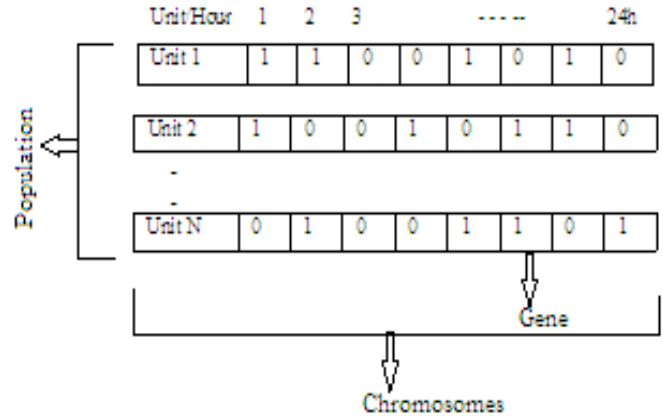


Fig. 2. Binary Code Representation for Unit Commitment

Step 4: Evaluate the fitness function for feasible solution and sort it for initial population.

Step 5: Store the best individuals from sorted list and perform crossover, mutation and selection process as shown in Fig.3 and 4.

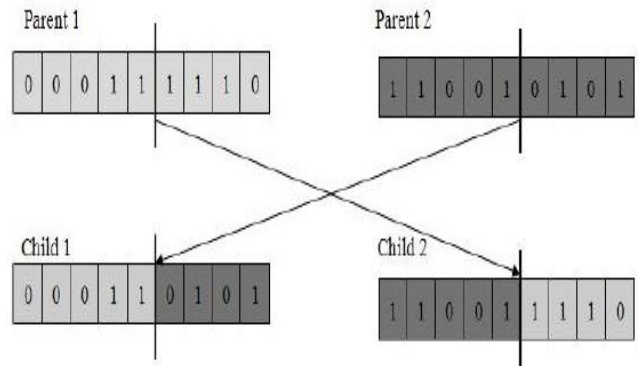


Fig. 3. Crossover Processing

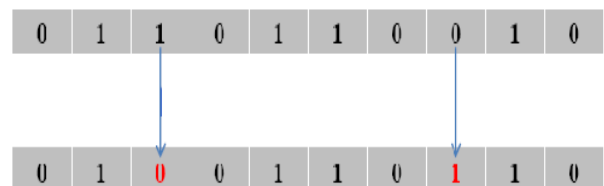


Fig. 4. Mutation Processing

Step6: Evaluate fitness for the mutated individuals and compare with the previous best individuals.

Step 7: Check for good convergence and get optimal solution or else go to step 1.

B. Flowchart for Memetic Algorithm

This proposed algorithm is shown in the flow chart Fig.5. By solving all sub-problems would require a considerable amount of time. MA terminates the evolution only when the evolution generation produces the best local optimum solution. When convergence is obtained program finds all the possible states for the given load demand for 24 hours and displays the power generated in individual units, generation fuel cost and start – up cost for individual demand.

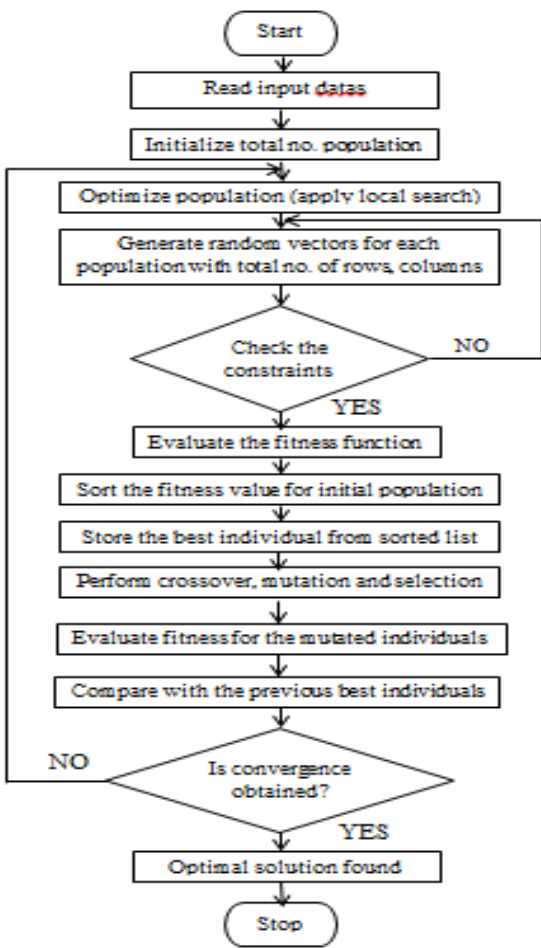


Fig. 5. Flowchart for Memetic Algorithm

IV. SIMULATION RESULT

A. Six-Bus Test System

Here, the standard IEEE test system is used to show the application of the proposed structure. The six-bus test system is shown in Fig. 3. The input data of thermal unit and generators dynamic data of wind are given in Table I, Table II and Table III, then the load data for 24h is given in Table IV.

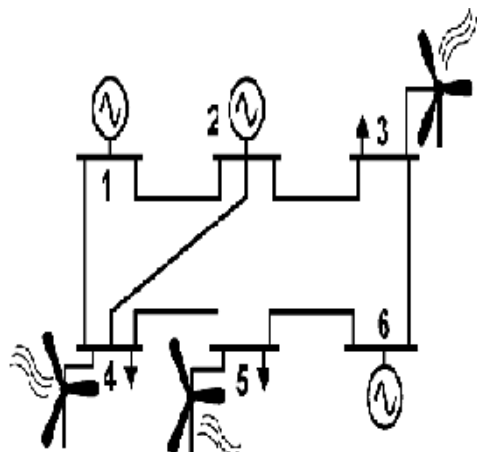


Fig. 6. Six-Bus Test System

TABLE I. INPUT DATA OF THERMAL UNIT FOR SIX-BUS SYSTEM

Parameters/ Units	T1	T2	T3
Bus.No.	1	2	6
Pmax (MW)	220	100	20
Pmin (MW)	100	10	10
a (MBtu)	176.9	129.9	137.4
b (MBtu/MWh)	13.5	32.6	17.6
c (MBtu/MW ² h)	0.1	0.1	0.1
Ini.State (h)	4	2	2
Min Up(h)	4	2	2
Max Down (h)	4	2	2
Ramp (MW/h)	55	50	20
StartUp Cost (MBtu)	100	200	20

TABLE II. GENERATOR DYNAMIC DATA OF WIND FOR THE SIX-BUS TEST SYSTEM

Gen. No	Bus No.	K	T _R	H	F _H	R	X _d
G1	1	0	8	7	0.15	0.04	0.061
G2	2	0.95	7	5.5	0.35	0.03	0.120
G3	6	0.98	9	3.5	0.25	0.05	0.181

TABLE III. WIND DATA FOR THE SIX BUS TEST SYSTEM

Units	Bus No.	Pmax (MW)	Pmin (MW)	Fixed Cost (Rs/MWyr)	Operating Cost (Rs/MWyr)
W1	3	60	0	50	625
W2	4	60	0	45	560
W3	5	60	0	40	495

TABLE IV. LOAD DEMAND DATA FOR 24 HOURS

Hour	Load(MW)	Hour	Load(MW)
1	280	13	220
2	300	14	220
3	400	15	500
4	320	16	280
5	340	17	440
6	390	18	370
7	410	19	270
8	480	20	480
9	280	21	500
10	340	22	300
11	380	23	390
12	420	24	240

B. Simulation of Unit Commitment and Frequency Control

The units are decided based on the load demand for 24h which is given in the Table V and the production cost is calculated for each hour. The overall production cost is Rs.12,62,957.5 and \$24,287.6

TABLE V. THERMAL-WIND GENERATOR SCHEDULING BY PROPOSED MEMETIC METHOD

Hour	Commitment schedule of Thermal and Wind Units						Production Cost(Rs)
	T1	T2	T3	W1	W2	W3	
1	1	0	0	0	1	0	41,586.9
2	1	0	1	0	1	0	42,116.3
3	1	1	1	0	1	0	46,506.2
4	1	1	0	0	0	0	12,376.8
5	1	1	1	0	0	0	12,906.2
6	1	1	1	1	0	0	50,406.2
7	1	1	0	1	0	1	79,576.8
8	1	1	0	1	1	1	1,13,176.8
9	1	0	0	0	1	0	41,586.9
10	1	1	1	0	0	0	12,906.2
11	1	1	0	0	1	0	45,976.8
12	1	1	0	1	0	1	79,576.8
13	1	0	0	0	0	0	11,186.9
14	1	0	0	0	0	0	11,186.9
15	1	1	1	1	1	1	1,13,706.2
16	1	0	0	0	1	0	41,586.9
17	1	1	1	1	0	1	80,106.2
18	1	1	0	1	0	0	49,876.8
19	1	0	0	1	0	0	45,486.9
20	1	1	0	1	1	1	1,13,176.8
21	1	1	1	1	1	1	1,13,706.2
22	1	0	1	0	1	0	42,116.3
23	1	1	1	1	0	0	50,406.2
24	1	0	1	0	0	0	11,716.3

Overall production cost (Rs)	12,62,957.5
------------------------------	-------------

To verify the above output and analysis, a simulation model was developed in MATLAB/Simulink. The simulation shows the frequency control using six bus test system. The six generating units are connected as a buses as shown in the single line diagram of test system. The variable speed constant frequency is produced using Permanent Magnet Synchronous Generator (PMSG). The frequency is maintained at standard value of 50Hz during continuous flow of wind and rated speed. When the speed of wind is reduced, thermal unit is connected to compensate the power production and frequency is maintained to the limit.

The fitness function of the algorithm is shown in the Fig.8 and output of the simulation model is depicted in the Fig.9 which gives the frequency within the limit. According to the proposed algorithm, the value is computed to the best local optimum as a waveform. By adding the generating units, the frequency is varied and controlled to the limit with $\pm 0.5\%$. The limit on the maximum frequency is at 50 Hz. And the operation of circuit breaker is done during generation i.e., the circuit breaker makes or breaks the circuit according to the need of power demand.

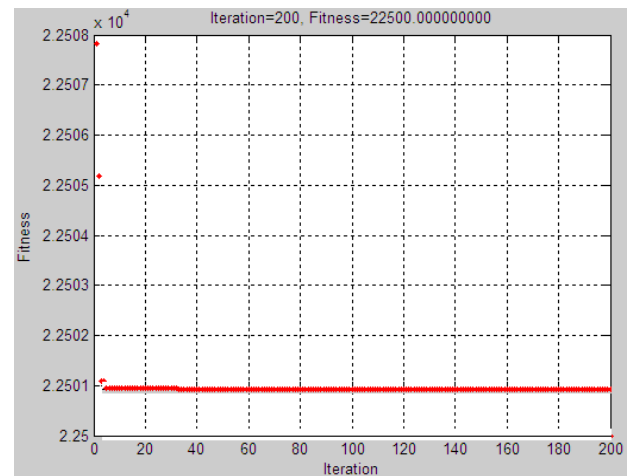


Fig. 8. Fitness Function

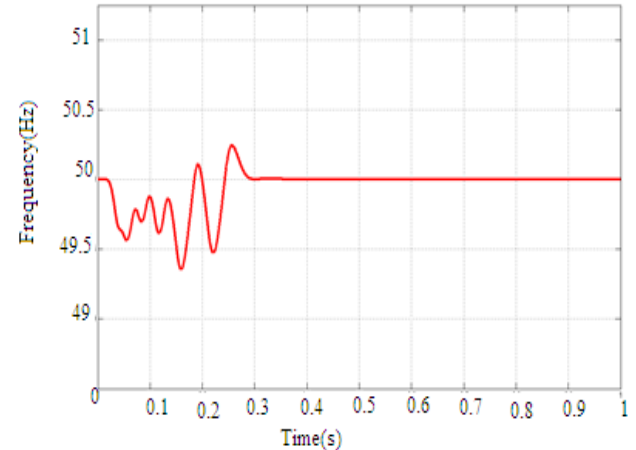


Fig 9. Output Waveform of Frequency Control

V. CONCLUSION

The minimum frequency after a sudden power imbalance is controlled using the optimization technique of Memetic algorithm in the IEEE six bus test system to achieve a higher-quality feasible solution. This test system is analyzed to exhibit the effectiveness of the proposed approach for frequency maintenance within the limit. The results shown that the proposed method which is applied for unit commitment & cost reduction is having well global searching as well as local searching performance. It is an efficient algorithm to solve the wind-thermal generation scheduling problem. Also, this scheduling model could be improved further by having better wind predictions. As forthcoming work, for systems with considerable hydro generation, different transfer function has to be derived to applicably model their governor response.

REFERENCES

- [1] P. M. Anderson and M. Mirheydar, "A low-order system frequency response model," *IEEE Trans. Power Syst.*, vol. 5, no. 3, pp. 720–729, 1990.
- [2] D. L. H. Aik, "A general-order system frequency response model incorporating load shedding: Analytic modeling and applications," *IEEE Trans. Power Syst.*, vol. 21, no. 2, pp. 709–717, 2006.
- [3] R. Doherty, G. Laror, and M. O'Malley, "Frequency control in competitive electricity market dispatch," *IEEE Trans. Power Syst.*, vol. 20, no. 3, pp. 1588–1596, 2005.
- [4] M. Lotfalian, R. Schlueter, D. Idizior, P. Rusche, S. Tedeschi, L. Shu, and A. Yazdankhah, "Inertial, governor, and AGC/economic dispatch load flow simulations of loss of generation contingencies," *IEEE Trans. Power App. Syst.*, vol. PAS-104, no. 11, pp. 3020–3028, 1985.
- [5] J. Restrepo and F. Galiana, "Unit commitment with primary frequency regulation constraints," *IEEE Trans. Power Syst.*, vol. 20, no. 4, pp. 1836–1842, 2005.
- [6] Chun-Lung Chen, "Optimal wind-thermal generating unit commitment", *IEEE Transactions on Energy Conversion*, vol. 23, no.1, March 2008 273.
- [7] M. A. Ortega-Vazquez and D. S. Kirschen, "Estimating the spinning reserve requirements in systems with significant wind power generation penetration," *IEEE Trans. Power Syst.*, vol. 24, no. 1, pp. 114–124, 2009.
- [8] H. Ahmadi and H. Ghasemi, "Maximum penetration level of wind generation considering power system security limits," *IET Gener. Transm. Distrib.*, vol. 6, no. 11, pp. 1164–1170, 2012.
- [9] Natalio Krasnogor and Jim Smith, "A tutorial for competent memetic algorithms: model, taxonomy, and design issues", *IEEE Transactions on Evolutionary Computation*, vol. 9, no. 5, October 2005.
- [10] Yan-Fu Li, Nicola Pedroni and Enrico Zio, "A Memetic Evolutionary Multi-Objective Optimization Method for Environmental Power Unit Commitment", *IEEE Transactions On Power Systems*, pp. 0885-8950, 2013.
- [11] D.Dasgupta and D.R.McGregor, "Thermal unit commitment using genetic algorithm", *IEE Proc-Gener, Transm, Distrib*, vol.141,no.5, September 1994.
- [12] Dionisis K. Dimitroulas, and Pavlos S. Georgilakis, "A new memetic algorithm approach for the price based unit commitment problem", *Applied Energy* 88 (2011) 4687–4699.
- [13] C. L. Chen and S. C. Wang, "Branch-and-Bound scheduling for thermal generating units," *IEEE Trans. Energy Convers.*, vol. 8, no.2, pp. 184–189, Jun. 1993.
- [14] K. Y. Huang, H. T. Yang, and C. L. Huang, "A new thermal unit commitment approach using constraint logic programming," *IEEE Trans. Power Syst.*, vol. 13, no. 3, pp. 936–945, Aug. 1998.
- [15] M. Carrion and J. M. Arroyo, "A computationally efficient mixed-integer linear formulation for the thermal unit commitment problem," *IEEE Trans. Power Syst.*, vol. 21, no. 3, pp. 1371–1378, 2006.
- [16] J. Valenzuela and A. E. Smith, "A seeded memetic algorithm for large unit commitment problems," *J. Heurist.*, vol. 8, pp. 173–195, 2002.
- [17] J. Ebrahimi, S. H. Hosseiniyan, and G. B. Gharehpetian, "Unit commitment problem solution using shuffled frog leaping algorithm," *IEEE Trans. Power Syst.*, vol. 26, no. 2, pp. 573–581, May 2011.
- [18] P. Moscato, "On Evolution, Search, Optimization, Genetic Algorithms and Martial Arts: Towards Memetic Algorithms" Pasadena, CA, USA: Caltech, 1989.
- [19] H. Ishibuchi, T. Yoshida, and T. Murata, "Balance between genetic search and local search in memetic algorithms for multiobjective permutation flowshop scheduling," *IEEE Trans. Evol. Computat.*, vol. 7, no. 2, pp. 204–223, 2003.
- [20] J. Ragland and N. P. Padhy, "Comparison of practical unit commitment solutions," *Elect. Power Compon. Syst.*, vol. 36, no. 8, pp. 844–863, 2008.

SELF HIRING USING SECURED EMBEDDED SYSTEM

^[1]R. Prem Kumar

A.P-III, Dept of EIE,

Sri Sai Ram Engineering College.

^[2]V.K.J. Murali Manohar Joshi
Dept of EIE, Sri Sairam
Engineering College
Joshi.eiae8494@gmail.com

^[3]R.Manikanda Prabhu
Dept of EIE, Sri Sairam
Engineering College
manikandaprabhu.rk@gmail.com

^[4]R.Arjun Kumar
Dept of EIE , Sri Sairam
Engineering College
arunramasamy@gmail.com

^[5]S.Madan Lal
Dept of EIE, Sri Sairam
Engineering College
Madansparkz13@gmail.com

Abstract— Motor Vehicle emissions contribute to air pollution and a major ingredient in the creation of smog in some large metropolitan cities around the world. Road transport is one of the biggest sources of pollution in India, contributing to poor air quality, noise disturbance etc. Instead of using carbon emitting vehicles for short distance travel especially inside social institutions, cycle transport can be used to save fuel. The paper objective is to reduce Air pollution and to enhance human physical being, by creating a simple, user-friendly secured embedded system for renting cycles in a semi-automated manner.

The existing pilot papers launched in various cities around the world are not very user-friendly. The proposed paper aims to create a simple secured but also economical system for renting cycles. The major proposed implementation is the creation of cycle docking centers inside the institution, factory or busy roads across the cities for every 500 meter range at least to facilitate the availability of cycles. The RFID card swipe system connected to a PIC microcontroller, to interact with the user by reading the RFID CARD and then details of the transport and payments are made by an interactive touch screen system .After making payment, four digit unique secure code is generated for number of required cycles from the dock area. The code must be re-entered by the user which is compared with the unique code by the PIC controller A special electromagnetic lock releases the appropriate cycles from the dock. The system automatically recomputes the cost on reaching the destination and additionally charge for any longer distance than entered in the input system according to the pre-programmed algorithm in which payment is based on the distance and idle time taken by the customer. This system is a friendly user interface making comfortable for the users. The use of cycles helps to reduce the emission of carbon monoxide, time saving and user friendly to the people who are all related to that social institution and Industries, etc.

Keywords —RFID, social institution.

I. Introduction

In this industrial era the effects of Pollution are a threat to the mankind. The air pollution has a tremendous effect causing most of the adverse effects. Particularly in large cities like Beijing etc the bad effects of the air pollution are already affecting the health of the civilians. There have been many strategies to eliminate or limit the effects of air pollution in many spheres of life. Ranging from international treaties to reduce global carbon emission levels to reducing live stocks to reduce methane emission is underway. On the other side of these ideas is to reduce the air pollution in the worst affected areas such as industrial areas. There has been intensive use of automobiles and process mechanisms which use fossil fuel for their operation. While the use of fossil fuels in operation of

the plant seems necessary, the automobiles which use an enormous amount of fossil fuel must be limited. Thus the reduction in the use of automobiles and encouraging the use of bicycle is clear way to reduce carbon levels, at least inside the industries. Thus a simple economical cycle hiring system using PIC microcontroller with electromagnetic locks and, a interface system using RFID cards and a Visual Basic application serves the purpose. The semi automated system uses an image oriented user interface to give a better experience and results in an economical system.

II. Design of interface and controller system

A. User Interface System

The RFID mechanism is used to interact with the controller system. Each user in the industry is provided with an RFID card to interface with the cycle hiring system. When swiping the RFID card the RFID reader reads the details from the card such as the account number, balance amount, password. Then the user is required to enter the password to enter into the system. After entering in the system the number of cycles required can be entered in the menu box. Then an Image displaying the various docking stations present in various locations is shown. The destination can be selected in the window. This selection of destination makes it comfortable for the user to view the various stations and select the destination.



Figure 1 : image showing stations

B. Controller System

After entering the destination, the user is required to enter the password at the docking station lock with the help of keypad. The password is compared with the card holder password by the controller. If the passwords are matched, the required number of cycles are dispatched from the station electromagnetic lock. At the same time, a software clock is started by the controller. After usage of the cycles, they are returned at any one of the docking stations. Similarly at the time of returning, the total time consumed is used to calculate the amount to be charged. If the user is found to underuse the cycle he may be charged a little bit more to compensate for the unavailability created.

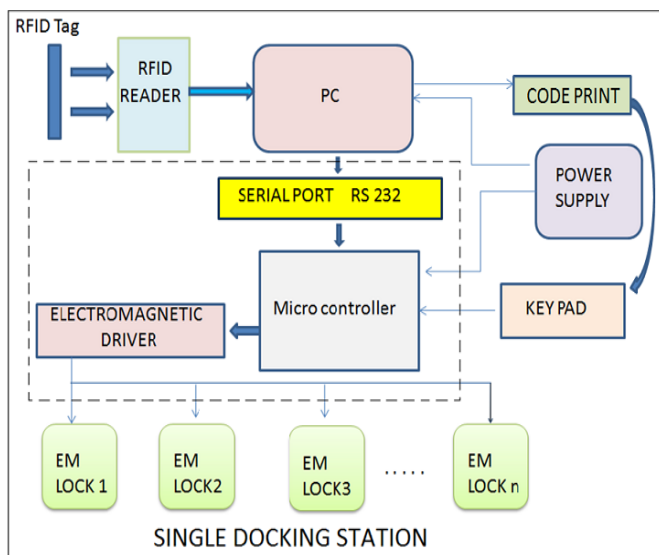


Figure 2: Block Diagram of a single docking station

III. System Components

The main task of this cycle hiring system is to provide the cycles to all the users in an social institution so that the air pollution in the particular vulnerable area and also to preserve the well being of the individuals with reduction in the fuel. The major concern about the system is that it must implement it with user friendly interface and at the same time economical in cost.

RFID CARD AND READER

The RFID card is used to obtain the details pertaining to the user. The obtained information is used for further processing. The details obtained from the card is used to search, get and update the details of the database created for the purpose. The RFID card and its reader actually use the induction principle in their operation. The RFID card when brought near a reader supplied with energy, induces a pattern of flux in the reader. The flux is modulated to get the details. The use of RFID cards is justified by the fact that it is most economical form of identification used in similar applications.

A. PIC16F882 Microcontroller

PIC microcontroller is widely used for experimental and modern applications because of its low price, wide range of applications, high quality and ease of availability. It is ideal for machine control applications, measurement devices, and study purpose and so on.

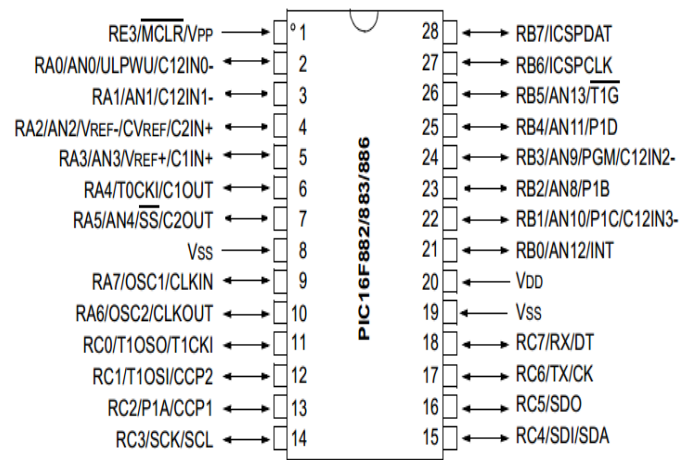


Figure 3. PIC16F882 28-Pin Diagram

The PIC16F882/883/884/886/887 has a 13-bit program counter capable of addressing a 2K x 14 (0000h-07FFh) for the PIC16F882, 4K x 14 (0000h-0FFFh) for the PIC16F883/PIC16F884, and 8K x 14 (0000h-1FFFh) for the PIC16F886/PIC16F887 program memory space. Accessing a location above these boundaries will cause a wraparound within the first 8K x 14 space. The data memory is partitioned into four banks which contain the General Purpose Registers (GPR) and the Special Function Registers (SFR). The Special Function Registers are located in the first 32 locations of each bank. The General Purpose Registers, implemented as static RAM, are located in the last 96 locations of each Bank. Register locations F0h-FFh in Bank 1, 170h-17Fh in Bank 2 and 1F0h-1FFh in Bank 3, point to addresses 70h-7Fh in Bank 0. The actual number of General Purpose Registers (GPR) implemented in each Bank depends on the device.

Electromagnetic Lock

The electromagnetic lock is used to dock the cycles in the docking station. The lock is actuated by a stepper motor when signaled by the microcontroller. The lock also consists of a proximity sensor and a limit switch to indicate the status of the availability of the cycles. The availability and Unavailability is received continuously and updated at the controller memory. Depending upon the register values of this memory the necessary controlling operations of dispatching and locking of the cycles occurs. The lock is welded to a particular stand like structure to lock more cycle to a dock.

G. Regulated Power Supply

Regulated power supply is an electronic circuit that is designed to provide a constant dc voltage of predetermined value across load terminals irrespective of ac mains fluctuations or load variations. The output from the regulated power supply may be alternating or unidirectional, but is nearly always DC. A regulated power supply essentially consists of an ordinary power supply and a voltage regulating device. The output from an ordinary power supply is fed to the voltage regulating device that provides the final output. The ac voltage, typically $230\text{ V}_{\text{rms}}$ is connected to a transformer which transforms that ac voltage to the level for the desired dc output. A bridge rectifier then provides a full-wave rectified voltage that is initially filtered by a Π (or C-L-C) filter to produce a dc voltage. The resulting dc voltage usually has some ripple or ac voltage variation. A regulating circuit uses this dc input to provide a dc voltage that not only has much less ripple voltage but also remains constant even if the input dc voltage varies somewhat or the load connected to the output dc voltage changes. The regulated dc supply is available across a voltage divider. A single power supply can provide as many as voltages as are required by using a voltage (or potential) divider. As illustrated in the figure, a potential divider is a single tapped resistor connected across the output terminals of the supply. The tapped resistor may consist of two or three resistors connected in series across the supply.

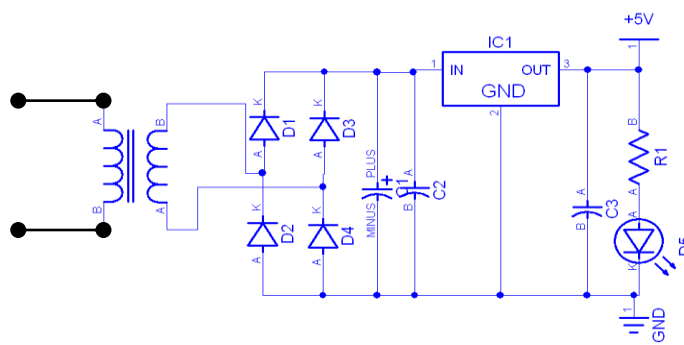


Figure 4. Regulated Power Supply

Visual Basic application

The application interface is created using Visual Basic software. The visual Basic software is used to actually create the application pages to interface with the user. The first page is the user login page with which the user can log in to the application. The second page receives the information about the number of cycles to be used followed by the selection of destination. After the selection the user is required to enter the password again in the keypad provided. If the passwords are matched then the application makes the controller to dispatch the cycles.

IV. STANDARD WORKING PROCEDURE OF THE SYSTEM

The main working of this system involves the identification of active users in the institution. Then the required number of RFID cards and estimated number of cycles are procured.

Then each card is registered by the administrator as using the interface application using the admin login page.

Admin User Setting

Figure 5: login page of the VB application

After the registration the user is accounted with the certain money by the administrator. After the amount is deposited the user can login and select the desired location by seeing the image of the various docking stations as below.

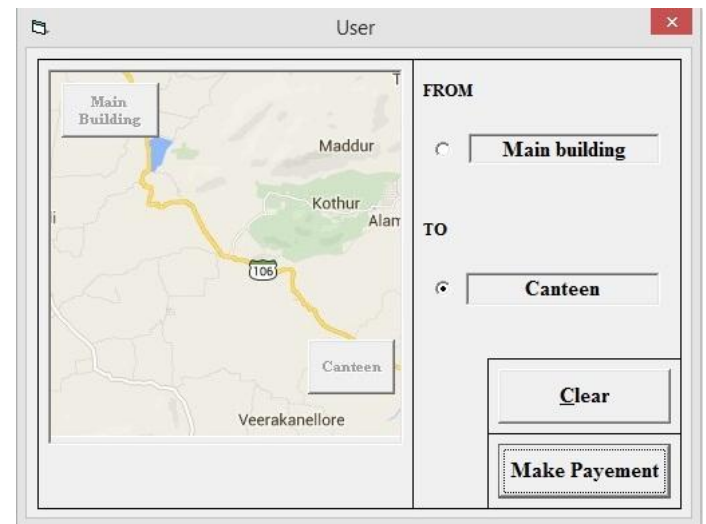


Figure 4: Selection of destination

After the usage when the user returns the cycle the proximity sensor and the limit switch indicate the return of the cycle and the timer in the application stops to indicate the total time taken.

V. CONCLUSION

This paper describes a new intelligent way of renting cycle in a semi automated manner which integrates new technologies available on the market to offer higher efficiency and considerable savings but with the economical design.. Another advantage obtained by the control system is

the intelligent management of the cycles. The system maintenance can be easily and efficiently planned from the centralization, allowing additional savings.

VI. Acknowledgment

The authors would like to thank Mr. . R. Premkumar, M.E (Asst Prof, Dept of EIE) who provided constant guidance and motivation to frame this paper. The authors would also like to thank the department of Electronics and Instrumentation who have always been our pillars of support and stood by us in times of need.

VII. Reference

- [1] Proposals for Introducing Public Bike Schemes in regional cities-Technical Feasibility study National Transport Authority ,30 June 2011
- [2] ‘Electronic Combination lock using PIC Microcontroller’ by Azzad Firdaus Bin Zolkepli Faculty of Electronic and computer Engineering, Universiti Teknikal Malaysia Melaka.
- [3] Employee Bike sharing Pilot Program Evaluation, Final report , California Department of Transportation, District 4,Transporattion sustainability center, University of California ,Berkeley, February 2011

Simulation and implementation of mixed conduction mode control for boost power factor conduction conversion

D.VIJAYASANKAR¹, A.PRATHAUPKUMAR², Mrs. M.PREETHI PAULINE MARY³
DEPARTMENT EEE, SATHYABAMA UNIVERSITY

Abstract

This paper presents a novel mixed conduction mode (MCM) digital controller with a digital controller (DCs) (DSP, PIC etc)- based discontinuous conduction mode (DCM) detection technique to realize total harmonic distortion (THD) and power factor improvements in boost power factor correction (PFC) converters operating in both continuous conduction mode(CCM) and (DCM) during a single ac line half-cycle. By using the integrated comparators found on many DCs, simplification and cost-reduction over existing DCM and zero-current detection methods are made possible. The boost converter operated in both DCM and CCM operation as a result the THD and power factor is improved during MCM operation. The different mode is simulated using MATLAB and compared their performance.

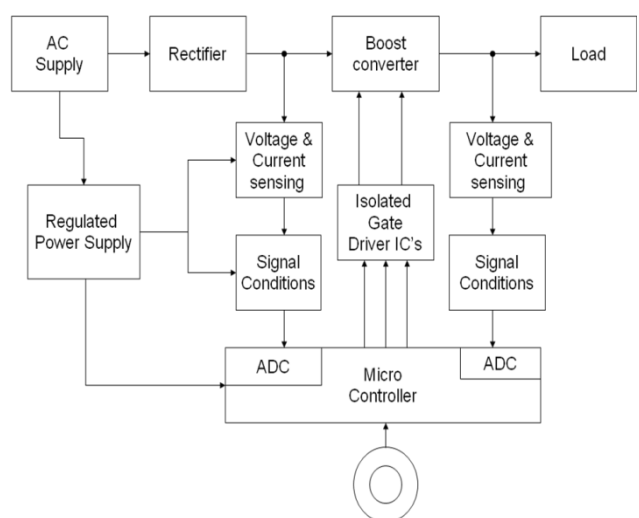
1 Introduction

The importance of meeting international energy standards and programs ,such as the IEC 1000-3-2 and ENERGY STAR's 8 PLUS program, to meet efficiency, input current harmonic and/or power factor requirements, has necessitated the development of advance circuits and control techniques simplifying compliance with these increasingly aggressive limits. Among these circuits, the boost power factor correction (PFC) converter of Fig.1 is a popular choice due to its well-known

dynamics and simplicity. By actively controlling the ac line current i_{ac} be sinusoidal and in-phase with the ac line voltage v_{ac} , commonly known as PFC the total harmonic distraction (THD) of i_{ac} and power factor of these electronic devices can be made to meet these recommendations, Complementing the rise in popularity of these standards, advances in digital control techniques and digital devices have enabled performance and cost advantages over analog controllers and techniques, providing incentive for manufacturers and designers to adopt digital controllers over their analog counterparts.

An important performance consideration of the boost PFC converter is the behavior of its inductor current i_L during a single switching cycle T_{sw} .

2. Block Diagram



3.Circuit Diagram

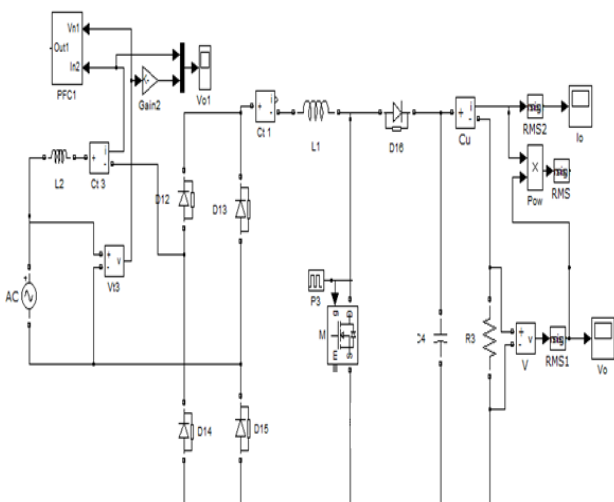


Fig.1 Circuit diagram

If the inductor current remains above zero for the full duration of the switching period, the converter is operating in continuous conduction mode (CCM). If, however, the inductor current falls to zero and remains at zero for a portion of the off period T_{off} , the mode of operation is known as discontinuous conduction mode (DCM). Generally, DCM is reserved for power levels under 300 W, due to its high current ripple, and sometimes variable switching frequency, necessitating more complex electromagnetic interference (EMI) filtering. In addition, converters designed for fully CCM operation may still operate in DCM at high-line and/or light-load conditions.

This behavior results in a third mode of operation called the mixed conduction mode (MCM) [7]. In the MCM, the boost PFC converter will operate in both CCM and DCM over a half line ac cycle. These three conduction modes are illustrated in Fig. 2. CCM and DCM boost PFC converters have significantly different small-signal dynamics, and if the boost PFC converter is designed for CCM operation, but instead operates in DCM, it will show increased input current distortion, leading to

degraded power quality. Consequently, a boost PFC converter in the MCM requires specialized control considerations for CCM and DCM operation, and it is therefore desirable to detect the mode of operation and/or provide zero current detection (ZCD) capability, enabling the use of the most appropriate and optimized control technique. Several existing methods to detect zero inductor current employ auxiliary windings to monitor the voltage across the boost inductor or use ancillary methods, either digital techniques or analog circuits, to detect DCM, or allow ZCD.

3.1 Boost converter

A boost converter (step-up converter) is a DC-to-DC power converter with an output voltage greater than its input voltage. It is a class of switched-mode power supply (SMPS) containing at least two semiconductor switches (a diode and a transistor) and at least one energy storage element, a capacitor, inductor, or the two in combination. Filters made of capacitors (sometimes in combination with inductors) are normally added to the output of the converter to reduce output voltage ripple. Power for the boost converter can come from any suitable DC sources, such as batteries, solar panels, rectifiers and DC generators. A process that changes one DC voltage to a different DC voltage is called DC to DC conversion. A boost converter is a DC to DC converter with an output voltage greater than the source voltage. A boost converter is sometimes called a step-up converter since it “steps up” the source voltage. Since power ($P=VI$) must be conserved, the output current is lower than the source current.

The key principle that drives the boost converter is the tendency of an inductor to resist changes in current. In a boost converter, the output voltage is always

higher than the input voltage. A schematic of a boost power stage is shown in Figure 2. When the switch is turned-ON, the current flows through the inductor and energy is stored in it. When the switch is turned-OFF, the stored energy in the inductor tends to collapse and its polarity changes such that it adds to the input voltage. Thus, the voltage across the inductor and the input voltage are in series and together charge the output capacitor to a voltage higher than the input voltage.

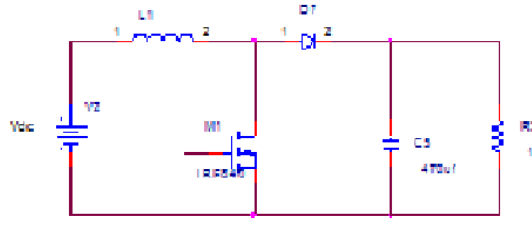


Fig : 2 boost converter

The basic principle of a Boost converter consists of 2 distinct states

- In the On-state, the switch S (fig:2) is closed, resulting in an increase in the inductor current;
- In the Off-state, the switch is open and the only path offered to inductor current is through the fly back diode D, the capacitor C and the load R. This result in transferring the energy accumulated during the On-state into the capacitor.
- The input current is the same as the inductor current as can be seen in figure 2. So it is not discontinuous as in the buck converter and the requirements on the input filter are relaxed compared to a buck converter.

When a boost converter operates in continuous mode, the current through the inductor (I_L) never falls to zero. Figure 4 shows the typical waveforms of currents and voltages in a converter operating in this mode. The output voltage can be calculated

as follows, in the case of an ideal converter (i.e. using components with an ideal behavior) operating in steady conditions:^[1]

During the On-state, the switch S is closed, which makes the input voltage (V_i) appear across the inductor, which causes a change in current (I_L) flowing through the inductor during a time period (t) by the formula:

$$\frac{\Delta I_L}{\Delta t} = \frac{V_i}{L} \quad (1)$$

At the end of the On-state, the increase of I_L is therefore:

$$\Delta I_{L_{On}} = \frac{1}{L} \int_0^{DT} V_i dt = \frac{DT}{L} V_i \quad (2)$$

D is the duty cycle. It represents the fraction of the commutation period T during which the switch is On. Therefore D ranges between 0 (S is never on) and 1 (S is always on).

During the Off-state, the switch S is open, so the inductor current flows through the load. If we consider zero voltage drop in the diode, and a capacitor large enough for its voltage to remain constant, the evolution of I_L is:

$$V_i - V_o = L \frac{dI_L}{dt} \quad (3)$$

Therefore, the variation of I_L during the Off-period is:

$$\Delta I_{L_{Off}} = \int_{DT}^T \frac{(V_i - V_o) dt}{L} = \frac{(V_i - V_o)(1 - D)T}{L} \quad (4)$$

As we consider that the converter operates in steady-state conditions, the amount of energy stored in each of its components has

to be the same at the beginning and at the end of a commutation cycle. In particular, the energy stored in the inductor is given by:

$$E = \frac{1}{2} L I_L^2 \quad (5)$$

So, the inductor current has to be the same at the start and end of the commutation cycle. This means the overall change in the current (the sum of the changes) is zero:

$$\Delta I_{L_{On}} + \Delta I_{L_{Off}} = 0$$

Substituting $\Delta I_{L_{On}}$ and $\Delta I_{L_{Off}}$ by their expressions yields:

$$\Delta I_{L_{On}} + \Delta I_{L_{Off}} = \frac{V_i DT}{L} + \frac{(V_i - V_o)(1 - D)T}{L} = 0$$

This can be written as:

$$\frac{V_o}{V_i} = \frac{1}{1 - D}$$

Which in turn reveals the duty cycle to be:

$$D = 1 - \frac{V_i}{V_o} \quad (6)$$

The above expression shows that the output voltage is always higher than the input voltage (as the duty cycle goes from 0 to 1), and that it increases with D, theoretically to infinity as D approaches 1. This is why this converter is sometimes referred to as a *step-up* converter.

4 Simulation

A. DCM operation

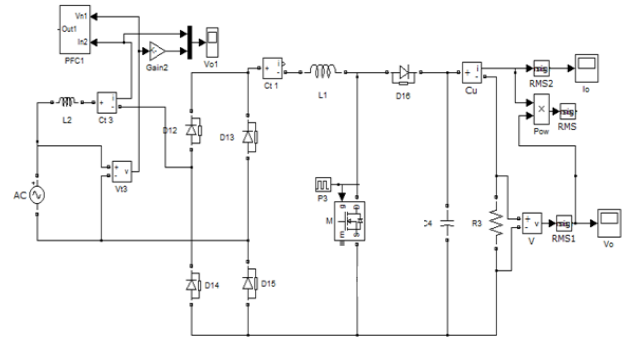
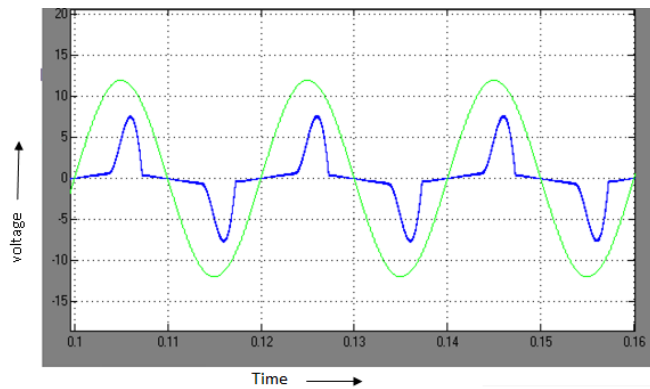


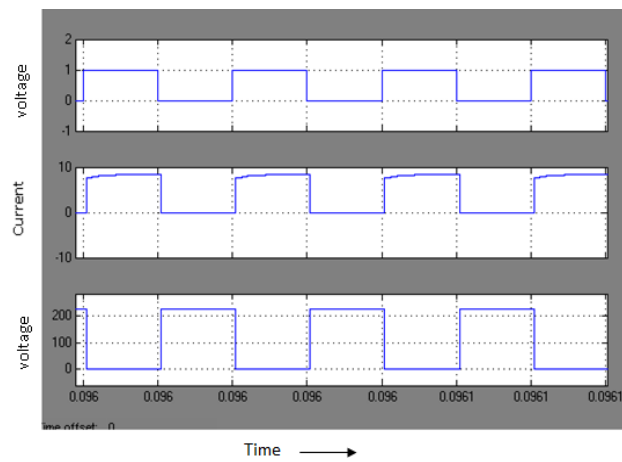
Fig:3 DCM Circuit diagram

To illustrate a possible scenario encountered in DCM operation during a single half-line ac cycle, Fig.3 provides triggering voltage and waveforms of the proposed detection and ensuing qualification logic for five hypothetical periods, $T_1 - T_5$. During T_1 , the converter is operation in CCM

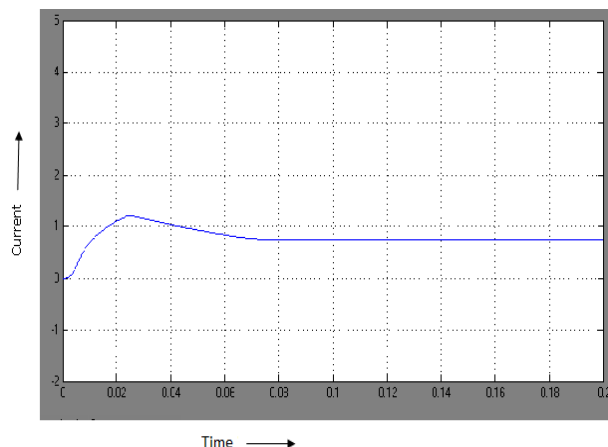
Fig 2 shows the boost converter circuit diagram. It consists AC source, rectifier boost converter and load. The boost converter is used to boost the voltage as well as to improve the input power factor and reduce the current harmonics as shown in fig 8 shows the input voltage and current waveform. Fig 9 shows the V_{gs} , I_{ds} and V_{ds} across switch 1. Fig 10 and fig 11 shows the output current and voltage in MCM operation. The output voltage is low during DCM operation and high in CCM operation. It is shown in tabular1 and figures 10 and 11. fig 12 show the current through inductor. Thus the proposed control technique has higher performance compare than conventional method.

Simulation Results:

DCM input voltage and current



DCM Vgs, Ids and Vds across switch S



DCM Output current

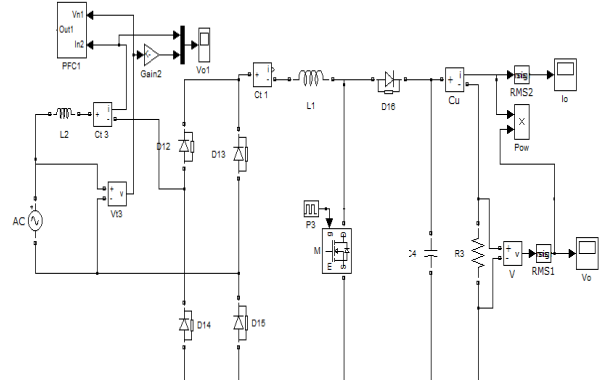
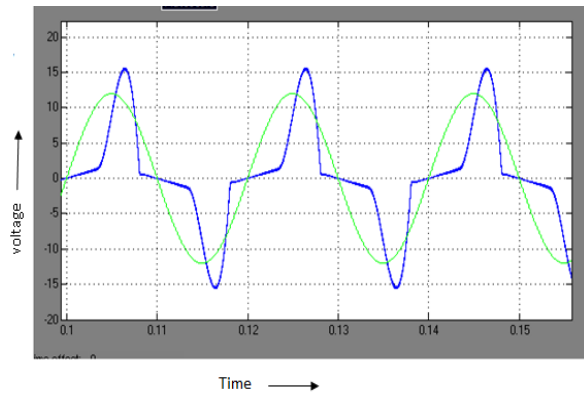
B.CCM Operation

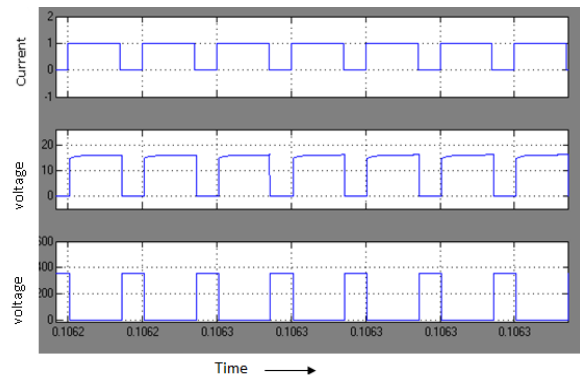
Fig.4 CCM Circuit diagram

Fig:3 shows the boost converter circuit diagram. It consists AC source, rectifier boost converter and load. The boost converter is used to boost the voltage as well as to improve the input power factor and reduce the current harmonics as shown in fig 8 shows the input voltage and current waveform. Fig 9 shows the Vgs, Ids and Vds across switch 1. Fig 10 and fig 11 shows the output current and voltage in MCM operation. The output voltage is low during DCM operation and high in CCM operation. It is shown in tabular1 and figures 10 and 11. fig 12 show the current through inductor. Thus the proposed control technique has higher performance compare than conventional method.

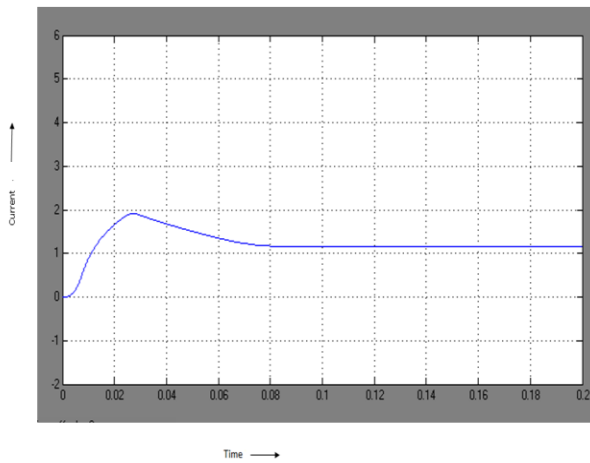
Simulation Results



CCM Input voltage and current



CCM Vgs, Ids and Vds across switch S



CCM Output current

C.MCM Operation

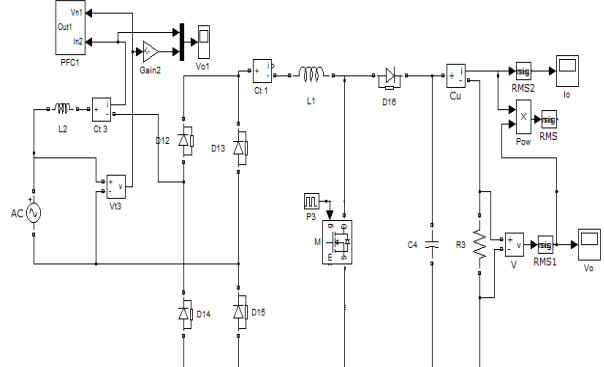


Fig: 4 MCM Circuit diagram

Fig 4 shows the boost converter circuit diagram. It consists AC source, rectifier boost converter and load. The boost converter is used to boost the voltage as well as to improve the input power factor and reduce the current harmonics as shown in fig 8 shows the input voltage and current waveform. Fig 9 shows the Vgs, Ids and Vds across switch 1. Fig 10 and fig 11 shows the output current and voltage in MCM operation. The output voltage is low during DCM operation and high in CCM operation. It is shown in tabular1 and figures 10 and 11. fig 12 show the current through inductor. Thus the proposed control technique has higher performance compare than conventional method.

Fig 4 shows the boost converter circuit diagram. It consists AC source, rectifier boost converter and load. The boost converter is used to boost the voltage as well as to improve the input power factor and reduce the current harmonics as shown in fig 8 shows the input voltage and current waveform. Fig 9 shows the Vgs, Ids and Vds across switch 1. Fig 10 and fig 11 shows the output current and voltage in MCM operation. The output voltage is low during

DCM operation and high in CCM operation. It is shown in tabular1 and figures 10 and 11. fig 12 show the current through inductor. Thus the proposed control technique has higher performance compare than conventional method.

Hence, *ZCD* flag and *DCM* flag remain at a logical low. During period *T*2 and at moment $d3T_{sw}$, the inductor current reaches zero and *ZCD* flag is triggered high. Subsequently, *DCM* flag is set to a logical high in succession with *DCMimm*, indicating the transition into DCM operation. Interrupts sourced from a *ZCD* flag event are disabled at this point and now additional zero-current events, such as DCM oscillation, are not serviced, preventing redundant DSP processing. With DCM operation detected upon entering the switching period of *T*3, *DCMimm* is reset low allowing the DSP to decide if *DCMflag* should be cleared, or left as-is during the next switching cycle.

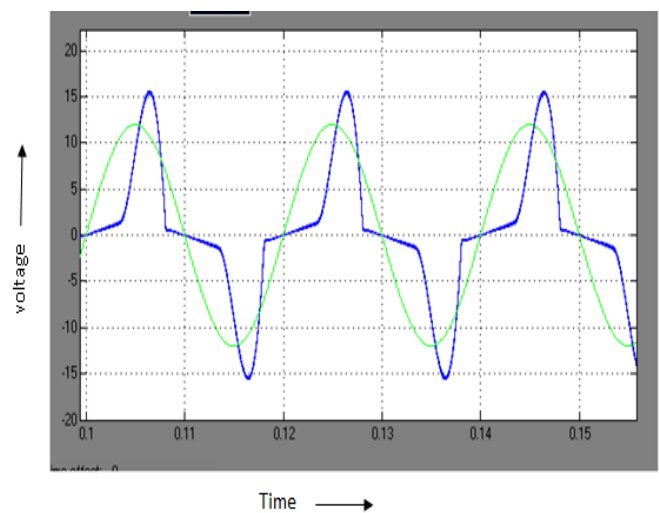
At $d5T_{sw}$, *DCMimm* flag is set in accordance with the zero current condition and *DCMflag* remains unchanged. In period *T*4, however, no zero current events are detected during the switching period, and thus, no *DCMimm* flag is set. The boost PFC converter has transitioned DCM operation to CCM operation, and *DCMflag* is cleared at the beginning of period *T*5.

Through careful selection of *DACref*, it can be assumed that the possibility of control law misapplication and resulting instability or performance degradation is minimized, ensuring an appropriate control law application to the associated mode of operation. If *DCMflag* is set during the immediate switching cycle, the DSP will use the DCM compensator coefficients in the subsequent switching cycles until CCM operation is detected. Inherently, due to the minimum time of one switching cycle

necessary to update the duty cycle for the next switching period, the DCM compensator will be delayed during each of its first initializations by an additional switching cycle. Similarly, the same principle of operation applies when *DCMflag* is cleared, thus indicating CCM operation.

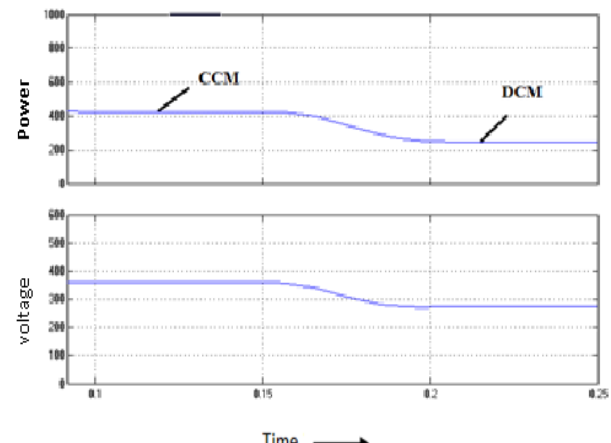
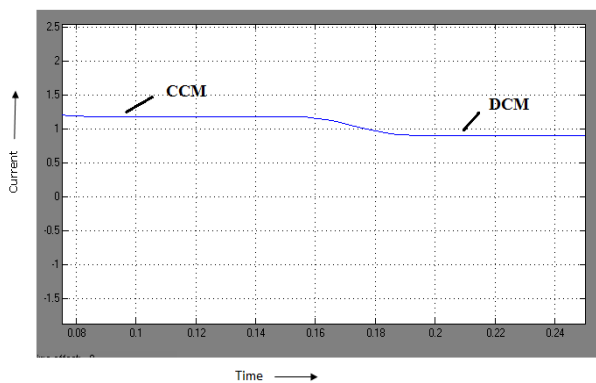
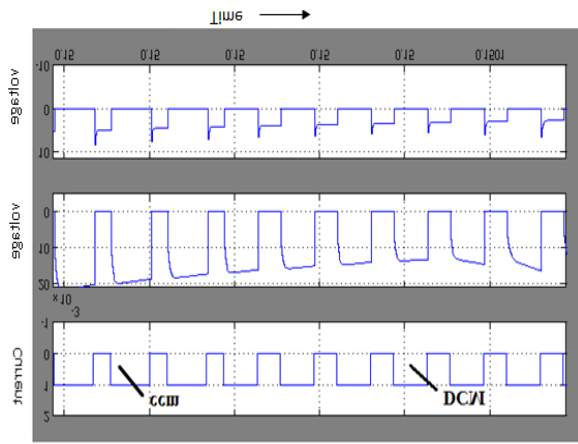
When *DCMflag* is cleared, the compensator will be updated to use the CCM compensator coefficients until *DCMflag* is set again. It is also worth noting that the DCM detection logic is modified to prevent the coefficients from being unnecessarily updated each switching cycle if the mode of operation has not changed. An advantage is that the PI controller structure can be recycled and employed for both DCM and CCM operation, where only a simple update of controller coefficients is required. In contrast to having two separate PI controllers with an associated larger memory footprint, savings in storage space is possible.

Simulation Results:



MCM Input voltage and current

PARAMETERS	DCM	CCM	MCM
INPUT PF	0.987	0.98	0.99
% THD	12.28	8.09	7.36
OUTPUT VOLATGE(V)	222	352	359
OUTPUT POWER(W)	162	408	424
OUTPUT CURRENT (A)	0.8	1.12	1.12 TO 0.8



D. Comparison of different modes of operation.

5. Conclusion

In this paper, a novel MCM control technique for boost PFC converters operating over a wide load range has been presented in order to realize improvements in power quality by lowering THD and improving power factor in comparison to a conventional digital control technique. In particular, a DCM detection method has been proposed using the added capabilities of a DCs with integrated comparators, allowing detection of DCM operation intervals, thereby enabling simplification and cost reduction over existing DCM and ZCD methods. By using knowledge of the detected mode of operation, a novel MCM controller was presented using appropriate compensator selection for the detected mode of operation. Additionally, a simple digital controller architecture that changes its compensator to suit DCM or CCM operation was introduced. When combined with the proposed DCM detection method, this MCM controller achieves less THD, and improves the power factor. Furthermore, additional reduction in THD and power factor improvement is seen over the entire load range when operated in MCM and pure DCM.

References:

- [1] Limits for Harmonic Current Emissions (Equipment Input Current < 16 A Per Phase), IEC 1000-3-2 Standard, 2001
- [2] 80 PLUS (2012). [Online]: Available: <http://www.plugloadsolutions.com>
- [3] R. W. Erickson and D. Maksimovic, Fundamentals of Power Electronics. Secaucus, NJ, USA: Kluwer, 2001.
- [4] D. Maksimovic, R. Zane, and R. Erickson, "Impact of digital control in power electronics," in Proc. IEEE Int. Symp. Power Semicond. Devices ICs, May 2004, pp. 13–22.
- [5] L. Huber, Y. Jang, and M. M. Jovanovic, "Performance evaluation of bridgeless PFC boost rectifiers," IEEE Trans. Power Electron., vol. 23, no. 3, pp. 1381–1390, May 2008.
- [6] D. M. Van de Sype, K. De Gusseme, A. P. M. Van den Bossche, and J. A. Melkebeek, "Duty-ratio feed forward for digitally controlled boost PFC converters," IEEE Trans. Ind. Electron., vol. 52, no. 1, pp. 108–115, Feb. 2005.
- [7] Fairchild Semiconductor Corporation, FAN7930 critical conduction mode PFC controller, FAN7930, Apr. 2010.
- [8] Y. Uno, "Power factor correction converter," U.S. Patent 2011/211377A1, May 2011

Voltage Sag compensation in Stand Alone Power System using SRF theory

J.Arun Venkatesh¹, A.Barrathi², S.Abarna², T.Ajitha²

¹Assistant Professor, ²UG Student

Department of EEE, KCG College of Technology, Chennai

Abstract—This paper presents a hybrid stand alone power system in which wind energy and solar energy are the sources. The solar energy is used to compensate for the power quality issues and also to supply the demand in the load which is not met by the wind energy. The wind and solar energy are interconnected using Dynamic voltage restorer (DVR). SRF theory is used as controller to compensate for the power demand and the power quality issues in the system.

Keywords— Wind energy, Solar energy, SRF theory, Hybrid stand alone power system.

I. INTRODUCTION

A stand-alone power system is an off-the-grid electricity system for locations that are not fitted with an electricity distribution system. The SAPS are places where grid cannot be connected and hence an alternative has to be met using some other forms of electrical energy sources. Typical SAPS include one or more methods of electricity generation, energy storage, and regulation. Electricity is typically generated by one or more of the following methods such as Solar panel, Wind turbine, Diesel or biofuel generator, etc., Storage is implemented using a battery. Stand-alone photovoltaic power systems are independent of the utility grid and may use solar panels only or may be used in conjunction with a diesel generator or a wind turbine. The two types of stand-alone photovoltaic power systems are direct-coupled system without batteries and stand alone system with batteries. In stand-alone photovoltaic power systems, the electrical energy produced by the photovoltaic panels cannot always be used directly. As the demand from the load does not always equal the solar panel capacity, battery banks are generally used. The battery banks can be replaced by using another generation source which may be either wind or diesel generator thus forming a hybrid system. The hybrid power plant is a complete electrical power supply system that can be easily configured to meet a broad range of remote power needs. There are three basic elements to the system - the power source, the battery, and the power management center. The power sources are a wind turbine, diesel engine generator, and solar arrays. The battery allows autonomous operation by compensating for the difference between power production and use. The power management center regulates power production from each of the sources, controls power use by classifying loads, and protects the battery from service extremes.

II. ENERGY SOURCES

A. Energy Sources

Natural resources such as oil, coal, or the sun, which can be used to provide power for light, heat, machines, etc. We are committed to the development of clean and renewable energy sources.

The world's energy resources can be divided into fossil fuel, nuclear fuel and renewable resources. Based on long-term availability the energy resources are classified as,

- Non-renewable energy resources.
- Renewable energy resources.

B. Non Renewable Energy

A non-renewable energy source is a source that does not restore itself at significant rate for sustainable economic extraction in meaningful human time-frames. An example is carbon-based, organic fuel. The organic material when subjected to changes with the aid of heat and pressure becomes a fuel such as oil or gas.

Disadvantages of Non-renewable Energy Resources

- Fossil fuels generate pollution. These pollutants degrade the environment, cause health hazards. Mainly carbon dioxide which causes global warming.
- Coal a petrochemical is used as raw material for chemical, pharmaceutical and paint industries. In long-term it is desirable to conserve coal for future needs.
- The waste materials in nuclear plants has radioactivity quotients of dangerous levels, it remains above the safe limit for long period and is health hazard.
- Possibility of accidental leakage of radioactive material from reactor is another safety issue.
- Non-renewable sources will finish up one day.
- Conventional sources are not sufficient to meet the growing demand.

Due to these reasons it has become necessary to identify non-conventional or renewable resources to reduce too much dependence on conventional or non-renewable resources. India is the only country having a full-fledged ministry devoted especially to developing new and renewable energy sources.

C. Maintaining the Integrity of the Specifications

A renewable energy source is natural source that can replenish in due time compared to the usage, either through biological reproduction or other naturally recurring processes. Renewable resources are a part of Earth's natural environment and the largest components of its ecosphere.

Advantages of Renewable energy

- Its acts as a solution to the energy problem for the stabilization of carbon dioxide emissions and other greenhouse gases. Replaces energy generation plants which use conventional sources lead to a reduction in

- the emission of pollutants such as sulphur and nitrogen oxides which cause acid rain.
- Domestic sources of energy and contribute to increasing energy independence and society of energy supply at the national level.
 - Geographically dispersed leading to the decentralization of the energy system making it possible for energy needs to be met at a local and regional level reducing losses from energy transmission.
 - They provide opportunities for rational use of energy sources because they cover wide range of energy needs.
 - Low operating costs which are not influenced by fluctuations in the international economy and especially in prices for conventional fuels.

16% of global energy consumption presently comes from renewable resources, 10% of energy from traditional biomass used for heating, and 3.4% from hydroelectricity. New renewable account for another 3% and are increasing rapidly. National renewable energy markets are projected to continue to grow strongly in the coming decade and beyond.

Renewable energy sources all over wide geographical areas in contrast to other energy sources which are concentrated in a limited number of countries to particular areas. Rapid deployment of renewable energy and energy efficiency is resulting in significant energy security, climate change mitigation, and economic benefits. In international public opinion surveys there is strong support for promoting renewable sources such as solar power and wind power. While many renewable energy projects are large-scale, renewable technologies are also suited to rural and remote areas and developing countries.

III. POWER QUALITY

Power Quality is mainly a distribution side problem. The term power quality refers to maintaining a near sinusoidal voltage at the distribution side at rated frequency and magnitude. The main cause of the power quality problems are due to lightning, Energisation of transformers and capacitors, sudden switching of heavy loads, failure of equipment and power electronic loads. Harmonics is a type of distortion. The harmonics may be in voltage or current. It is mainly caused due to power electronic converters and power electronic loads. The measure of voltage harmonics is known as THD and current harmonics is TDD.

The Power Quality problem, harmonics can be compensated by using filters. The STATCOM used in the distribution system is known as D-STATCOM. The D-STATCOM has the property of high speed control of reactive power to provide voltage stabilization, flicker suppression. In the D-STATCOM the voltage source converter is designed by using GTO or IGBT. Protects the utility transmission or distribution system from voltage sags and/or flicker caused by rapidly varying reactive current demand. Provides leading or lagging reactive power to achieve system stability during transient conditions in utility. In industrial facilities to compensate for voltage sag and flicker caused by non-linear dynamic loads, enabling such problem loads to co-exist on the same feeder as more sensitive loads. Instantaneously

exchanges reactive power with the distribution system without the use of bulky capacitors or reactors.

Voltage Sag

A short duration drop in voltage is known as voltage sag. The common causes are startup of large appliances or motors; faults on the electric delivery system. Voltage sag is referred to as voltage dips. IEEE defines voltage sag as a reduction in voltage for a short time. The duration of Voltage Sag is less than 1 minute but more than 8 milliseconds (0.5 cycles to 1 minute). The magnitude of the reduction is between 10 percent and 90 percent of the normal root mean square (RMS) voltage at fundamental frequency (50 HZ). Sag is a decrease of rms voltage to a value between 0.1 and 0.9 p.u. Voltage sags differ from other voltage reduction disturbances. Other voltage reduction disturbances often occur intermittently, like voltage flicker, while voltage sag occurs once for a short time. Compared to other power quality problems affecting industrial and commercial end users, voltage sags occur most frequently. They reduce the energy being delivered to the end user and cause computers to fail, adjustable speed drives to shut down and motors to stall and over heat. Solutions to voltage sag problems include equipment that protects loads that are sensitive to voltage sags.

IV. DYNAMIC VOLTAGE RESTORER

DVR injects a voltage component which is connected in series with the supply voltage, thus compensating the voltage sags and swells on the load side. Control response is of the order of 3msec, ensuring a secure voltage supply under transient conditions. The main function of a DVR is the protection of sensitive loads from voltage sags/swells coming from the network. The DVR is located on the basis of sensitive loads. If a fault occurs on other lines, DVR inserts series voltage V_{dvr} and compensates load voltage to pre fault value. The momentary amplitudes of the three injected phase voltages are controlled in such a way to eliminate any detrimental effects of a bus fault to the load voltage. The structure of DVR is shown in fig 1.

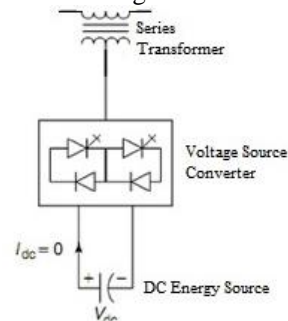


Fig 1. Dynamic Voltage Restorer

V. SYSTEM DESCRIPTION

The hybrid stand alone power system is achieved by having the source as a combination of wind energy and solar energy. The wind energy is used to supply the power to the load and the solar energy is used to supply the power when the wind energy does not give enough power to load and to compensate for the power quality issues in the system connected using wind energy. The hybrid system is represented in fig 2.

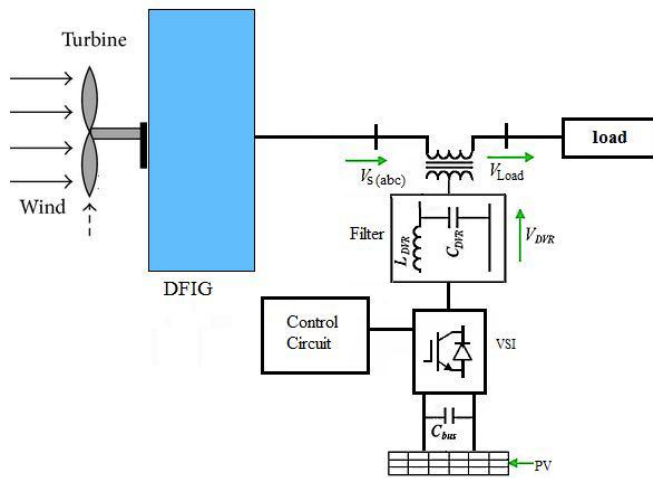


Fig 2. Hybrid Stand alone power system

VI. SIMUALTION RESULTS

The simulation is carried out for the test system using MATLAB/Simulink environment. The following equations explains about the synchronous reference frame theory which is used as controller in the system.

$$\begin{bmatrix} V_d \\ V_q \\ V_0 \end{bmatrix} = \frac{2}{3} \begin{bmatrix} \cos \omega t & \cos(\omega t - 2\pi/3) & \cos(\omega t + 2\pi/3) \\ -\sin \omega t & -\sin(\omega t - 2\pi/3) & -\sin(\omega t + 2\pi/3) \\ 1/2 & 1/2 & 1/2 \end{bmatrix} \begin{bmatrix} V_a \\ V_b \\ V_c \end{bmatrix}$$

$$\begin{bmatrix} V_a \\ V_b \\ V_c \end{bmatrix} = \begin{bmatrix} \cos \omega t & -\sin \omega t & 1 \\ \cos(\omega t - 2\pi/3) & -\sin(\omega t - 2\pi/3) & 1 \\ \cos(\omega t + 2\pi/3) & -\sin(\omega t + 2\pi/3) & 1 \end{bmatrix} \begin{bmatrix} V_d \\ V_q \\ V_0 \end{bmatrix}$$

The output waveforms that are obtained for voltage sag compensation is represented in fig 4. The sag occurs for a duration of 0.1 sec during which the voltage is at the level 0.78 pu and the voltage injected is at 0.2 pu to bring the system voltage back to 0.98 pu. Thus the sag is mitigated in the system.

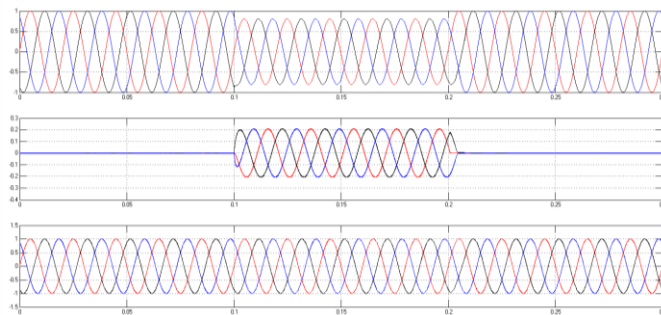


Fig 3. Output Waveforms

VII. CONCLUSION

A standalone WECS using DVR supported by PV, controlled by Synchronous Reference Frame Theory technique and Hysteresis Controller is implemented to protect the loads from power quality problems. The above simulation results shows that DVR is able to mitigate power quality problems such as voltage sag. Since WECS and PV combined it is used as renewable and pollution free. The wind energy can be replaced by other renewable energy source which can supply

energy continuously. The system can be developed with any optimization algorithms to get better results.

REFERENCES

- [1] A. Ghosh and G. Ledwich, Power Quality Enhancement using Custom Power devices, Kluwer Academic Publishers, London, 2002.
- [2] P. Jayaprakash, Bhim Singh, D. P. Kothari, A. Chandra, Kamal-Al-Haddad, "Control of Reduced Rating Dynamic Voltage Restorer with Battery Energy Storage System" *Power System Technology and IEEE Power India Conference, 2008. POWERCON 2008*.
- [3] Arindam Ghosh, Amit Kumar Jindal and Avinash Joshi, "Design of a capacitor supported dynamic voltage restorer for unbalanced and distorted loads" *IEEE Trans. on Power Delivery, vol.19, no. 1, pp. 405-413, Jan 2004*.
- [4] Amit Kumar Jindal, Arindam Ghosh and Avinash Joshi, "Critical load bus voltage control using DVR under system frequency variation," *Electric Power Systems Research, Vol. 78, No. 2, pp. 255-263, Feb. 2008*.
- [5] M.I. Marei, E.F. El-Saadany, M.M.A. Salama, "A New Approach to Control VR Based on Symmetrical Components Estimation," *Power Delivery, IEEE Transactions on , vol.22, no.4, pp.2017-2024, Oct. 2007*.
- [6] B. Singh, A. Adya, J. Gupta, "Power Quality Enhancement with DSTATCOM for Small Isolated Alternator feeding Distribution System" *Power Electronicsand Drive Systems 2005, (PEDS 2005)*
- [7] Investigation on D-STATCOM and DVR operation for voltage control in Distribution networks with a new control strategy.*Hojat Hashemi, Farhadshahnia, S.H. Hosseini. IEEE2007*
- [8] Metin Kesler, Engin Ozdemir "Synchronous-Reference-Frame-Based Control Method for UPQC Under Unbalanced and Distorted Load Conditions" *IEEE Transactions on Industrial Electronics, Vol. 58, no. 9, September 2011*.

Wireless Control of Prototype of PMDC Motor Using PI and Fuzzy Logic

Harini Sreerengarajan, Rajarajeswari A K, Sangita S

Department of Electrical and Electronics Engineering
Meenakshi Sundararajan Engineering College
Chennai, India

Abstract— Wireless technology is widely used to control industrial application nowadays. The control system uses wireless communication to transmit commands between the control station and the controlled object or process. This system will control the status of a PMDC motor, speed and direction of rotation (enabled by an external switch). The speed control technique is done by the PWM technique involving duty ratio control. The duty ratios can be chosen according to the user requirements, which are generated by the microcontroller, according to the required speed.

A prototype of PMDC motor which adopts a chopper based drive is used in this paper. The proposed design communicates with a remote control unit using Bluetooth. Proposed logic drive is implemented using ARM7 microcontroller unit. The ARM processor houses a Bluetooth module, acting as a slave. A handheld device serves the purpose of a master. A Proportional & Integral and Fuzzy Logic Controller are made to drive the PMDC motor individually. It acts as a feedback to the motor to reduce settling time. The simulation results are intended to show small ripple in rotational speed and fast response to change.

Index Terms— Wireless, PMDC, PI Controller, Fuzzy Controller, MATLAB, Bluetooth, ARM 7, PWM

A.INTRODUCTION

Microprocessor based power electronic drives have been a simulating area of research since the advent of microchip fabrication technology. In this paper, a wireless DC motor drive is proposed in order to provide a cost effective and remote control of Permanent Magnet DC (PMDC) motor for home and industrial applications.

In the proposed design, the parameters such as average value of voltage waveform and hence the speed of the motor is controlled by Microcontroller Unit (MCU). The design consists of a commanding and a control mechanism where communication between the commanding and control unit is made possible through a blue tooth module.

The idea of this paper involves around both power loss reduction and wireless control. It is a very practical idea as wireless technology is becoming increasingly more available. Hence the ability to control a motor though a wireless connection from a phone or PC could considerably enhance flexibility. The idea of using blue tooth as the wireless medium was also a big motivation for this paper as this technology is ubiquitous. A comprehensive understanding of how it works has also been done simultaneously.

The goal of this paper is to design a controller that will be able to run a permanent magnet DC motor wirelessly within a close proximity to the motor. The space was facilitated to us by VI Microsystems, Chennai.

B.OVERVIEW OF PMDC MOTOR

The PMDC motor used here uses a 24 v supply. These motors are used where high starting/acceleration torque is needed. The speed control and variation in these types of motors are done differently as the flux of PMDC motor remains constant. Therefore the only way of controlling the speed is to vary the armature voltage. Hence these motors are employed only in those systems where speed control below base speed is required.

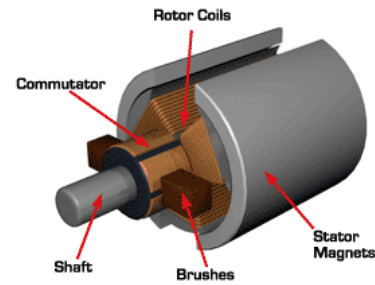


Fig 1. PMDC Motor. Image Courtesy ...

The field poles of this motor are essentially made of permanent magnet. A PMDC motor mainly consists of two parts - stator and rotor. Here the stator is a steel cylinder. The magnets are mounted in the inner periphery of this cylinder. The permanent magnets are mounted in such a way that the N – pole and S – pole of each magnet are alternatively faced towards armature as shown in the figure. In addition to holding the magnets on its inner periphery, the steel cylindrical stator also serves as low reluctance return path for the magnetic flux. Although field coil is not required in permanent magnet dc motor, still it is sometimes found that they are used along with permanent magnet as, the lost magnetic strength can be compensated by field excitation through these field coils. Generally, rare earth hard magnetic materials are used for these permanent magnets. The rotor of PMDC motor is similar to other DC motors. The rotor or armature of permanent magnet

dc motor also consists of core, windings and commutator. Armature core is made of number of varnish insulated, slotted circular lamination of steel sheets. By fixing these circular steel sheets one by one, a cylindrical shaped slotted armature core is formed. The varnish insulated laminated steel sheets are used to reduce eddy current loss in armature of permanent magnet dc motor. These slots on the outer periphery of the armature core are used for housing armature conductors in them. The armature conductors are connected in a suitable manner which gives rise to armature winding. The end terminals of the winding are connected to the commutator segments placed on the motor shaft. Like other dc motors, carbon or graphite brushes are placed with spring pressure on the commutator segments to supply current to the armature.

Open loop control

In the open loop control once when the input is applied to the motor, it rotates at a speed less than or greater than the rated value. Time taken for the motor to achieve set speed condition is equal to the motor actual speed, is large which

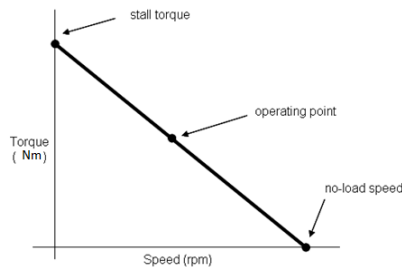


Fig 2 Speed – Torque characteristics

increases the settling time for the motor. Hence, closed loop control is adopted where less erroneous value as well as faster settling time is achieved.

Closed loop control

Speed is controlled by varying the voltage applied to the armature. Feedback devices sense the motor speed and send this information to the controller (either PI or Fuzzy logic controller) to vary its output voltage up or down to keep speed at or near the set value. Feedback technique employed here is MOC sensor which senses the speed of motor

At the no load, the speed is maximum and at the point where the torque is maximum the motor stops rotating and it draws maximum current. This current is called stalling current.

Applications

- Battery powered devices like wheel chairs and cordless power tools
- Conveyers
- Door openers
- Welding equipment
- Electric fuel pumps
- Marine engine starters
- Electric drills and saber saws.
- X-ray and tomographic systems

- Small PMDC motors are used for automobile heaters, air conditioner blowers, wind shield wipers, fans, and radio antennae.

C. BLOCK DIAGRAM

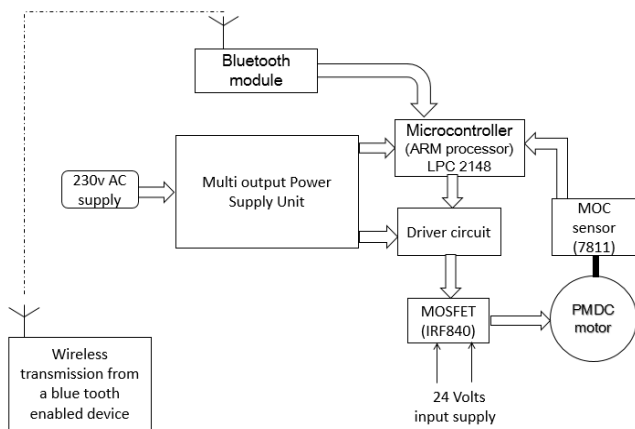


Fig 3 Overall Block Diagram

The block diagram consists of multi output power supply unit, the microcontroller, the driver circuit and an MOC sensor setup with a PMDC motor. The microcontroller facilitates wireless communication by an attachable Bluetooth module acting as a slave. The Bluetooth enabled motor speed commanding device acts as a Master.

Components

The Multi Output Power Supply block consists of 2 step down transformers with multiple taps, 18 V and 9V output respectively, followed by a bridge rectifier section along with capacitive filters and regulators. Voltage regulators 7805 and 7812 maintain a 5V and 12 V DC outputs respectively.

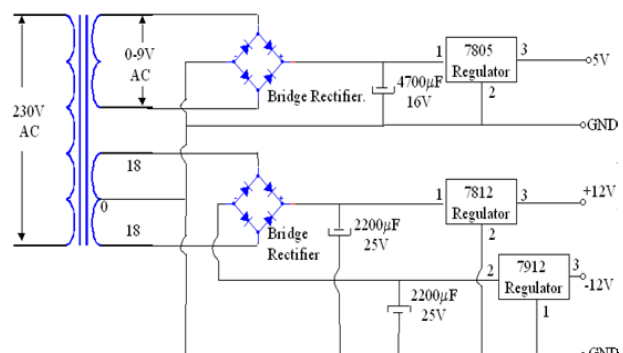


Fig 4 Power Supply Circuit

The **driver circuit** connecting the microcontroller output to the MOSFET has three main components – the opto coupler, the inverter and the driver IC. The opto coupler

(6N137) is used to isolate the power circuit of the MOSFET and the microcontroller unit hence ensuring safety from spikes. This results in an inverted output, calling for an inverter. These are then driven (or amplified) by the driver IC (IR2110). All these signals travelling are pulse width modulated waves which are finally given to the MOSFET switch which runs the motor.

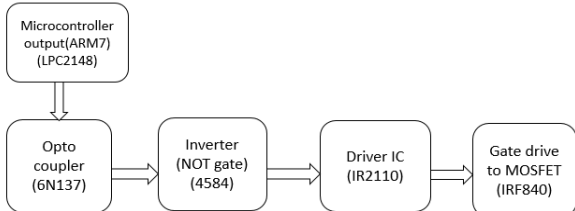


Fig 5 Driver Block Diagram

Pulse Width Modulation

Speed control for this motor can be easily done by the armature control method where the supply voltage is varied by a rheostat. But this leads to power loss in the form of heat from a rheostat. Hence, we go for the PWM control which reduces this loss by using a power electronic switch.

Pulse width modulation speed control works by driving the motor with a series of “ON-OFF” pulses and varying the duty cycle, the fraction of time that the output voltage is “ON” compared to when it is “OFF”, of the pulses while keeping the frequency constant.

The power applied to the motor can be controlled by varying the width of these applied pulses and thereby varying the average DC voltage applied to the motors terminals. By changing or modulating the timing of these pulses the speed of the motor can be controlled, i.e., the longer the pulse is “ON”, the faster the motor will rotate and vice versa.

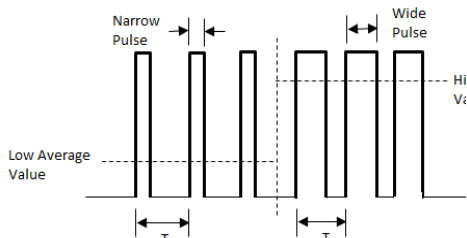


Fig 6. PWM Representation

Here, T represents total time period. The narrow and wide pulses (T_{on}) determine the duty cycle.

$$\text{Duty cycle} \equiv T_{\text{on}} / T$$

The use of pulse width modulation to control a small motor has the following advantage: the power loss in the switching transistor is small because the transistor is either fully "ON" or fully "OFF". As a result the switching transistor has a much reduced power dissipation giving it a linear type of control resulting in better speed stability. Also the amplitude of

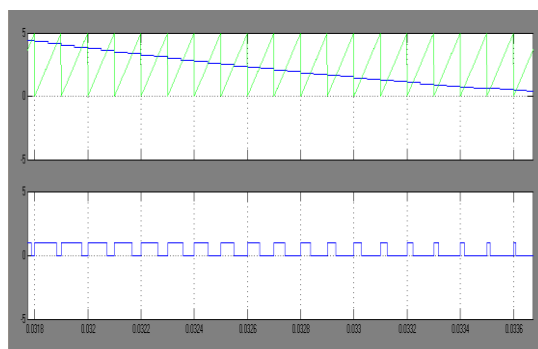


Fig 7. PWM Wave Generation

the motor voltage remains constant. Hence, stalling at slower speeds can be avoided.

To produce a PWM pulse train, the signal is compared with the carrier wave (sawtooth waveform here). When the latter is less than the former, the PWM signal is in high state (1); otherwise, it is in low state (0).

D. HARDWARE DESCRIPTION

LPC2148

The LPC 2148 microcontroller is based on a 32-bit ARM7TDMI-S CPU with real time emulation and embedded trace support. The TDMI stands for:

‘T’- Thumb architecture instruction (reduces code by more than 30% with a minimal performance penalty if the size of a program is a concern.)

‘D’- Debug extension.

'M'-enhanced Multiplier which can be enabled using PLL.

'I'- embedded ICE macro cell extension, with a high speed flash memory of 512 kB. To enable maximum clock rate, it is designed with a 128 bit wide memory interface and unique accelerator architecture.

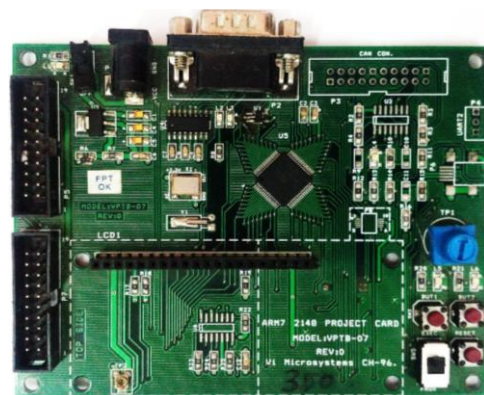


Fig 8. LPC 2148 Embedded Board

LPC 2148 has a 3 stage instruction pipeline with a Von-Neumann Architecture. The average instruction cycle time is approximately 32 ns with a 60 MHz operation. Due to its portable size and low power consumption, it is ideal where miniaturization is the key requirement such as access control

and point of scale. Serial communication ranges from USB 2.0, multiple UARTs, SPI, SSI to i2C-bus and on chip SRAM of 40kB. Various 32-bit timers, single or dual 10-bit ADCs, 10-bit DAC, PWM channels and 45 fast GPIO lines with 9 edge or level sensitive external interrupt pins are present.

The pin connect block allows selected pins of the microcontroller to have more than one function. Configuration registers control the multiplexers to allow connection between the pin and on chip peripherals. The Pin Controlled Module with its pin select registers defines the functionality of the microcontroller in a given hardware environment.

The General Purpose Parallel (GPIO) registers, when enabled, are relocated to the local ARM bus to provide the fastest possible I/O timing. These registers are byte addressable. The ADC is of 10-bit successive approximation type capable of performing more than 400000 10-bit samples per second. ADC0 has six channels and ADC1 has eight channels. The DAC is also 10 bit with a buffered output.

Applications

- Communication gateways
- Soft modems
- Voice recognition
- Medical systems.
- Any embedded application requiring a large buffer size and high processing power.

Optocoupler (6N137)

An optocoupler also referred to as an opto isolator, photo coupler or photo OS- is a piece of an electric circuit that transfers electricity between two other parts without allowing them to make a direct connection. An opto coupler is essentially an optical transmitter and an optical receiver connected by a nonconductive barrier. It uses a beam of light



Fig 9. Optocoupler Pin Configuration

to transfer energy from one circuit element to another, and it can handle incoming voltages of upto 2500V (rms). Optocouplers are most often used to separate two circuit elements that are operating on extremely different voltages. This prevents damage to the part working at a lower voltage. They also work to keep the two elements from being damaged by reverse voltage or power surges because of this trait, opto

Input	Enable	Output
H	H	L
L	H	H
H	L	H
L	L	H

Fig 10. Optocoupler Truth Table

couplers are best utilized in associated with on off switches and the transfer of digital data. They are commonly ground between a transmitter and a receiver in an electric circuit. 6N137 contains high emitting diode and a one chip photo IC. It is packaged in an 8 pin DIP and is TTL compatible.

As indicated in the truth table, it not only isolates the system by also inverts the output obtained. The default state is high (since the input '0' is assumed as default) and stays high if the enable is low. When the input is high, the LED glows emitting rays which will ground the receiving circuit. Hence, the output is low. When the output is low, there is no current flow from Vin to ground and hence the input voltage is obtained at the output.

Applications:

1. I/O isolation for MCUs (Micro Controller Units).
2. Noise suppression in switching circuits.
3. Signal transmission between circuits of different potentials and impedances.

Inverter

The NOT gate does logical negation on the digital bits. The NOT gate here is used in the driver. The Opto Coupler transmits the signals in an inverted form as discussed above. Hence, to re-invert the signals, the NOT gate is used.

Driver IC

The driver IC translates TTL or CMOS logical signals, to a higher voltage and higher current, with the goal of rapidly and completely switching the gate of a MOSFET. Essentially, it is a voltage level shifter with an amplifier. This driver receives its signal from the NOT gate which negates the inversion done by the optocoupler.

The IR2110/IR2113 are high voltage, high speed power MOSFET and IGBT drivers with independent high and low side referenced output channels.

Logic inputs are compatible with standard CMOS or LSTTL output, down to 3.3V logic. The output drivers feature a high pulse current buffer stage designed for minimum driver cross-conduction. Propagation delays are matched to simplify use in high frequency applications. The floating channel can be used to drive an N-channel power MOSFET or IGBT in the high side configuration which operates up to 500 or 600 volts.

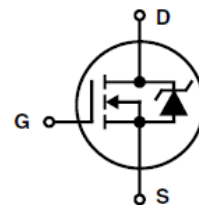


Fig 11. MOSFET Internal Diagram

MOSFET

The metal–oxide–semiconductor field-effect transistor (MOSFET, MOS-FET, or MOS FET) is a type of transistor

used for amplifying or switching electronic signals. The main advantage of a MOSFET transistor over a regular transistor is that it requires very little current to turn on (less than 1mA), while delivering a much higher current to a load (10 to 50A or more). However, the MOSFET requires a higher gate voltage (3-4V) to turn on.

Applications

- Switching regulators
- Relay drivers
- Variable Frequency Drives
- SMPS

MOC Sensor

MOC7811 sensor is used to count the number of rotations of the aluminium disc connected to the motor shaft. It consists of IR LED and Photodiode mounted facing each other enclosed in plastic body. This is normally used as positional sensor switch (limit switch). It has four legs: 2 legs for diode and 2 for transistor. Both are inbuilt, no external connection required. When light emitted by the IR LED is blocked because of alternating slots of the encoder disc logic level of the photo diode changes. This change in the logic level can be sensed by the microcontroller or by discrete hardware. Current limiting resistance is required.

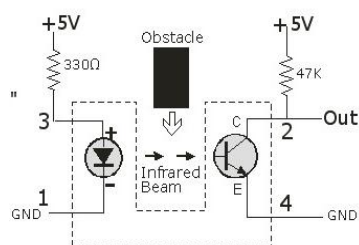


Fig 12. MOC Sensor Working

The above is the internal diagram of the MOC Sensor. The IR Led here is always ON. Hence, it acts as a base signal for the photo transistor and it conducts giving an output of 0. When it is cut by an obstacle, the IR signal is cut and the transistor fails to conduct. The input voltage of 5 V would be available at the Output pin. The transistor output voltage can be 30 V (maximum).

Applications

- DC motor position / velocity control
- Position and velocity servomechanisms
- Factory automation robots
- Numerically controlled machinery
- Computer printers and plotters

Bluetooth Module

Bluetooth is a wireless technology standard for exchanging data over short distances (using short-wavelength UHF radio waves from 2.4 to 2.485 GHz) from fixed and mobile devices and building personal area networks (PANs).

It uses a radio technology called frequency-hopping spread spectrum. Bluetooth divides transmitted data into

packets, and transmits each packet on one of 79 designated Bluetooth channels. Each channel has a bandwidth of 1 MHz. Bluetooth 4.0 uses 2 MHz spacing, which accommodates 40 channels. The first channel starts at 2402 MHz and continues up to 2480 MHz in 1 MHz steps. It usually performs 1600 hops per second, with Adaptive Frequency-Hopping (AFH) enabled.

Bluetooth is a packet-based protocol with a master-slave structure. One master may communicate with up to seven slaves in a piconet. All devices share the master's clock. Packet exchange is based on the basic clock, defined by the master, which ticks at 312.5 µs intervals. Two clock ticks make up a slot of 625 µs, and two slots make up a slot pair of 1250 µs. In the simple case of single-slot packets the master transmits in even slots and receives in odd slots. The slave, conversely, receives in even slots and transmits in odd slots. Packets may be 1, 3 or 5 slots long, but in all cases the master's transmission begins in even slots and the slave's in odd slots.

The Bluetooth module consists of a Bluetooth Serial Interface (HC-05) and a Bluetooth adapter (HC – M6). Bluetooth serial module is used for converting serial port to Bluetooth. It has two modes: master mode and slaver device. This even number named device is defined as the master or the slaver as a part of the factory setting and cannot be changed.

The main function of Bluetooth serial module is replacing the serial port line, like:

1. There are two MCUs want to communicate with each other. One connects to Bluetooth master device while the other one connects to slave device. Their connection can be built once the pair is made.

This Bluetooth connection is equivalently linked to a serial port line connection including RXD, TXD signals. And they can use the Bluetooth serial module to communicate with each other.

2. When MCU has Bluetooth slave module, it can communicate with Bluetooth adapter of computers and smart phones. Then there is a virtual communicable serial port line between MCU and computer or smart phone.

Communication between two Bluetooth modules requires at least two conditions:

- (1) The communication must be between master and slave.
- (2) The password must be correct.

This is connected to one of the pins of the microcontroller and assigned a password. This acts as the slave device and the Bluetooth enabled phone or PC will be the master device. Once the password is verified with the slave, the master can start sending messages regarding the speed of the motor which is to be set as the reference. Hence, the reference is effectively communicated to the microcontroller.

E. SOFTWARE TOOLS

Introduction To PI and Fuzzy Logic

PI Controller

The Proportional control generates the output proportional to the given input. The integral control is used to eliminate small errors. The Proportional-Integral-Derivative

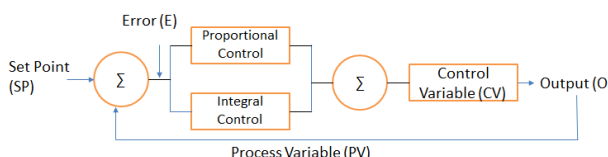


Fig 13. Schematic of PI controller

(PID) controller provides accurate output but the settling time taken to achieve the ideal condition is large. Hence the Proportional-Integral (PI) controller is used where the settling time is comparatively small. The PI controller is essentially a low pass filter.

The process variable is the current speed of motor, the set point is the speed defined by the user as reference speed and the control variable is the output from the PI controller.

The equations describing the controller:

- $E = SP - PV$
- Integral = Integral + E
- Control Variable = $(K_p * E) + (K_i * I)$

Where, K_p = Proportional Constant and K_i = Integral Constant

Generally $0.1 < K_i < 1$ and $0.01 < K_p < 1$.

The advantages and disadvantages of a properly designed PI controller are as follows:

- Improves damping and reduces maximum overshoot.
- Increases rise time.
- Decreases bandwidth.
- Improves gain margin and phase margin.
- Filters out high frequency noise.

The actual setup in the simulation of controlling of PMDC motor using PI controller consists of the PMDC motor whose speed is directly controlled by the MOSFET. Initially the supply voltage is applied across the motor through the MOSFET. Whenever the MOSFET receives the gate pulse the motor rotates.

In the simulations, the speed obtained from the motor is in rps (rotation per second). Hence to convert it to the actual rpm (rotation per minute) value, the rps value is multiplied with the constant 30/pi.

The rpm is then compared with the set speed and the output is fed to the PI controller. The PI controller on receiving the input provides the reference output which is compared with the saw tooth carrier wave and the output is given as the gate drive to the MOSFET. ($K_p=0.1$ and $K_i=1$ here).

Fuzzy Logic Controller

In recent years, the number and variety of applications of fuzzy logic have increased significantly. The applications range from consumer products such as cameras, camcorders, washing machines, and microwave ovens to industrial process control, medical instrumentation, decision-support systems, and portfolio selection. Fuzzy logic has two different meanings. In a narrow sense, fuzzy logic is a logical system, which is an extension of multi valued logic. However, in a wider sense fuzzy logic (FL) is almost synonymous with the theory of fuzzy sets, a theory which relates to classes of objects with unsharp boundaries in which membership is a matter of degree. Even in its more narrow definition, fuzzy logic differs both in concept and substance from traditional multi valued logical systems. In effect, much of FL may be viewed as a methodology for computing with words rather than numbers. Although words are inherently less precise than numbers, their use is closer to human intuition. Furthermore, computing with

words exploits the tolerance for imprecision and thereby lowers the cost of solution. Another basic concept in FL, which plays a central role in most of its applications, is that of a fuzzy if-then rule or, simply, fuzzy rule.

When the exact analytical model of the controlled system is uncertain or difficult to be characterized, intelligent control techniques such as fuzzy logic control (FLC), neural network control, or genetic algorithm may allow better performance.

Intelligent control approaches try to imitate and learn the experience of the human expert to get satisfactory performance for the controlled plant. The FLC has been found particularly suitable for controller design when the plant is difficult to model mathematically due to its complexity, nonlinearity, and/or imprecision. Hence, the FLC is widely applied in a considerable variety of engineering fields today because of its adaptability and effectiveness.

The FLC architecture approximates the way of expert operation intuitiveness; this makes it attractive and easy to incorporate heuristic rules that reflect the experience of human experts into the controller. Recently, fuzzy control theory has been widely studied, and various types of fuzzy controllers have also been proposed in the base paper to improve the drive performance further. In these research works, the main techniques utilized to enhance the self-adaptability and performance of the FLC are scaling factor (SF) tuning, rule base modification, inference mechanism improvement, and membership function redefinition and shifting. Among these techniques, SF tuning is the most used approach, and it has a

	NB	NM	NS	ZE	PS	PM	PB
NB	VB	VB	VB	B	SB	S	ZE
NM	VB	VB	B	B	MB	S	VS
NS	VB	MB	B	VB	VS	S	VS
ZE	S	SB	MB	ZE	MB	SB	S
PS	VS	S	VS	VB	B	MB	VB
PM	VS	S	MB	B	B	VB	VB
PB	ZE	S	SB	B	VB	VB	VB

Fig 14. General Rule Base

significant impact on the performance of an FLC.

Today, home appliance applications require more and more features such as motor speed adaptations to multipurpose accessories, user friendly interfaces, and security features. Such new requirements can be achieved through a low-end microcontroller-based electronic control using the fuzzy logic approach. Nowadays, most of fuzzy logic-based controls are only limited to a complicated ranking management of user interfaces, sensors, and actuators, corresponding to a slow software speed operation. This paper proposes a totally

different use of fuzzy logic. In this case, fuzzy logic is implemented in a standard microcontroller to regulate the speed of a PMDC motor by a real time adjustment of the motor speed. This microcontroller directly tunes the motor current by means of a chopper converter. Starting from a basic food-processor application, the paper practically shows how a fuzzy logic approach can be applied to build a closed speed regulation loop from a very low cost tacho-generator. The paper gives the practical procedure to define the input parameters and to build fuzzy logic rules when using the fuzzy logic development tool. Finally, the major benefits of this paper lie in an original approach where fuzzy logic is applied to fast “real-time” regulation loop without requiring any specific expertise in conventional methods of regulation. Benefits are discussed and concrete results are given.

So far in this paper:

This paper consists of a fuzzy logic control to vary the speed of the motor. The membership functions which are seven in number vary from the largest value in negative to the largest value in positive. The output is a fuzzified result of the two input functions, namely, error in speed and change in error. They can be explained as follows:

Error: The difference of the current speed of the motor to the reference speed, i.e the set speed is the error. This is calculated by:

$$e(k) = r(k) - y(k)$$

$e(k)$ = error in speed

$r(k)$ =required speed

$y(k)$ = existing speed

This speed input is given by means of a closed loop.

Change in error: The change in error, Δe is the ratio of the change in speeds to the change in the selected speed slab. This is calculated by the formula:

$$\Delta e(k) = e(k) - e(k - 1) = y(k - 1) - y(k),$$

if $r(k) = r(k - 1)$

$\Delta e(k)$ = change in error

k is the instant of occurrence

Label & Membership functions	Description (Based on Speed)	Speed output range (defining constants)
NB-Trapezoidal	Negative big	[2208 -1802 -1320 -869.8]
NM-Triangular	Negative medium	[-1320 -759.5 -198.7]
NS-Triangular	Negative small	[-870.6 -193.8 2.19]
ZE-Triangular	Zero	[-192.9 3.143 199.1]
PS-Triangular	Positive small	[2.19 198.6 840.2]
PM-Triangular	Positive medium	[199.6 760.4 1321]
PB-Trapezoidal	Positive big	[846 1322 2006 2686]

Fig 15. Combined Rule Base for Output MP

The PI-like fuzzy controller (PIFC) is driven by a set of control rules rather than constant proportional and integral gains. The main difference between both controllers is that the STFC includes another control rule base for the gain updating factor α . Adaptability is necessary for fuzzy controllers to ensure acceptable control performance over a wide range of load variations regardless of inaccurate operating knowledge or plant dynamic behaviour.

Here, a discrete-time controller with two inputs and a single output is considered.

From Fig., the error e and change of error Δe are used as the input variables, which are defined as

$$e(k) = r(k) - y(k)$$

$$\Delta e(k) = e(k) - e(k - 1)$$

$$= y(k - 1) - y(k), \text{ if } r(k) = r(k - 1)$$

where r and y denote the reference command and plant output, respectively. Indices k and $k - 1$ represent the current and previous states of the system, respectively. The controller output is the incremental change of the control signal $\Delta u(k)$. The control signal can be obtained by

$$u(k) = u(k - 1) + \Delta u(k).$$

The linguistic values ZE, VS, S, SB, MB, B, and VB represent zero, very small, small, small big, medium big, big, and very big, respectively.

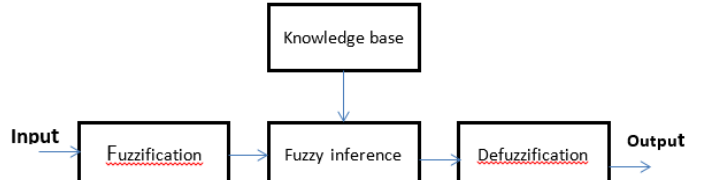


Fig 16. Schematic of FLC

Δe_{err}	NB	NM	NS	ZE	PS	PM	PB
NB	NB	NB	NB	NS	NVS	NVS	ZE
NM	NB	NM	NS	NS	NVS	ZE	PVS
NS	NB	NS	NVS	NVS	ZE	PS	PS
ZE	NS	NS	NVS	ZE	PVS	PS	PS
PS	NS	NS	ZE	PVS	PVS	PS	PB
PM	NVS	ZE	PVS	PS	PS	PM	PB
PB	ZE	PVS	PVS	PS	PB	PB	PB

Here, except for the two fuzzy sets at the outmost ends (trapezoidal MFs are considered), symmetric triangles with equal bases and 50% overlap with adjacent MFs are chosen.

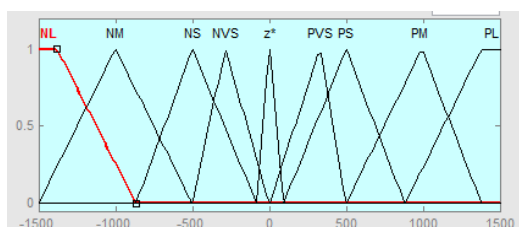
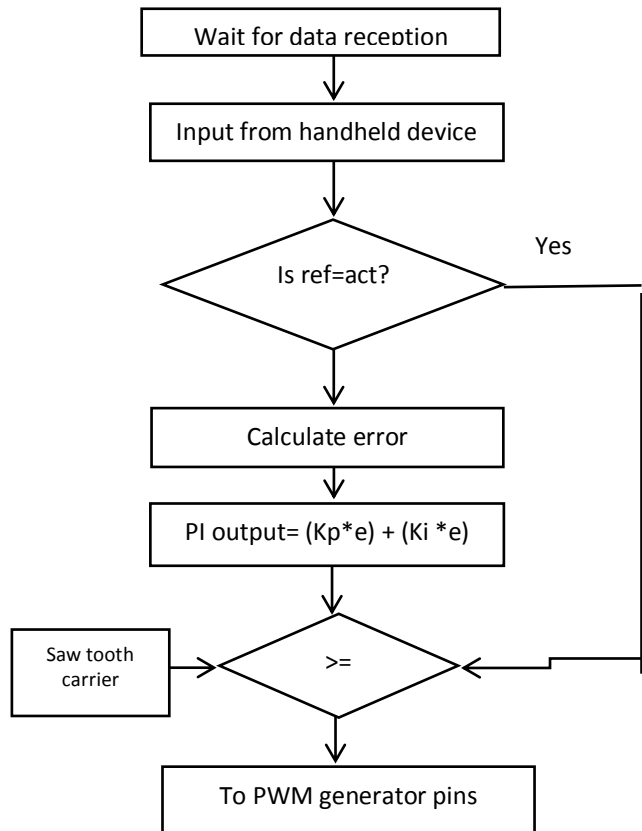
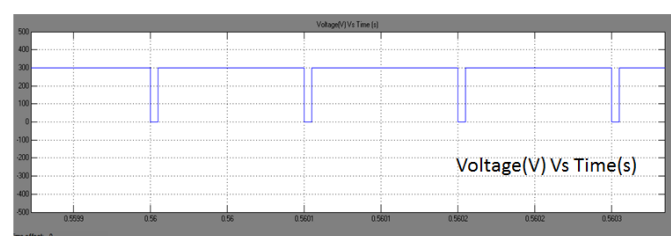
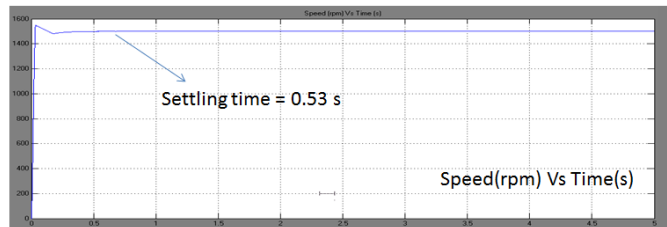
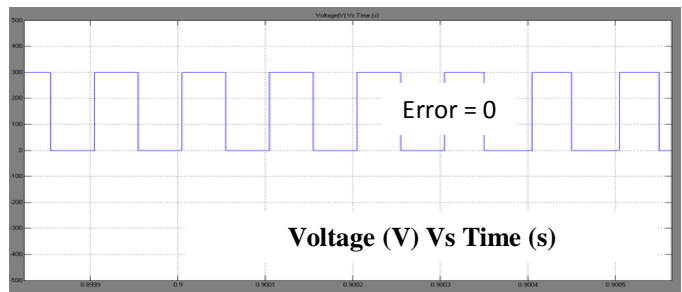
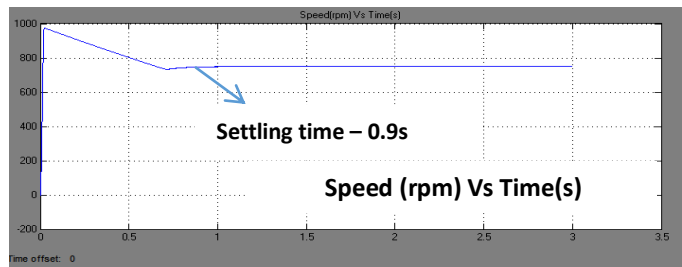
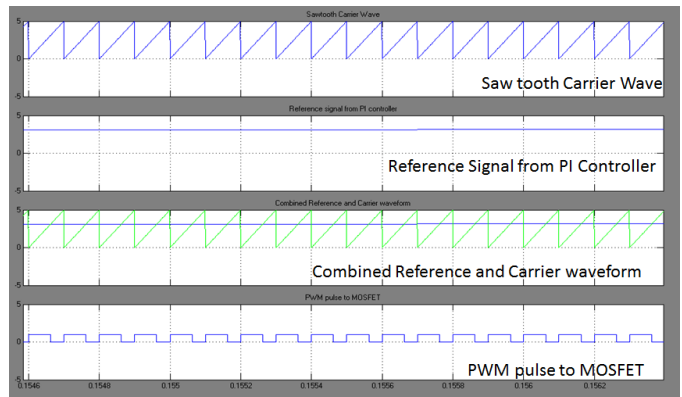


Fig 16a. General Membership Functions

Simulations

Simulink, developed by MathWorks, is a data flow graphical programming language tool for modeling, simulating and analyzing multi domain dynamic systems. Its primary interface is a graphical block diagramming tool and a customizable set of block libraries. It offers tight integration with the rest of the MATLAB environment and can either drive MATLAB or be scripted from it

F. RESPONSE OF THE PI CONTROLLER FLOWCHART**SPEED AND VOLTAGE WAVEFORMS – 1500 RPM****G. SPEED AND VOLTAGE WAVEFORMS – 750 RPM****REFERENCE AND CARRIER WAVEFORMS**

FOR FLC

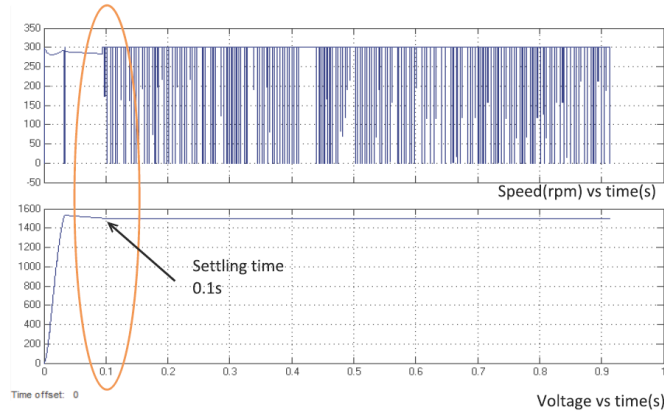


Fig.17 Settling time in FLC

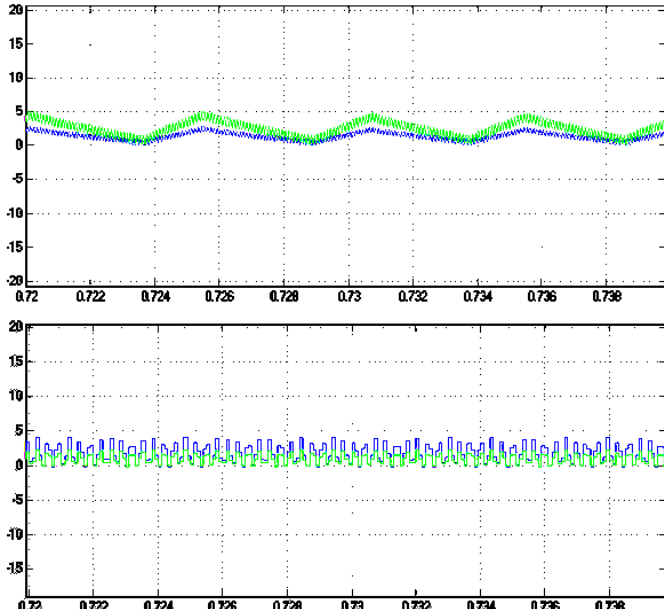


Fig 17.a Current and torque waveforms of PMDC motor via FLC based feedback

Flowchart for FLC system

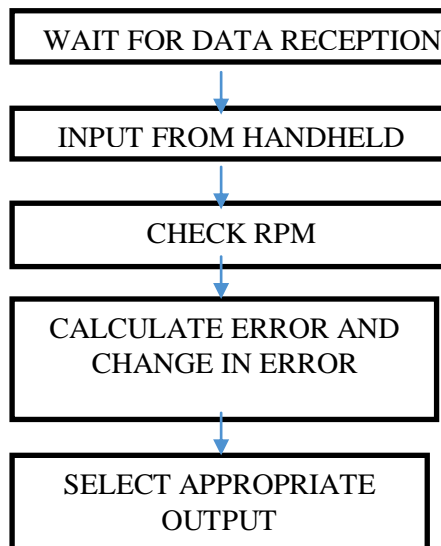
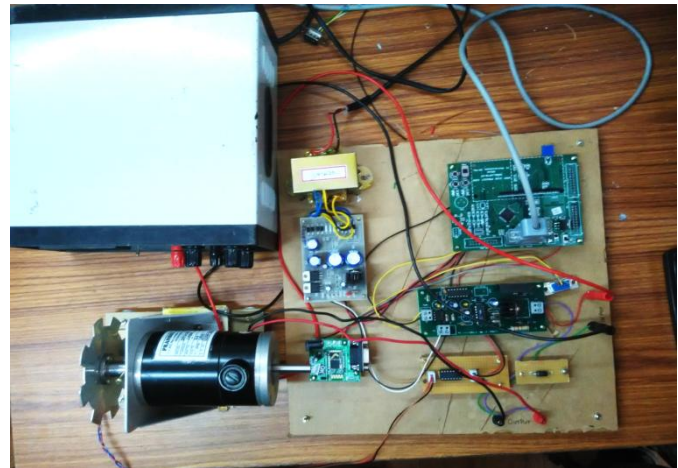
**G . IMPLEMENTATION AND TESTING***Hardware Implementation*

Fig. 18. Hardware

Android Application

Here android application is used to send speed to the motor. First the blue tooth enabled device is paired with the Bluetooth module in the hardware setup using password. Once the pairing is done, the current speed of the motor is displayed in the display screen. The speed at which the motor is to be operated is set by the user as set speed and the change in speeds are observed.

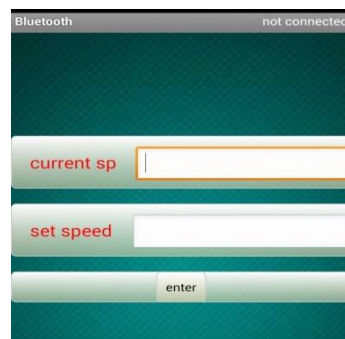


Fig 19. Speed transfer via blue tooth

Testing

The real time comparison of PI and Fuzzy is done using lab view and the results thus obtained are similar to that of simulation results.

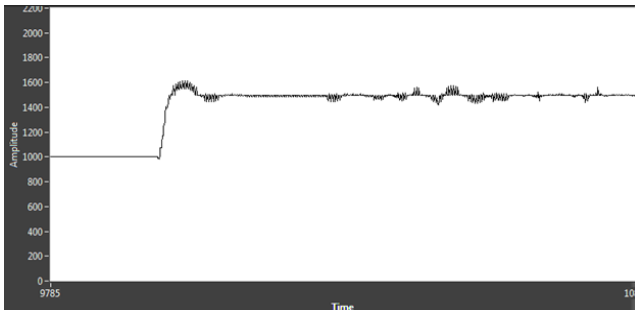


Fig 20. PI controller - 1500 rpm

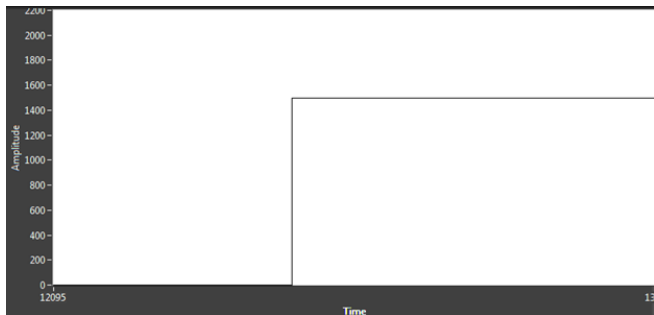


Fig 20 a. Fuzzy controller - 1500 rpm



Fig 20 b. Fuzzy controller – dynamic operation.

H. CONCLUSION

A closed loop control system was implemented based on PI and Fuzzy Logic Controllers. The motor was able to run at the various speed set by the user. In the simulation and the actual implementation, fuzzy logic controller was found to have a better settling time and a higher initial torque than the PI controller. The motor was given the speed command from a distance not more than 10 metres from a phone and was observed to perform efficiently, more so, with the FLC.

The future scope is as follows. This same idea can be applied on multiple drives to make them run at same or different speeds. The fuzzy settling times can be reduced by adding more membership functions and reducing their widths. Also, Bluetooth can be replaced by an internet level cloud control by using the CC3000 IC and hence is not bound by physical distance. This can also be extended to different types of motors in the industry so as to help them achieve complete automation.

I. ACKNOWLEDGMENT

We would like to thank Mrs. Rajeswari K, HOD of the EEE Department for her constant motivation and support during the entire term of the paper. We would also like to thank Mr. Suresh of VI Microsystems for imparting technical knowledge on par with the industrial standards.

J. REFERENCES

- [1] “Hybrid PID-Like Fuzzy Logic Speed Drive of Switched Reluctance Motor”, 2012, Ali Maleki Majid Valianpour Ashkan Mohammadi Saeed Darabi
- [2] Special Electrical Machines by Dhayalini
- [3] Automatic Control Systems by Benjamin C. Kuo
- [4] en.wikipedia.org
- [5] Power Electronics by P S Bhimbra
- [6] “A Modified PI-Like Fuzzy Logic Controller for Switched Reluctance Motor Drives”, Shun-Chung Wang and Yi-Hwa Liu, Member, IEEE
- [7] “New Self-Tuning Fuzzy PI Control of a Novel Doubly Salient Permanent-Magnet Motor Drive” Ming Cheng, Senior Member, IEEE, Qiang Sun, and E. Zhou
- [8] “A Prototype Implementation of a Digital Controlled Rectifier-Based PMDC Motor Drive” Muhammad Usman Rafique, Umama Rashid, Saba Iqbal, Qasim Shafique, Sehrish Jabeen

Congestion Management in Electricity Market by Demand Response Program

¹ V.Uma, ² P.Lakshmi , ³ V.Gomathi

¹Associate Professor, ²Professor, ³Assistant Professor

Department of Electrical and Electronics Engineering

¹ St. Joseph's College of Engineering, ^{2,3} Anna University, Chennai, India

selvirathi@gmail.com, umafiji2007@gmail.com, gomesvg@annauniv.edu

Abstract: Transmission system congestion is a serious issue for the Independent System Operator (ISO) as it violates the various operating limits of the system. Congestion Management plays an important role in operation of power system. In this paper, congestion management is done by Demand Response Program (DRP). Time Of Use (TOU) and Curtailable Demand Response Programs (CDRP) have been focused. DR is modeled considering both TOU and CDRP methods using the single period load models based on load elasticity concept. Fuel cost is calculated in both methods of congestion management. Numerical studies based on IEEE 30 bus system are performed for the evaluation of the proposed method.

Keywords: Congestion Management, Demand Response, TOU, CDRP

NOMENCLATURE

$E(i)$	Self elasticity of the demand in i-th hour
p	Electricity price (\$/MWh)
p_0	Initial electricity price (\$/MWh)
D_0	Initial demand value (MWh)
D	Customer demand after DR (MWh)
A	Incentive of CDRP (\$/MWh)
N_D	Total number of demand buses
N_{Di}	Number of blocks requested by demand 'i'
N_g	Total number of generator buses
$pen(i)$	Penalty given to i-th bus for not participating in DR program (\$)
$B(D(i))$	Income of customer with demand D in i-th hour (\$)
$P_{Di,k}$	Power block k that demand 'i' is willing to buy at price λ_{Dik}
P_{Di}	Power consumed by demand 'i'
P_{gj}	Power produced by generator 'j'
ΔP_{gj}^+	Increment in power of generator 'j' after DR
ΔP_{gj}^-	Decrement in power of generator 'j' after DR

d_i

0/1 variable. It is equal to 1 if the demand 'i' participates in DR and 0 otherwise

N_{reD}

Number of responsive demands

r_{Di}^{down}

Price offered by demand 'i' to decrease its power schedule for congestion management

I INTRODUCTION

In power system, congestion means a situation in which the transmission lines cannot accommodate all line flows requested by market participants, due to lack of capacity of the transmission systems concerned. The network loading has to be maintained within limits for secure operation of power system. Congestion may also cause increase in the electricity prices. Due to congestion in the transmission network some of the power transactions dispatch may be cancelled out. Hence, congestion has to be resolved quickly.

The set of actions taken by the system operator (SO) to relieve congestion are referred to as Congestion Management. Demand Response programs are used to relieve congestion. DR is defined by Department of Energy (DOE) as: "Changes in electric usage by end-use customers from their normal consumption patterns in response to changes in the price of electricity over time, or to incentive payments designed to induce lower electricity use at times of high wholesale market prices or when system reliability is jeopardized" [1].

Demand Response (DR) activities are also defined as "actions voluntarily taken by a consumer to adjust the amount or timing of energy consumption". In this paper Time Of Use (TOU) and Curtailable DR methods are used. The demand reaction to price is analyzed for self elastic loads. The numerical results are shown and the effect of running TOU and CDRP programs individually are discussed.

Congestion management is performed using both demand response and FACTS devices in [2].

Curtailable demand response program is used and the results are compared with only FACTS and only DR and combination of both. Market and re-dispatch cost is calculated for all the three cases.

Emergency Demand Response Program (EDRP), one of the incentive based DR program is used for congestion management in [3]. Different methods of congestion management are discussed briefly. The values of reduction in demand are calculated for various incentives. It is seen that there is a greater reduction in demand with increase in incentive. IEEE 30 bus system is considered for case study and congestion management is performed.

The demand responsiveness can play a major role in competitive electricity markets, particularly in the case of congestion [4]. The impacts of congestion are alleviated as the demand elasticity increases. Demand elasticity tends to lower the congestion costs.

The benefits of demand response are cost reduction, reliability of system, market efficiency, customer service, market power reduction [5]. A brief discussion on incentive based DR is given along with DR promotion principals.

Based on historical demand, price data and short term load forecasting, ISO tries to reduce peak demand. The ISO tries to prevent occurring spike prices by running EDRP [6]. The impact of demand elasticity, incentives and electricity prices on load are test and analyzed by EDRP and TOU demand response programs.

The activities designed to influence consumer demand in short term to reduce peak demand is demand response [7]. Typically, load management includes:

- (i) Incentive-based programs
 - a) Direct Load Control (DLC)
 - b) Curtailable Demand Response Program (CDRP)
 - c) Demand Bidding
 - d) Emergency Demand Response Program (EDRP)
 - e) Capacity Market Program (CMP)
 - f) Ancillary Service Market Program (ASMP)
- (ii) Time-based programs
 - a) Time Of Use (TOU) program
 - b) Real Time Pricing (RTP) program
 - c) Critical Peak Pricing (CPP) program

This paper presents the congestion management method by time based and incentive based DR program. The control variables are demand power, incentive, penalty and electricity price. Optimal power flow algorithm is carried for

the test system to obtain the results. Fuel cost is also calculated by both the methods.

In TOU program, the electricity prices in the low peak period will be cheap, in the off-peak period will be moderate and will be high in the peak period. By running this program, the customers especially who are able to move their consumption will adjust themselves with the prices. So, the peak demand will be reduced and loads will transfer from the peak period to off-peak or low periods.

In CDRP, customers who intend to reduce a portion of their load based on ISO announcements will participate in this program. The ISO will pay them a significant amount of money as an incentive for those who reduce the demand and penalty is assigned for those who don't reduce the demand.

II ECONOMIC MODEL OF ELASTIC LOADS

An economic load model represents the change of the customer's demand with respect to change of electricity price, the incentive given to customers and the penalty charged to customers. This is formulated for the participation of customers in DR programs. Those customers who participate in DR programs are referred to as "responsive demands".

The price elasticity of demand can be defined as the ratio of the relative change in demand to the relative change in demand [3].

$$E = \frac{\partial D}{\partial P} = \frac{P_0}{D_0} \cdot \frac{dD}{dP} \quad (1)$$

If the electricity prices vary for different periods, then the demand reacts one of the following [3]:

- a) Some loads are not able to move from one period to another (e.g. illuminating loads) and they could be only "on" or "off". Such loads are called self elastic loads and they have a negative value.
- b) Some loads could be transferred from the peak period to the off-peak or low periods. Such loads are called cross elastic loads and they always have positive value.

A. Economic Load Model Based on TOU

Assuming that the customer changes his demand from (initial value) to $D(i)$, based on the value of electricity price, we have:

$$\Delta D(i) = D_0(i) - D(i) \quad (MWh) \quad (2)$$

The customer's benefit S(\$), for the i-th hour will be as following:

$$S(D(i)) = B(D(i)) - D(i) \cdot \rho(i) (\$) \quad (3)$$

To maximize the customer's benefit, $\frac{\partial S}{\partial D(i)}$ should be equal to zero:

$$\frac{\partial S}{\partial D(i)} = \frac{\partial B(D(i))}{\partial D(i)} - \rho(i) = 0 \quad (4)$$

$$\frac{\partial B(D(i))}{\partial D(i)} = \rho(i) \quad (5)$$

The benefit function can be defined as [2]:

$$B(D(i)) = B(D_0(i)) + \rho_0(i)[D(i) - D_0(i)] \left\{ 1 + \frac{D(i) - D_0(i)}{2E(i) \cdot D_0(i)} \right\} \quad (6) \quad 0 \leq P_{Di,k} \leq P_{Di,k}^{\max} \quad \forall i = 1, \dots, N_D, k = 1, \dots, N_{Di}$$

$$\frac{\partial B(D(i))}{\partial D(i)} = \rho_0(i) \left\{ 1 + \frac{D(i)}{E(i) \cdot D_0(i)} - \frac{1}{E(i)} \right\} \quad (7)$$

Considering (6) and (8):

$$\rho(i) = \rho_0(i) \left\{ 1 + \frac{D(i)}{E(i) \cdot D_0(i)} - \frac{1}{E(i)} \right\} \quad (8)$$

The demand response to price variation will be as following:

$$D(i) = D_0(i) \cdot \left\{ 1 + \frac{E(i)[\rho(i) - \rho_0(i)]}{\rho_0(i)} \right\} \quad (9)$$

The estimated demand in (9) depends on electricity price during peak, off-peak and low peak hour which are to be predicted by system operator.

B. Economic Load Model Based on CDRP

The change of the customer's demand with respect to changing of the electricity price, the incentive and penalty given to the consumers, is used as in [2]. This model is represented as following:

$$D(i) = D_0 \cdot \left(\frac{\rho(i) + A(i) + pen(i)}{\rho_0(i)} \right)^{E(i)} \quad (10)$$

The estimated demand in (10) depends on electricity price, incentive and penalty given to customers.

IV. PROBLEM FORMULATION

The problem formulation for auction-based market clearing and congestion management by DR is discussed below.

A. Auction-based Market Clearing

Customers can bid a price at which they would be willing to curtail their loads during times of congestion. The ISO clears the market without considering the line flow constraints. A modified auction dispatch based on bidding can be formulated as:

$$Max: \sum_{i=1}^{N_D} \sum_{k=1}^{N_{Di}} (A_{Di,k} P_{Di,k}) - \sum_{j=1}^{N_G} C_j(P_{G,j}) \quad (11)$$

Subject to:

$$0 \leq P_{Di,k} \leq P_{Di,k}^{\max} \quad \forall i = 1, \dots, N_D, k = 1, \dots, N_{Di} \quad (12)$$

$$P_{G,j}^{\min} \leq P_{G,j} \leq P_{G,j}^{\max} \quad \forall j = 1, \dots, N_G \quad (13)$$

$$\sum_{i=1}^{N_D} \sum_{k=1}^{N_{Di}} P_{Di,k} = \sum_{j=1}^{N_G} P_{G,j} \quad (14)$$

The first term in objective function (11) represents the sum of accepted demand bids times to the corresponding bid prices and the second term is the generation cost.

The constraint (12) specifies the size of the demand bids. The constraint (13) ensures that every generator if running, should run between its minimum and its maximum limits.

B. Congestion Management by Demand Response Program

In general, both generation and demand re-dispatch is demand response. So, to manage congestion, the amount of demand reduction by CDRP and TOU is calculated. In auction-based market clearing, the dispatch is performed without taking network limitations such as transmission line and voltage limit constraints. To manage congestion due to such limits, the problem is formulated as:

$$Min: \sum_{j=1}^{N_G} |C_j(\Delta P_{G,j})| + \sum_{i \in red} r_{Di}^{\text{down}} \Delta P_{red,i}^{\text{down}} d_i \quad (15)$$

Subject to:

$$\sum_{j=1}^{N_G} \Delta P_{G,j}^+ = \sum_{\substack{k=1 \\ k \neq j}}^{N_G} \Delta P_{G,k}^- \quad (16)$$

$$\Delta P_{gj}^+ + \Delta P_{gk}^- - \Delta P_{reD} = 0 \quad \forall j = 1, \dots, N_G \quad (17)$$

$$-P_{ij}^{max} \leq P_{ij} \leq P_{ij}^{max} \quad \forall ij = 1, \dots, NL \quad (18)$$

$$V_i^{min} \leq V_i \leq V_i^{max} \quad \forall i = 1, 2, \dots, n \quad (19)$$

$$P_{gj}^{min} \leq P_{gi}^0 \pm \Delta P_{gj} \leq P_{gj}^{max} \quad \forall j = 1, \dots, N_G \quad (20)$$

The objective function (15) contains two parts. The first term is the payments received by generator for changing the output from the original generation and the second term shows the payment received by responsive demands to reduce their load.

The set of equality constraints (16) denotes that the sum of increase in power generation in all buses must be equal to the decrease of power generated in all buses. This implies that the algebraic sum of power increment or decrement on all buses must be equal to zero. The equality constraints (17) ensure that the change in generated power must be equal to the change in loads of responsive demands.

The set of inequality constraints (18) enforces line capacity limits. The inequality constraint (19) ensures that the voltage values in all buses are within limits. Constraints (20) confirm that the rescheduled generators stay within the maximum and minimum power outputs.

V. RESULTS AND DISCUSSION

A case study based on IEEE 30-bus system is presented in this section. Topology, line, generator and demand data can be found in [12].

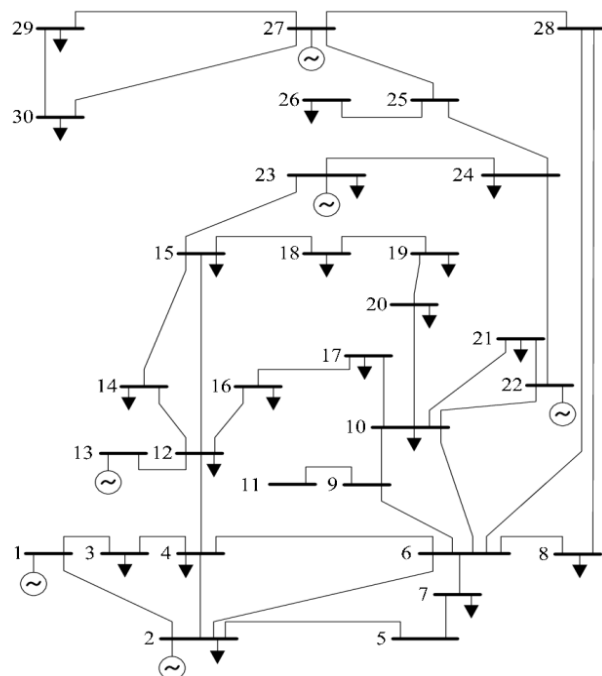


Fig. 1. IEEE 30 bus system

Fig.1 depicts the IEEE 30bus system. It has 6 generators, 21 loads and 41 transmission lines.

A. Auction-based market clearing

The auction dispatch clears the generators production by using the initial demand values according to (11)-(14). The auction results for generator are provided in Table1.

Table 1 Auction results

Generator No.	Bus No.	Generation (MW)
1	1	57.44
2	2	36.84
3	13	48.73
4	22	25.60
5	23	22.48
6	27	29.47

Based on severity index, the line 12-16 is tripped for congestion creation. The line 12-13 gets overloaded and congestion management is performed by both CDRP and TOU individually.

B. DR program implementation to relieve congestion

Seven load buses are selected based on generation shift factor to participate in demand response program [2].The price of electricity in DR programs is assumed to be equal to 50 \$/MWh.

Table 2 Selected responsive demands for participation in demand response program

Demand response number	Bus number
1	7
2	8
3	12
4	17
5	19
6	21
7	30

Table 2 shows the demand buses participating in CDRP and TOU demand response programs.

The elasticity values for the demand response participants are shown in Table 3.

Table 3 Self and Cross elasticity

	Peak	Off-Peak	Low
Peak	-0.1	0.016	0.012
Off-Peak	0.016	-0.1	0.01
Low	0.012	0.01	-0.1

From Table 3, it is seen that the values of self elasticity are negative and the cross elasticity values are positive.

B.1. Congestion management by CDRP

Demand values of responsive loads after CDRP implementation are shown in Table 4.

Table 4 Demands of responsive loads by CDRP

Responsive load bus number	Initial Demand (*10 MW)	Change in Demand after DR (*10 MW)
7	22.8	22.5162
8	30	29.6265
12	11.2	11.0606
17	9	8.8880
19	9.5	9.3817
21	17.5	17.2821
30	10.6	10.4680

According to the results obtained in Table 4 it is viewed that there is an average decrease of about 1.2% in each demand after DR.

The results of congestion management by CDRP for an incentive and penalty of 100\$ and 150 \$ per MWh is provided in Table 5.

Table 5 Variation of Generation due to CDRP

Generator Number	Bus number	Initial Generation (MW)	Change in Generation after CDRP (MW)
1	1	57.44	62.45
2	2	36.84	39.76
3	13	48.73	33.76
4	22	25.60	27.69
5	23	22.48	24.15
6	27	29.47	31.81

From Table 5, the generators in bus number 1, 2, 22, 23 and 27 increases the generation and the generator in bus 13 decrease the generation from the values obtained in auction based results.

B.2. Congestion management by TOU

Congestion management by TOU is presented in Table 7. The electricity price during off-peak and peak hour is considered as 250 and 300 \$ per MWh.

Demand values of responsive loads during off-peak and peak hours after implementation of TOU are shown in Table 6.

Table 6 Demands of responsive loads during low peak, off-peak and peak hour

Responsive load bus number	Initial Demand (*10 MW)	Change in Demand after DR (*10 MW)	
		Off-peak	Peak
7	22.8	21.88	21.66
8	30	28.8	28.5
12	11.2	10.752	10.64
17	9	8.640	8.550
19	9.5	9.120	9.025
21	17.5	16.8	16.625
30	10.6	10.176	10.07

From table 6, it is seen that there is a greater decrease in demand value during peak hour when compared with off-peak hour. During peak hour there is an average decrease of 5% of demand and during off-peak hours there is an average decrease of 4% of demand.

The results of generation re-dispatch for congestion management by TOU during off- peak(11:00 to 16:00)and peak hour (6:00 to 10:00and 17:00 to 21:00) is given in Table 7.

Table 7 Generation Variation of all generators due to congestion management by TOU during off-peak and peak hour

Generator Number	Bus number	Initial Generation (MW)	Generation Rescheduling Values (MW)	
			During off-peak hour	During peak hour
1	1	57.44	60.99	60.98
2	2	36.84	38.3	38.3
3	13	48.73	14.30	13.19
4	22	25.60	38.3	38.3
5	23	22.48	22.68	22.68
6	27	29.47	41.84	41.84

From Table 7, the generators in bus number 1, 2, 22, 23 and 27 increases the generation and the generator in bus 13 decrease the generation from initial values as obtained in auction based results.

The fuel cost of generator after congestion management by CDRP and TOU demand response program is presented in Table 8.

Table 8 Fuel cost before and after using DR

		Fuel Cost (\$)
Normal Case (without DR)		691.4370
With CDRP		645.8644
With TOU	Off-peak	642.6181
	Peak	639.5858

V. CONCLUSION

This paper evaluates the two types of demand response programs namely Time Of Use and Curtailable Demand Response Program. The economic load model of each program is given for social welfare maximization. The main objective is to relieve congestion and results obtained under both the programs show that based upon the incentives, penalty and electricity prices considered congestion

management by TOU relieves congestion at least cost when compared with CDRP. On a future note, congestion management can be done by other different types of DR program and the results can be compared. In addition, two DR programs can be combined together and check if the results obtained are encouraging.

VI. REFERENCES

- [1] Albadi MH, El-Saadany EF, "Demand Response in Electricity Markets: An Overview", Power engineering society general meeting, IEEE 2007;2007. P. 1-5.
- [2] A. Yousefi, T.T. Nguyen, H. Zareipour, O.P. Malik "Congestion Management Using Demand Response and FACTS Devices", Electrical Power and Energy Systems, 2012.
- [3] E. Shayesteh, M. Parsa Moghaddam, S. Tahernejhad, M. K. Sheikh-EL Eslami "Congestion Management using Demand Response Programs in Power Market", IEEE Conference, 2008.
- [4] Bompard E, Carpaneto E, Chicco G, Gross G, "The Role of Load Demand Elasticity in Congestion Management and Pricing" Power Engineering Society Summer Meeting, IEEE 2000, vol. p. 2229-34.
- [5] Arani A.B., Yousefian R., Khajavi P. and Monsef H., "Load Curve Characteristics Improvement by Means of Optimal Utilization of Demand Response Programs," IEEE Conference, 2011.
- [6] H. Aalami, G. R. Yousefi and M. Parsa Moghadam, "Demand Response Model Considering EDRP and TOU Programs", accepted for presentation in IEEE/PES Transmission and Distribution Conference & Exhibition, 2008, Chicago, USA.
- [7] Peter B., Laurent D. Michel, Peter Friedland and Che Guan "Load Forecasting and Demand Response ,," IEEE Conference, 2010.
- [8] Strbac G, "Demand Side Management: Benefits and Challenges", Energy Policy 2008; 36:4419-26.
- [9] M. Shahidehpour, H.Yatim, and Z. Li, Market Operations in Electric Power Systems. New York: Wiley, 2002.
- [10] E. Shayesteh, M. Parsa Moghaddam, R.Haghifam, M.K. Sheikh-EL-Eslami, "Security-Based Congestion Management By Means Of Demand Response Programs", Paper accepted for presentation at 2009 IEEE.
- [11] A. J. Wood, B.F. Wollenberg, "Power Generation Operation and Control", New York: Wiley 1996.
- [12] P. Khajavi, H. Abniki, A.B. Arani, "The Role of Inventive Based Demand Response Programs in Smart Grid", IEEE 2011.
- [13] Bompard E, Wene L, Napoli R., " Network Constraint Impacts on the Competitive Electricity Markets under Supply-side Strategic Bidding", IEEE Trans Power System 2006; 21:160–70.

A Structure Of 360° Solar Tracking System Using PLC And SCADA

K.S.DHANAM JAYAM
dhanamjayam619@gmail.com
 044-25952905
 DEPARTMENT OF EEE
 SATHYABAMA UNIVERSITY
 CHENNAI,INDIA

D.SUSITRA
 ASSISTANT PROFESSOR
 DEPARTMENT OF EEE
 SATHYABAMA UNIVERSITY
 CHENNAI,INDIA

Abstract— Electricity plays a key role in our daily lives but the energy sources to electric power has been used in abundance and so

researchers were compelled to find an alternate source of power leading to the discovery of solar power converted into electricity using solar panels. These types of panels can be used in a stable form for both single axis as well as for dual axis. In a fixed form their efficient is low were as in a tracking system the panel is made to move either in single axis or dual axis. In a single axis, it tracks only in an east to west direction with respect to the sun and it has a better efficient than panels in fixed form. But in a dual axis system the panels is made to rotate in all four directions and dual axis has proved more efficient than both fixed panels and single axis system

Keywords: solarpanel,LDR,Relay,DCGearedmotor,PLC,SCADA

I. INTRODUCTION

Solar energy is the energy extracted from the rays issued from the sun in the form of heat and electricity. This energy is essential for all life on Earth. It is a renewable resource that is clean, economical, and less pollution compared to other resources and energy. Therefore, solar energy is rapidly gaining notoriety as an important means of expanding renewable energy resources. The main object for this paper is to develop the suntracking solar system model which is follow the movement of the sun regardless of the motor speed. Beside that it is to improve the overall electricity generation using axis sun tracking system. Light Dependent Resistor(LDR) has been choosen as the sensor because it is commonly used in suntracking system. The programmable logical controller(PLC) will gives the pluse to the driver to progress the motor. For the DC motor driver bi-directional control using relay. The motor controller has been choosen to rotate clockwise and counter clockwise easily. This paper is covered for the dual axis and is designed for low power and residential usage application.

From the reference paper of Ashok kumar saxena & V.Dutta (1990) the Solar tracking can be achieved in closed loop and open loop and the controller is capable of acquiring photovoltaic and metrological data from a photovoltaic system. The disadvantages of this system are the tracking system using versatile microprocessor based controller life is short, Bill lane (2008) presented the system which is able to track and follow sunlight intensity in order to collect

maximum solar power and it is usually cheaper in terms of cost per watt. The disadvantages are this is a far more cost effective solution than purchasing additional solar panel. Y.J.Huang (2009) explained that Solar energy is the most powerful resource that can be used to generate power high efficiency of light-electricity transformation and the mechanism is simple & saves power. The disadvantages are when the internal temperature of a solar cell panel is over 85-100 degree, the set will get damage and different voltage ¤t. Asmara Hid Ponniran (2011) he constructed a system model that can be applied in the residential area for alternative electricity generation especially for non-critical & low power appliances and the main disadvantage of the single axis tracker is that it can only track the daily movement of the sun and not the yearly movement, K.Sreenivasa Rao & M.Mahesh (2012) explained that the efficiency of the proposed system can be increased around 64% on a summer in sunny day. The disadvantages of the paper is the cost of tracking is very high and not economical using processor. The organization of this paper is as follows section II discuss about solar system tracker. Section III discuss about Hardware Implementation , Section IV discuss about simulation and Section V presents conclusion.

II. SOLAR SYSTEM TRACKER

A solar tracker is an electro-mechanical system used on behalf of orienting a solar panel from the sun. It is used in different applications such as the transportation signaling, lighthouses, emergency phones installed in the highways etc. Its main objective is to find the maximum sun radiations in order to get maximum charge from the batteries. There are several ways in which electricity can be generated from sun. Photovoltaic's (PV) has been mainly developed for small and medium-sized applications, such as calculator charged by solar cell to the PV power plant. For large -scale generation, concentrating solar thermal power plants have been more common, however new multi-megawatt PV plants have been built recently. A photovoltaic cell (PV cell) is a specialized

semiconductor that converts visible light into direct current (DC). Some PV cells can produce DC electricity from infrared (IR) or ultraviolet (UV) radiation. Photovoltaic cells are an integral part of solar-electric energy generation. Solar energy only generates DC electricity from sun, which in turn can be used in many applications such as: charging batteries, powering equipment, etc. They produce electric energy as long as light shines.

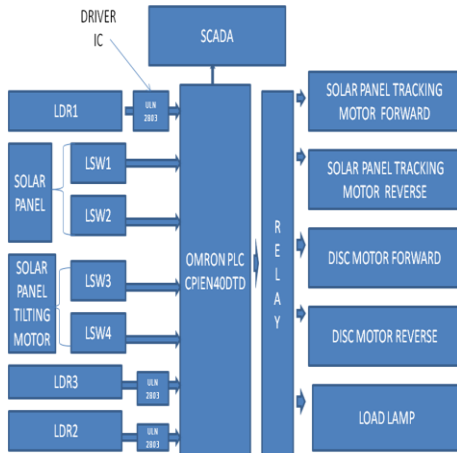


Fig 1: Block diagram of dual axis solar tracker

SCADA: Supervisory Control and Data Acquisition systems are used to control dispersed assets where centralized data acquisition is as important as control. SCADA systems integrate data acquisition systems with data transmission systems. HMI software is used to provide a centralized monitoring and control system for numerous process inputs / outputs.

PLC: A programmable logic controller, is used for automation of industries, such as control of machinery on factory assembly lines. It uses less wiring and it is easier and faster to make change.

LIMIT SWITCH: Limit switch is a sensor that provides feedback to keep some physical value (for example, pressure, temperature, or distance) within a preset range. These electromechanical devices are triggered by physical contact, translating mechanical signals into electrical. There are four limit switches and limit 1&2 switches are used to the solar panel and limit 3&4 switches are used for the tilting.

RELAY: Relay is a switching device associated with the benefit of switching high load signals with low control signals. Heavy loads such as motor and lamps can be controlled with the help of low signals.

DC GEARMOTOR: A geared DC Motor has a gear assembly attached to the motor. The gear assembly helps in increasing the torque and reducing the speed.

LIGHT DEPENDENT RESISTOR (LDR): The light dependent resistor (LDR) are used in the circuit to sense the change in the sun's position.

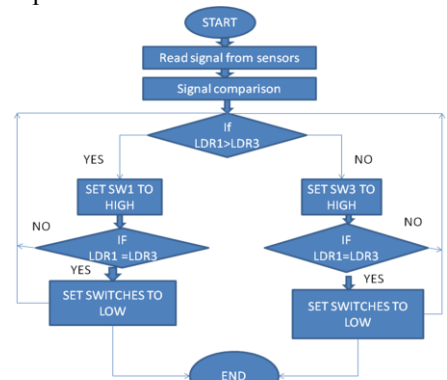


Fig 2 Flow chart of dual axis tracker

The algorithmic steps for the dual axis tracking system is given below

Step 1: Start the procedure of PLC Programming

Step 2: Read the signal from sensors

Step 3: Convert the signal from A to D and then compare the signal

Step 4: If $LDR1 > LDR3$ then set SW1 to high and if $LDR1 < LDR3$ then set SW3 to high

Step 5: If $LDR1 = LDR3$ then switches will be in original position and if not equal then the procedure will repeat again from step 4 (SW1 & SW3 are the switches).

Step 6: End the procedure.

The organization of this paper is as follows section III discuss about hardware implementation and Solar tracker system

III. HARDWARE IMPLEMENTATION

3.1 SOLAR PANEL:

A photovoltaic module or photovoltaic panel is a packaged interconnected assembly of photovoltaic cells, also known as solar cells. A typical silicon PV cell is composed of a thin wafer consisting of an ultra-thin layer of phosphorus-doped (N-type) silicon on top of a thicker layer of boron-doped (P type) silicon. Regardless of size, a typical silicon PV cell produces about 0.5 – 0.6 volt DC under open-circuit and no-load conditions. The current (and power) output of a PV cell depends on its efficiency and size (surface area), and is proportional to the intensity of sunlight striking the surface of the cell. The photovoltaic module, known more commonly as the solar panel, uses light energy (photons) from the sun to generate electricity through the photovoltaic effect. The majority of modules use wafer-based crystalline silicon cells or a thin-film cell based on cadmium telluride or silicon. Crystalline silicon, which is commonly used in the wafer form in photovoltaic (PV) modules, is derived from silicon, a

commonly used semi-conductor. The solar panel used in the proposed system is of 5W power rating



Fig 3: 5w solar panel plate

3.2 SENSORS:

LDR (LIGHT DEPENDENT RESISTOR):

It is a device whose resistivity is a function of the incident electromagnetic radiation. Hence, they are light sensitive devices. They are also called as photo conductors, photo conductive cells or simply photocells. A photo resistor or light dependent resistor or cadmium sulphide (CdS) cell is a resistor whose resistance decreases with increasing incident light intensity. A photo resistor requires a power source because it does not generate Photocurrent a photo effect is manifested in the change in the material's electrical Resistance. They are made up of semiconductor materials having high resistance. Sensor can be defined as a device which receives a signal and converts it into electrical form which can be further used for electronic devices. LDR are used in the circuit to sense the change in the sun's position.

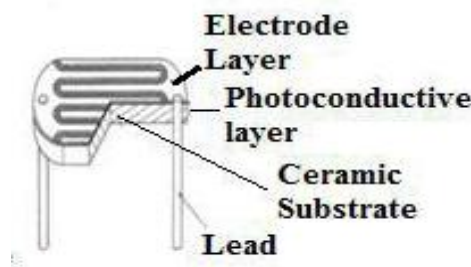


Fig 4: Block diagram of LDR

3.3 PLC (PROGRAMMABLE LOGIC CONTROLLERS):

IT is used for automation of typically industrial electromechanical processes, such as control of

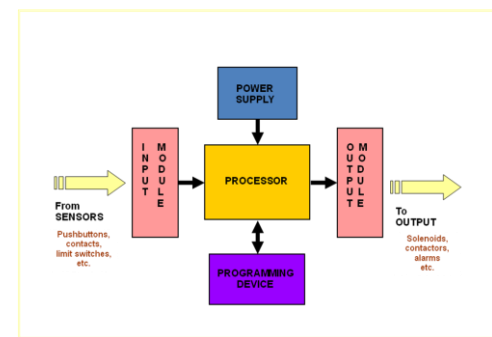
machinery on factory assembly lines, amusement rides, or light fixtures. PLCs are used in many industries and machines. PLCs are designed for multiple analogue and digital inputs and output arrangements, extended temperature ranges, immunity to electrical noise and resistance to vibration and impact. Programs to control machine operation are typically stored in battery-backed-up or non-volatile memory. The organization of this paper is as follows section 3.3.1 discuss about PLC size.

3.3.1 PLC SIZE:

SMALL - it covers units with up to 128 I/O's and memories up to 2 Kbytes.- these PLC's are capable of providing simple to advance levels or machine controls.

MEDIUM - have up to 2048 I/O's and memories up to 32 Kbytes.

LARGE- *the most sophisticated units of the PLC family. They have up to 8192 I/O's and memories up to 750 Kbytes.-can control individual production processes or entire plant.* The organization of this paper is as follows section discuss about components of PLC.



MAJOR COMPONENTS OF A COMMON PLC

Fig 5: Components of PLC

3.3.2 PLC OPERATION:

While the PLC is running, the scanning process includes the following four phases, which are repeated continuously as individual cycles of operation

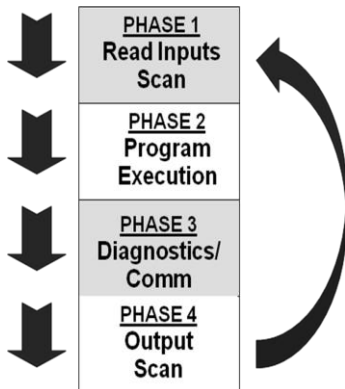


Fig 6: Operation of PLC

3.3.4 PLC COMMUNICATIONS

SERIAL COMMUNICATION:

PLC communications facilities normally provide serial transmission of information.

COMMON STANDARDS

RS 232

Used in short-distance computer communications, with the majority of computer hardware and peripherals.

Has a maximum effective distance of approx. 30 m at 9600 baud.

Local Area Network (LAN)

Local Area Network provides a physical link between all devices plus providing overall data exchange management or protocol, ensuring that each device can “talk” to other machines and understand data received from them.

LANs provide the common, high-speed data communications bus which interconnects any or all devices within the local area.

LANs are commonly used in business applications to allow several users to share costly software packages and peripheral equipment such as printers and hard disk storage.

RS 422 / RS 485

Used for longer-distance links, often between several PCs in a distributed system. RS 485 can have a maximum distance of about 1000 meters. The organization of this paper is as follows discuss about PLC communication ports.

PLC COMMUNICATION PORTS

Changing resident PLC programs - uploading/downloading from a supervisory controller (Laptop or desktop computer).

Forcing I/O points and memory elements from a remote terminal.

linking a PLC into a control hierarchy containing several sizes of PLC and computer.

Monitoring data and alarms, etc. via printers or Operator Interface Units (OIUs). The organization of this paper is as follows section 3.4 discuss about scada.

3.4 SCADA:

(SCADA (supervisory control and data acquisition) is a type of industrial control system (ICS). Industrial control systems are computer controlled systems that monitor and control industrial processes that exist in the physical world. The organization of this paper is as follows section 3.5 discuss about relay.

3.5 RELAY

This device consists of a coil of wire covered with an iron core. When electricity is applied to this coil of wire it becomes magnetised, The A,B&C are terminals a SPDT Switch controlled by an electro magnet. When v1 & v2 are ON condition, the electromagnet acts on the SPDT switch so that the B, C terminals are connected. When the electricity is disconnected, then A&C terminals are connected.

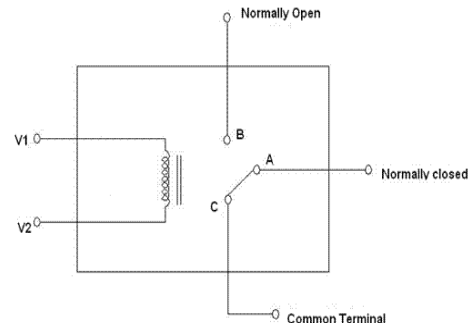


Fig 7: Relay Circuit Diagram

3.6 DC GEARED MOTOR

A geared DC Motor the rotor shaft is also connected with motor.

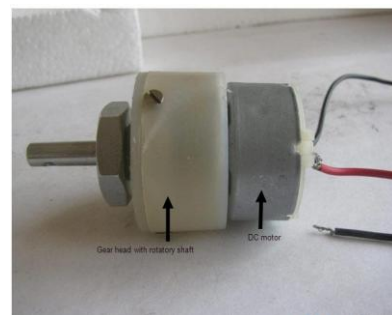


Fig 8: Geared DC Motor

The speed of motor is counted in terms of rotations of the shaft per minute and is termed as RPM .The gear assembly helps in increasing the torque and reducing the speed.

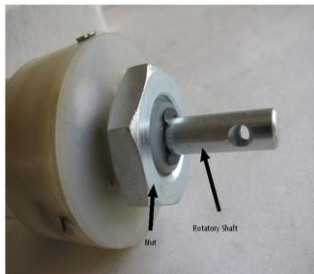


Fig 9: Nut & Rotor Shaft is connected in gear motor

A nut is placed near the shaft which helps in mounting the motor to the other parts of the assembly. This method where gears reduce the speed of the vehicle but increase its torque is known as gear reduction. The organization of this paper is as follows section 3.9 discuss about stand .

3.9 STAND ASSEMBLY

The frame for the solar panel is made up of L shaped steel rod. The length is 35cm and width is 65cm.

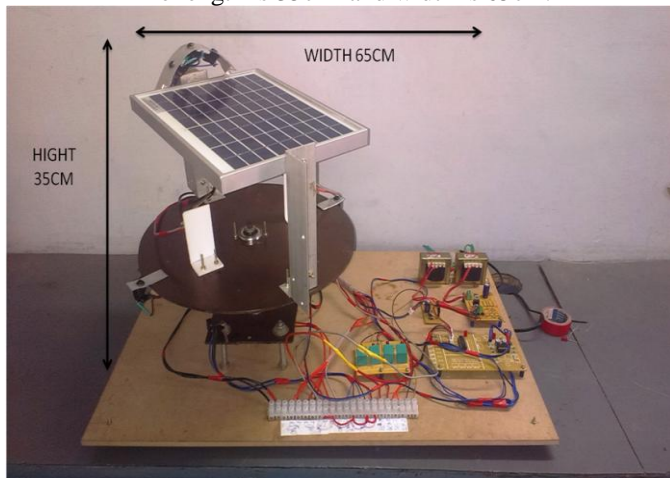


Fig 10: Hardware Setup.

3.8 ULN AND COMPARATOR CIRCUIT:

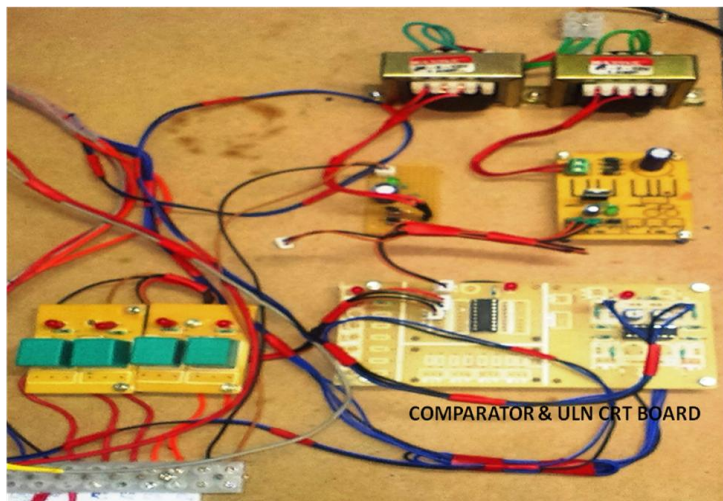


Fig 11: Comparator and ULN circuit board.

3.9 ULN 2803:

ULN stands for Ultra Low Noise. ULN2803 is an Integrated Circuit (IC) chip with a high voltage/current Darlington transistor array. The chip takes low level signals (TTL, CMOS, PMOS, NMOS - operate at low voltages and currents) and acts as a relay, switching a high level signal on the opposite side. It is an 18-pin IC configuration that includes eight transistors. Pins 1-8 receive the low level signals and pin 9 is grounded. Pin 10 is connected to the positive power supply. Pins 11-18 are the outputs that generate strong signals.

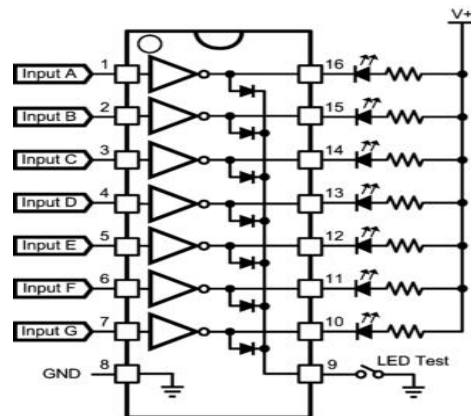


Fig 12: ULN Configuration

A TTL signal operates with signals between 0.0 and 0.8V that is considered low, and 2.2 to 5.0V that is considered high. The maximum power available on a TTL signal does not exceed 25mW which is not suitable for powering relay coil. The organization of this paper is as follows section IV discuss about simulation.

IV SIMULATION

The Simulation diagram of dual axis solar tracking panel using PLC and SCADA is shows in Fig 13. It is used to monitor and any damage caused we can easily rectify the system. The simulation is developed through the INTOUCH SOFTWARE. The ladder logic is transfer to the PC to PLC using RS232 cable and HOST LINK used to open and fix the com ports then simulation will work. The USB cable from the PLC connect to the system used to monitor and control the solar panel system. The slides are used to know when the LDR's are sensed then the switches will go to high and the solar panel will move to the directions where LDR's are sensed and the battery used to store the energy and supply to the industry.

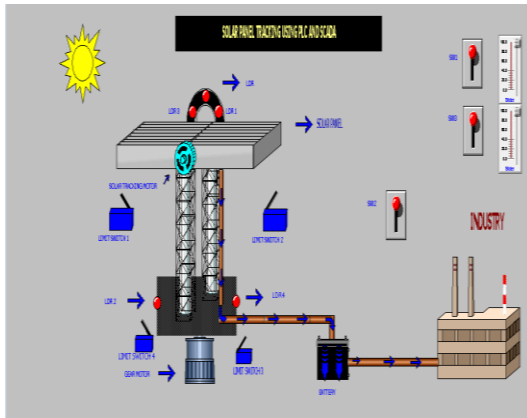


Fig 13 Simulation of the paper.

HARDWARE SYSTEM ASSEMBLY



Fig 14 Hardware setup

In the hardware assembly the tilting plate is used to rotate the panel and the solar panel range is 12volts and 5watts. There are six inputs and four outputs. The six inputs are four limit switches and two LDR's. The four Limit switches are used to east, west, forward and reverse and two LDR's are east and west .The four outputs are motor1&2 and motor1 is used to the disc purpose and motor2 is used to the solar panel. In the hardware setup the input supply is 230volts and using step down transformers (0-12v) the supply will step down to 12volts. The regulated pin used to send the regulated power supply to the comparator IC and ULN2803. The unregulated power supply will go to the PLC supply as DC. The LDR's are used to sense the light and when the torch light is keep on the east LDR then the solar panel move to the east direction .The LDR west is sensed then the solar panel move to the west direction. The Limit Switch is used to protect the panel due to over rotating. From the tabulation the dual axis is more efficiency than the single axis and the readings are taken at 1pm the single axis panel got 10.2 volts and the dual axis got 11.6volts.

READING TABULATION:

HOURS	SINGLE AXIS (VOLTS)	DUAL AXIS (VOLTS)
6AM	4.4V	5.7V
7AM	5.5V	5.9V
8AM	5.9V	6.4V
9AM	6.5V	8.9V
10AM	7.9V	9.6V
12PM	9.03V	11.3V
1PM	10.2V	11.6V
2PM	10.5V	11.9V
3PM	9.6V	10.9V
4PM	8.3V	10.6V

V CONCLUSION:

In this paper a solar tracker is realized to capture maximum power from sunlight. The position of maximum capture of power is stored in memory.

The stored data can be applicable for many applications such as Large photo voltaic panels can track the sun all the day light and by that it give above 65% efficiency in generating electricity.

Solar heaters is also tracking sun during day light and by that less panels are required at the initial cost while in the home automation systems, this system is also needed in turning light ON and Off and also for opening and closing the curtains.

REFERENCES:

1. Asmarashid Ponniran, Ammar Hashim, Arifuddin Joret ,(2011,"A Design of Low Power Single Axis Solar Tracking System Regardless of Motor Speed", International Journal of Integrated Engineering, Vol. 3 No. 2(2011) pg:5-9.
2. Ashok Kumar Saxena and V.Dutta,(1990), "A VERSATILE MICROPROCESSOR BASED

*CONTROLLER FOR SOLAR TRACKING” , IEEE .
Pg:1105-1109*

3. *Bill Lane,(2008), “Solar Tracker”, Department of Electrical and Computer Engineering Cleveland State University,Pg:1-17*
4. *Dhanabal.R , Bharathi.V, Ranjitha.R , Ponni.A, Deepthi.S ,Mageshkannan, (2013,” Comparison of Efficiencies of Solar Tracker systems with static panel Single-Axis Tracking System and Dual-Axis Tracking System with Fixed Mount” International Journal of Engineering and Technology (IJET).pg.no:1925-1933*
5. *Sreenivasa Rao.K, M. Mahesh (2012) , “ARM Based Solar Tracking System ” International Journal of Modern Engineering Research (IJME) Vol.2, Issue.4,pg:2504-2507.*

PERFORMANCE ANALYSIS OF PMSM USING DIRECT TORQUE CONTROL

Nuthalapati Mani Deepika Prasanthi^{1,a}, Mrs. Jayarama Pradeep^{2,b}

¹PG Scholar, ²Associate Professor

St. Joseph's College of Engineering, Chennai-600119, Tamil Nadu, India
prasanthinnlr@gmail.com^a, jaya_7pradeep@yahoo.com^b

Abstract: The permanent magnet synchronous machine(PMSM's) are used in many applications that required rapid torque response and high performance operation. The increase of electromagnetic torque in a permanent magnet synchronous machine is proportional to the increase of angle between stator and rotor flux linkages and this can be obtained by adjusting rotating speed of stator flux linkages as fast as possible. DTC is receiving increasing attention as it eliminates current controllers and low dependence on motor parameters. In this paper the basic theory of operation for the control technique is presented. A simulation model is developed in MATLAB/SIMULINK and performance comparison of proposed DTC with conventional PI is provided. Simulation results demonstrate the better dynamic response in torque and speed for the proposed drive over a wide speed range.

Keywords: Permanent magnet synchronous machine(PMSM's), Direct Torque Control(DTC), High dynamic response, Stator flux linkages.

I Introduction: PMSM motors are being increasingly used in different industry sectors in new applications or as alternatives to induction motors in current applications. This is due to their many advantages including high efficiency, compactness, fast dynamics and high torque to inertia ratio [1]. The PMSM is a nonlinear, multi variable and high coupling system. It has the complication in output torque and stator current function relation. To get good control performance the magnetic field and torque can be decoupled by using vector control, which is also easier to implement [2].

In the indirect torque control scheme, currents are regulated by using PWM or hysteresis controllers, which operate in the rotor reference frame. Before switching the inverter, the modified current errors are transformed to the stator by a dq-1 transformation using measured rotor position from an encoder. Current controllers followed by hysteresis or PWM comparators are not used in DTC systems.

DTC, first proposed for induction motors, can be applied to all AC machine drives. In addition it seems to become an alternative for the classic variable speed AC drives. The basic idea of DTC is to choose the best voltage vector, which makes the flux rotate and produce the desired torque. During this rotation, the

amplitude of the flux rests in a predefined band. Thus it is almost constant. The torque is estimated using measured currents and estimated fluxes. Switching commands of inverter come directly from a look up table.

II PMSM Modelling

The following assumptions will be made for this research:

1. Saturation will be taken into account through parameter changes
2. The machine induced Electro-Motive Force (EMF) is sinusoidal
3. Eddy currents and hysteresis losses are negligible
4. There are no field current dynamics.

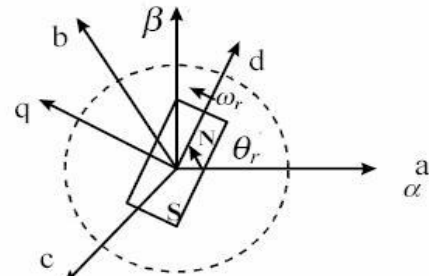


FIGURE 1. PM MACHINE REFERENCE FRAMES.

In Figure 1, the magnetic axes of the three stator windings are labeled a, b and c. From this three dimensional coordinate based system two possible results for the Park transformation are commonly used. The first one is labeled α - β and is attached to the "a" phase axis. The other case, which will be used in the analysis of this research, is attached to the rotating magnetic axis of the rotor, and is usually called the d - q rotor flux reference frame. The machine modeling starts in the "abc" reference frame with the following set of equations.

Voltage equations are given by

$$V_q = R_s i_q + \omega_r \lambda_d + \rho \lambda_q \quad (1)$$

$$V_d = R_s i_d - \omega_r \lambda_q + \rho \lambda_d \quad (2)$$

Flux linkages are given by

$$\lambda_q = L_q i_q \quad (3)$$

$$\lambda_d = L_d i_d + \lambda_f \quad (4)$$

Substituting equations (3) and (4) in (1) and (2)
 $V_d = R_s i_d + \omega_r L_q i_q + \rho(L_d i_d + \lambda_f) \quad (5)$

$$V_q = R_s i_q - \rho L_q i_q + \omega_r (L_d i_d + \lambda_f) \quad (6)$$

Arranging equations (5) and (6) in matrix form

$$\begin{bmatrix} V_q \\ V_d \end{bmatrix} = \begin{bmatrix} R_s + \rho L_q & \omega_r L_d \\ -\omega_r L_q & R_s + \rho L_d \end{bmatrix} \begin{bmatrix} i_q \\ i_d \end{bmatrix} + \begin{bmatrix} \omega_r \lambda_f \\ \rho \lambda_f \end{bmatrix} \quad (7)$$

The developed motor torque is given by

$$T_e = (3/2)(P/2)(\lambda_d i_q - \lambda_q i_d) \quad (8)$$

The mechanical torque equation is

$$T_e = T_L + B\omega_m + J(d\omega_m/dt) \quad (9)$$

Solving for rotor mechanical speed from equation (9)

$$\omega_m = \int((T_e - T_L - B\omega_m)/J) dt \quad (10)$$

and $\omega_m = \omega_r(2/P)$

In rotor reference frame the torque equation

is modelled as,

$$T = 0.75P(L_d - L_q)I_d I_q + 0.75P(\omega_m I_q) \quad (11)$$

Torque=Reluctance torque + excitation torque

III Direct Torque Control

The working principle for the basic DTC is to select a voltage vector based on the error between requested and actual (sensed and estimated) values of torque and flux, rotor position estimation. DTC has the capability to work without any external measurement sensor for the rotors mechanical position. To satisfy the correct direction of rotation of a PMSM, the rotor position is required at the motor start up. DTC is simple because it does not require any kind of current regulators, rotating reference frame transformation or a PWM generator. The advantages of the DTC is to eliminate the dq-axis current controllers, associated transformation networks, and the rotor position sensor. The disadvantages are low speed torque control difficulty, high torque and current ripple value, variable switching frequency, high noise level in low

speed range. Three signals affect the control action in a DTC system. They are namely.

1. Torque
2. The amplitude of the stator flux linkage
3. Angle of the resultant flux vector (angle between flux vector of stator and rotor)

The estimator obtains the torque and flux signal. Regulation of these two signals is done by the help of two hysteresis controllers. The rotor position estimator

and the hysteresis controller give output signals to the switching table who in turn selects switching of the three inverter legs, and applies a set of voltage vectors across the motor terminals. For counter-clockwise operation, If the sensed torque is lesser than the required the voltage vector which keeps Ψ_s rotation in the same direction as previous is chosen. The moment in which the measured torque is greater than the reference, the voltage vector which keeps Ψ_s rotation in the opposite direction is applied. By selecting the voltage vector in this manner, the stator flux vector is rotated all the times It's rotational direction is obtained by the torque hysteresis controller output. If the estimated flux linkage is lesser than the required value then $\Phi=1$. Same case applies to the torque.

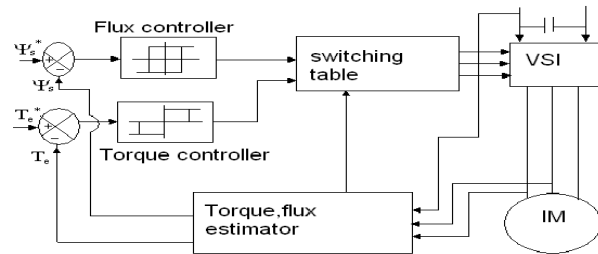


FIGURE 2. SCHEMATIC OF DIRECT TORQUE CONTROL

Torque and flux hysteresis comparators to find out the correct commands for control purpose a flux and a torque hysteresis comparators can be used. The comparators calculate the error between the required values and estimated values, and hence obtain if the flux and torque vector.

TABLE 1 :VECTOR SELECTION TABLE

C_ϕ	C_T	Sector I	Sector II	Sector III
1	1	$V_2(110)$	$V_3(010)$	$V_4(011)$
	0	$V_7(111)$	$V_0(000)$	$V_7(111)$
	-1	$V_6(101)$	$V_1(100)$	$V_2(110)$
0	1	$V_3(010)$	$V_4(011)$	$V_5(001)$
	0	$V_0(000)$	$V_7(111)$	$V_0(000)$
	-1	$V_5(001)$	$V_6(101)$	$V_1(100)$

C_ϕ	C_T	Sector IV	Sector V	Sector VI
1	1	$V_5(001)$	$V_6(101)$	$V_1(100)$
	0	$V_0(000)$	$V_7(111)$	$V_0(000)$
	-1	$V_3(010)$	$V_4(011)$	$V_5(001)$
0	1	$V_6(101)$	$V_1(100)$	$V_2(110)$
	0	$V_7(111)$	$V_0(000)$	$V_7(111)$
	-1	$V_2(110)$	$V_3(010)$	$V_4(011)$

The properties of DTC can be characterized as follows:

- Torque and flux can be changed very fast by changing the references

- High efficiency & low losses - switching losses are minimized because the transistors are switched only when it is needed to keep torque and flux within their hysteresis bands
- The step response has no overshoot
- No coordinate transforms are needed, all calculations are done in stationary coordinate system
- No separate modulator is needed, the hysteresis control defines the switch control signals directly
- There are no PI current controllers. Thus no tuning of the control is required
- The switching frequency of the transistors is not constant. However, by controlling the width of the tolerance bands the average switching frequency can be kept roughly at its reference value. This also keeps the current and torque ripple small. Thus the torque and current ripple are of the same magnitude than with vector controlled drives with the same switching frequency.
- Due to the hysteresis control the switching process is random by nature. Thus there are no peaks in the current spectrum. This further means that the audible noise of the machine is low
- The intermediate DC circuit's voltage variation is automatically taken into account in the algorithm (in voltage integration). Thus no problems exist due to dc voltage ripple (aliasing) or dc voltage transients

IV Simulation Results

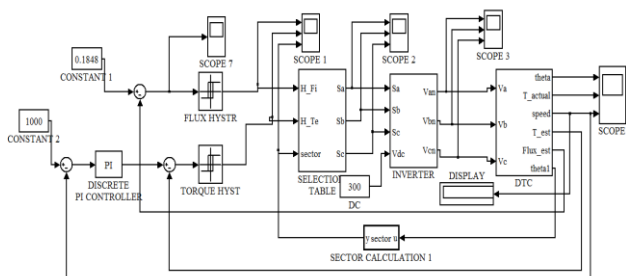


FIGURE 3. SIMULINK MODEL OF DTC CONTROL OF PMSM

Parameter Specification: $K_p = 0.008$; $K_I = 0.1$; $R = 4.765$; $L = 0.014$; $J = 4.4047 \times 10^{-5}$; $B = 0.043$; $\lambda = 0.1848$; $T_L = 0.6$

Speed Waveform

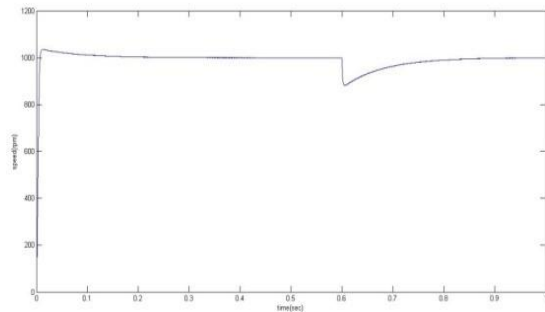


FIGURE 4. SPEED WAVEFORM

Torque Waveform

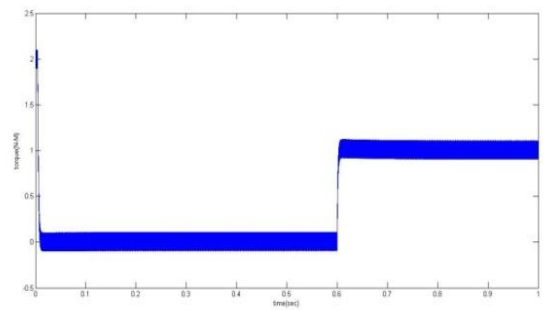


FIGURE 5. TORQUE WAVEFORM

Waveform For Comparison Of Speed Between PI and DTC

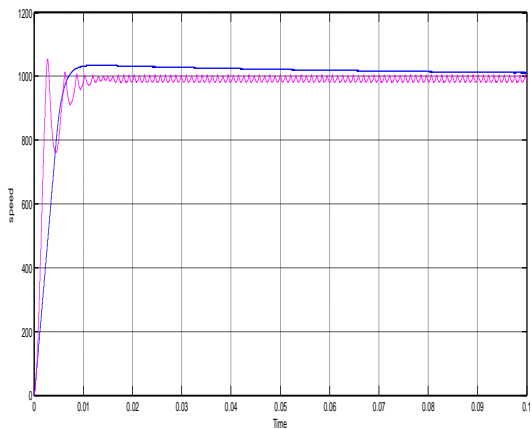


FIGURE 6. COMPARISON WAVEFORM OF SPEED BETWEEN PI AND DTC

It is seen that more ripples are observed when we are using PI controller and the amount of ripple decreases when we go for direct torque control of PMSM. Better dynamic response in torque and speed is observed when we are using DTC control of PMSM.

Waveform For Comparison Of Torque Between PI and DTC

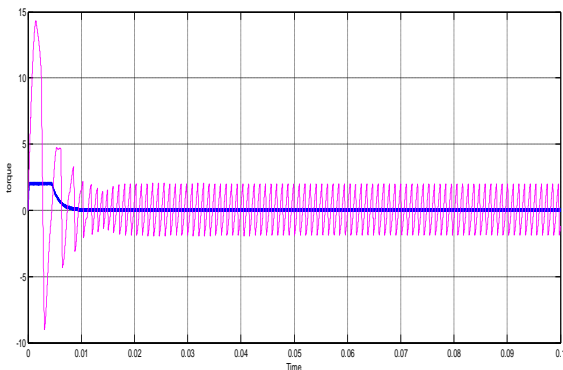


FIGURE 7. COMPARISON WAVEFORM OF TORQUE BETWEEN PI AND DTC

V Conclusion

Motor criteria such as durability, high performance, high power factor, easy and cheap control, low maintenance demands have led to a new type of motor excited by permanent magnets. In this paper, a mathematical model for the Permanent magnet synchronous motor is developed. The direct torque control technique is used to control the PMSM motor. In the performed simulation certain stator flux and torque references are compared to values estimated from the motor parameters and errors are sent to the hysteresis comparators. The outputs of the flux and torque comparators are used to determine the appropriate voltage vector and stator flux space vector. The simulation model is developed in MATLAB/SIMULINK. Performance comparison of proposed DTC with conventional PI is provided which demonstrate better dynamic response in torque and speed over a wide speed range.

References

- [1] Chen Junfeng, Permanent Magnet Motor [M], (Beijing, China achine press, 2002).
- [2] Zhonghui Zhang and Jiao Shu, Matlab Based Permanent Magnet Synchronous Motor Vector Control Simulation, IEEE, 978-1-4244-5540-9/10
- [3] Simon D. Wilson, Paul Stewart *Senior Member IEEE*, and Benjamin P. Taylor.: 'Methods of Resistance Estimation in Permanent Magnet Synchronous Motors for Real-Time Thermal Management'.
- [4] G.Kohlrusz, D.Fodor.: 'Comparison Of Scalar And Vector Control Strategies of Induction Motors' Hungarian Journal of Industrial Chemistry Veszprem, Vol. 39, no.2, pp.265-270, 2011.

- [5] P. Pillay and R. Krishnan, "Modeling of permanent magnet motor drives," *IEEE Trans. Ind. Electron.*, vol. 35, no. 4, pp. 537–541, Nov. 1988.
- [6] P. Pillay, R. Krishnan, "Modeling, Simulation and Analysis of PM Motor Drives, Part I: the Permanent Magnet Synchronous Motor Drive", *IEEE transactions on Industry Applications*, Vol. 25, NO. 2, March/April 1989..
- [7] L. Zhong, M. F. Rahman, "A Direct Torque Controller for Permanent Magnet Synchronous Motor Drives", *IEEE Trans. On Energy Conversion*, Vol. 14, No.3, September, 1999.
- [8] S. Dan, F. Weizhong, H. Yikang, "Study on the Direct Torque Control of Permanent-Magnet Synchronous Motor Drives", Fourth IEEE International Conference on Power electronics and Drive System, October 22-25, Bali, Indonesia, p.571-574.
- [9] L. Zhong, M. F. Rahman, W.Y. Hu, K.W. Lim, "Analysis of Direct Torque Control in Permanent Magnet Synchronous Motor Drive", *IEEE Trans. On Power Electronics*, Vol. 12, No.3, May, 1997.

A STABILITY ANALYSIS FOR GRID CONNECTED WIND FARM WITH BATTERY

Mr. V.AJAY ¹, Mr. P.REYNORD ², Mr. R. SREEKANTH ³

¹v.ajay1994@gmail.com, ²reynord@gmail.com, ³reach.sreekanth@gmail.com

^{1,2}UG Scholar, Department of EEE, St. Joseph's College of Engineering,Chennai-119, India

³ Assistant Professor, Department of EEE, St.Joseph's College of Engineering, Chennai-119,India

Abstract- The fluctuating nature of wind has been a great disadvantage in wind energy. Due to the wind fluctuation caused by the wind its effect on the power system to which it is connected will increase too. Normally, when wind speed is higher than the normal speed the power generation is more and if wind speed is lesser than rated speed power generation is lesser. This implies that power generation will depend on the wind speed. A Doubly-Fed Induction Generator (DFIG) is used which is useful for extracting more power from lower wind speed.

In this paper we deal with the stability problems which is optimized using batteries. When the power generation from the wind farm is more, battery will be an energy storage device and if the demand is more than the generation battery will act as a compensating device. In this operation both rectifier and inverter operation will takes place. The voltage from the battery is free from fluctuations and can be supplied to grid.

Keywords- DFIG, Wind farm, battery unit, inverter, rectifier, grid

I. INTRODUCTION

Electricity has been a great demand and it is essential for the modern world. Non-Renewable energy sources like fossil fuels are depleting by time as the consumption of power increases day by day. So the alternative way for producing energy is the use of renewable energy like solar, wind, hydro and tidal. The renewable sources also have some effects like weather dependence, power fluctuations and stability problems. These problems will have adverse effect on wind energy and in the future the generation from wind energy will have a large penetration in the complete power generation. As the power generation is proportional to wind speed a Doubly fed Induction Generator is used for providing fixed frequency and voltage to synchronize with the grid. The stability problems in the system should be decreased which can be done by a battery for the smoothening the power fluctuations.

The battery is connected to the grid system and if the actual power output (P_{prod}) of the wind farm is higher than calculated demand (P_{calc}), the battery will be charged; on the other hand, if the power output (P_{prod}) is lower than the calculated demand power (P_{calc}), then the battery will be discharged.

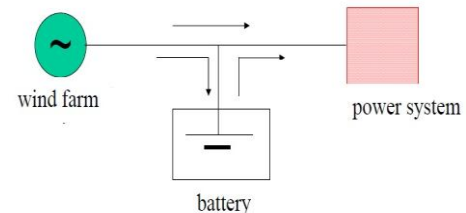


Fig. 1: Wind farm with battery connected to power system
The actual charging state of battery is very important and it is done by a rectifier and discharging of power from battery is done by inverter. The main aim to us battery is to compensate the difference between the calculated and actual wind power feeding into the system and increasing the system performance.

II. DOUBLY FED INDUCTION GENERATOR

Wind Mill converts mechanical energy produced by the turbine to electrical energy as wind turbine is coupled to generator. Wind farm is a collection of wind turbines producing many Mega Watt (MW) of power. Doubly-fed Induction Generator (DFIG) belongs to variable-speed wind turbine. In DFIG the rotation speed of wind turbine rotor varies but it produces constant voltage and frequency.

A. Construction of DFIG

The DFIG is an induction machine with a wound rotor where the rotor and stator are both connected to electrical sources, hence the term 'doubly-fed'. The generator system operates in both a sub-synchronous and super-synchronous mode. The DFIG stator circuit is connected directly to the grid while the rotor winding is connected via slip-rings to a three-phase converter and to the grid. The rotor circuit of two converters one is grid side converter (Cgrid) and other is rotor side converter (Crotor) interconnected by a DC link capacitor.

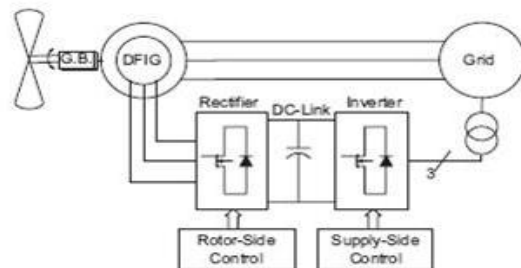


Fig. 2: DFIG construction

The AC currents thus produced by the generator are converted to DC currents by an AC/DC converter (rotor side converter- Crotor), then converted again to AC current by another AC/DC converter (grid side converter-Cgrid) which are synchronous with the AC network. The placement of capacitor as a dc-link for storing energy, in order to keep the voltage variations very small. The rotor side converter (Crotor) is used to control the torque production and powerfactor of the DFIG through direct control of the rotor currents. It will operate at varying frequencies corresponding to the variable rotor speed requirements based on the wind speed. The DC capacitor will store power produced by the rotor side converter and the voltage at the DC terminals will be converted to AC and supplied to grid by grid side converter. This is used to regulate the voltage of the DC link between the two Converters. The back-to-back arrangement of the converters provides fixed voltage and constant frequency by using its mechanism for converting the variable voltage and frequency output of the generator (as its speed changes). The output is compliant with the grid and also power losses in the circuit is reduced.

B.Torque production in DFIG

The DFIG consists of stator windings and rotor windings connected directly to the grid. The stator windings are therefore energized by the grid to create the stator magnetic field. The rotor windings are energized by the converter to establish the rotor magnetic field. Torque is created by the interaction of the rotor magnetic field with the stator magnetic field. The magnitude of the generated torque is dependent on both the strength of the two magnetic fields, and the angular displacement between the two. If the magnetic fields are completely aligned, as in two bar magnets with poles in north and south direction, there is no torque generated. However if the two magnets are placed orthogonal to each other, with the north and south poles displaced perpendicularly, the attraction will be the strongest and thus the generated torque the greatest. The output power of turbine is given by

$$P_m = C_p(\lambda, \beta) (\rho A/2) V_{wind}^3$$

Where, P_m is Mechanical output power of the turbine (W),

C_p is performance coefficient of the turbine,

ρ is the air density (kg/m^3),

A is the turbine swept area (m^2),

V_{wind} is wind speed (m/s),

λ is ratio of tip speed ratio

β is the blade pitch angle (deg).

C.Power flow in DFIG

There are multiple aspects to the power flow to fully grasp the DFIG operation. The basis for injecting or absorbing active power is the varying operation of the DFIG when it goes from sub-synchronous speed to super-synchronous speed. Active power flows as a function of slip. At synchronous speed W_s (when the required rotor speed for a given power level is exactly equal to W_s), the

magnetic field of the rotor rotates at the same speed as the stator magnetic field. The DFIG then essentially operates as a synchronous machine with DC current in the rotor windings, meaning no active power will be generated in the rotor windings and therefore all active power from the DFIG machine will flow from the stator to the grid. When the wind speed increases, the speed of the rotor must change in order to optimize the efficiency of the system and rotor speed increases above synchronous speed, resulting in a negative slip and super-synchronous operation. In this operation, power flows to the grid from both the stator windings and the rotor windings. As the wind speed decreases, rotor speed decreases, and the machine operates in sub-synchronous mode, with a positive slip. Under these circumstances, the rotor must absorb active power from the grid, essentially borrowing power for rotor winding excitation

BATTERY UNIT

The battery unit has been used with wind turbine and the power system for smoothening power output fluctuations from the windfarm at one point common coupling (PCC) and for storing energy. The battery is used for features like

- large power and energy density,
- large power capacity,
- fast access time,
- large efficiency (up to 90%)
- relatively prolonged life time (15 years or 2500 cycles)
- Due to large pulse power factor, they are able to feed higher power than the rated one into the system

If the power produced by means of wind is higher than the demand then the power produced is stored in battery and if power produced is lesser then the stored power is supplied from battery to the grid

A.INVERTER

A device that converts DC power into AC power at desired output voltage and frequency is called an Inverter. In three phase inverters which is used for high power applications consists six semiconductor switches which is given gate pulse by variety of techniques. One of the most commonly used technique is pulse width modulation (PWM). The Sinusoidal pulse width modulation (SPWM) is used. In this method the pulselwidth is varied in proportion to the amplitude of a sine wave ($V_{control}$) evaluated at the centre of the same pulse. The gating signals are generated by comparing a sinusoidal reference signal with a triangular carrier(V_{tri}) wave and the resulting drive signals cause multiple turn-on of the inverter switches in each half-cycle with variable pulse width to produce a quasi-sine wave of load voltage

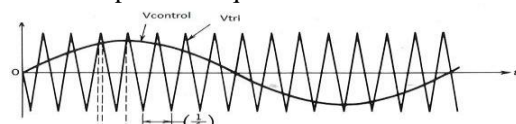


Fig. 3: Sine wave is compared with triangular wave

B.RECTIFIER

Rectifier is used to convert AC voltage to DC voltage. The rectification process is done by constructing it using a universal bridge. Three-phase controlled rectifiers have a wide range of applications, from small use to high voltage direct current (HVDC) transmission systems. The supply

for rectifier will be from grid and it converts the AC to DC to store in the battery .It will take place when the power produced by the wind farm is higher than the demand and the battery will be charged to the rated capacity

III. SIMULATION RESULTS

The DFIG connected with the battery unit is integrated with the power system. Its model constructed in the simulink has shown below

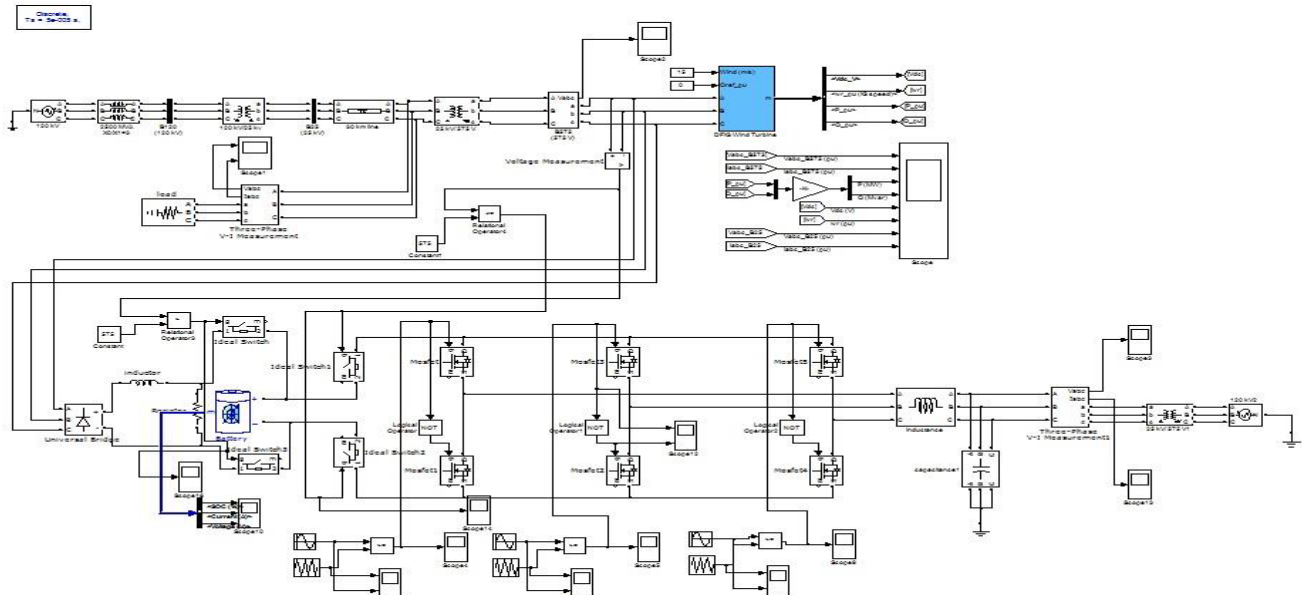


Fig. 4: Integration of grid with windfarm connected with battery unit

The DFIG produces a voltage of 575 V with wind speed constant which is stepped up to 25 KV and transmitted through a transmission line. The 25 KV is again stepped up to 120 KV and then supplied to grid. The simulation results are furnished here.

The voltage characteristics of DFIG during constant and variable speed is presented in below figures.

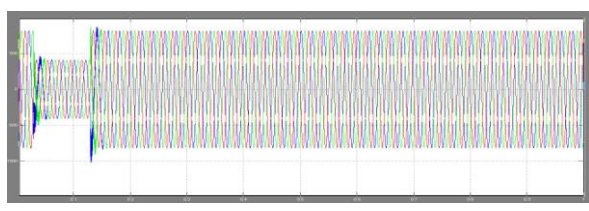


Fig. 4: Voltage characteristics of DFIG during constant speed

The above diagram shows the output if DFIG during constant speed of 15 m/s. The oscillations are present

initially which is smoothened at the end and the upcoming waveform shows voltage characteristics at variable speed.

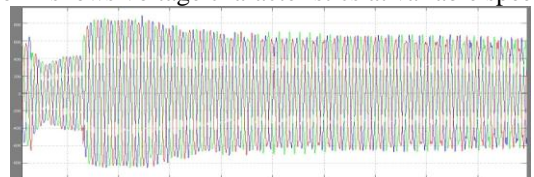


Fig. 5: Voltage characteristics of DFIG during variable speed

The following characteristics shows the inverted voltage waveform from the inverter connected with battery which is supplied to grid when the wind power lesser than the demand.

Fig. 6: Voltage waveform from the battery

This waveform shows that the voltage waveform from the battery which is free from fluctuations. This voltage when supplied to grid improves the system performance.

CONCLUSION

The application of batteries as a backup of a large wind farms can be very interesting from the point of view of power system stability. In the power systems with large wind penetration, where the disconnection of a wind generation can lead to the system instability. The wind turbine (DFIG) connected with the grid has been modelled and battery unit is modelled with an inverter and rectifier. The grid system is integrated with the battery unit and the

voltage waveforms are analysed. The battery act as a power buffer and also act as an energy storage device. The storage of wind energy is also a possible solution for compensating the problems of fluctuation in the power produced by the wind energy due to weather dependency and fluctuating nature. This shows the use of batteries will improve the system performance.

VI. REFERENCES

- 1. ERVIN SPACHIĆ, GERD BALZER and AREFEH DANESH SHAKIB** paper about the “The Impact of the ‘Wind farm-Battery’ Unit on the Power system stability and control”.
- 2. P. Kundur, Power System Stability and Control,** New York: McGraw-Hill, 1994.
- 3. Prof. Dr. MANFRED STIEBLER,** Presented a detailed work on Wind energy system for electrical power generation.
- 4. Ankit Gupta, S.N. Singh, Dheeraj K. Khatod** presented a paper on Modeling and Simulation of Doubly Fed Induction Generator Coupled With Wind Turbine-An Overview.
- 5. MICHAEL A. SNYDER** presented a work on “Development of Simplified Models of Doubly-Fed Induction Generators (DFIG)”.
- 6. Dr. John Fletcher and Jin Yang** presented a work on Introduction to Doubly-Fed Induction Generator for Wind Power Applications.
- 7. A. DaneshShakib, G. Balzer** presented a work on “Optimization of Battery Application for Wind Energy Storage”.
- 8. S. MÜLLER, M. DEICKE, & RIK W.D. DONCKER** presented a work on Doubly Fed Induction Generators.
- 9. T.ACKERMANN (2005),** describes the basics concepts and details of wind power in power systems.
- 10. E. Spahić, G.Balzer, W.Münch and B.Hellmich,** “Wind energy storages - possibilities”, PowerTech 2007, Lausanne, Switzerland, July.
- 11..E. Spahić and G. Balzer,** “The Application of Batteries as a Backup of Large Wind Farms”, which describes about the Large Scale Integration of Wind Power and Transmission Systems for Offshore Wind Farms, Paper No. 43, Delft, The Netherlands, October 2006

A Power Oscillation Damper For Variable Speed Wind Generator

R.Kishore¹,R.Durga Prasad²,Jayarama Pradeep³,R.Sreekanth⁴

¹kishoresubu@gmail.com,²rdp.uniqueone@gmail.com

³jayapradeepkp@gmail.com,⁴reachsreekanth@gmail.com

^{1,2}UG Scholar,Department of EEE, St.Joseph's college of engineering,Chennai-119,India

³Associate Professor,Department of EEE,St.Joseph's college of engineering,Chennai-119,India

⁴Assistant Professor,Department of EEE,St.Joseph's college of engineering,Chennai-119,India

ABSTRACT: A new robust power oscillation damper (POD) design for a doubly fed induction generator based- wind turbine is proposed. The POD structure is specified by the second-order lead/lag compensator with single input signal. The formulation of POD parameters are optimized using mixed H₂/H_∞ control. The POD parameters are optimized by the firefly algorithm and tuning of Lead-Lag compensator

I. INTRODUCTION

The power system oscillation with poor damping is a challenging problem in the power system stability and control. The undamped power oscillation may cause the wide area blackouts and loss of system synchronism. Due to oscillation, the voltage variation is been stabilized by the power system stabilizer (PSS) for a long time. Nevertheless, the PSS may cause the degradation in the quality of voltage control.

On the other hand it is increasingly important that wind generation continue to operate during periods of fault in the grid. The penetration of wind power has reached levels high enough to affect the quality and stability of the grid. According to grid codes issued by utilities, tripping of wind turbines following grid fault is not allowed. To maintain Grid voltage the reactive power supply is a must. Main ancillary services in a power system are power-frequency control and voltage control. These services must be provided by each generator connected to the grid. In order to provide the ancillary service of voltage, generators must have some reactive power capability as required by the corresponding grid codes. Recently, the most widely used variable wind turbine is the Doubly Fed Induction Generator type (DFIG) because it can operate at a wider range of speed depending on the wind speed or other specific operation

so that the damping performance against system disturbances and the robustness under system uncertainties are satisfied.

Keywords—Power oscillation damper, mixed H₂/H_∞ control, doubly fed induction generator, firefly algorithm.

requirements. Thus it allows for a better capture of wind energy, and dynamic slip control and pitch control In addition, to that comparing the results of system stability DFIG's behavior is much better than IG, of its capability of decoupling the control of output active and reactive power.

The power oscillation damping controllers in these works satisfactorily provide the stabilizing effect. Nevertheless, these controllers have been designed at one operating point. Under various operating conditions, parameters variation, several disturbances, and system nonlinearity etc., they may not withstand such system uncertainties and fail to stabilize the system. To overcome this problem, the robust control design of power oscillation damper (POD) of DFIG.

II. General form of generation in a DFIG system

The general scheme of electrical energy's generation from the wind power on the basis of using doubly-fed induction generator is shown in Figure 1. The stator is considered to be connected to the grid directly whereas the rotor is connected to it via back-to-back converter. Rotor side converter is a current regulate-voltage source inverter and grid side converter is a PWM inverter.

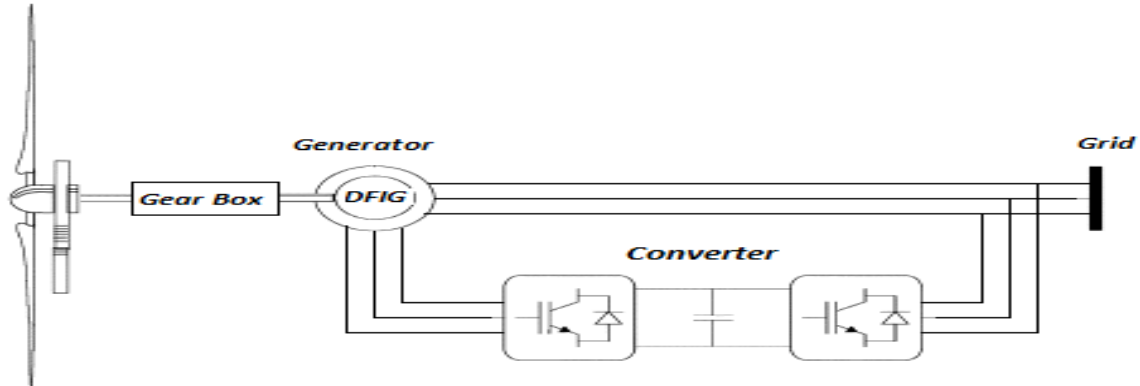


Fig. 1. General form of electrical energy's generation from the wind power on the induction generator

III. Power equations of wind turbine

Amount of power extracted by the wind turbines is as follows:

$$P_m = C_p P_w \quad (1)$$

$$P_w = 1/2\pi\rho R^2 V_w^3$$

Where $m P$ is the mechanical power that is extracted from the wind by the wind turbine, $w P$ is the actual wind power, ρ is the air density, R is the radius of the blades in wind turbine, $w V$ is the wind speed and $p C$ is the efficiency index ($p C$). The efficiency index ($p C$) represents the part of the actual wind energy that is extractable by wind turbine and is depended to the blades is described by

$$C_p = f(\gamma, \beta)$$

$$\gamma = R \frac{\omega_t}{V_w}$$

Where γ is the ratio of turbine blades tip speed to wind speed, β is the blade angle and is the turbine blades rotational speed. In wind turbine simulation, generation torque is represented by

$$T_a = \frac{P_m}{\omega_t} = \frac{1}{2} \frac{\rho\pi R^2 C_p V_w^3}{\omega_t}$$

Where $a T$ is the torque in turbine shaft

IV. Machine equation

The equations of induction machines in the dq reference frame, with the speed 'ω' of and neglecting zero parameter is given by

$$V_{ds} = R_s i_{ds} - \omega \varphi_{qs} + \frac{d\varphi_{ds}}{dt}$$

$$V_{qs} = R_s i_{qs} + \omega \varphi_{ds} + \frac{d\varphi_{qs}}{dt}$$

$$V_{dr} = R_r i_{dr} - (\omega - \omega_r) \varphi_{qr} + \frac{d\varphi_{dr}}{dt}$$

$$V_{qr} = R_r i_{qr} - (\omega - \omega_r) \varphi_{dr} + \frac{d\varphi_{qr}}{dt}$$

Where V_{ds} and V_{qs} are the d- and q-axis stator voltages, V_{dr} and V_{qr} are the d- and q-axis rotor voltages, i_{ds} and i_{qs} are the d-and q-axis stator currents, and i_{dr} and i_{qr} are the d- and q-axis rotor currents. R_s and R_r are the per-phase stator and rotor resistances referred to the stator, ψ_{ds} and ψ_{qs} are the d- and q-axis stator flux linkages ,and ψ_{dr} and ψ_{qr} are the d- and q-axis rotor flux linkages. ω is the speed of rotation of the dq frame, and ω_r is the rotor electrical angular velocity. . The developed electromagnetic torque T is given by:

$$T_{em} = \frac{3P}{4} (i_{qs}\varphi_{ds} - i_{ds}\varphi_{qs})$$

The equation relating the speed of rotation and applied mechanical torque is given by

$$J \frac{d\omega_m}{dt} = T_{mech} + T_{em}$$

Where 'J' is the polar moment of inertia of the machine and prime mover referred to the induction machine shaft.

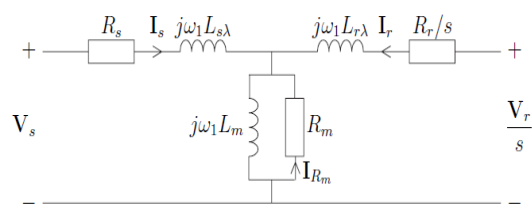


Fig. 2: Equivalent circuit of the DFIG.

V. Dc link model

The energy, W_{dc} , stored in the dc-link capacitor, C_{dc} , is given by

$$W_{dc} = \left(\frac{1}{2}\right)C_{dc}V_{dc}^2$$

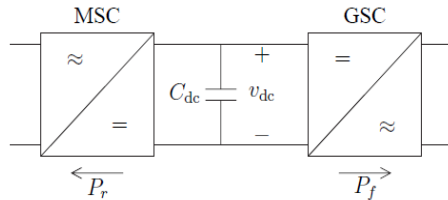


Fig. 3: DC-link model

Where V_{dc} is the dc-link voltage. In Fig. 16 an equivalent circuit of the dc-link model, where the definition of the power flow through the grid-sideconverter (GSC) and the machine side converter (MSC) is shown. Moreover, if the losses in the actual converter can be considered small and thereby be neglected, the energy in the dc-link capacitor is dependent on the power delivered to the grid filter, P_f , and the power delivered to the rotor circuit of the DFIG is

$$\frac{dW_{dc}}{dt} = \left(\frac{1}{2}\right)C_{dc}\frac{dV_{dc}^2}{dt} = -P_f - P_r$$

The dc-link voltage will vary as

$$C_{dc}\frac{dV_{dc}}{dt} = -P_f - P_r$$

Means that $P_f = -P_r$ for a constant dc-link voltage.

VI. Proposed system

i. POD model

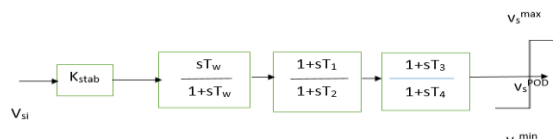


Fig.4. Structure of POD

The linearized state equation is used to represent the system model. The structure of the POD equipped with DFIG is a second-order lead/lag compensator as depicted in Fig. 6. The POD consists of a stabilizer gain K_{stab} , a washout filter with time constant $T_w=10$ s, and two phase compensator blocks with time constant T_1 , T_2 , T_3 and T_4 . V_s^{\min} and V_s^{\max} are minimum and maximum output signal V_s^{POD} . The washout signal ensures that the POD output is zero in the steady-state. The input signal V_{si} is the active power

flow in the transmission line between bus 2 and bus 3. The output signal V_s^{POD} is subjected to an anti-windup limiter. The gain determines the amount of damping introduced by the POD while the phase compensator block provides the appropriate lead/lag compensation of the input signal.

ii. System model

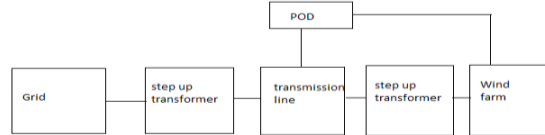


Fig.5. Block diagram of wind farm connected to Grid

Circuit description:

The wind farm consists of totally 6 wind mills each of generating capacity 1.5MW, 575V with initial frequency of 60 Hz (assumption case). The output of the wind farm is been stepped-up to 11KV and it is transmitted through a transmission line of Distributed parameters, because in case of lumped parameters the magnetization inductance effect is higher (30Km). Later the transmitted voltage is been stepped up further for a voltage of 120 KV for synchronizing of the Grid parameters (Phase, Voltage and Frequency), thus it is connected to the grid.

The POD is connected transmission line and voltage is taken as the reference for damping of oscillation then the stabilized voltage is been given to the PLL circuit (Phase Locked loop) or the Qref circuit. Thus the Qref calculated is taken as the controlling parameter for damping out oscillation in the real power (P) from output of DFIG.

As already the parameters are optimized using the firefly algorithm or it can be tuned using trial and error method for stabilization of the voltage and the real power. The results are published below:

VII. Simulation results

The above system is debugged and compiled in Matlab 7.10.0(R2010a) software

Without POD:

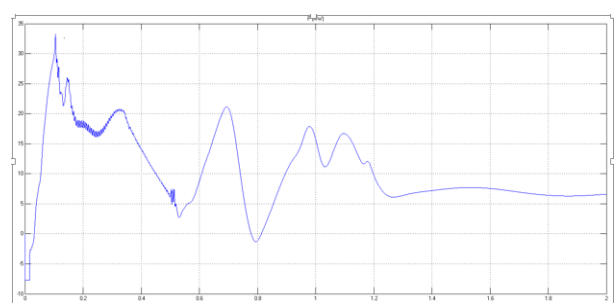


Fig.6. Active power from wind farm without POD

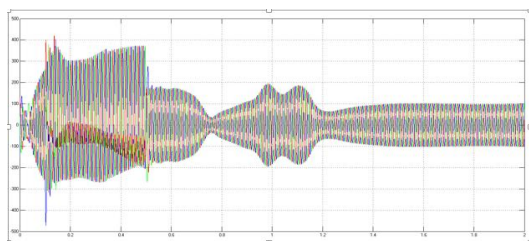


Fig.7. Current from wind farm without POD
With POD

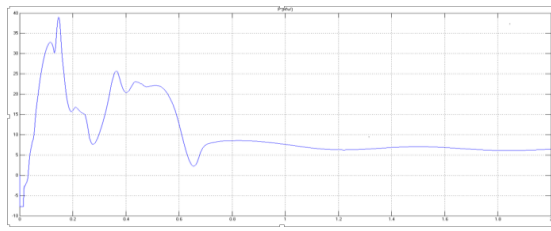


Fig.8. Active power from wind farm With POD

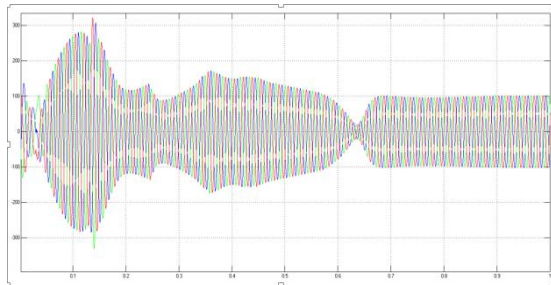


Fig.9. Current from wind farm with POD

DC Link Voltage in both the cases

The above results are generated by developing Harmonics in the Grid side. The values of the Harmonics are

Parameters	Values
Amplitude	A: -2 pu B: 8 pu
Order	A: 2 B: 2
Phase	A: 0 (deg) B: 30(deg)
Sequence	A: Negative B: Negative

The main advantage of POD over the Power system stabilizer is the power system stabilizer stabilizes the voltage but does not damp out harmonics the below result proves it

VIII. Comparative result:

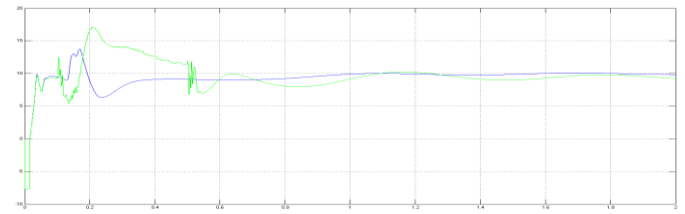
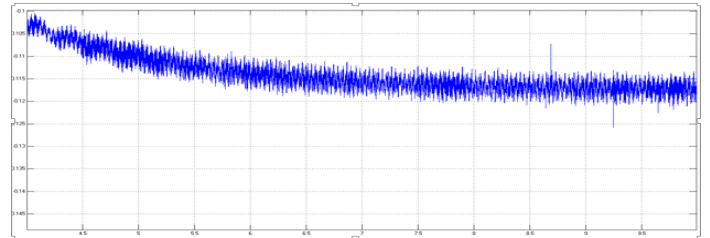


Fig.10. Comparative Power output from wind farm with and without POD

Fig.6 depicts the power of existing system without Power oscillation damper, from this graph it shows that the settling time of power in existing system takes a long time to settle approximately at 1.35s. In Fig.8 the power in the same existing system is settled faster at 0.6s using the power oscillation damper. The comparison of power for both the system is shown in the Fig.10, similarly the current variation in both the system is also shown. It shows the DC link voltage between the grid side converter and the rotor side converter, it has to be maintained at a constant value so that the power flow between the grid and the rotor will be smooth and free from both harmonics & ripples.

IX. Optimization Technique

Firefly algorithm

The firefly algorithm is a high level algorithm used for generate, find or select a lower level application inspired by the flashing behavior of fireflies. The primary purpose for a firefly's flash is to act as a signal system to attract other fireflies. The FA algorithm is explained as follow:

- 1) Generate initial population of fireflies with random positions and light intensity.
- 2) Evaluate the objective function in for each firefly and check constrain in .
- 3) Ranking the fireflies by their light intensity.
- 4) Move all fireflies toward brighter ones x_i .
- 5) When the maximum number of iterations is arrived, stop the process.
- 6) Otherwise go to process 2.

$$x_i = x_i \beta_0 e^{-\gamma r_{ij}^2} (x_j + x_i) + \alpha (\text{rand} - 0.5)$$

Where α is the randomization parameter, rand is the random number in (0, 1), β_0 is the attractiveness at $r=0$, r is distance between any two fireflies i and j at x_i and x_j , and γ is light absorption coefficient.

X. Conclusion

A new robust POD design with specified structure based on a mixed $H2/H\infty$ control for DFIG-based wind turbine is been proposed in this paper. The POD with the structure of second-order lead/lag compensator with single input signal is very practical for actual system. The optimization of POD parameters is carried out so that the high stabilizing performance and robustness can be achieved. Solving the optimization problem by FA, the controller parameters of POD are automatically obtained. Simulation results in a single machine infinite bus will confirm the proposed POD is robust than the conventional POD under various heavy power flows, severe faults, wind speeds, and patterns of wind.

References

1. P. Kundur, *Power system stability and control*, McGraw-Hill, 1994.
2. MUHAMMAD H. RASHID, *Power Electronics Handbook*.
3. M. Grant and S. Boyd, "CVX: Matlab software for disciplined convex programming, version 1.21," <http://cvxr.com/cvx>, Feb.2011.
4. S.Muller, M.Deicke and Rik.W De Doncker, *Doubly fed Induction Generator system for Wind Turbine*.
5. F. M. Hughes, O. A-Lara, N. Jenkins, and G. Strbac, "A power system stabilizes for DFIG-based wind generation", *IEEE Trans. Power Systems*.
6. A.H.M.A. Rahim, and I.O. Habiballah, "DFIG rotor voltage control for system dynamic performance enhancement", *Electric Power System Research*.
7. F. Milano. *Power system analysis toolbox (PSAT)*, Documentation for PSAT version 2.1.6.
8. H. Bevrani, and T. Hiyama "Robust decentralized PI based LFC design for time delay power system", *Energy conversion and Management* Ekanayake, J. and Jenkins, N. (2004).
9. Comparison of the response of doubly fed and fixed-speed induction generator wind turbines to changes in network frequency.
10. Pena, R.; Clare, J.C. & Asher, G.M. (1996). Doubly fed induction generator using back-to-back PWM converters and its application to variable-speed wind energy generation,

DYNAMIC MATHEMATICAL MODELLING OF PMSM AND PARAMETRIC SENSITIVITY ANALYSIS USING VECTOR CONTROL

Snekha. E
 2nd year PG scholar/Department of EEE
 St. Joseph's College of Engineering
Snekha27@gmail.com

Mrs.Jayarama Pradeep
 Associate professor/ Department of EEE
 St. Joseph's College of Engineering
jaya_7pradeep@yahoo.co.in

Abstract - This paper deals with the comparison of PI controlled PMSM and fuzzy-PI controlled PMSM system. The PMSM servo system is a nonlinear time-varying complex system. The controller is used as the speed controller in PMSM control system, which can adjust the controller parameters according to the speed error and the derivative of speed error change. The simulation model of PMSM control system is established using Matlab/Simulink toolbox, Based on the rotor field oriented control of permanent magnet synchronous motor. The results of traditional PI control are not satisfactory to the higher degree of accuracy condition. But the fuzzy control system has the major advantage in complex, time lag, time varying and non-linear system control. The fuzzy-PI controller has the advantages of both PI control and fuzzy control, so it can get better control performance. The simulation results show that, the system can run smoothly and the fuzzy-PI controller have less regulating time and it is stronger, robust compared to the traditional PI controller.

Keywords- Permanent Magnet Synchronous Machine, Vector Control, PI Controller, fuzzy-PI controller.

I. INTRODUCTION

In the vector-controlled permanent magnet synchronous motor (PMSM) drive, the outer speed loop provides the reference value of the current for the inner current loop and any disturbance in the speed controller output would cause erroneous currents, thus degrading the system performance. Hence, proper operation of the speed controller is of great importance for the appropriate drive performance. The use of proportional plus integral (PI) controller suffers from performance degradation under system disturbances due to the fixed proportional gain and integral time constant [1],[2]. This problem can be overcome with fuzzy logic controller (FLC) [2], [3]. An FLC is free from mathematical modeling and is based on the linguistic rules formed from the experience with the system [3]. But as compared to the PI controller, the FLC involves approximations, increased complexity, more computations and higher memory

requirements. The performance of the FLC is superior only under transient conditions while the performance of the PI controller is superior under the steady-state condition[4]. Gain scheduled PI speed controllers have been reported but suffer from the need of apt selection of the limits for controller gains and the rate at which they would change [5].

This paper deals with the comparative analysis between the performance of PI and Fuzzy-PI based PMSM system. Simulation is carried out using MATLAB/Simulink toolbox to demonstrate the better dynamic response in torque and speed proposed drive over a wide speed range for different values of parameters.

II. MODELLING OF PMSM

The following assumptions will be made for this research:

1. Saturation will be taken into account through parameter changes
2. The machine induced Electro-Motive Force (EMF) is sinusoidal
3. Eddy currents and hysteresis losses are negligible
4. There are no field current dynamics.

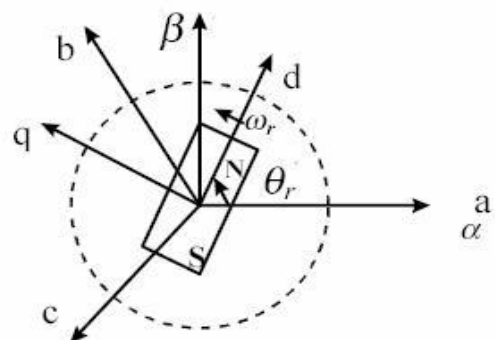


Figure 1. PM machine reference frames.

In Figure 1, the magnetic axes of the three stator windings are labeled a, b and c. From this three dimensional coordinate based system two possible results for the Park transformation are commonly used. The first one is labeled α - β and is attached to the "a" phase axis. The other case, which will be used in the analysis of this research, is attached to the rotating magnetic axis of the rotor, and is usually called the d - q rotor flux reference frame. The machine modeling starts in the "abc" reference frame with the following set of equation

Voltage equations are given by

$$V_q = R_s i_q + \omega_r \lambda_d + \rho \lambda_q \quad (1)$$

$$V_d = R_s i_d - \omega_r \lambda_q + \rho \lambda_d \quad (2)$$

Flux linkages are given by

$$\lambda_q = L_q i_q \quad (3)$$

$$\lambda_d = L_d i_d + \lambda_f \quad (4)$$

Substituting equations (3) and (4) in (1) and (2)

$$V_d = R_s i_d + \omega_r L_q i_q + \rho (L_d i_d + \lambda_f) \quad (5)$$

$$V_q = R_s i_q - \rho L_q i_q + \omega_r (L_d i_d + \lambda_f) \quad (6)$$

Arranging equations (5) and (6) in matrix form

$$\begin{bmatrix} V_q \\ V_d \end{bmatrix} = \begin{bmatrix} R_s + \rho L_a & \omega_r L_d \\ -\omega_r L_a & R_s + \rho L_d \end{bmatrix} \begin{bmatrix} i_q \\ i_d \end{bmatrix} + \begin{bmatrix} \omega_r \lambda_f \\ \rho \lambda_f \end{bmatrix} \quad (7)$$

The developed motor torque is given by

$$T_e = (3/2)(P/2)(\lambda_d i_q - \lambda_q i_d) \quad (8)$$

The mechanical torque equation is

$$T_e = T_L + B\omega_m + J(d\omega_m/dt) \quad (9)$$

Solving for rotor mechanical speed from equation (9)

$$\omega_m = \int((T_e - T_L - B\omega_m)/J) dt \quad (10)$$

and $\omega_m = \omega_r(2/P)$

In rotor reference frame the torque equation

is modelled as,

$$T = 0.75P(L_d - L_q)I_d I_q + 0.75P(\omega_m I_q) \quad (11)$$

Torque = reluctance torque + excitation torque

Torque is related to d axis and q axis currents, since $L_d \leq L_q$. For surface mounted $L_d = L_q$. Second term contributes to negative torque if flux weakening control is used.

III. PROPOSED SYSTEM

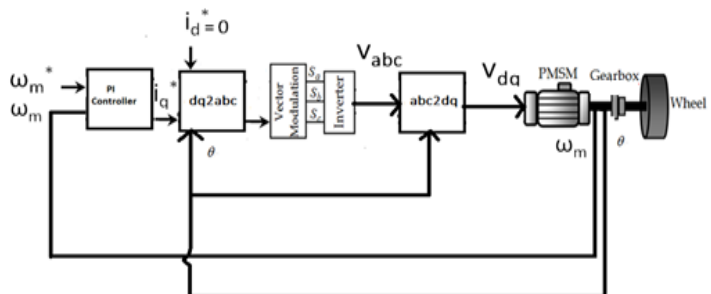


Figure 2. Proposed Block Diagram with PI

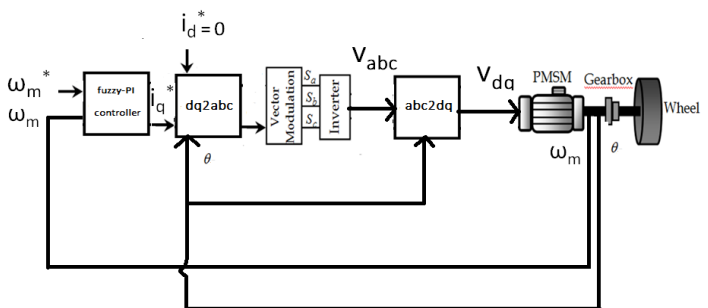


Figure 3. Proposed Block Diagram with Fuzzy-PI

In the proposed system, the PMSM machine is mathematically modeled and the speed feedback is taken. The original speed is compared with the reference speed and the speed error is fed to the PI controller/ Fuzzy-PI controller for generating proper q-axis reference current. The d-axis reference current is set to zero. Then dq to abc transformation is done to generate switching signals for voltage source inverter. Again the output of VSI is converted to dq reference frame to feed PMSM. Thus the PMSM is vector controlled. The comparative analysis is made between the performance of PI and Fuzzy-PI based PMSM system.

TABLE II

RULE TABLE FOR FUZZY SYSTEM

DUTY	CYCLE	CHANGE IN SPEED ERROR						
		NB	NM	NS	Z	PS	PM	PB
SPEED ERROR	NB	NB	NB	NB	NB	NM	NS	Z
	NM	NB	NB	NB	NM	NS	Z	PS
	NS	NB	NB	NM	NS	Z	PS	PM
	Z	NB	NM	NS	Z	PS	PM	PB
	PS	NM	NS	Z	PS	PM	PB	PB
	PM	NS	Z	PS	PM	PB	PB	PB
	PB	Z	PS	PM	PB	PB	PB	PB

IV. SIMULATION BLOCK AND RESULTS FOR VECTOR CONTROL OF PMSM

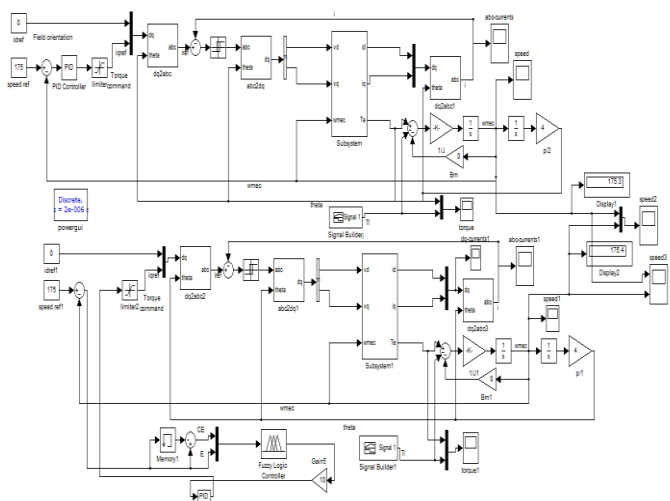


Figure 4. Simulation Block For Vector Control Of PMSM With PI and Fuzzy-PI Controllers.

CASE I : The simulation result at No-Load Condition with controller gains KP =1.0, KI = 0.5.

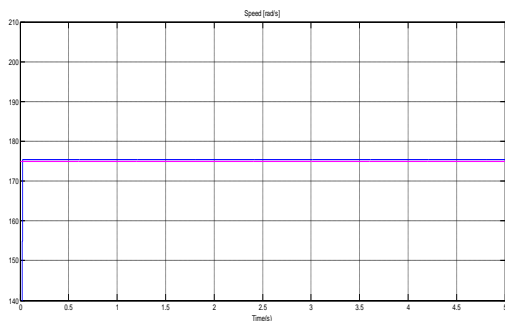


Figure 5. Speed curve of fuzzy-PI system at no load

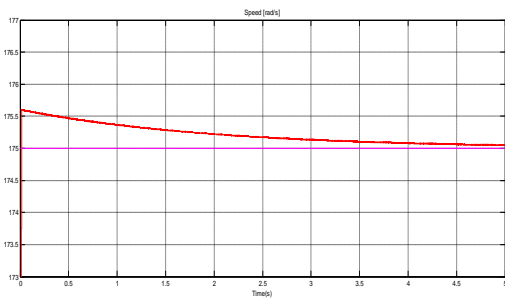


Figure 6. Speed curve of PI system at no load

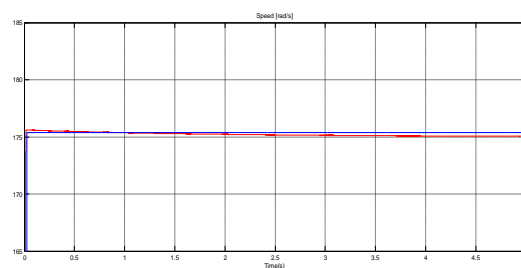


Figure 7. Comparison of speed curves between fuzzy-PI and PI system at no load

Figure 5,6 shows that, at no load condition, the overshoot will occur in PI controlled system, but overshoot is reduced in Fuzzy-PI controlled system.

CASE II: The simulation result when sudden change in load is applied from no-load to 1.5 Nm load at 0.5 sec, at this point wave form is distorted or there is a fluctuation in speed for a few second

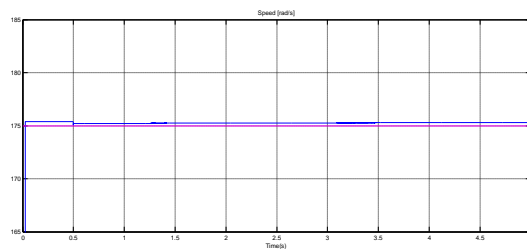


Figure 8. Speed curve of fuzzy-PI system at load condition

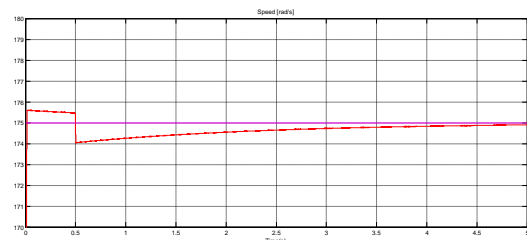


Figure 9. Speed curve of PI system at load condition

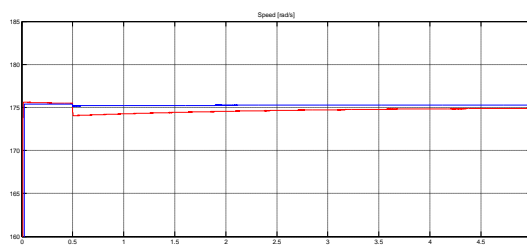


Figure 10. Comparison of speed curves between fuzzy-PI and PI system at load condition

Figure 10 shows that, In PI system, after the disturbance the speed is regained at time 5sec, but in Fuzzy-PI system there is no such big fluctuation in speed after the disturbance at 0.5 sec. It tends to remain stable near the reference speed of 175 rad/s. This is the major advantage of Fuzzy-PI controller.

TABLE III
PARAMETER SPECIFICATION

Armature resistance, R_a	2.875 ohms
d axis inductance, L_d	8.5Mh
q axis inductance, L_q	8.5Mh
Moment of inertia, J	$8 * 10^{-4}$ J/m ³
Flux density, B	0 wb/m ²
Number of poles, p	8
P gain, k_p	1
I gain, k_i	0.5
Rated power , P	1.1KW
Rated voltage, V	220V
Rated speed, ω_m	3000rpm
Reference speed	175rads/s

V.CONCLUSION

The PMSM is a nonlinear, multi variable and high coupling system. Here comparative analysis is made between the performance of PI and Fuzzy-PI based PMSM system. The PI and Fuzzy-PI controllers are used as the speed controller in PMSM control system, which can adjust the controller parameters according to the speed error. The vector control system has the prominent advantage in complex, time lag, time varying and non-linear system control. Based on the vector control of PMSM, the simulation model of PMSM control system is established using Simulink toolbox of Matlab. Reference speed is set, and load disturbance is given in both pi and fuzzy-pi based PMSM circuit. After the disturbance, the speed in PI based PMSM drops initially then tends to attain reference speed. There is no such drastic change of speed in fuzzy-PI based PMSM. The speed remains stable, which is the advantage of fuzzy-PI based PMSM circuit.

REFERENCES

- [1] B.K.Bose, Modern Power Electronics And AC Drives. Upper Saddle River, Nj: Prentice-Hall, 2002.
- [2] Amit Vilas Sant , K. R. Rajagopal , and Nimit K. Sheth, "Permanent Magnet Synchronous Motor Drive Using Hybrid PI Speed Controller With Inherent and Noninherent Switching Functions, " IEEE Transactions On Magnetics, Vol. 47, No. 10, October 2011.
- [3] M. N. Proc. 1999 Uddin and M. A. Rahman, "Fuzzy logic based speed control of an IPM synchronous motor drive," in *IEEE Can. Conf.Electr. Comput. Eng.*, May 9–12, 1999, pp. 1259–1264.
- [4] A. V. Sant and K. R. Rajagopal, "PM synchronous motor speed control using hybrid fuzzy PI with novel switching functions," *IEEE Trans. Mag.*, vol. 45, no. 10, pp. 4672–4675, Oct. 2009.
- [5] S. R. Panda, J. Lim, P. K. Bash, and K. S. Lock, "Gain scheduled PI speed controller for PMSM drive," in *Proc. 23rd Int. Conf. Ind. Electron.,Control Instrum.*, 1997, pp. 925–931.
- [6] Madhumita Chakraborty, Comparative Analysis of Speed Control of PMSM using PI-Controller and Fuzzy Controller, in International Journal of Scientific & Engineering Research, Volume 4, Issue 7, July-2013 103 ISSN 2229-5518

A Probability Based Approach for Unit Commitment and Economic Dispatch in Powered Microgrids

P.SHARLY SOPHIA , R.SREEKANTH M.E.,

Abstract: This paper is based on the cost –benefit analysis for optimal sizing of an energy storage system in a microgrid. Microgrid are entities that coordinates DERs(Distributed Energy Resources)in a consistently more decentralized way, thereby reducing the control burden on the grid and permitting them to provide their full benefits. The objective function is to minimize the overall cost of fuel cost ,which is used to determine the least cost unit commitment problem and the associated dispatch, while meeting the load ,environmental and system requirements is considered. A probability based concept is introduced the probability that microgrid is capable of meeting the local demand in self-sufficient manner. The main problem is formulated as a mixed integer UC problem, which is used to solve in analytical closed forms. Microgrid is the solution to fulfill the commitment of reliable power delivery for future power delivery for future power systems. The cost associated with DG energy production and start up and shut down decisions, along with possible profits.

Index terms: Distributed generators, probability of self-sufficiency, economic dispatch, renewable energy resources, unit commitment (UC).

I.INTRODUCTION

Today's electrical infrastructure has remain unchanged for about some years. Economic, technology and environmental incentives are changing the features of electricity generation and transmission. Centralized power systems are giving way to local scale distributed generations. At present, there is a need to assess the effects of large scale numbers of distributed generators and short-term storage microgrid.

Due to this combination of conventional and renewable sources, the unit commitment becomes more crucial and more complicated in the management of a microgrid. Microgrid is a low voltage intelligent distribution networks comprising various distributed generators, storage devices and controllable loads which can be operated as interconnected or as islanded system. A *microgrid* is an integrated system consists of a set of distributed generators(DGs), wind turbines(WT), microturbine (MT),fuel cells(FC), which functions cooperatively to furnish the cooperation in parallel with, autonomously of, the traditional electricity microgrid.

The operation of a microgrid involves finding the least cost dispatch of the DGs that reduces the total operating cost, while meeting the electrical load and satisfying various technical, environmental and operating constraints. The unit commitment problem in a power system involves determining the start-up and shut down costs, which is used to meet forecasted demand over a future short term period. The special features of microgrids introduce further restrictions as well as simplifications to the optimization task that needs to be addressed. This optimization technique is developed for the considered short-term DER scheduling problem. The objective function is to minimize operational costs while satisfying the microgrid load demand. All the DER and energy-storage units must be operated within their lower and upper output limits. The output of the power optimization technique considers the operation limits of the supply options, load demand, sell/purchase power costs from the connected grid, and the operating costs, total fuel costs of the DERs.

Unit commitment

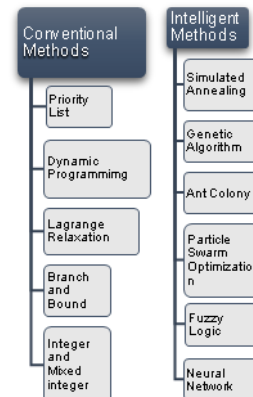


Fig.1 Conventional and intelligent methods

Therefore, the main objective function becomes minimizing fuel costs represented by the difference between the profit and the cost. The fundamental constraints of economic dispatch problem are the load demand and spinning reserve capacity. Additionally, some practical operation constraints of generators, i.e. ramp rate limits are taken into consideration. In the scheduling period, the problem is formulated as a mixed-integer optimization nonlinear programming problem is solved by a Lagrange optimization. To solve the

microgrid DER scheduling problem, a solution algorithm is proposed and implemented under MATLAB Graphically represented. Results are then presented to show the usefulness of the proposed algorithm. Micro-grid system is currently a conceptual solution to fulfill the reliable power delivery for future power systems. Renewable power sources such as wind and fuel cell, microturbine offer the best potential for emission free power for future micro-grid systems.

II.PROBLEM FORMULATION

Objective function of UC is to minimize the total cost of the units in the grid.

$$TC = \sum_{t=1}^T \sum_{i=1}^N u_{i,t} (FC_{i,t} + MC_{i,t} + STC_{i,t}) \quad (2.1)$$

where,

i = unit,

t = time interval,

u_i = unit status indicator of a unit where 1 means ON and 0 means OFF

TC = total cost of all units,

FC = fuel cost function of a unit,

MC = maintenance cost function of a unit,

STC = start - up cost function of a unit

A.Model of Forecasted Wind Power

Wind power is the electrical power generated by wind turbine, the actual power p_w almost depends on the wind speed v_w when other limitations are fixed or changed slowly. In principle v_w is a random variable and varies continuously over time. To find the relationship between the wind speeds and wind power the following linear model is adopted:

$$p_w = \begin{cases} w_r & v_r \leq v \leq v_{out} \\ \frac{(v - v_{in})w_r}{v_r - v_{in}} & v_{in} \leq v \leq v_r \\ 0 & \text{else} \end{cases} \quad (2.2)$$

B.Costs for MT and FC

The operating cost of an FC and MT includes the fuel cost, maintenance cost, and start cost,

Fuel costs: The fuel cost of DGs are considered of unit i in time interval t can be expressed as,

$$FC_{i,t}(p_{i,t}) = a_i p_{i,t}^2 + b_i p_{i,t} + c_i \quad (2.3)$$

Maintenance costs: The maintenance costs for DGs are based on forecasts with real-time situations, which is assumed to be proportional to the produced power. The maintenance costs of unit i in time interval t is,

$$MC_{i,t}(p_{i,t}) = d_i p_{i,t} \quad (2.4)$$

Start-up costs: The generator start -up costs depends upon the time the unit has been off prior to a start-up costs of unit i in time interval t can be exponential cost curve can be expressed as,

$$STC_{i,t} = (HSC_i + CSC_i [1 - \exp(-\frac{TD_{i,t}}{\rho_i})]) \cdot (1 - u_{i,t} - 1) \quad (2.5)$$

The total cost per day,

$$TC = \sum_{t=1}^T \sum_{i=1}^N u_{i,t} (FC_{i,t} + MC_{i,t} + STC_{i,t}) \quad (2.6)$$

C. Energy storage system

The problem of mitigating power intermittences and load mismatches is an important task in renewable powered microgrids is a challenging task. When there is peak demand, the forecasted wind power is smaller than the actual value,(i.e. underestimate),the supplied power is likely to be larger than the actual electricity demand, in that case the ESS will be functioning in charging state to store more power in electrical or renewable energy, which can be dispatched later in the power shortage.

The charge and discharge limits, c_{\min} and c_{\max} , it specify the minimum and maximum energy storage in the better bank. In this work, the starting and ending limits are both are selected as c_{\min} for the purpose of energy balance of the ESS.

D. Unit and operation constraints

Maximum and minimum output limits: The output power of the DGs in stable operation is given by upper and lower limits as follows:

$$p_i^{\min} \leq p_{i,t} \leq p_i^{\max} \quad (2.7)$$

Minimum up/down time :Once a DG is switched ON it operate continuously for some number of times before it can be switched OFF ,also certain number of hours should have to pass before DG is in online after being switched OFF. Mathematically we have,

$$(TU_{i,t-1} - MUT_i)(u_{i,t-1} - u_{i,t}) \geq 0 \quad (2.8)$$

$$(TU_{i,t-1} - MUT_i)(u_{i,t} - u_{i,t-1}) \geq 0$$

Ramp Rates: Thermal units are often subjected to ramp rate limits that specify the amount of unit generation which can increase or decrease during one scheduling period. In microgrids, small DGs units ramp rate up from 0 to full load in order of several minutes.

Emission Limits: To reduce the greenhouse gas footprint, we impose hourly emission limits on all the DGs, It is expressed as,

$$\sum_{i=1}^N u_{i,t} E_{i,t}(p_{i,t}) \leq \zeta \quad (2.9)$$

Operating Reserves: In the event of a power supply disruption operating reserve constraints that generate more power to the system which brings online immediately (spinning reserve) or within a short interval (supplementary reserves) .In microgrid the DGs operating reserves are expressed as follows,

$$\sum_{i=1}^N (p_i^{\max} - u_{i,t} p_{i,t}) \geq R_t \quad (2.10)$$

Probability of self-sufficiency: When microgrid cannot meet the power demand based on the local generating units, it can switch to grid-connected mode and purchase energy from upstream macro grid, for better understandings the impacts of operational mode on total operating cost, we propose the use of probability-based concept, which indicates that target probability that when microgrid is isolated without purchasing energy from the microgrid. As we assume that both demand forecast error Δ_d and Δ_w wind power error can be modeled as independent distributed random variables. The power balance constraint can be expressed as

$$p(\sum_{i=1}^N p_{i,t} u_{i,t} + p_{w,t} + \Delta_w \geq D_t + \Delta_d) \geq PSS \quad (2.11)$$

III .WIND MODEL

Wind energy converters wind power to electrical power. Typical systems range from 30 kW to 1.5 MW for wind farms of multiple units. Hub-heights are around 80 meters, and rotor diameters are 65 m. Rotor construction is either variable (pitch regulation) or non-variable, conversion from power flows in one direction feeding grid towards the load.

3.1 MODELLING OF WIND TURBINE

The wind turbine is characterized by non-dimensional curves of the power coefficient C_p , as a function of both tip speed ratio e , and the blade pitch angle, ϵ . The tip speed ratio e is the ratio of linear speed at the tip of blades to the speed of the wind. It can be expressed as follows

$$\lambda = \frac{\Omega R}{V_w} \quad (3.1)$$

Where R is the wind-turbine rotor radius, Ω mechanical angular velocity of the Wind-turbine rotor and V_w is the wind velocity. For the wind turbine used in the study, the following form approximates C_p as a function of e and ϵ

$$C_p = (0.44 - 0.0167\beta) \sin[\frac{\pi(\lambda-3)}{15-0.3\beta}] - 0.00184(\lambda-3)\beta \quad (3.2)$$

Where ρ is the air density and A is the swept area by the blades.

$$T_m = \frac{1}{2} \rho A C_p V_w^2 w / \lambda \quad (3.3)$$

IV.SOLUTION METHODOLOGY

4.1LAGRANGE RELAXATION SOLUTION

In the Lagrange relaxation technique these disadvantages disappear. This method is based on a dual optimization approach as introduced.

We start by defining the variable U_i^t as:

$$U_i^t = 1 \text{ if unit } i \text{ is on-line during period } t$$

$U_i^t = 0 \text{ if unit } i \text{ is off-line during period } t$

The objective function of the unit commitment problem:

1. Loading constraints:

$$P_{load}^t - \sum_{i=1}^N p_i^t U_i^t = 0 \text{ for } t=1\dots T \quad (4.1)$$

2. Unit limits:

$$U_i^t P_i^{\min} \leq P_i^t \leq U_i^t P_i^{\max} \text{ for } i=1\dots N \quad \text{and} \quad t=1\dots T \quad (4.2)$$

3. Unit minimum up- and down-time constraints. Note that other constraints can easily be formulated and added to the unit commitment problem. These include transmission security constraints generator fuel limit constraints, and system air quality constraints in the form of limits on emissions from fossil-fired plants, spinning reserve constraints, etc.

4. The objective function is:

$$\sum_{t=1}^T \sum_{i=1}^N [F_i(P_i^t) + startup \cos t_{i,t}] U_i^t = F(P^t, U^t) \quad (4.3)$$

The unit commitment problem requires that we minimize the Lagrange function, above, subject to the local unit constraints 2 and 3, which can be applied to each unit separately. Note:

1. The cost function, $F(P_i^t, U_i^t)$, together with constraints 2 and 3 are each separable over units. That is, what is done with one unit does not affect the cost of running another unit, as far as the cost function and the unit limits (constraint 2) and the unit up- and down-time (constraint 3) are concerned.
2. Constraints 1 are coupling constraints across the units so that what we do to one unit affects what will happen on other units if the coupling constraints are to be met.

$$q^*(\lambda) = \max_{\lambda^t} q(\lambda) \quad (4.4)$$

$$q(\lambda) = \min_{P_i^t, U_i^t} \mathcal{L}(P, U, \lambda)$$

(4.5)

This is done in two basic steps:

Step 1.Find a value for each λ^t which move $q(\lambda)$ toward a larger value.

Step 2.Assuming that the λ^t found in step 1 are now fixed, find the minimum of \mathcal{L} by adjusting the values of P^t and U^t

$$\begin{aligned} \mathcal{L} = & \sum_{t=1}^T \sum_{i=1}^N [F_i(p_i^t) + start up cost_{i,t}] U_i^t + \\ & \sum_{t=1}^T \lambda^t (P_{load}^t - \sum_{i=1}^N p_i^t U_i^t) \end{aligned} \quad (4.6)$$

$$\begin{aligned} \mathcal{L} = & \sum_{t=1}^T \sum_{i=1}^N [F_i(p_i^t) + start up cost_{i,t}] U_i^t + \\ & \sum_{t=1}^T \lambda^t P_{load}^t - \sum_{t=1}^T \sum_{i=1}^N \lambda^t p_i^t U_i^t \end{aligned} \quad (4.7)$$

The second term above is constant and can be dropped (since the I^t are fixed). Finally, we write the Lagrange function as

$$\mathcal{L} = \sum_{i=1}^N \left(\sum_{t=1}^T \{ [F_i(P_i^t) + \text{start up cost}_{i,t}] U_i^t - \lambda^t P_i^t U_i^t \} \right) \quad (4.8)$$

Here, we have achieved our goal of separating the units from one another. The term inside the outer brackets; that is:

$$\sum_{t=1}^T \{ [F_i(P_i^t) + \text{start up cost}_{i,t}] U_i^t - \lambda^t P_i^t U_i^t \} \quad (4.9)$$

)

can be solved separately for each generating unit, without regard for what is happening on the other generating units. The minimum of the Lagrangian is found by solving for the minimum for each generating unit over all time periods; that is:

$$\min q(\lambda) = \sum_{i=1}^N \min \sum_{t=1}^T \{ [F_i(P_i^t) + \text{start up cost}_{i,t}] U_i^t - \lambda^t P_i^t U_i^t \}$$

Subject to,

$$U_i^t P_i^{\min} \leq P_i^t \leq U_i^t P_i^{\max} \quad (4.11)$$

V. SIMULATION RESULTS AND DISCUSSION

In this paper, a micro grid system model of two micro turbine, fuel cell and wind, and one energy storage system for a scheduling time horizon of 24 hour is considered. Micro turbine are small generators that burn gas and liquid to create high speed rotation that turns an electrical generator. Fuel cell technology uses an electrochemical process to generate electricity, polymer electrolyte fuel cells also known as proton exchange membrane are particularly attracted for micro grids that require rapid start-up and quick response to load change. The wind speed data is assumed in this work it's an variable load were lagrangian algorithm is used in which the values are assumed from 70 to 190,to understand the impact of PSS on the total operating cost, three different operation are considered, which are PSS=90%, PSS=70%, PSS=50%. The input parameters are considered in this work the forecasted wind power is generated and we assume v_m remains unchanged in one scheduling period (i.e., 1h) and vary independently between different scheduling periods.

Table 1 Parameters of distributed generators

Unit	a_i	b_i	c_i	α^* 10^{-4}	β^* 10^{-4}	γ^* 10^{-4}	Pmax (kw)
MT1	20	50	100	6.49	-5.55	4.09	30
MT2	100	40	140	5.64	-6.05	2.54	75
FC	10	20	20	3.38	-3.35	5.33	100

Based on the aforementioned cost models and system constrains, first formulate the UC optimization problem using Lagrangian algorithm which used to determine loads and commitments of DGs such that the total cost is minimized , power demand is met, and the system constrains are satisfied. To understand the impact of PSS on the total operating cost operation are considered, which are PSS=90%, PSS=70%, PSS=50%.

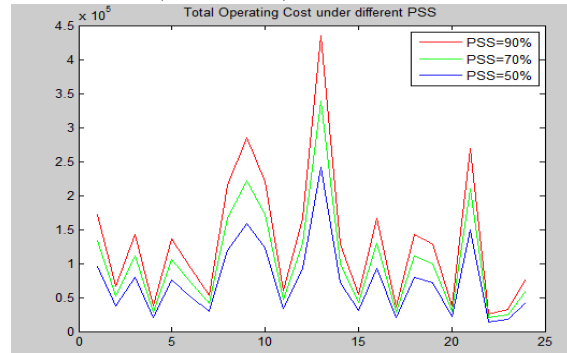
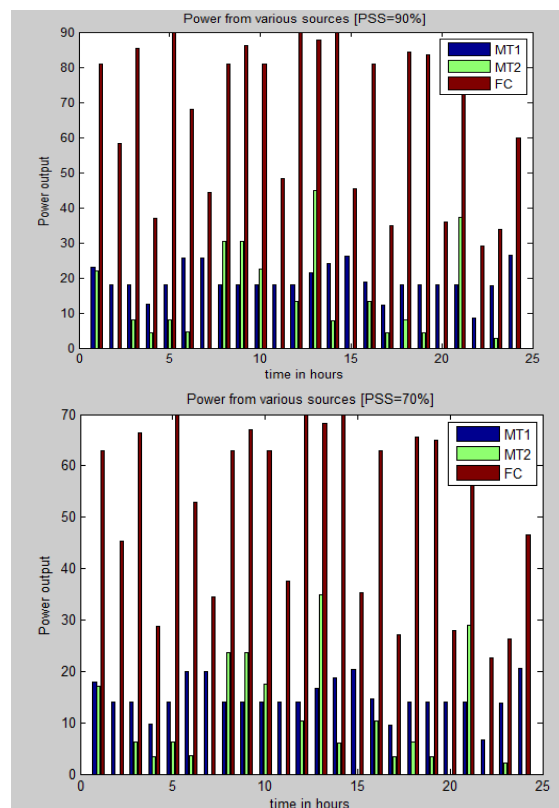


Fig 2.Total operating cost under different PSS
(4.10)

Table 2.Unit commitment of the DGs with targets

unit	Hours(1-24)
MT1	1 1 1 1 1 1 1 1 1 1 1 1 1 1 1 0 0 0 1 1 1 1 1 0 0 0
MT2	1 1 1 1 1 1 1 1 1 1 1 1 1 1 1 1 0 0 0 0 1 1 1 1 1 0 0 0
FC	1 0 1 1 1 1 1 1 0 0

(a)



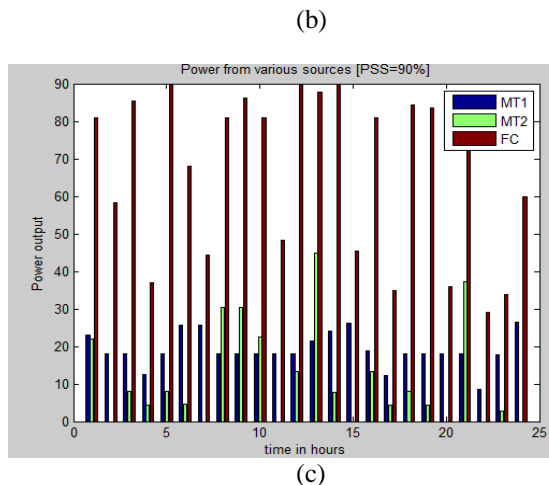


Fig 3.Forecasted demand and wind power and DGs under PSS targets a) PSS=50%,b) PSS=70%,c) PSS=90%

Table 2 depicts the UC status of the DGs for the case of PSS=70% over a period of 24h. Fig 3 shows that an FC is the most preferred power source among the DGs and contributes during the scheduling period, MT2 contributes the least and is always the last one to be turned ON. We incorporate the Energy storage system into micro grid setting and the impact of ESS, the effectiveness of the ESS on the achieved PSS, data samples of the wind are employed to calculate PSS of the micro grid. It is observed from fig (b) that for all the PSS targets, the proposed approach successfully meets the design targets the absence of ESS. The micro grid is more capable of functioning self-sufficiently as the capacity of ESS increases. The achieved PSS hits an upper limit when the capacity of ESS is larger than a threshold. The renewable energy source based generation systems are used for solving the unit commitment problem.

Table3.Optimal dispatch of generation in mw (without wind)

P1	P2	P3
30.0000	25.9013	100.0000
30.0000	6.8109	69.1086
30.0000	18.9047	100.0000
23.8906	4.8281	49.2813
30.0000	16.9026	100.0000
30.0000	8.4474	85.4738
28.8906	5.8281	59.2813
30.0000	33.9014	100.0000
30.0000	43.9004	100.0000
30.0000	34.9039	100.0000
30.0000	6.2659	63.6593
30.0000	24.9011	100.0000

30.0000	59.9018	100.0000
30.0000	13.9026	100.0000
29.5156	5.9531	60.5313
30.0000	24.9011	100.0000
23.5781	4.7656	48.6563
30.0000	18.9047	100.0000
30.0000	13.9026	100.0000
24.2031	4.8906	49.9063
30.0000	41.9060	100.0000
19.5156	3.9531	40.5313
22.0156	4.4531	45.5313
30.0000	7.5410	76.4100

5.1 The impact of ESS

We incorporate the ESS into the microgrid setting and study the impact of ESS achieved level of microgrid. We observe that all targets, the proposed approach successfully meets the targets in the absence of ESS. For example the microgrid achieve PSS=56%,PSS=74%,PSS=93% when the PSS targets are set as 50%,70%,90% the microgrid capable of functioning self-sufficiently as the capacity of ESS increases and achieved PSS hits and upper limit when capacity of ESS is larger than threshold.

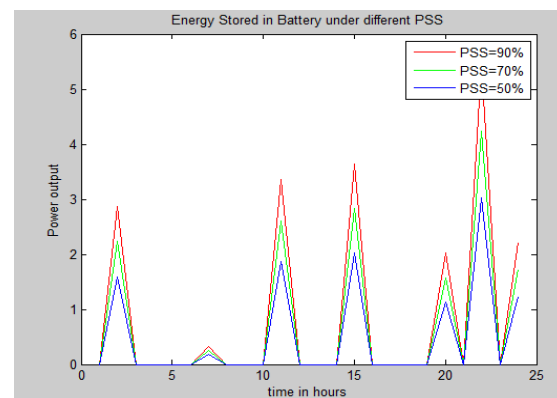


Fig 4.Energy stored in battery under different PSS

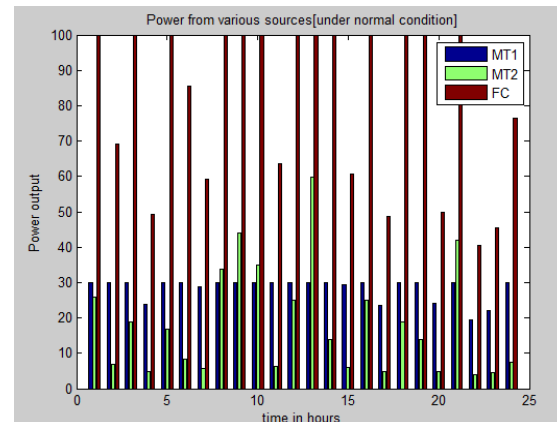


Fig 5. Power from various sources

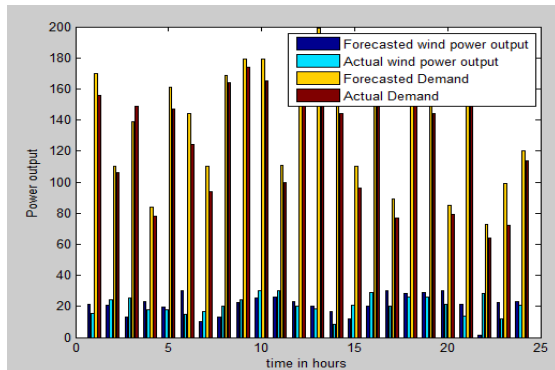


Fig 6.Wind power output and demand

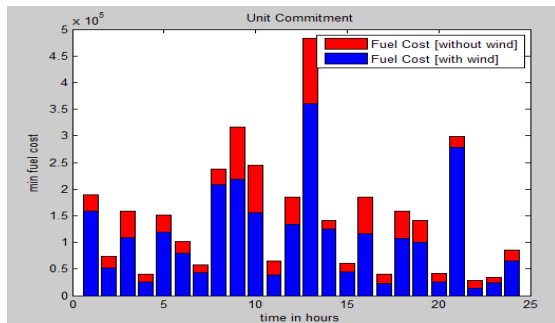


Fig 7.Unit commitment

Table 4.Total generation cost

WITH WIND	WITHOUT WIND
158440	189880
052580	73810
109240	158260
025120	40670
119370	151010
079310	102000
43100	58360
208350	238050
219070	316240
155080	244980
039130	65740
134060	184760
361050	482980
125670	141640
045120	60790
1115690	184760
2280	39670
107420	158260
99890	141640
25910	41680
277940	299050
13720	27810

24750 | 34860

The method which is proposed in this work for minimizing the total operating cost per day during different PSS targets has been achieved without loss of optimality and with lower complexity than the existing algorithms. Power from wind which reduces fuel cost .thus, renewable energy sources helps in producing power in the absence when grid is off-line

VI. CONCLUSION

The unique characteristics of renewable powered micro grid have brought new challenges to the classic unit commitment optimization task of UC. The cost, constraint, and availability functions make the optimal power setting for each plant a complex surface. The optimal commitment and dispatch solutions using a Lagrangian algorithm .This leads to the conclusion that a power-sharing scheme aimed at maximizing the financial benefits in a micro grid. The results shows the capability of proposed approach can easily modified to incorporate other types of DGs or RESS.

REFERENCES

- [1] IEEE transactions on smart grid, vol. 3, no. 1, march 2012 Investigation of Economic and Environmental-Driven Demand Response Measures Incorporating UC was proposed by Amir Abdollahi, Mohsen Parsa Moghaddam, Masoud Rashidinejad and Mohammad Kazem Sheikh-Eslami.
- [2] IEEE transactions on industry applications, vol. 41, no. 3, fuel consumption minimization of a micro grid was proposed by carlos a. hernandez-aramburo,Tim c and nicolas mugniot.
- [3] IEEE transactions on energy conversion, vol. 17, no. 1, March 2002 Market Constrained Optimal Planning for Wind Energy Conversion Systems Over Multiple Installation Sites was proposed by S. Roy.
- [4] IEEE transactions on power delivery, vol. 20, no. 2, April 2005 Online Optimal Management of PEM Fuel Cells Using Neural Networks was proposed by Ahmed M. Azmy and Istvan Erlich.
- [5] IEEE transactions on industrial electronics, vol. 58, no. 4, April 2011 Plug-in Vehicles and Renewable Energy Sources for Cost and Emission Reductions was proposed by Ahmed Yousuf Saber, and Ganesh Kumar Venayagamoorthy.
- [6] IEEE Transactions on power systems, vol. 26, no. 4, November 2011 A Statistical Model for Wind Power Forecast Error and its Application to the Estimation of Penalties in Liberalized Markets was proposed by Saurabh Tewari, Charles J. Geyer, and Ned Mohan.

QUASI Z SOURCE INVERTER FOR CONSUMER APPLICATION

Ms.V.Brinda¹, Mrs.S.P.Vedhavalli M.E²

¹PG Scholar, St. Joseph's College of Engineering, Chennai, India.

²Assistant Professor, St. Joseph's College of Engineering, Chennai, India.

¹rose.brinda30@gmail.com ²vedavalliprabhu@gmail.com

Abstract --- This paper proposes a new topology of the energy-stored quasi-z-source inverter the characteristic of the proposed solution is analyzed in detail and compared to that of the existing topology. A strategy is proposed with the related design principles to control the new energy-stored quasi-z-source inverter when applied to the PV power system. They can control the inverter output power and manage the battery power, simultaneously. The voltage boost and inversion, and energy storage are integrated in a single-stage inverter. A real PV panel is used in the grid-tie test of the proposed energy-stored quasi-z-source inverter, which demonstrates three operational modes suitable for application in the PV power system.

Keywords—Energy storage, photovoltaic (PV) power generation, power conversion, quasi-Z-source inverter (qZSI).

I.INTRODUCTION

Power converter topologies employed in the PV power generation systems are mainly characterized by two- or single-stage inverters. The single-stage inverter is an attractive solution due to its compactness, low cost, and reliability. However, its conventional structure must be oversized to cope with the wide PV voltage variation derived from changes of irradiation and temperature. The two-stage inverter topology applies a boost dc/dc converter to minimize the required kilovolt ampere rating of the inverter and boost the wide-range input voltage to a constant desired output value. However, the switch in the dc/dc converter will increase the cost and decrease the efficiency. [1][2] The Z-source inverter (ZSI) presents a new single-stage structure to achieve the voltage boost/buck character in a single power conversion stage, which has been reported in applications to PV systems. This type of converter can handle the PV dc voltage variations over a wide range without overrating the inverter. As a result, the component count and system cost are reduced, with improved reliability due to the allowed shoot through state.[3][4] Recently proposed quasi-Z-source inverters have some new attractive advantages more suitable for application in PV systems shown in fig1. The

QZSI circuit differs from that of a conventional ZSI in the LC impedance network interface between the source and inverter. The unique LC and diode network connected to the inverter bridge modify the operation of the circuit, allowing the shoot-through state which is forbidden in traditional VSI. This network will effectively protect the circuit from damage when the shoot through occurs and by using the shoot-through state, the (quasi-) Z-source network boosts the dc-link voltage. [9][10] This will make the PV system simpler and will lower cost, because of the following: 1) the quasi-z-source inverter draws a constant current from the PV panel, and thus, there is no need for extra filtering capacitors; 2) the quasi-z-source inverter features a lower component (capacitor) rating; and 3) the quasi-z-source inverter reduces switching ripples seen by the PV panels. In addition, the intermittent and unscheduled characteristics of solar power limit the applicability of PV systems. [5] Therefore, much of the literature suggests the addition of an energy storage system (ESS) to work in conjunction with PV power generation to make its output power continuous, stable, and smooth. Without requirements of any additional dc/dc converters or components, the quasi-z-source inverter with energy storage was first proposed for PV power generation system.[6] This system is able to do the following simultaneously: 1) produce the desired output ac voltage to the grid/load; 2) regulate the battery state of charge (SOC); and 3) control the PV panel output power (or voltage) to maximize energy production. The authors presented its basic principle and analyzed the charging, discharging, and discontinuous conduction mode (DCM) during battery discharge operation. The intermittent and unscheduled characteristics of solar power limit the applicability of PV systems. Therefore, much of the literature suggests the addition of an energy storage system (ESS) to work in conjunction with PV power generation to make its output power continuous, stable, and smooth. Moreover, when applied as a grid-connected system, it implements other important auxiliary services normally provided by special

and expensive equipment electrical power quality control, load peak demand control. Most of the existing ESS technologies employ a bidirectional dc/dc converter to manage the batteries which makes the system complex, increases its cost, and decreases its reliability.

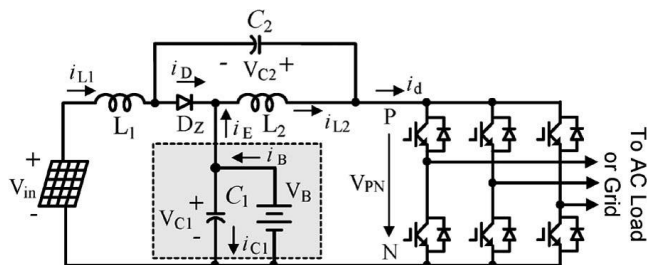


Fig.1 New energy-stored qZSI for PV power generation.

In today's climate of growing energy needs and increasing environmental concern, alternatives to the use of non-renewable and polluting fossil fuels have to be investigated. One such alternative is solar energy. Solar energy is quite simply the energy produced directly by the sun and collected elsewhere, normally the Earth. The sun creates its energy through a thermonuclear process that converts about 650,000,0001 tons of hydrogen to helium every second. The process creates heat and electromagnetic radiation. The heat remains in the sun and is instrumental in maintaining the thermonuclear reaction. The electromagnetic radiation (including visible light, infra-red light, and ultra-violet radiation) streams out into space in all directions. Only a very small fraction of the total radiation produced reaches the Earth. The radiation that does reach the Earth is the indirect source of nearly every type of energy used today. The exceptions are geothermal energy, and nuclear fission and fusion. Even fossil fuels owe their origins to the sun; they were once living plants and animals whose life was dependent upon the sun. Much of the world's required energy can be supplied directly by solar power. More still can be provided indirectly.

The practicality of doing so will be examined, as well as the benefits and drawbacks. In addition, the uses solar energy is currently applied to will be noted. Due to the nature of solar energy, two components are required to have a functional solar energy generator. These two components are a collector and a storage unit. The collector simply collects the radiation that falls on it and converts a fraction of it to other forms of energy (either electricity and heat or heat alone). The storage unit is required because of the non-constant nature of solar energy; at certain times only a very small amount of radiation will be received.

At night or during heavy cloud cover, for example, the amount of energy produced by the collector will be quite small. The storage unit can hold the excess energy produced during the periods of maximum productivity, and release it when the productivity drops. In

practice, a backup power supply is usually added, too, for the situations when the amount of energy required is greater than both what is being produced and what is stored in the container. Methods of collecting and storing solar energy vary depending on the uses planned for the solar generator. In general, there are three types of collectors and many forms of storage units. The three types of collectors are flat-plate collectors, focusing collectors, and passive collectors. Flat-plate collectors are the more commonly used type of collector today. They are arrays of solar panels arranged in a simple plane. They can be of nearly any size, and have an output that is directly related to a few variables including size, facing, and cleanliness. These variables all affect the amount of radiation that falls on the collector. Often these collector panels have automated machinery that keeps them facing the sun. The additional energy they take in due to the correction of facing more than compensates for the energy needed to drive the extra machinery. Focusing collectors are essentially flat-plane collectors with optical devices arranged to maximize the radiation falling on the focus of the collector. These are currently used only in a few scattered areas. Solar furnaces are examples of this type of collector. Although they can produce far greater amounts of energy at a single point than the flat-plane collectors can, they lose some of the radiation that the flat-plane panels do not.

II Z – SOURCE INVERTER

The network employs a unique impedance circuit to couple the converter main circuit to that of the power source in order to obtain the unique features that cannot be achieved using conventional VSI or CSI. The Z-source inverter (ZSI) has been reported suitable for residential PV system because of the capability of voltage boost and inversion in a single stage shown in fig.2. The unique feature about Z- source inverter is that the output voltage can be anywhere from zero to infinity. The inverter can perform both buck and boost operation and provide a wide range of output voltage which is not possible in conventional voltage source and current source inverters.[8][11]

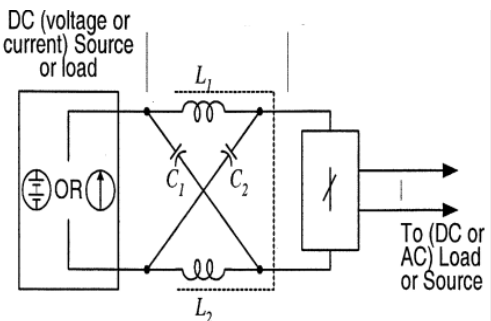


Fig:2 Z-source inverter

The Z source inverter has nine permissible switching states which has an extra state compared to the conventional inverters. The extra switching state arises from the shoot through state of the network in which two switches of the same leg is switched ON and conduct simultaneously which is not possible in conventional inverters. Z-source inverter is one of quite new ideas designed to renewable energy system, mainly fuel cell and photovoltaic. In the Z-source inverter, a special Z-network is introduced and shoot-through states may be used in similar manner as in Current Source Inverter. ZSI employs a unique impedance network (or circuit) to couple the converter main circuit to the power source, load, or another converter, for providing unique features that cannot be observed in the traditional voltage and current source inverters where a capacitor and inductor are used respectively. The Z-source converter overcomes the conceptual and theoretical barriers and limitations of the traditional voltage source and current source inverters and provides a novel power conversion concept.

III QUASI-Z-SOURCE INVERTER

The quasi z-source inverter (QZSI) is a single stage power converter derived from the Z-source inverter topology, employing a unique impedance network. The conventional Voltage source inverter and Current source inverter suffer from the limitation that triggering two switches in the same leg or phase leads to a source short and in addition, the maximum obtainable output voltage cannot exceed the dc input, since they are buck converters and can produce a voltage lower than the dc input voltage. Both Z-source inverters and quasi-Z-source inverters overcome these drawbacks; by utilizing several shoot-through zero states. A zero state is produced when the upper three or lower three switches are fired simultaneously to boost the output voltage. Sustaining the six permissible active switching states of a VSI, the zero states can be partially or completely replaced by the shoot through states depending upon the voltage boost requirement. [6][7]Quasi-Z-source inverters (QZSI) acquire all the advantages of traditional Z source inverter. The impedance network couples the source and the inverter to achieve voltage boost and inversion in a single stage. By using this new topology, the inverter draws a constant current from the Photovoltaic array and is capable of handling a wide input voltage range. It also features lower component ratings, reduces switching ripples to the Photovoltaic panels, causes less EMI compared to the traditional ZSI. The quasi-z-source inverter draws a constant current from the PV panel. There is no need for extra filtering capacitors. The quasi-z-source inverter features a lower component (capacitor rating). The quasi-z-source inverter reduces switching ripples seen by the PV panels. Quasi-Z source inverter overcome the aforementioned disadvantages of conventional CMI through combining quasi z source network and H-bridge module together because of the qZS inverter's buck/boost

and inversion in a single stage . The second-harmonic voltage and current ripples always exist in each module of CMI. A huge dc-link capacitor is required in each H-bridge module of traditional CMI to limit the voltage ripple. Similarly, the qZS-CMI also has the 2ω voltage and current ripples in each qZSI module. Some literatures focus on analyzing and eliminating low-frequency ripples of each capacitor voltage and inductor current . An ac equivalent model is built to analyze the ripples of the qZSI module in the model contains five equations, where the coupled relationship makes the analysis and design

A.MODES OF OPERATION

There are two operating modes based on quasi z-source network.

I. Mode 1:

This mode will make the inverter short circuit via any one phase leg, combinations of any two phase legs, and all three phase legs which is referred to as the shoot through state . As a result, the diode Dz is turned off due to the reverse-bias voltage. Its equivalent circuit is shown in Fig.3. During this time interval, the circuit equations are presented as follows:

$$C \frac{dV_{C1}}{dt} = i_B - i_{L2} \quad \dots(1)$$

$$C \frac{dV_{C2}}{dt} = - i_{L1} \quad \dots(2)$$

$$L \frac{di_{L1}}{dt} = V_{in} + V_{C2} \quad \dots(3)$$

$$L \frac{di_{L2}}{dt} = V_{C1} \quad \dots(4)$$

where i_{L1} , i_{L2} , and i_B denote the currents of inductors L_1 and L_2 and the battery, respectively; V_{C1} , V_{C2} , and v_{in} denote the voltages of capacitors C_1 and C_2 and the PV panel, respectively; C denotes the capacitance of capacitors C_1 and C_2 ; and L denotes the inductance of inductors L_1 and L_2 .

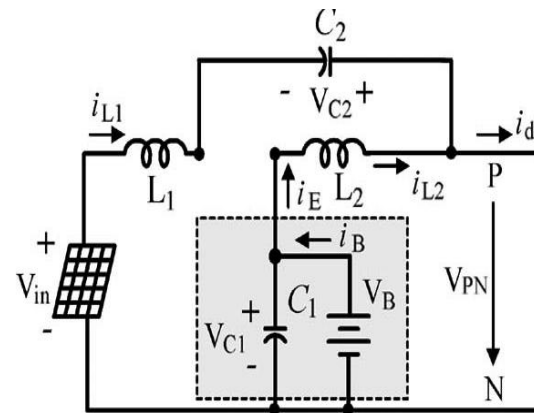


Fig.3Operating modes in the CCM. Mode I

II Mode 2:

This mode will make the inverter operate in one of the six active states and two traditional zero states, which is referred to as the non-shoot-through state shown in fig.4. A continuous current flows through the diode Dz, and its equivalent circuit.[6]

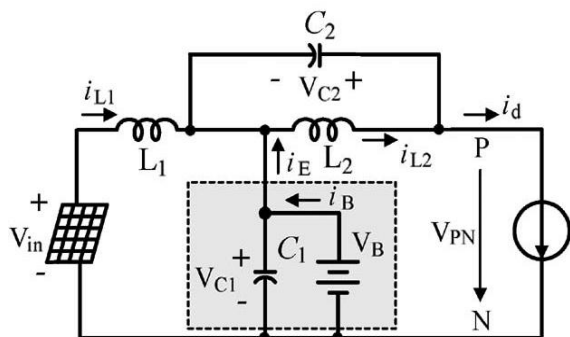


Fig.4 Operating modes in the CCM Mode II.

During this time interval, the circuit equations are presented as follows:

$$C \frac{dV_{C1}}{dt} = i_B + i_{L1} - i_d \quad \dots \dots \dots (5)$$

$$C \frac{dV_{C2}}{dt} = i_{L2} - i_d \quad \dots \dots \dots (6)$$

$$L \frac{di_{L1}}{dt} = V_{in} - V_{C1} \quad \dots \dots \dots (7)$$

$$L \frac{di_{L2}}{dt} = -V_{C2} \quad \dots \dots \dots (8)$$

where i_d is the load current going to the inverter.

B.SINUSOIDAL PULSE WIDTH MODULATION TECHNIQUE

The voltage source inverter that use PWM switching techniques have a DC input voltage that is usually constant in magnitude. The inverter job is to take this DC input and to give AC output, where the magnitude and frequency can be controlled. There are several techniques of Pulse Width Modulation (PWM).The efficiency parameters of an inverter such as switching losses and harmonic reduction are principally depended on the modulation strategies used to control the inverter. In this design the Sinusoidal Pulse Width Modulation (SPWM) technique has been used for controlling the inverter as it can be directly controlled the inverter output voltage and output frequency according to the sine functions. Sinusoidal pulse width modulation (SPWM) is widely used in power electronics to digitize the power so that a sequence of voltage pulses can be generated by the on and off of the power switches. The PWM inverter has been the main choice in power electronic for decades, because of its circuit simplicity and rugged control scheme. Sinusoidal Pulse Width Modulation switching technique is commonly used in industrial applications or solar electric vehicle applications.[4]

SPWM techniques are characterized by constant amplitude pulses with different duty cycles for each period

in this fig.5. The width of these pulses are modulated to obtain inverter output voltage control and to reduce its harmonic content. Sinusoidal pulse width modulation is the mostly used method in motor control and inverter application. In SPWM technique three sine waves and a high frequency triangular carrier wave are used to generate PWM signal. Generally, three sinusoidal waves are used for three phase inverter. The frequency of these sinusoidal waves is chosen based on the required inverter output frequency. The carrier triangular wave is usually a high frequency (in several KHz) wave. The switching signal is generated by comparing the sinusoidal waves with the triangular wave. The comparator gives out a pulse when sine voltage is greater than the triangular voltage and this pulse is used to trigger the respective inverter switches. In order to avoid undefined switching states and undefined AC output line voltages in the VSI, the switches of any leg in the inverter cannot be switched off simultaneously. The ratio between the triangular wave & sine wave must be an integer N, the number of voltage pulses per half-cycle, such that, $2N = f_c/f_s$. Conventional SPWM signal generation technique for three phase voltage source inverter.

C.COMPARISON OF SINE & TRIANGULAR PWM

A PWM control technique for QZSI, with modified carrier for active and shoot through states is presented. While the zero states of traditional VSI are replaced by shoot through states, the active states should remain unaltered, for the shape of output voltage waveform to be preserved. This technique uses sine wave as both reference and carrier. The simple boost control method used here employs two constant voltage envelopes which are compared with the sine carrier wave. Whenever the magnitude of sine carrier wave becomes greater than or equal to the positive constant magnitude envelope (or) lesser than or equal to the negative constant magnitude envelope, pulses are generated and they control the shoot through duty ratio D_o . These pulses serve as firing signals for the switches in the inverter.

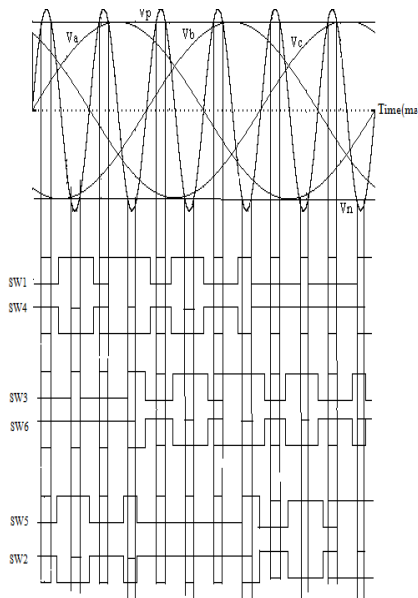


Fig.5 Schematic of Sine PWM

D.CONTROL TECHNIQUE FOR PV PANEL:

The PV-panel-power-based control system, where the PV panel voltage V_{in} and current i_{L1} are sensed to calculate the PV actual power that is used to pursue a demand PV panel voltage V_{in} through the MPPT algorithm. In the same way as the conventional voltage-source inverter, the output power of the quasi-z-source inverter can be controlled on the basis of the d-q model in fig.6. Three-phase grid currents and voltages are measured and transformed to get the d- and q-axis components, i.e., from three-phase a-b-c frame to two-phase stationary coordinate $\alpha-\beta$ frame and, finally, to two-phase rotation coordinate d-q frame[9][10]

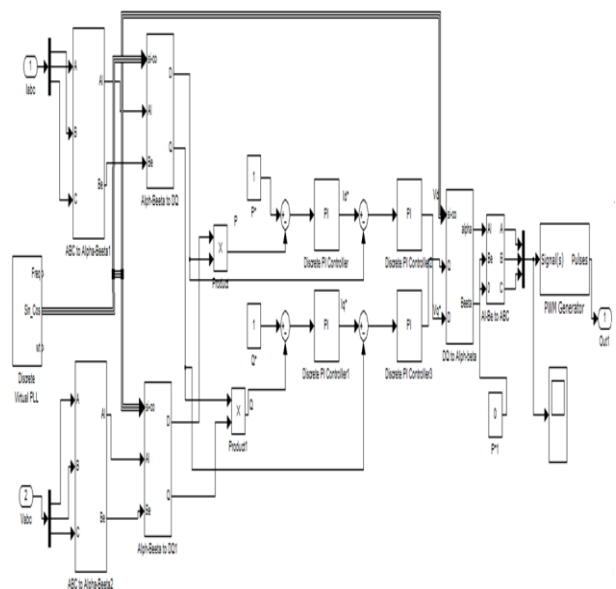


Fig.6 PV-panel-power-based qZSI–battery PV power generation system.

In the practical implementation, a feed forward control will speed up the response by a steady-state shoot-through duty ratio. The active power and reactive power closed-loop controls are combined with d and q-axis current component closed-loop controls to produce three-phase desired voltage signals V_a^* , V_b^* , and V_c^* (related to the modulation index M), which will force the actual active power P_{out} and reactive power Q_{out} to track the given powers P_{out}^* and Q_{out}^* respectively. The existing simple boost control and maximum constant boost control for ZSI/QZSI are preferable to integrate the duty ratio D and three-phase voltage signals V_a^* , V_b^* , and V_c^* in the sinusoidal pulse width modulation . The simple boost control will be used in the demonstration of experiments later.

Simulation result:

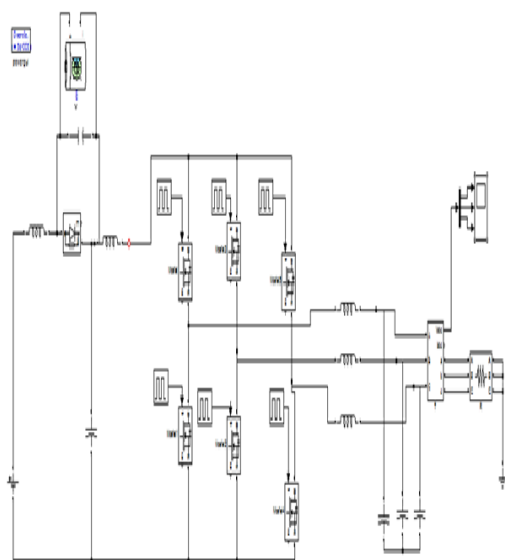


Fig:7 Simulation of Existing qZSI with battery for PV power generation

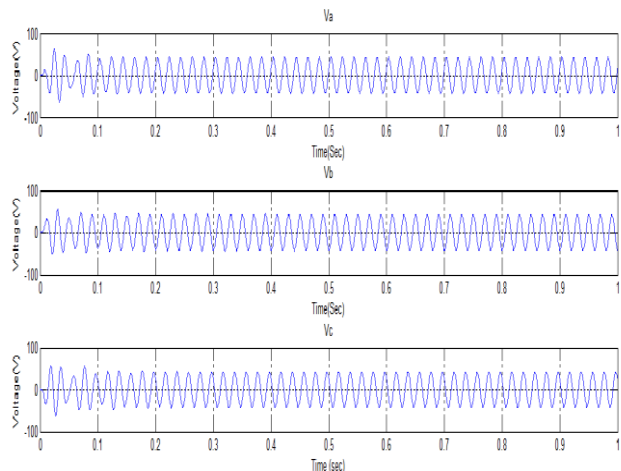


Fig:8 Simulation result of Existing qZSI with battery for PV power generation

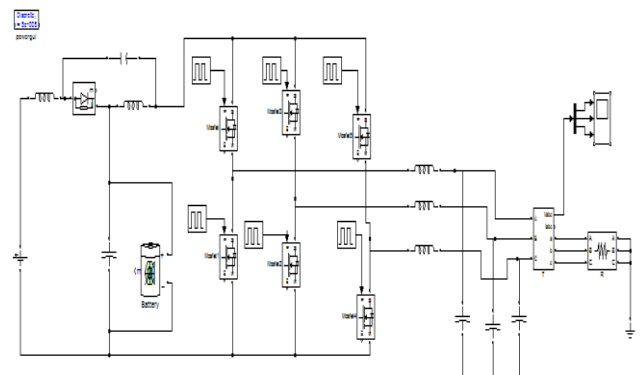


Fig:9 Simulation of New energy-stored qZSI for PV power generation

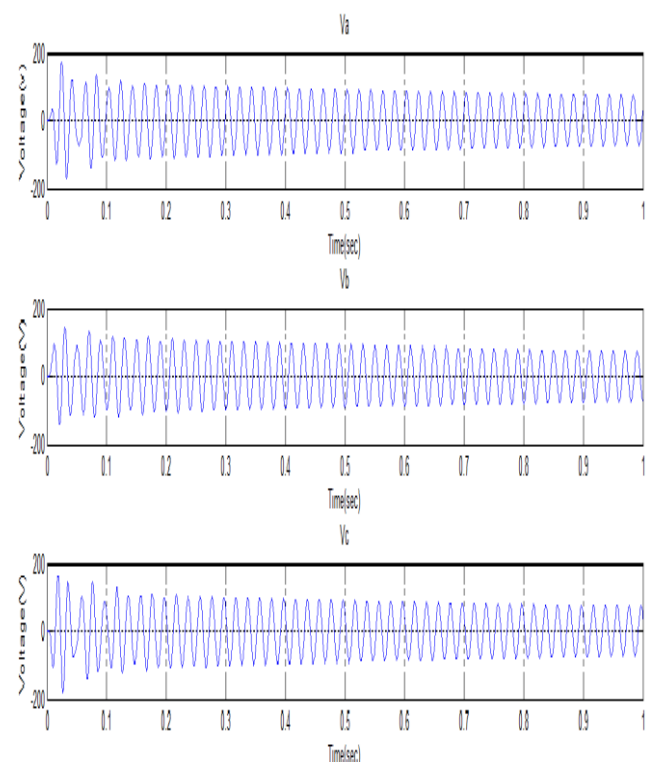


Fig:10 Simulation result of New energy-stored qZSI for PV power generation

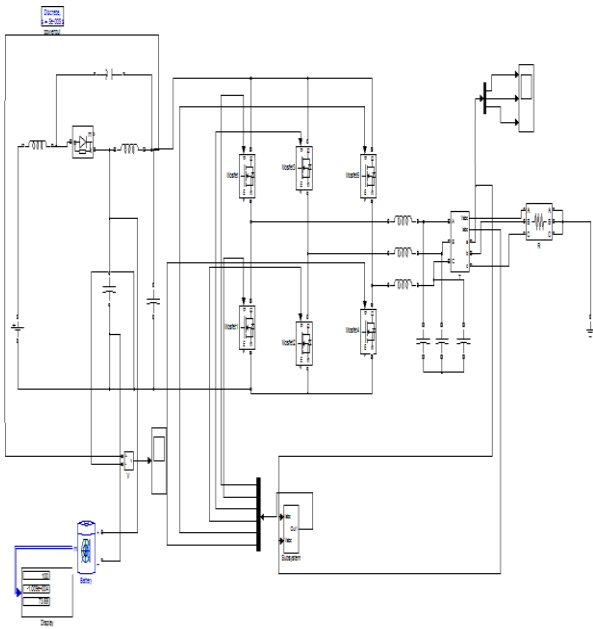


Fig:11 Simulation of PV-panel-power-based qZSI-battery PV power generation system.

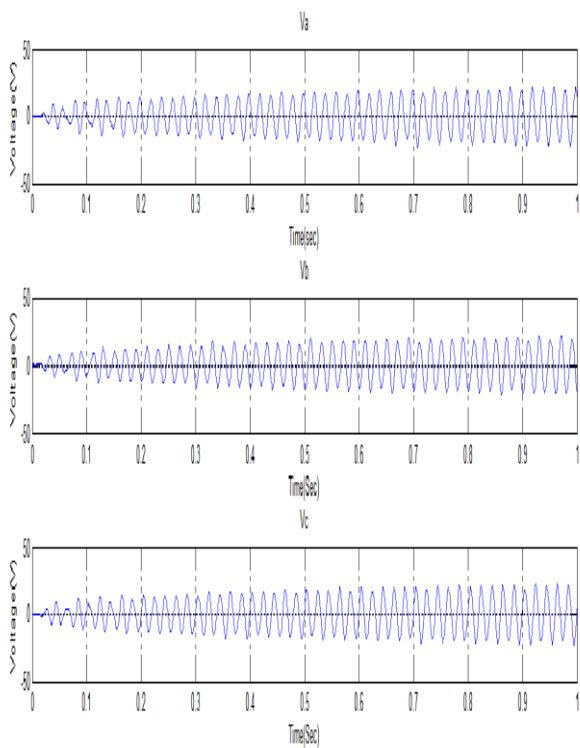


Fig:12 Simulation result of PV-panel-power-based qZSI-battery PV power generation system.

CONCLUSION:

In this paper, a novel topology for an energy-stored quasi-z-source inverter has been proposed to overcome the shortcoming of the existing solutions in PV power system. A strategy has been proposed to control the new circuit topology, and their design methods have been presented by employing a small-signal model and a Bode plot. The theoretical analysis, simulations, and experimental results presented in this paper clearly demonstrate that the proposed energy-stored quasi-z-source inverter and the suggested a control method can effectively track the MPP in the PV module and inject the active/reactive power into the grid by the inverter, independently, as well as control the battery power flow.

REFERENCE:

- 1.Y. Li, J. Anderson, F. Z. Peng, and D. Liu, "Quasi-Z-source inverter for photovoltaic power generation systems," in *Proc. 24th Ann. IEEE Applied Power Electronics Conf. Exposition (APEC2009)*, Washington,DC, Feb. 15–19, 2009, pp. 918–924.
- 2.X. Wang, Z. Fang, J. Li, L. Wang, and S. Ni, "Modelling and control of dual-stage high-power multifunctional PV system in d - q - o coordinate," *IEEE Trans. Ind. Electron.*, vol. 60, no. 4, pp. 1556–1570, Apr. 2013.
3. E. S. Sreeraj, K. Chatterjee, and S. Bandyopadhyay, "One cycle controlled single-stage, single-phase voltage sensor-less grid-connected PV system," *IEEE Trans. Ind. Electron.*, vol. 60, no. 3, pp. 1216–1224, Mar. 2013.
4. J. Chavarria, D. Biel, F. Guinjoan, C. Meza, and J. Negroni, "Energy balance control of PV cascaded multilevel grid-connected inverters for phase-shifted and level-shifted pulse-width modulations," *IEEE Trans. Ind. Electron.*, vol. 60, no. 1, pp. 98–111, Jan. 2013.
5. D. Vinnikov, I. Roasto, R. Strzelecki, and M.Adamowicz, "Step-up DC/DC converters with cascaded quasi-z-source network," *IEEE Trans. Ind. Electron.*, vol. 59, no. 10, pp. 3727–3736, Oct. 2012.
- 6.J. Anderson and F. Z. Peng, "A class of quasi-Z-source inverters," in *Conf. Rec. IEEE IAS Annu. Meeting*, Edmonton, AL, Canada, Oct. 2008, pp. 1–7.
- 7.. D. Vinnikov and I. Roasto, "Quasi-Z-source-based isolated DC/DC converters for distributed power generation," *IEEE Trans. Ind. Electron.*, vol. 58, no. 1, pp. 192–201, Jan. 2011

8.Y. Huang, M. Shen, F. Z. Peng, and J. Wang, “Z-source inverter for residential photovoltaic systems,” *IEEE Trans. Power Electron.*, vol. 21, no. 6, pp. 1776–1782, Nov. 2006.

9. S. Jain and V. Agarwal, “Comparison of the performance of maximum power point tracking schemes applied to single-stage grid-connected photovoltaic systems,” *IET Elect. Power Appl.*, vol. 1, no. 5, pp. 753–762, Sep. 2007.

10. M. Shen, J. Wang, A. Joseph, F. Z. Peng, L. M. Tolbert, and D. J. Adams,“Constant boost control of the Z-source inverter to minimize current ripple and voltage stress,” *IEEE Trans. Ind. Appl.*, vol. 42, no. 3, pp. 770–778, May/Jun. 2006.

11.F. Z. Peng, “Z-source inverter,” *IEEE Trans. Ind. Appl.*, vol. 39, no. 2,pp. 504–510, Mar./Apr. 2003.

Analysis With PWM Control of Cuk and Boost Dual Input Dual Output Dc-Dc Converter

Maris Anto. M

2nd year PG scholar/Department of EEE
St.Joseph's College of Engineering
Chennai, India
maris.anto06@gmail.com

Mr.H.UmeshPrabhu

Assistant Professor/Department of EEE
St.Joseph's College of Engineering
Chennai, India
prabhuumesh2013@gmail.com

Abstract— Among the available renewable energy resources, the wind and photo voltaic energy is being widely utilized because of their abundance and sustainability to generate electricity. In this paper, a new topology, fed by DC supply and solar energy system is configured using Cuk and Boost converter Dual input Dual Output Dc-Dc converter. This configuration allows the two sources to supply the load separately (PV/DC supply) or simultaneously together depending on the availability of the energy sources. The main purpose of this fusion is to meet our daily demand effectively and to get an uninterrupted power supply. By combining these two intermittent sources the system's power transfer efficiency and reliability can be improved significantly.

I. INTRODUCTION

The utilization of naturally occurring renewable energy sources as an alternative energy supply has been assuming more importance of less power generation utilizing solar rays, geothermal energy, wind force and wave force has become a reality. Consumption of energy based on fossil fuels is considered to be the major factor for global warming and environment degradation. They are abundant, pollution free, distributed throughout the earth and recyclable. When a source is unavailable or insufficient to meet the load demand, the other energy source can compensate for the difference in load. Several PV power systems with MPPT control have been proposed and discussed in works.

Most of the systems use a separate DC/DC boost converter connected in parallel in the rectifier stage to perform the MPPT control for each of the renewable energy power sources. This converter has three inductors that can shape the input current and feed the output load. Photovoltaic cell is a solid state electronic source that converts the energy of light directly into electricity by the photovoltaic effect. Thus the output voltage will be very low and not much efficient. A Cuk boost converter is a power converter with an output DC voltage greater than its input DC voltage. Load may be battery or any DC load.

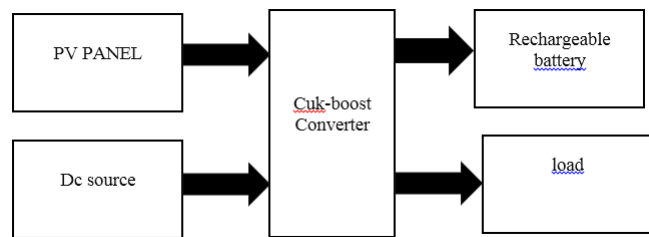


Fig.1 BLOCK DIAGRAM OF CUK-BOOST CONVERTER

Fused Cuk boost Converter:

The fig.2 shows the fusion of Cuk-boost converter it has dual inputs and dual outputs .The first input is from a PV cells and the second input is from a Dc source. The converter which controls the supply towards the load. According to climatic conditions the converter schedules the input source either from PV or from dc source. The output of the boost which is used for any applications or dc fans. The output of the Cuk is used to store the energy in rechargeable battery. The Cuk converter can either operate in continuous or discontinuous current mode. However, unlike these converters, it can also operate in discontinuous voltage mode. This converter consists of V_{in} , V_{PV} and capacitors C_1 , and C_2 , C and inductor L_1 , L_2 , L MOSFET switch and freewheeling diodes D_1 and D_2 , D_3 and D and resistors V_{o1} and V_{o2} .

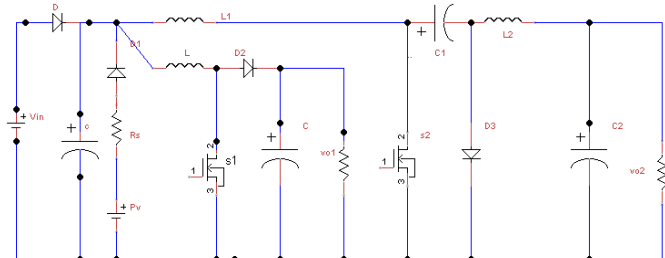


Fig.2. Equivalent Circuit of Cuk boost converter

From Fig.3, we can see that the operation switch S_1 , S_2 are in ON condition. During the operation switch S_1 , S_2 are in ON condition. The current flows through L inductor charges through S_1 and L_1 charges through S_2 .The Capacitor C discharges towards the r-load(V_{o1}) and Diode D_2 and D_3 are in off state and also C_1 is discharged towards the S_2,C_2,L_2 and S_2,R -load(V_{o2}) when L_2 is charged while C_2 discharges.

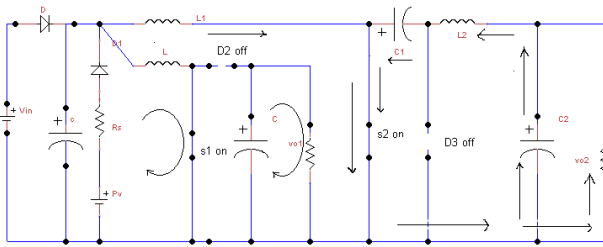


Fig.2. Equivalent Circuit During Switch-on

From Fig.3, we can see that the operation switch \$S_1, S_2\$ are in OFF condition. The Current flows through \$L\$ and inductor current discharges through \$L, D_2, C\$ and \$L, D_2, R\$-Load(\$V_{O1}\$). \$L_1\$ discharges through \$L, C_1, D_3\$ and \$L_2\$ discharges through \$L_2, D_3, C_2\$ and \$L_2, D_3, R\$-Load(\$V_{O2}\$).

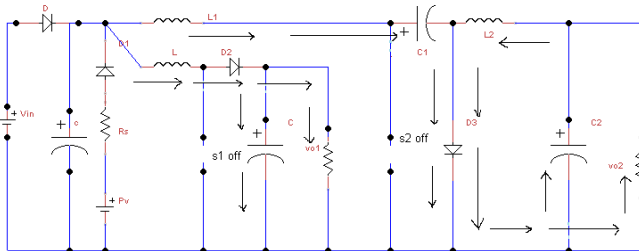


Fig.3 Equivalent Circuit During Switch-off

II. BOOST CONVERTER

The boost is a popular non-isolated power stage topology, sometimes called a step-up power stage. Power supply designers choose the boost power stage because the required output is always higher than the input voltage. The input current for a boost power stage is continuous, or non-pulsating, because the output diode conducts only during a portion of the switching cycle. The output capacitor supplies the entire load current for the rest of the switching cycle. Inductor L and capacitor C make up the effective output filter. The capacitor equivalent series resistance (ESR), RC, and the inductor dc resistance, RL, are included in the analysis. Resistor R represents the load seen by the power supply output.

A power stage can operate in continuous or discontinuous inductor current mode. In continuous inductor current mode, current flows continuously in the inductor during the entire switching cycle in steady-state operation. In discontinuous inductor current mode, inductor current is zero for a portion of the switching cycle. It starts at zero, reaches peak value, and return to zero during each switching cycle. It is desirable for a power stage to stay in only one mode over its expected operating conditions because the power stage frequency response changes significantly between the two modes of operation.

$$\Delta V_C = \frac{I_{AK}}{f_c} \quad (1.1)$$

$$\Delta I = \frac{V_s t_1}{L} \quad (1.2)$$

$$V_a = \frac{V_s}{1-K} \quad (1.3)$$

$$V_S = \frac{L \Delta I}{t_1} \quad (1.4)$$

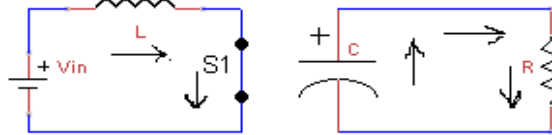


Fig .4 MODE 1

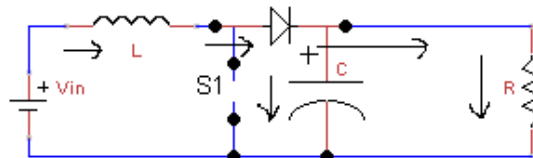


Fig .5 MODE 2

III. CUK CONVERTER

CUK is essentially a boost converter followed by a buck converter with a capacitor to couple the energy. It uses a capacitor as its main energy-storage component, unlike most other types of converters which use an inductor. It is an inverting converter, so the output voltage is negative with respect to the input voltage that has an output voltage magnitude that is either greater than or less than the input voltage magnitude. Its schematic diagram can be seen in Fig. 3.2

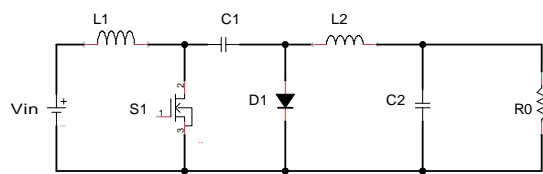


Fig 3.7 Cuk converter

The voltage conversion ratio of the Cuk converter is given by

$$V_O = -V_{in} \left[\frac{D}{(1-D)} \right] \quad (1.1)$$

$$L_1 = V_{in} \left[\frac{T_1}{(\Delta I_1)} \right] \quad (1.2)$$

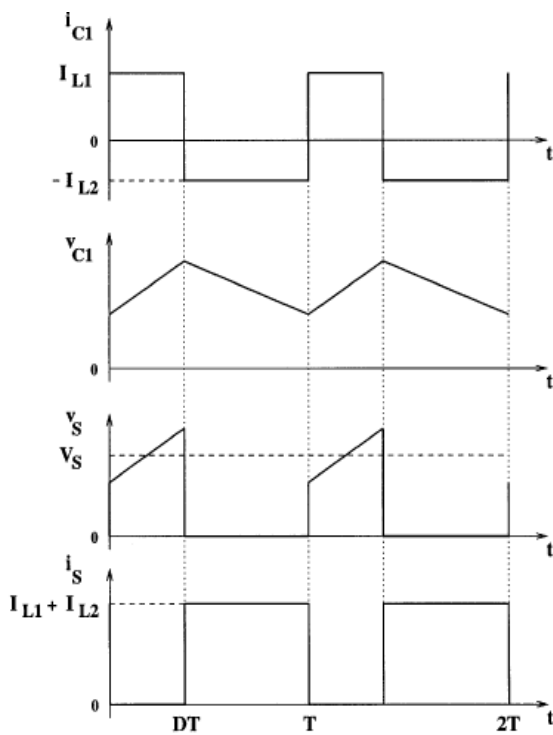
$$L_2 = V_{in} \left[\frac{T_2}{(\Delta I_2)} \right] \quad (1.3)$$

$$C_1 = I_{in} \left[\frac{(1-D)}{(f \Delta V C_1)} \right] \quad (1.4)$$

$$C_2 = D \left[\frac{V_{in}}{g_1 C_1 C_2 f^2} \right] \quad (1.5)$$

VSIMULATION RESULTS

The MATLAB/SIMULINK model of Cuk boost converter is depicted in Fig.7 below.



Converters	Output voltages		
	0.5	0.6	0.7
Buck	4.83	23.63	31.84
Boost	18.72		
Cuk	11.28	23.28	34.26
Cuk Boost	V _{o1} = 69.49 V _{o2} = - 10.88	V _{o1} =84.43 V _{o2} =-10.87	V _{o1} =89.4 V _{o2} =- 29.51

TABLE.II COMPARISON OF OUTPUT VOLTAGE

COMPONENT RATINGS

CONVERTER	L ₁	L ₂	L ₀	C ₁	C ₂	C ₀
CUK CONVERTE	5mH	2mH	2mH	100 μ F	47 μ F	47 μ F
CUK BOOST CONVERTER	5mH	2.64mH	0.02mH	47 μ F	47 μ F	47 μ F

For $V_{in} = 12$ V, Switching Frequency $f = 25$ KHz, Duty Cycle $K = 75\%$, $R_o = 10\Omega$

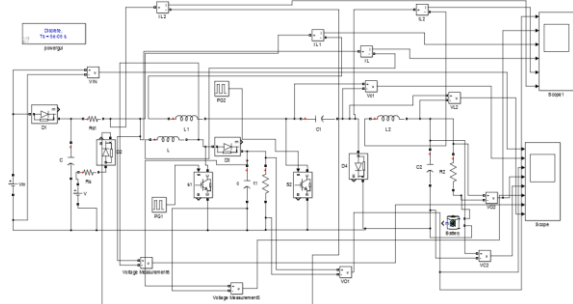


Fig.7 Simulink model of Cuk Boost Converter

Fig.7 shows the model of Cuk boost converter. Here the MOSFET switch is turned ON using pulse generator with 50% duty ratio and the output voltage is obtained.

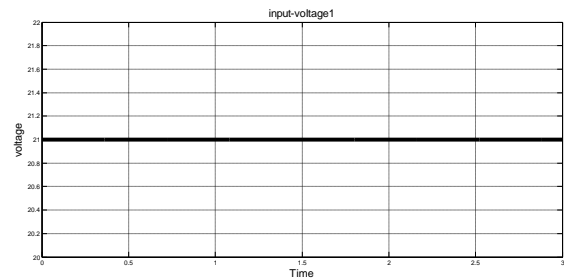
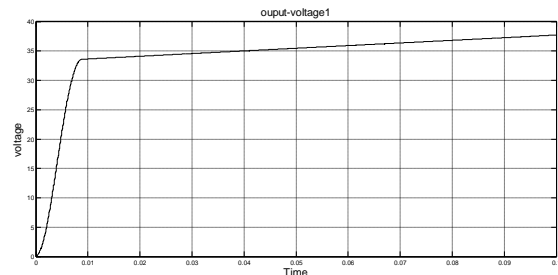
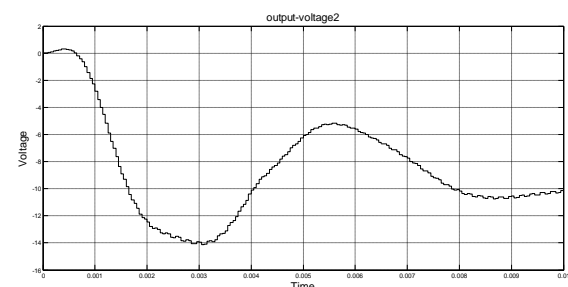


Fig.8 Input Voltage

Fig.9 Output Voltage(V_{o1})Fig.10 Output Voltage(V_{o2})

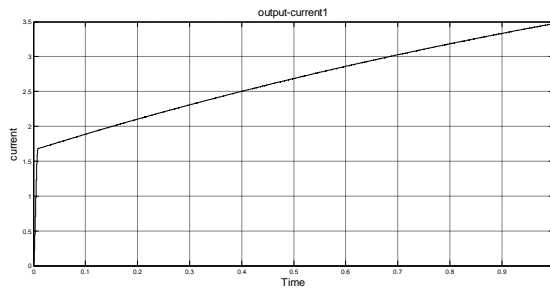


Fig.11Output Current1 Waveform of boost converter

Fig.11 shows the load current waveform of the boost converter

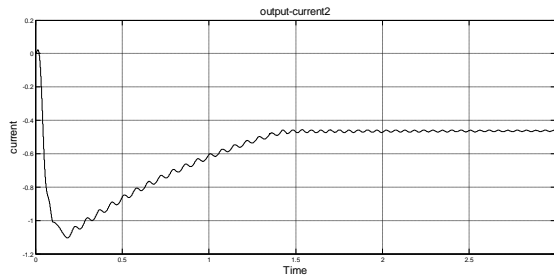


Fig.12 Output current2 waveform of cuk converter

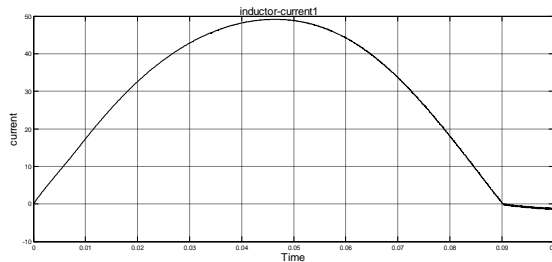


Fig.13 Output current waveform of cuk converter

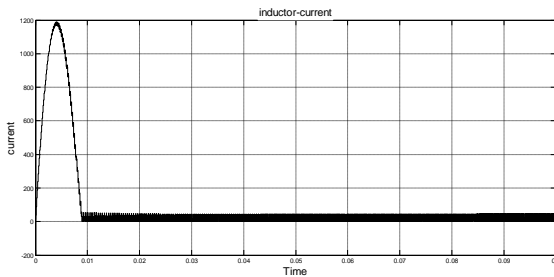


Fig.14 Output inductor current waveform of boost converter

the renewable energy power sources. The structure proposed by is a fusion of the Cuk and boost converter. The converter has three inductors that can shape the input current and feed the output load. The converter can give two parallel outputs at the same time.thus the efficiency of the converter can be improved by using fused converter topology.

REFERENCES

- [1] Aaden Safari and SaadMekhilef, “Simulation and hardware implementation of incremental conductance MPPT with direct control method using Cuk converter,” IEEE Trans. on Ind. Electron., vol. 58, no. 4, pp. 1154– 1161, April 2011.
- [2] Y. Qiu, C. V. Liempd, B. O. H. Veld, P. G. Blanken, and C. V. Hool, “5 μW-to-10 mW input power range inductive boost converter for indoor photovoltaic energy harvesting with integrated maximum power point tracking algorithm,” in Proc. IEEE Int. Solid-State Circuits Conf. Mar. 2011, pp. 118–120.
- [3] Rashid “Handbook on Power Electronics ”Pearson Publications.
- [4] TIMOTHY ROSS, “Fuzzy Logic with Engineering Applications”, Third Edition.
- [5] LUO F.L., “Luo converters – voltage lift technique,” Proceedings of the IEEE Power Electronics special conference IEEE-PESC’98,Fukuoka, Japan, 17-22, pp. 1783-1789, May. 1998.
- [6] M.Namnabat, M. BayatiPoodeh, S. Eshtehardiha, “Comparison the control methods in improvement the performance of the DC-DC Converter,” The 7th International Conference on Power Electronics. October 2007, pp. 246-251.
- [7] P. Comines and N. Munro, “PID controllers: recent tuning methods and design to specification”, in IEEE Proc. Control Theory Application, vol.149, no.1, pp.46-53, Jan 2002.
- [8] Rashid, M.H.: ‘Power electronics: circuits, devices and applications’ (Prentice Hall, Englewood Cliffs,, NJ, USA, 1993, 2nd edn.)
- [9] Massey, R.P., and Snyder, E.C.: ‘High-voltage single-ended DC-DC converter’. IEEE Power Electronics Specialists Conf., Record 1977, June 1977, pp. 156–159

VI CONCLUSION

The fused cuk boost converter which performs the step up and step down voltage. By using fused converter we can obtain more output voltage than the buck converter. Most of the systems use a separate DC/DC boost converter connected in parallel to perform the MPPT control for each of

SOFT START OF BOOST CONVERTER FED DC MOTOR FOR HIGH POWER APPLICATIONS

T D SUDHAKAR

Associate Professor

Electrical and Electronics Engineering
St. Joseph's College of Engineering
Chennai, India
t.d.sudhakar@gmail.com

A V VIGNESWARAN

Undergraduate Student

Electrical and Electronics Engineering
St. Joseph's College of Engineering
Chennai, India
vigneswaran1194@gmail.com

M VIJAY NISHANTH

Undergraduate Student

Electrical and Electronics Engineering
St. Joseph's College of Engineering
Chennai, India
vijaymnishanth@gmail.com

Abstract—The major drawback that occurs while starting a dc motor is the presence of high armature current. This initial current can have dangerous effects on the dc motor such as damage of windings, high initial losses and creation of false operation of protective devices. It may also lead to poor power factor, low efficiency and reduces the lifetime of the machine. Hence, there is a need to reduce the high initial starting current for better working of the dc motor and it is known as Soft Starting of DC motor. This paper aims at providing means for soft start of boost converter fed DC motor through two methods, namely, resistor start method and hysteresis control of armature current.

The first method is the conventional method of starting a dc motor which includes starting resistances to the motor armature circuit initially and later on they are tapped off from the armature circuit after the settling time. The second one aims at including a chopper circuit with a hysteresis controller to armature circuit to restrict the high armature current.

Keywords—Soft start, DC motor, hysteresis control, resistor start

I. INTRODUCTION

The DC motor is usually started by connecting DC voltage source to its armature circuit which results in high armature current initially. This high initial armature current is due to the absence of back electromotive force (emf) during the starting conditions. It is because during starting, the initial speed is zero and as the back emf (electromotive force) is proportional to the motor speed, the back emf (electromotive force) is also zero.

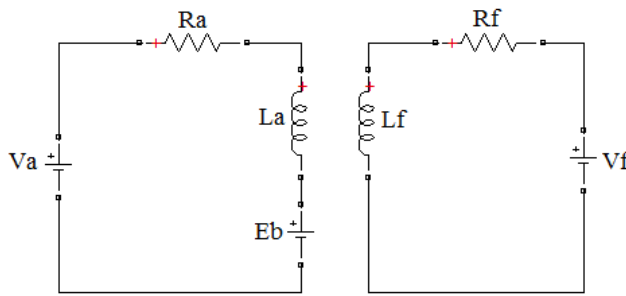


Fig. 1. Equivalent Circuit of DC Motor

Usually the field resistance (R_f) is large and the armature resistance (R_a) is very small. A normal DC shunt machine is modeled and simulated using MATLAB and the following values of armature current was obtained from figure 1. The peak values of the initial armature current are up to 93 A for a 5HP DC motor, which is 6 times the rated current value of 15.5 A.

A. Boost converter

It steps up the input DC voltage based on the values of inductor and capacitor. The Boost Converter Simulink diagram is shown in figure 2. The Design Procedure is as follows [1][2]:

1. Let us assume the frequency, voltage ripple, current ripple and output voltage of the circuit to be a constant.
2. Find the duty cycle using, $V_o = V_{in}/(1-D)$ -----(1)
3. Find the inductance and capacitance using,

$$L = (V_{in} * D) / (dI * f) \quad \text{-----(2)}$$

$$C = (I_o * D) / (dV * f) \quad \text{-----(3)}$$

where

L -Inductance of Boost Converter

C -Capacitance of Boost Converter

D -Duty Cycle

f -Frequency =25 KHz

V_{in} -Input Voltage

V_o -Output Voltage

dV- Ripple Voltage

dI -Ripple Current

The output voltage and current waveforms are shown in figure 3 and 4 respectively.

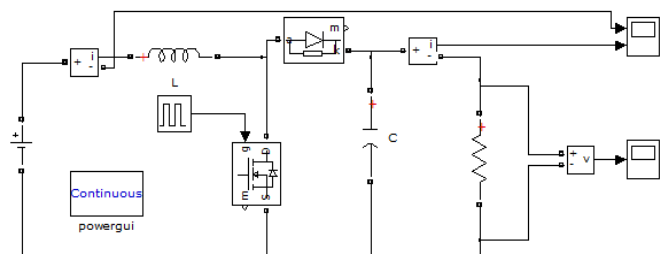


Fig.2. Boost Converter with R load

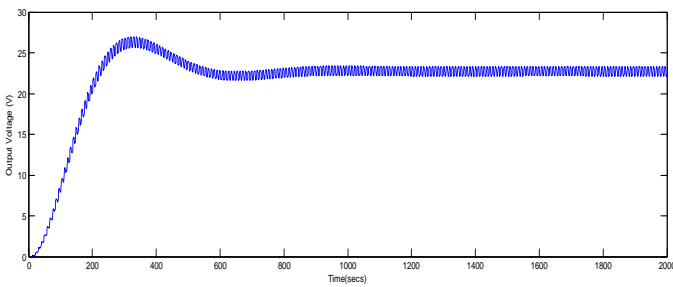


Fig. 3. Output voltage of Boost Converter with R Load

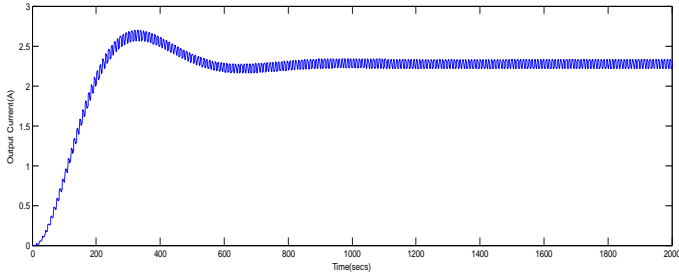


Fig. 4. Output current of Boost Converter with R Load

B. Boost Converter with Motor load

For study purpose take motor specifications as 5HP, 240V, 1750RPM, Field voltage=300V, $V_{in} = 120$ V and $V_o = 240$ V. Assuming $f = 25e3$ Hz, $dI = 5\%$, $dV = 5\%$, the values of parameters are obtained as $D = 0.5$, $L = 2.724e-4$ H, $C = 146.8e-6$ F. The Boost converter has the output voltage of 236V approximately for an input of 120V with the given design parameters. The Simulink diagram of Boost Converter with motor load is shown in figure 5. The output current is approximately 23A with input current being 50A after proper settling time. The resultant current waveforms are as shown below in figure 6[4][5].

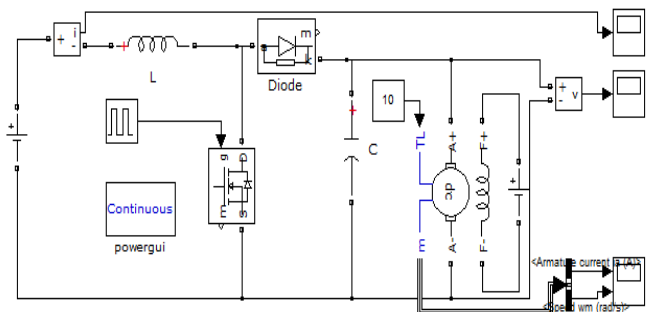


Fig. 5. Boost Converter with motor load

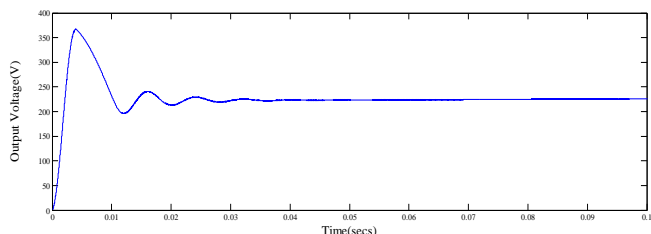


Fig. 6. Output voltage of Boost Converter fed Motor Load

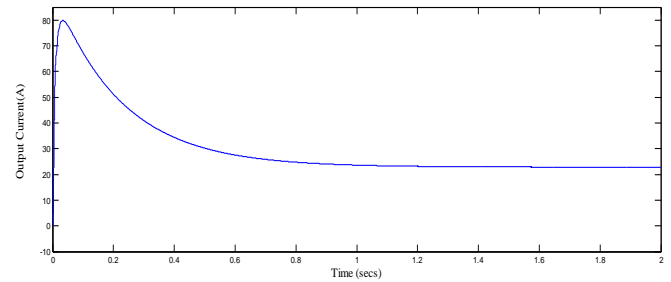


Fig. 7. Output Current of Boost Converter fed Motor Load

II. METHODS OF STARTING

In order to reduce the high starting current, the two methods which have been proposed are[3][5]:

- A. Resistor Start Method
- B. Chopper circuit including hysteresis controller

A. Resistor Start Method

In conventional method of resistance starting, all the resistances are included in the armature circuit initially so that the armature current is lowered due to increased resistance. Gradually the resistors are removed as the motor speeds up. But the major drawback of this method is the wastage of power at each start-up manoeuvre across the resistors.

B. Chopper Circuit Method

To overcome the disadvantage of power wastage, the boost converter with hysteresis controller is used to restrict the high armature current. The function of the hysteresis controller is to monitor and control the armature current between two pre-set threshold values. The new disadvantage that arises because of introducing the chopper circuit is the creation of ripples in armature current.

III. SIMULINK MODELS OF THE STARTING MEANS

A. Resistor Start Method

The conventional way of limiting starting current is to insert starting resistors into the armature circuit in series as shown. These starting resistors are removed gradually as the motor speeds up. The time for moving from one resistor tap to another is usually calculated using the steady state analysis of DC motor.

Generally, five to eight resistors are placed in series with the armature circuit. These parts are generally short-circuited by means of an ideal switch triggered by a step wave appropriately at required time. The Simulink block of starting resistors is as shown below in figure 8 and the Simulink model is as shown in figure 9[5].

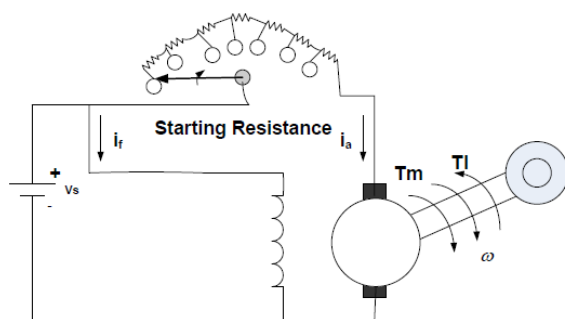


Fig. 8. Schematic Representation of Resistor Starter in DC Motor

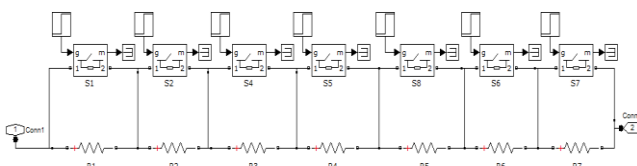


Fig. 9. MATLAB/Simulink Block of starting resistors

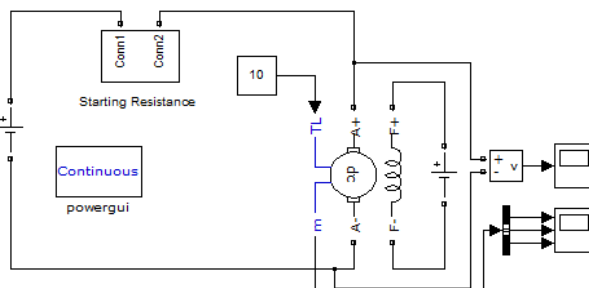


Fig. 10. Simulink Model of Resistor Start Method

The results of the simulations are shown below in the following figure 10. It is observed that the maximum value of armature current does not exceed twice the rated value.

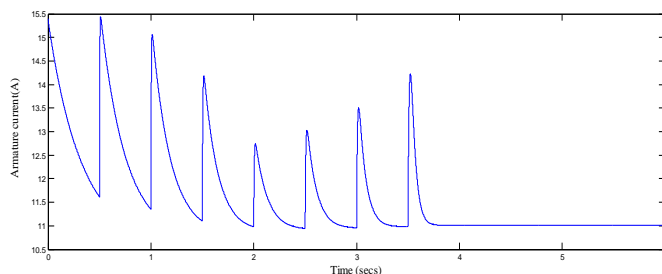


Fig. 11. Simulink Results using starting resistors

B. Chopper Circuit Method with hysteresis controller

The second method of controlling the armature current is to use a hysteresis controller with the already existing converter circuit. The hysteresis controller deals with the control of switching of MOSFET between the set maximum and minimum values. The circuitry shown in figure 11 is used for the hysteresis control of armature current and the resultant output waveforms of the respective Simulink models are represented as below in figure 12[5].

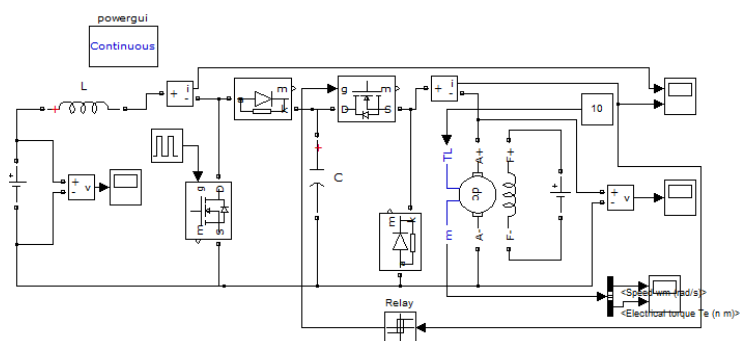


Fig. 12. Simulink Model of Chopper Circuit Method

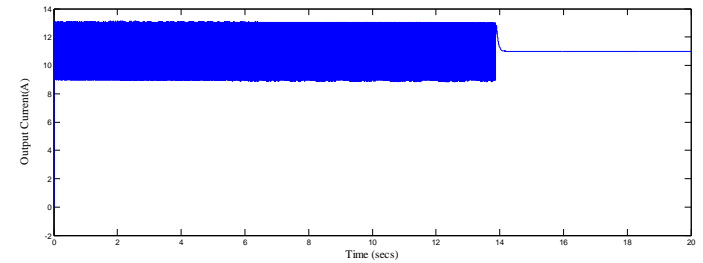


Fig. 13. Resultant output current waveforms obtained using Hysteresis control

IV. CONCLUSION

The development of Simulink models for the means of soft starting up of DC motor is the major work of this phase. Based on the simulation results, the latter method of chopper circuit with hysteresis controller seem to reduce the initial armature current and avoid wastage of energy present in the conventional resistor start method.

The major disadvantage of the method is the longer settling time and the high damping oscillations which may damage the armature windings. The Longer settling time is due to the narrow window of control and also due to high peak overshoot of armature current initially and slow change in current due to inductance.

The conventional method of resistor start method is advantageous in this aspect because it provides an effective means of reducing the armature current with comparatively shorter settling time of 4 seconds but this is achieved at the expense of wastage of useful power at the included resistors.

References

- [1] P. C. Sen, Principles of Electric Machines and Power Electronics, John Wiley & Sons Inc., New York, 1989.
- [2] M. H. Rashid, Power Electronics: Circuits, Devices, and Applications Prentice Hall, New Jersey, 1988
- [3] Mammar Taleb, A paper on Matlab/Simulink Models For Typical Soft Starting Means For A DC Motor, International Journal of Electrical & Computer Sciences IJECS-IJENS Vol: 11 No: 02
- [4] P.S.Bimbhra, A Book on Power electronics, Khanna Publishers, New Delhi, 1991
- [5] D.M.Hasaneen, Adel A. Elbaset Mohammed A paper Design and simulation of DC/DC Boost Converter, December 2008.

Design of H6 transformer less full bridge grid tied inverters

VELAYUDHAM ^{1a*}, SETHURAMAN A ^{1b}

Mr.K.SIVAKUMAR^{2a}, Dr.T.D.SUDHAKAR^{2 b}

¹UG Scholar, St. Joseph's College of Engineering, Chennai, India.

^{2a}Assistant Professor, St. Joseph's College of Engineering, Chennai, India.

^{2a}Associate Professor, St. Joseph's College of Engineering, Chennai, India.

[^avel090993@gmail.com](mailto:a.vel090993@gmail.com), [^bsethuram976@gmail.com](mailto:b.sethuram976@gmail.com)

Abstract:: This concept has been proposed in order to bring in high efficiency and low cost. The aim of H6 transformer less inverter is to bring in low leakage currents. The power loss and power device costs are very much reduced when compared to the existing topologies. Passive filters have been used in order to reduce harmonics. This concept can be extended to solar applications with small changes in the circuit.

Keywords: Transformer less inverters, grid tied inverters, low leakage currents, common mode leakage currents.

I.INTRODUCTION:

As we come across power demand now a days to a greater extent we are pushed in a situation to find for an alternative source of energy. So this new concept of H6 transformer less inverter is mainly a solar based application. This method is mainly proposed in order to bring low leakage currents, reduction in cost, reduced conduction losses, and reduction in thermal stress. The leakage currents in PV system has been shown below.

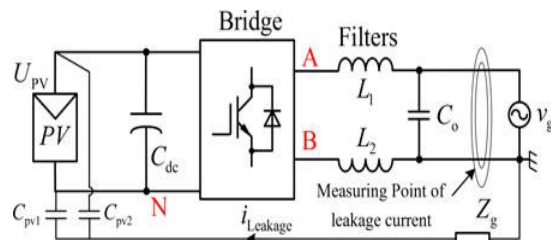


Fig. 1. Leakage current path for transformer less PV inverters.

The transformer less inverters are installed in low power distributed PV generation systems. When transformers are removed, there arises leakage current and capacitance effect which have been reduced to a greater extent using passive filters when compared to the existing systems. DC voltage utilization is half the value in half bridge inverters whereas it is full incase of full bridge inverters. So with the use of large number of PV panels will help in obtaining the required output voltages. The common mode voltage is kept constant in all the modes during its operation in this H6 topology set up. The current ripples are also high which has been compensated with unipolar SPWM differential mode characteristics.

II.H6 topology

The existing system is a full bridge inverter with 5 switches namely the H5 topology. With the addition of one single switch the operation still remains the same but with only change during the negative half cycle so that the diode freewheeling loss, conduction losses, switching losses have been reduced to a very greater extent.

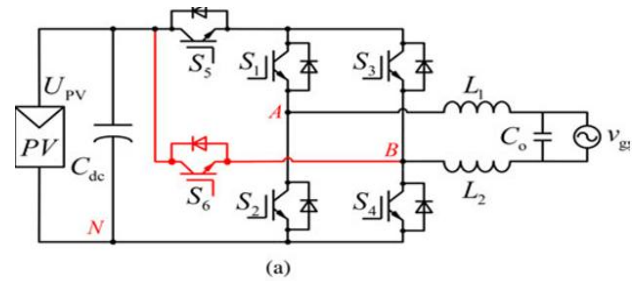


Fig 2. Circuit diagram of proposed H6 topology

III. Modes of operation

There are two primary modes namely positive half cycle and negative half cycle in which there are further two modes active mode and freewheeling modes in positive half cycle and negative cycle.

Mode I is the active mode in the positive half period of the utility grid voltage. S1, S4 , and S5 are turned ON, when these switches are turned on the diodes across each switches also operate and the other switches are turned OFF. The inductor current is flowing through S1, S4 , and S5 . $v_{AN} = UPV$, $v_{BN} = 0$; thus, $v_{AB} = UPV$, and the CM voltage $v_{CM} = (v_{AN} + v_{BN})/2 = 0.5UPV$.

Mode II is the freewheeling mode in the positive half period of the utility grid voltage only the switch S1 is turned ON; the other switches are turned OFF. The inductor current is flowing through S1 and the antiparalleled diode of S3. $v_{AN} = v_{BN} \approx 0.5UPV$; thus, $v_{AB} = 0$, and the CM voltage $v_{CM} = (v_{AN} + v_{BN})/2 \approx 0.5UPV$.

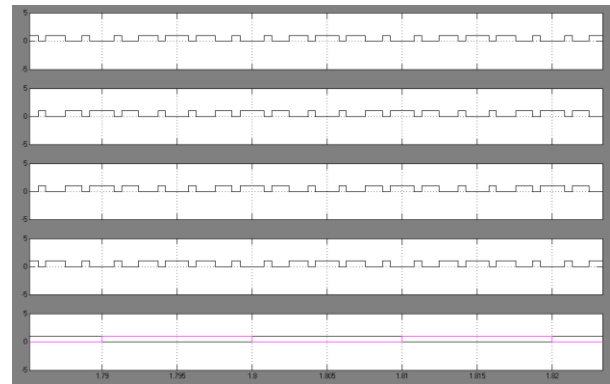
Mode III is the active mode in the negative half period of the utility grid voltage, S2, S3, and S6 are turned ON; the other switches are turned OFF. The inductor current is flowing through S2 and S6. Although S3 is turned ON, there is no current flowing through it, and the switch S3 has no conduction loss in this mode. Nevertheless, in the H5 topology, the inductor current flows through S2, S3, and S5 . Therefore, the conduction loss of proposed topology is less than that of H5 topology. In this mode, $v_{AN} = 0$, $v_{BN} = UPV$; thus, $v_{AB} = -UPV$, and the CM voltage $v_{CM} = (v_{AN} + v_{BN})/2 = 0.5UPV$.

Mode IV is the freewheeling mode in the negative half period of the utility grid voltage, S3 is turned ON, and the other switches are turned OFF. The inductor current is flowing through S3 and the antiparalleldiode of S1 . $v_{AN} = v_{BN} \approx 0.5UPV$; thus, $v_{AB} = 0$, and the CM voltage $v_{CM} = (v_{AN} + v_{BN})/2 \approx 0.5UPV$.

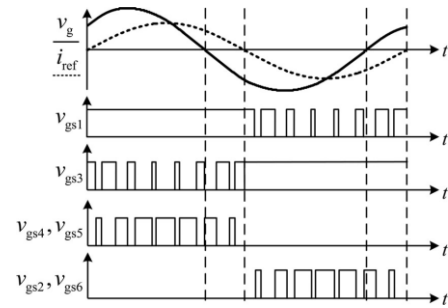
IV.Results

The various graphs for the above explained modes of operation has been shown below.

The gate signals for all the 6 switches have been shown below.

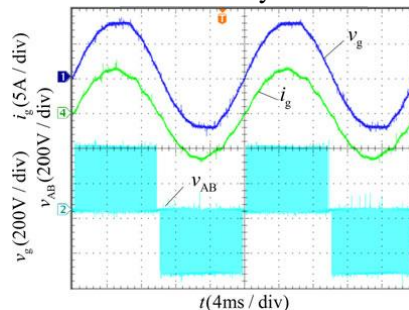


These switching pulses are given to various switches using corresponding sine and carrier signals.



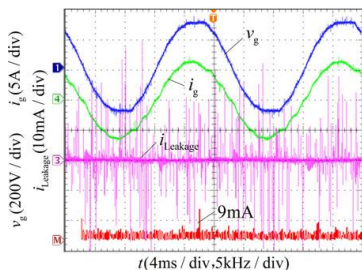
Schematic of gate drive signals with power factor other than unity

The above graph shows the schematic of d gate drives signals with power factor other than unity



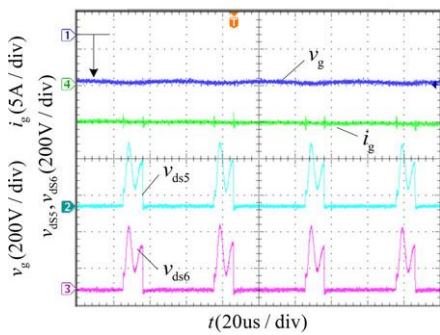
DM characteristic of H6 topology.

The above characteristic graph represents the DM characteristics of the proposed topology which is far better than the existing topology



CM voltage and leakage current in H6 topology. (a) CM voltage. (b) Leakage current.

The common mode voltage graphs have been shown above which is also a better output when compared to the existing H5 topology.



Drain-source voltages in H6 topology. (a) Voltage stress on S5 and S6 . (b) Detailed waveforms

The drain source characteristics have been shown in above graph for both existing and proposed topologies.

V. Conclusion

In this paper, a family of novel H6 full-bridge topologies is proposed for the transformer less PV grid-tied inverters. An extra Switch is inserted to the H5 topology for forming a new current path and for the purpose of reducing conduction loss.

Therefore, in the active modes, the inductor current of the proposed H6 topology flows through two switches during one of the half line periods and through three switches during another half-line period. The proposed H6 topology has achieved the minimum conduction loss, and also has featured with low leakage currents.

The excellent DM performance is achieved like the isolated full-bridge inverter with unipolar SPWM. Therefore, the proposed H6 topologies are good solutions for the single phase transformer less PV grid-tied

inverters. Low Conduction Losses in the Power Devices when compared to the existing topologies. Low Conduction Losses in Switched Capacitors with Low Switching Losses. Also Losses in the Filter Inductor is very low and CM Current is fully eliminated.

VI. References

- [1] S. B. Kjaer, J. K. Pederson, and F. Blaabjerg, "A review of single-phase grid-connected inverters for photovoltaic modules," *IEEE Trans. Ind. Appl.*, vol. 41, no. 5, pp. 1292–1306, Sep/Oct. 2005.
- [2] F. Blaabjerg, Z. Chen, and S. B. Kjaer, "Power electronics as efficient interface in dispersed power generation systems," *IEEE Trans. PowerElectron.*, vol. 19, no. 5, pp. 1184–1194, Sep. 2004.
- [3] B. Sahan, A. N. Vergara, N. Henze, A. Engler, and P. Zacharias, "A single Stage PV module integrated converter based on a low-power current source Inverter," *IEEE Trans. Ind. Electron.*, vol. 55, no. 7, pp. 2602–2609, Jul.2008.
- [4] M. Calais, J. Myrzik, T. Spooner, and V. G. Agelidis, "Inverters for single Phase grid connected photovoltaic systems—an overview," in Proc. IEEE PESC, 2002, vol. 2, pp. 1995–2000.
- [5] F. Bleiberg, Z. Chen, and S. B. Kjaer, "Power electronics as efficient interface in dispersed power generation systems," *IEEE Trans. Power Electron.*, vol. 19, no. 5, pp. 1184–1194, Sep. 2004.
- [6] Q. Li and P. Wolfs, "A review of the single phase photovoltaic module integrated converter topologies with three different dc link configuration," *IEEE Trans. Power Electron.*, vol. 23, no. 3, pp. 1320–1333, May2008.
- [7] O. Lopez, F. D. Freijedo, A. G. Yepes, P. Fernandez-Comesana, J. Malvar, R. Teodorescu, and J. Doval-Gandoy, "Eliminating ground current in a transformerless photovoltaic application," *IEEE Trans. Energy Convers.*, vol. 25, no. 1, pp. 140–147, Mar. 2010.
- [8] R. Gonzalez, J. Lopez, P. Sanchis, and L. Marroyo, "Transformerless Inverter for single-phase photovoltaic systems," *IEEE Trans. Power Electron.*, vol. 22, no. 2, pp. 693–697, Mar. 2007.
- [9] H. Xiao and S. Xie, "Leakage current analytical model and application In single-phase transformerless photovoltaic grid-connected inverter," *IEEE Trans. Electromagn. Compat.*, vol. 52, no. 4, pp. 902–913, Nov.2010.

- [10] VDE-AR-N 4105: Power Generation Systems Connected to the Low-Voltage Distribution Network—Technical Minimum Requirements for the Connection to and Parallel Operation with Low-Voltage Distribution Networks, DIN_VDE Nomo, 2011–08.
- [11] B. Yang, W. Li, Y. Gu, W. Cui, and X. He, “Improved transformer less Inverter with common-mode leakage current elimination for a photovoltaic grid-connected power system,” IEEE Trans. Power Electron., vol. 27, no. 2, pp. 752–762, Feb. 2012.
- [12] R. Gonzalez, E. Gubia, J. Lopez, and L. Marroyo, “Transformerless singlephase multilevel-based photovoltaic inverter,” IEEE Trans. Ind. Electron., vol. 55, no. 7, pp. 2694–2702, Jul. 2008.
- [13] H. Xiao and S. Xie, “Transformerless split-inductor neutral point clamped Three-level PV grid-connected inverter,” IEEE Trans. Power Electron vol. 27, no. 4, pp. 1799–1808, Apr. 2012.
- [14] L. Zhang, K. Sun, L. Feng, H. Wu, and Y. Xing, “A family of neutral point Clamped full-bridge topologies for transformerless photovoltaic grid-tied Inverters,” IEEE Trans. Power Electron., vol. 28, no. 2, pp. 730–739, Feb. 2012.
- [15] German Patent Wechselrichter: DE 19642522C1 Apr. 1998.
- [16] Y. Gu, W. Li, Y. Zhao, B. Yang, C. Li, and X. He, “Transformerless inverter with virtual DC bus concept for cost-effective grid-connected PV power systems,” IEEE Trans. Power Electron., vol. 28, no. 2, pp. 793–805, Feb. 2012.
- [17] M. Victor, F. Greizer, S. Bremicker, and U. Hübner, “Method of converting a direct current voltage from a source of direct current voltage, more specifically from a photovoltaic source of direct current voltage, into a alternating current voltage,” U.S. Patent 7 411 802, Aug. 12, 2008.
- [18] S. Heribert, S. Christoph, and K. Jurgen, “Inverter for transforming a DC voltage into an AC current or an AC voltage,” Europe Patent 1 369 985 (A2), May 13, 2003.
- [19] W. Yu, J. Lai, H. Qian, and C. Hutchens, “High-efficiency MOSFET inverter with H6-type configuration for photovoltaic no isolated ac-module applications,” IEEE Trans. Power Electron., vol. 26, no. 4, pp. 1253–1260